

# Finite element analysis of the closed stiffener to crossbeam connection in OSDs using the hot spot stress approach

D.J. van der Ende



# Finite element analysis of the closed stiffener to crossbeam connection in OSDs using the hot spot stress approach

## Master of Science thesis

Delft University of Technology  
Faculty of Civil Engineering and Geosciences  
Department of Structural Engineering

Author: D.J. van der Ende  
Student number: 4247116  
Graduation committee: Prof.dr. M. (Milan) Veljkovic TU Delft  
Dr.ir. M.A.N. (Max) Hendriks TU Delft  
W. (Weijian) Wu MSc. TU Delft  
Prof.dr.ir. J. (Johan) Maljaars TNO

Cover image: Weesperbrug, Weesp.

<https://www.nationalestaalprijs.nl/project/verkeersbrug-weesperbrug>



## PREFACE

This thesis on the finite element analysis of the longitudinal to transverse stiffener connection in an orthotropic steel deck (OSD) has been written to obtain the Master of Science degree at the Delft University of Technology. The research is fulfilled at the Organization for Applied Scientific Research: TNO Delft, at the department of Structural Reliability.

First of all I would like to thank Prof.dr.ir. Johan Maljaars for giving me the opportunity to write my thesis at TNO. Your enthusiasm and knowledge about fatigue really inspired me and I've learned a lot from your guidance. Furthermore, I would like to thank Weijian Wu for being my daily supervisor from the University, your knowledge about the finite element software Abaqus and guiding me throughout the project has been invaluable for my work. I would also like to thank Ir. Bas Wijnbeld from Rijkswaterstaat, your experience from practice was really helpful.

Special thanks to Prof.dr. Milan Veljkovic for your judgement and feedback during the meetings and providing me valuable guidance. Furthermore I would like to thank Dr.ir. Max Hendriks for your interest in my thesis. The judgement of my committee members really improved the quality of this thesis.

Furthermore, I am grateful to two other master students, Navid Nikraftar and Sayantan Pandit, who performed a similar research on different fatigue details. Their feedback and brainstorm sessions were really helpful in completing this thesis.

I would also like to thank my family and friends for their support during this research and being there for me. Special thanks to my mother and good friend Fahim who have been there for me all the time and took care of the relaxing moments. Even though you had no knowledge about the topic, listening to me while I was facing difficulties really helped me to see the light at the end of the tunnel again.

Enjoy reading this research report.

D.J. van der Ende  
Brielle, August 2020

## ABSTRACT

An Orthotropic Steel Deck (OSD) is susceptible to fatigue and this forms an important design criterium. In this research the rib-to-crossbeam connection with a cope hole is studied using Finite Element Methods (FEM). The fatigue assessment is performed with the hot spot stress method making use of surface stress extrapolation. Two fatigue cracks are investigated: the crack initiating from lower weld end in the rib, and the crack which appears at the weld toe of the rib-to-crossbeam connection and propagating in the crossbeam at some distance from the soft toe of the cut-out.

Engineering firms widely use shell elements to model the structure, instead of solid elements. The modelling and computational time is limited when compared to the solid element. When a comparison is made between the results from the solid and shell FE models, a scatter in results is often seen. This thesis studies the difference of shell and solid element modelling in the hot spot stress calculation of OSDs. Improvement of the shell element modelling is given based on the FE analysis using various shell element modelling techniques and compared with solid element models which represent as a reference.

Three different weld modelling techniques are applied to shell FE model: IIW, Eriksson and a combination of the first two approaches. The weld modelling techniques for the shell FE model are first applied on a simple single sided fillet welded transverse stiffener connection. In this study both the deformations and hot spot stress are compared. The conclusions of the single sided fillet welded connection are used for the full OSD specimen to investigate if similar conclusions are also valid.

A small parametric analysis is performed to investigate the difference in hot spot stress for pure in-plane and out-of-plane rotation of the crossbeam. In this study the different weld modelling techniques for the shell FE models are included. Furthermore, the difference between the stress perpendicular to the weld toe and the principal stress is investigated, since it is concluded that a biaxial stress state occurs in the crossbeam. In the extensive parametric analysis two different studies are performed: one based on the influence of the loading positions, the second study is based on different thicknesses of the parts of the OSD. One axle type C from fatigue load model 4 (FLM4) is considered. Based on the loading positions study the critical loading positions, i.e. which result in the highest stress range, are further investigated.

From both the fillet welded transverse stiffener specimen and the full OSD specimen it is concluded that the shell FE model in which use is made of the combined weld modelling technique, gives the largest improvement. The ratio between shell and solid FE models of the obtained hot spot stress is reduced from a factor 1.25 to a factor 1.05 for the lower weld toe crack in the rib. The regular shell FE model is not suitable for the crack in the crossbeam, since the stresses cannot be captured well from the structural intersection point.

For the crack in the trough, the mean value of the hot spot stress ratios is equal to 1.04 for both the old and new OSD variant and the coefficient of variation (CV) is equal to 0.8% and 2.2% respectively. For the crack in the crossbeam, the mean values are equal to 0.80 and 0.76 for the old and new OSD variant respectively. The CV is equal to 1.9% and 2.0% for the old and new OSD variant respectively. Furthermore, the stress gradient and the stress at 40mm from the weld toe show similar results when compared with the solid FE models. The coefficient of variation for both investigated cracks is low, i.e. below 5%, thus the ratio between obtained hot spot stress of the shell with combined weld and solid FE models is consistent.



## Contents

Preface .....	i
Abstract.....	ii
1. Introduction .....	1
1.1. Background .....	1
1.2. Problem definition .....	2
1.3. Scope and limitations.....	3
1.4. Methodology.....	3
1.5. Outline.....	4
2. Literature review.....	6
2.1. Fatigue.....	6
2.2. S-N curves .....	7
2.3. Orthotropic Steel Deck (OSD) .....	8
2.4. Fatigue strength assessment methods .....	18
2.5. Fatigue load models (FLM).....	25
2.6. Finite element analysis .....	27
2.7. Performed research on different modelling techniques (shell and solid) .....	31
3. Validation of FEM models .....	35
3.1. Validation: single sided fillet welded longitudinal attachment connection .....	35
3.2. Validation: OSD in Stevinlab II.....	45
4. Fatigue assessment based on HSS method reference models .....	59
4.1. HSS results from experiments.....	59
4.2. HSS results from Finite element models.....	59
4.3. Comparison FE model solid and experimental results.....	60
5. Transverse stiffener connection: weld modelling techniques shell FE model.....	61
6. Parametric studies .....	67
6.1. General information of parametric studies .....	67
6.2. Small Parametric analysis .....	70
6.3. Parametric study I and II: loading positions and different geometries .....	90
6.4. Further investigation parametric studies.....	101
7. Results and discussion .....	112
8. Conclusions and recommendations.....	115
8.1. Conclusions .....	115
8.2. Recommendations .....	116
Annex A1 .....	117
Annex A2 .....	123

Annex B .....	126
Annex C .....	128
Annex D .....	130
Annex E .....	134
Annex F .....	140
Annex G .....	143
Annex H .....	150
Annex I .....	156
Annex J .....	160
Annex K .....	169
References .....	171

# 1. INTRODUCTION

## 1.1. Background

Orthotropic steel decks (OSD) are widely used in bridges due to their high load bearing capacity in combination with low weight and fast erection speed (Wu W. , Kolstein, Veljkovic, Pijpers, & Vorstenbosch-Krabbe, 2017). An OSD is made out of different parts: main girders, a deck plate, crossbeams and troughs, also called longitudinal closed stiffeners or ribs, which is shown in Figure 1.1. These different components are connected by welding. In combination with cyclic loading, due to the traffic, OSD bridges are susceptible to fatigue damage (Li, Suzuki, Hashimoto, & Sugiura, 2017). In the last years fatigue cracks are found in multiple bridges which consist of OSD's (Kolstein, 2007). A fatigue crack will first initiate and then propagate and based on the location of the crack, a part of the structure may not be able to resist the loads which can cause failure of the overall structure. The fatigue life is depending on different aspects: the fatigue detail class, the stress range and the intensity of the cyclic loading.

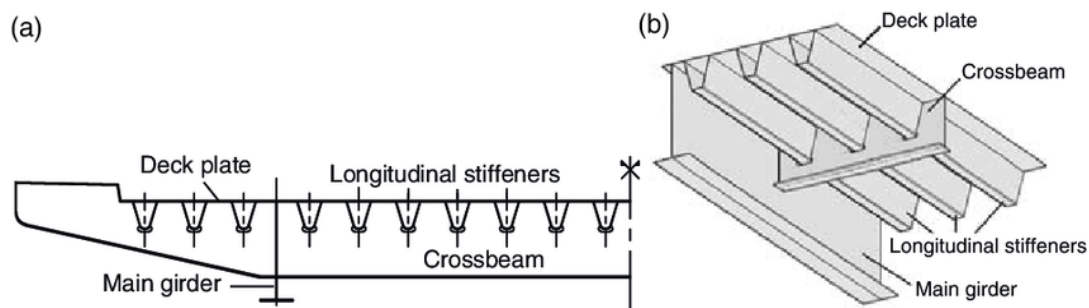


Figure 1.1 Overview OSD (Freitas, Kolstein, & Bijlaard, 2011)

In an OSD fatigue cracks can occur at different locations. One location is the rib-to-deck joint, in which a further distinction can be made between two different locations: at the crossbeam or in-between the crossbeams. Another location is the longitudinal closed stiffener (trough), and crossbeam joint. This thesis will focus on the latter joint.

Multiple guidelines and standards are available for the fatigue life analysis, e.g. Det Norske Veritas (DNV GL, 2016), EN1993-1-9 (EN1993-1-9, 2011), and the International Institute of Welding (Niemi, Fricke, & Maddox, 2018). Each design code or recommendation is based on a large amount of experiments for different connections. These different types of connections are assigned to so-called detail classifications or FAT classes. Each of the classifications comprises of a so-called S-N curve with which it is possible to calculate the fatigue life. The detail categories are based on standard and simple connections.

Obtaining the fatigue life of the OSD can be quite challenging because of the complex geometry, for example a crossbeam with or without cope holes, and complex load transfer of the structure. For determination of the stresses at the connections of the bridge finite element models are commonly used. With the use of the FE analysis, it is possible to acquire the required stresses at the joints with a complex geometry. Different fatigue assessment methods can be used for determining the stresses: (modified) nominal stress method, hot spot stress method and the effective notch method. The hot spot stress method and (modified) nominal stress method are included in (EN1993-1-9, 2011) while for the effective notch recommendations can be found in the IIW recommendations: International Institute of Welding (Hobbacher, 2014). Each method has his advantages or limitations. Engineering

firms widely use the hot spot stress method, because it is a straightforward and fast method with an acceptable accuracy. With the hot spot stress method, the stresses are extrapolated at the weld toe. When finite element modeling is used, the IIW (Niemi, Fricke, & Maddox, 2018) gives recommendations on how apply this method, while the (EN1993-1-9, 2011) gives no recommendations at all. The structural hot spot stress is the summation of the membrane stresses and the bending stresses. The non-linear stress peak due to the notch is excluded in this method.

All mentioned assessment methods have their limitations and care should be taken for which method to choose. The element type, for instance shell or solid elements, and the corresponding element size also have an influence on the outcome of the obtained stress range. The accuracy of the outcome is also depending on how detailed the model is. Normally, a more detailed model gives more local information of the fatigue strength calculation, at the cost of a considerably higher modelling and computational time.

## 1.2. Problem definition

As mentioned in the previous section, OSDs are susceptible to fatigue problems and in the last years a lot of bridges had difficulties with this phenomenon. To calculate the fatigue life of bridges use is made of finite element modelling. Engineering firms widely uses shell elements to model the structure, instead of solid elements. Shell elements are 2D elements and give a good approximation of the results if the thickness is a fraction of the width and length of the element. With shell elements the structural elements are modelled based on the middle planes of the elements. The thickness of the element is given as a property. Solid elements are elements which represents the structure in a three-dimensional manner. The variation throughout the thickness taken into account with solid elements. Solid elements give the most accurate approximation of the results, when compared with experiments, since they are the closest to the real-life situation, but they do have some downsides. The modelling and computational time for the model will drastically increase when solid elements are used to model the whole structure. When a comparison is made between the results from the solid and shell FE models, a scatter in results is often seen.

The results from shell elements can overestimate or underestimate the stresses when compared with the solid elements. Overestimation of the stresses will result in a shorter fatigue life and thus an overdesigned structure which will result in a more expensive structure. Underestimation of the stresses when compared with solid elements can result in unsafe structure which is not desirable. It is interesting to do further research on the differences in stresses between solid and shell elements models. **At this moment it is not clear if and how the stresses obtained from a shell FE model can be related to the stresses obtained from a solid FE model in a consistent way.**

At the moment TNO and Rijkswaterstaat (RWS) are performing research to update EN1993-1-9 (EN1993-1-9, 2011). An overview of the different detail categories of the OSD with closed and open stiffeners are given in table 8.8 and 8.9. Those tables will be updated with the next revision of the Eurocode. The idea is that those updated tables will have modelling requirements for the use of solid and shell elements. The results of this thesis can be used for the development of those modelling requirements.

The main aim of this thesis is to carry out research for suitable approaches for the complex connection of the rib-to-crossbeam connection with a cope hole in an OSD bridge. The main task of this thesis is to find a consistent method to relate the stress range obtained from the shell FE model, with the hot

spot stress obtained from the solid FE model, by keeping the model as ease of applicability as possible. This leads to the following research question:

***“What is the most consistent method to relate the stress range, obtained with shell FE modelling, with the hot spot stress range, obtained from solid FE modelling, at the rib-to-crossbeam connection with cope hole?”***

The following sub-questions should be investigated and answered first to obtain an answer to this main research question:

- 1) *What is the influence of different loading positions on the stresses at the hot spot location of the rib-to-crossbeam connection with a cope hole in the OSD bridge?*
- 2) *What is the influence of the geometry, old and new OSD design, on the stress range at the hot spot locations at the above-mentioned connection?*
- 3) *What are the differences in the hot spot stress range ( $\Delta\sigma_{HSS}$ ) between the solid and shell FE models, based on the different fatigue details for the critical loading positions?*
- 4) *With which weld modelling techniques can the differences of the shell and solid FE model be reduced for obtaining the hot spot stress?*

In the end an overview of the most suitable and consistent method will be given. Also, recommendations about the possible relation of the results from the finite element model based on shell and solid elements will be given.

### 1.3. Scope and limitations

The rib-to-crossbeam connection with a cope hole will be the focus of this master thesis. The fatigue life assessment of the reference models is determined with the hot spot stress method based on surface stress extrapolation. Both the ‘old’ and ‘new’ OSD geometries, with several configurations, will be investigated. This means that the dimensions of those structural elements will differ. Several geometric variants of the old and new OSD will be studied based on commonly used configurations. The following two fatigue cracks are investigated: longitudinally in the trough starting from the weld end at the weld toe adjacent to a cope hole and in the crossbeam parallel to the weld toe at some distance from the soft toe, as can be seen in Figure 1.2.



Figure 1.2 Fatigue cracks from weld toe to trough and crossbeam (Kolstein H. , 2007)

### 1.4. Methodology

In this master thesis FE modelling will be used to model the available experiments. Different element types are compared in this research: shell elements and solid elements. The software Abaqus 2019 is used for the modelling of the structure. First a simple connection, which is investigated by (Lee, et al., 2010) is validated based on the stresses. This connection consists of two plates, one main and one

attachment, which are connected to each other by fillet welds. In this FE model the geometric, boundary conditions and loading uncertainties are further investigated. This is done to see the effect on the stresses when one parameter is adapted. After the validation of the simple connection, the orthotropic steel deck which is currently being tested at the Stevinlab of the Delft University of Technology, is modelled and validated. The validation is based on the experimental results by (Wu & Kolstein, 2020). The first model consists of a shell element model. In the second model a small sub-solid model is made at the location of interest. To keep the uncertainties in the FE model as limited as possible, the actual geometry of the troughs and welds, and the actual location of the strain gauges, at the connection with the longitudinal closed stiffener with the crossbeam, is measured. This validation ensures that the outcome of the different models is reliable. Also the boundary conditions are closely investigated to limit those uncertainties. The fatigue life assessment of both the simple connection and OSD is based on the hot spot stress method using surface stress extrapolation.

After determination of the hot spot stress of the above mentioned OSD, a parametric study in which also finite element modelling is used, is performed. In this parametric study the effect of different parameters, on the stress range, is analyzed. This analysis is performed for a single sides fillet welded transverse attachment joint and an OSD specimen. Different weld modelling techniques are investigated for the shell FE models. The critical loading positions in the OSD specimen are determined based on a DLOAD subroutine in which one axle type C from FLM4 is moved over the deck plate. Based on the results from the parametric study, the most accurate and consistent weld modelling technique for obtaining the hot spot stress range is determined.

## 1.5. Outline

In chapter 2 the overview of the literature research is given. In this literature research the following parts are investigated to get a better understanding of the research question and problem: fatigue, fatigue strength assessment methods, OSD general, performed research on the trough to crossbeam connection and finite element modelling based on solid and shell elements.

In chapter 3 an overview of the reference finite elements models is given in which a distinction is made between a simple joint and the full OSD specimen. Both reference models are made with shell and solid elements. First the validation is done of a relatively simple case, which is a single sided fillet welded longitudinal stiffener joint, in which the influence of the different parameters on the stress range will be investigated. After this investigation the more complex case, which is the OSD currently being tested at the Delft University of Technology is validated.

In chapter 4 the hot spot stress method is used as the fatigue assessment method for the reference models. The obtained hot spot stresses of both the shell and solid FE model are compared with the experimental results from the OSD.

In chapter 5 different weld modelling techniques for the shell FE models are investigated based on single sides fillet welded transverse stiffener connection. Both the hot spot stress and the deformations of the different weld modelling techniques are compared with the solid FE model.

In chapter 6 the parametric analysis is performed and the results of the two investigated variants are discussed. In this parametric analysis the critical loading positions for the investigated cracks are determined based on a DLOAD subroutine. Furthermore, a comparison is made between the differences in results of the hot spot stress for the solid and shell FE models.

In chapter 7 a summary of the obtained results of all previous chapters is given and the results are discussed.

The conclusions and recommendations of this research are given in chapter 8.



## 2. LITERATURE REVIEW

In this chapter an overview of the information retrieved from the literature research is given. The literature research can be subdivided in different parts: fatigue, S-N curves, general information about the OSD, fatigue strength assessment methods, recommendations from codes or guidelines and finite element modelling based on solid or shell elements.

### 2.1. Fatigue

The classical definition of fatigue is obtained from the ASM handbook (ASM Handbook, Volume 19: Fatigue and Fracture, 1996): “fatigue is the progressive, localized and permanent structural change that occurs in a material subjected to repeated or fluctuating strains at nominal stresses that have maximum values less than the tensile strength of the material”.

#### Fatigue crack growth

The growth of a fatigue crack can be divided in three different stages: crack initiation stage, crack propagation stage and the last stage which is the final fracture (Smith, 1994). In Figure 2.1 an overview of those three stages is shown. The crack initiation starts at locations where a large stress range occurs due to for instance: size and shape of the weld, local weld defects, or geometrical discontinuities. This stage is the most complex stage in fatigue and a lot of research have been performed. The second stage is the crack propagation period in which the cracks develops from a microcrack to a macrocrack. In this stage the microcrack will further grow in a direction which is perpendicular to the tensile stress. Factors which have an influence on the crack propagation are: material properties, geometry and the stiffness of the specific detail. The last stage is the final fracture, or rupture, in which the propagation of the crack weakens the structure to that point that fracture can occur. The total number of cycles to failure is the number of cycles for the crack initiation, plus the number of cycles for the crack propagation ( $N_f = N_i + N_p$ ) (Smith, 1994). The number of cycles for crack initiation is relatively high, for high cycle fatigue, when compared with the number of cycles for crack propagation. When the stress level is increased the number of cycles for crack propagation will dominate, and the number of cycles for crack initiation will decrease. The final failure of the specimen can be either ductile or brittle.

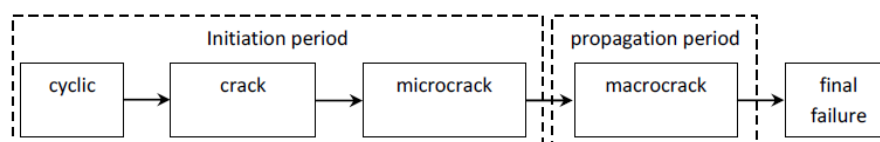


Figure 2.1 Different fatigue stages

An orthotropic steel deck is exposed to cyclic traffic load. This cyclic load will cause stress ranges in the structure. An important aspect is the intensity of this stress range. Highway bridges have more heavy traffic, like trucks, when compared with local bridges. This will result in relatively large stress ranges and high load cycles and consequently those two aspects play a major role in constructions which are sensitive for fatigue. In several OSD bridges in the Netherlands fatigue cracks are found: the Galecopperbrug and Van Brienoordbrug (Leendertz, 2008).

Cracks in OSD's can occur at different locations (Kolstein, 2007):

- At the location of the deck plate and trough connection, between or at the crossbeam;
- At the connection of the trough with the crossbeam, without or with cope holes;
- At the location of the splice welded joint of the troughs.

The focus of this thesis is on the rib-to-crossbeam connection with a cope hole, thus only the cracks which can initiate over here are included in this research.

## 2.2. S-N curves

In a S-N curve, also known as the Wöhler curve, a graphical representation of the stress magnitude and the number of cycles until failure, on a logarithmic scale is shown. On the horizontal axis the number of cycles until failure (N) is shown, while on the vertical axis the stress magnitude is shown (Smith, 1994). S-N curves are based on experimental results in which specimens are tested under repetitive loading conditions. During these experiments the stress range and the number of cycles until failure are measured. As can be seen from Figure 2.2, the experimental results show a large scatter in the data. To take this into account a design curve, also named characteristic curve is used. A 100% survival probability will result in very conservative structures which are not economical desirable, so a probability of survival of 97.7% or 95% is evaluated statistically based on the mean curve.

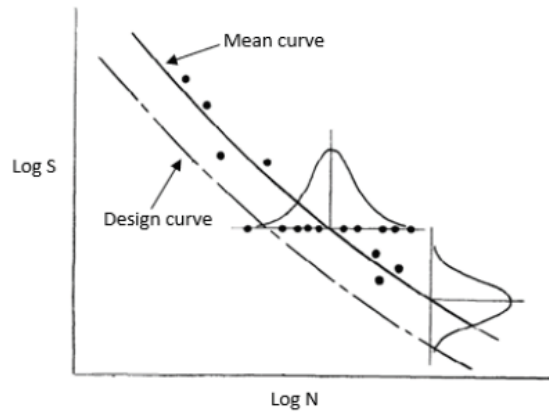


Figure 2.2 S-N curve with mean and characteristic curve (Bak, 2015)

### Detail categories

Detail categories are based on standardization of commonly used joints. These detail categories represent the stress range at failure, which occurs when 2 million load cycles are applied. The detail categories which can be found in EN1993-1-9 (EN1993-1-9, 2011) or the IIW recommendations (Niemi, Fricke, & Maddox, 2018), are based on the characteristic curve based on experiments. Due to the detail category it is relatively simple to perform a verification of a standard connection.

A S-N curve for different detail categories is shown in Figure 2.3. Three different points are important in this figure: 1, the detail category, 2, the CAFL, constant amplitude fatigue limit and 3, the COL, cut-off limit. The detail category corresponds with the stress range at 2 million load cycles, the constant amplitude fatigue limit with the stress range at 5 million load cycles and the cut-off limit with the stress range at 100 million load cycles (Mashiri & Zhao, 2007). When stress ranges with a constant amplitude are applied which are below the CAFL, the fatigue life will be infinite. When stress ranges with a non-constant amplitude are applied which is below the COL, the fatigue life will also be infinite. The slope of the graph between the detail category and the CAFL is equal to  $m=3$  and from the CAFL to the COL equal to  $m=5$  (Leonetti, Allaix, Maljaars, & Hashemi, 2017). The constant amplitude fatigue limit,  $\Delta\sigma_D$ , and the cut-off limit,  $\Delta\sigma_L$ , can be calculated with the following equations:

$$\Delta\sigma_D = \left(\frac{2}{5}\right)^{\frac{1}{3}} * \Delta\sigma_C$$

$$\Delta\sigma_L = \left(\frac{5}{100}\right)^{\frac{1}{5}} * \Delta\sigma_D$$

Several different effects, which are not taken into account in the design stress of the fatigue assessment, are included in the detail categories. These effects are: residual stresses and weld imperfections due to welding. The stress concentrations due to the weld geometry and detail geometry are included by the detail category or the design stress. Which stress concentrations are taken into account is depending on the fatigue assessment method which is used for the calculation of the stress range.

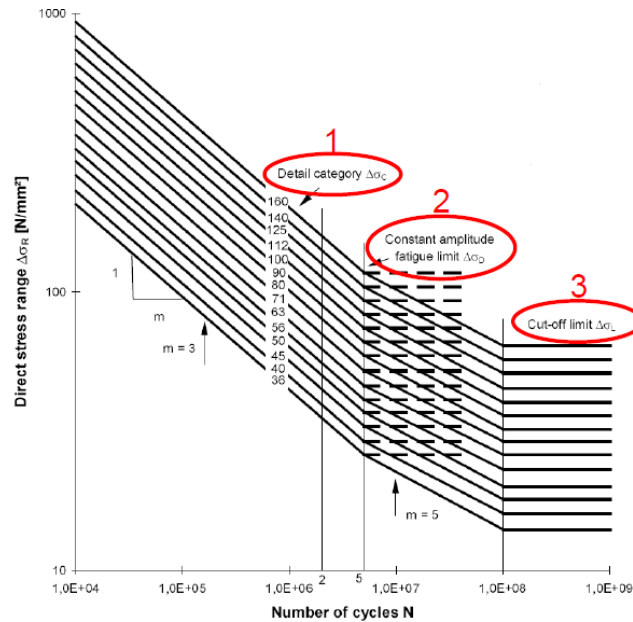


Figure 2.3 S-N curve with different detail categories from Eurocode (EN1993-1-9, 2011)

### 2.3. Orthotropic Steel Deck (OSD)

An orthotropic steel deck (OSD) is a structure which consists of a deck plate, main girders, closed stiffeners (troughs) and crossbeams. To make the manufacturing easier, a cope hole can be applied in the crossbeam. The troughs can be discontinuous, in which they are fitted between the crossbeams, or continuous in which they are passing through the crossbeam by cut-outs. The longitudinal stiffeners provide support to the deck plate and can be open or closed stiffeners. This research focusses on closed stiffeners only.

An overview of an OSD is shown in Figure 2.4 in which: 1: deck plate, 2: welded connection between trough and deck plate, 3: connection between crossbeam and trough, 4: cope hole in crossbeam and 5: stiffener splice joint.

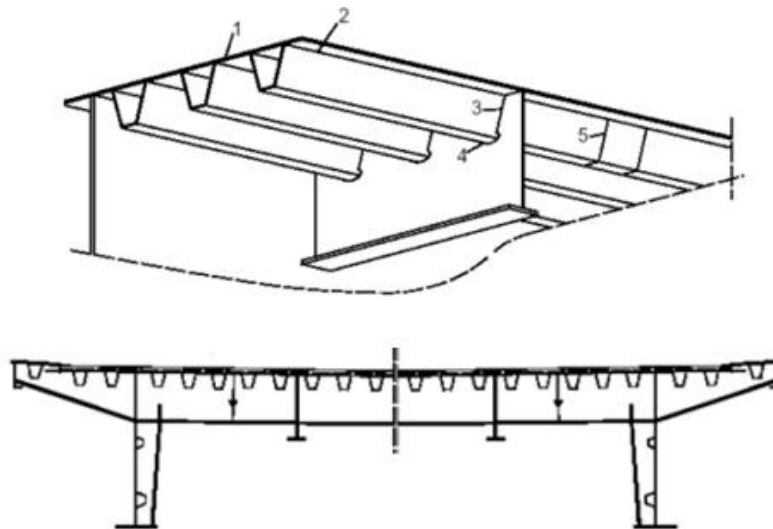


Figure 2.4 Overview OSD (EN1993-2, 2011)

### 2.3.1. Behavior of OSD under loading

When traffic passes the bridge, the deck will deform and due to the deformation of the supporting main girders, this will result in axial, shear and bending stresses in the primary system. As mentioned before, the OSD consists of different parts. This means that also the local behavior of the system needs to be verified. A distinction is made between the local behavior of the troughs and the local behavior of the crossbeams.

#### Local behavior deck plate and trough connection

The troughs are connected by the deck plate and a local load can be applied above or between the stiffeners, see Figure 2.5. As can be seen from the figure, the deck plate will deform both between the web of the troughs and between the troughs, and the deformation for both load cases will be different. The local deformation of the deck plate will result in bending stresses at the connection with the troughs. Another distinction can be made if the deck plate and trough connection is between crossbeams or at the crossbeam. When the connection of the deck plate and trough is between the crossbeams, the deformation will be the same as in Figure 2.5. If the connection of the trough and deck plate is at the location of the crossbeam, another situation will occur. Due to the much larger stiffness of this connection, which can be schematized as a fixed connection, it will only deform locally between the webs of the trough. Consequently, this will result in higher local bending stresses when compared with the connection between the crossbeams (Kolstein, 2007).

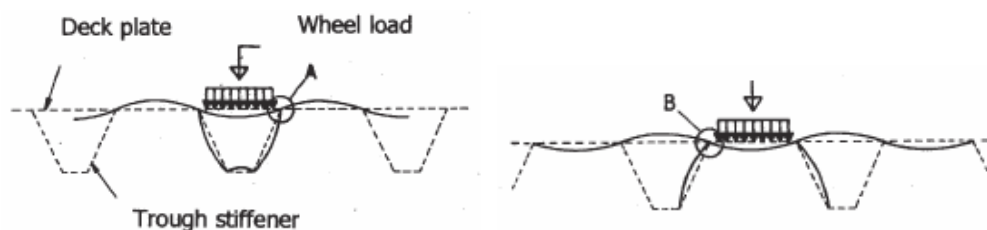


Figure 2.5 Local wheel load deck plate (Kolstein, 2007)

#### Local behavior crossbeam and trough connection

The trough to crossbeam connection can be seen as a complex connection since two highly stressed elements are connected with each other. Depending on where the load is applied the behavior of the orthotropic steel deck will be different. The crossbeams can be schematized as a beam which is supported at its ends by the main girders. When a load is applied at the location of the crossbeam, the

crossbeam will deform and this results in in-plane rotation, see Figure 2.6a. Another possibility is when the load is applied between the crossbeams. In this case the stiffener can be schematized as a continuous beam which is supported by the crossbeams. The connection between the troughs and crossbeams are welded, so the in-plane deformation of the troughs will result in out-of-plane rotation of the crossbeam, see Figure 2.6b (Aygül, 2012).

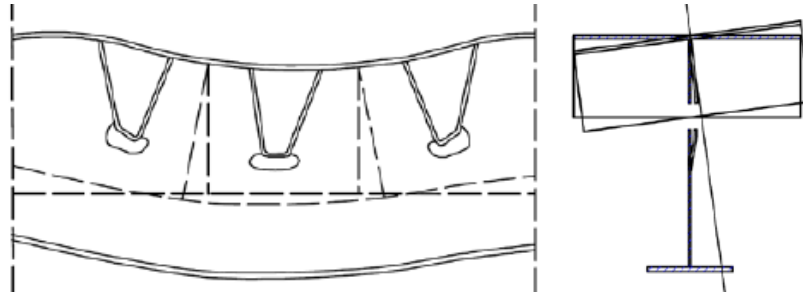


Figure 2.6 (a) In-plane rotation crossbeam and (b) out-of-plane rotation crossbeam (EN1993-2, 2011)

### 2.3.2. Fatigue cracks in trough to crossbeam connection

At the crossbeam to trough connection cracks can occur at different locations. A distinction needs to be made between discontinuous and continuous troughs. An overview of the detail with a discontinuous trough, and a continuous trough with a cope hole is shown in Figure 2.7.

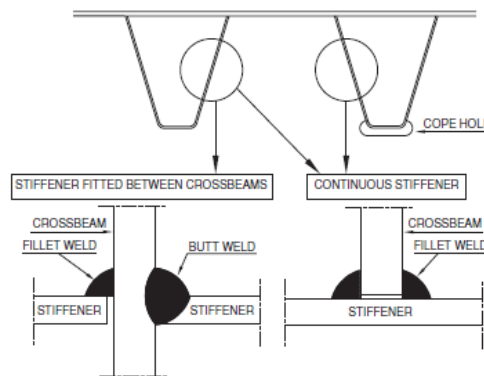


Figure 2.7 Geometries of crossbeam to trough connection (Kolstein, 2007)

In the discontinuous troughs, in which they are fillet welded between crossbeams, three different fatigue cracks are possible (Kolstein, 2007):

- From the root through the weld throat, see Figure 2.8 left;
- From the weld toe through the crossbeam, Figure 2.8 crack C2;
- From the weld toe through the trough, Figure 2.8 crack C1.

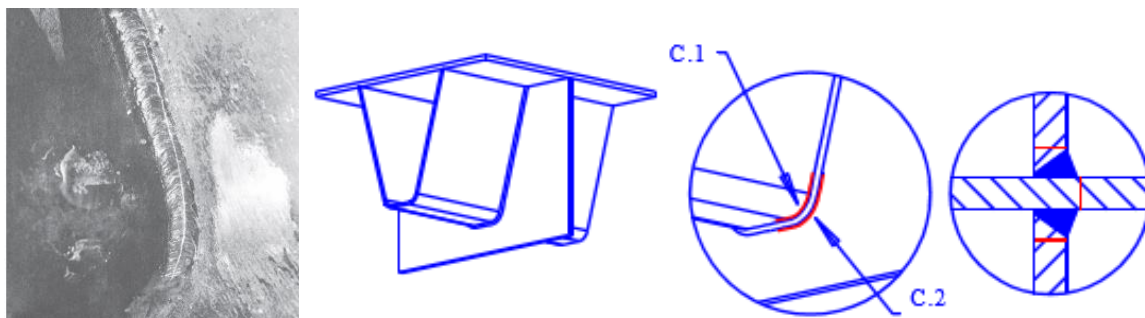


Figure 2.8 Overview cracks with trough fitted between crossbeams (Leendertz, 2008)

If continuous troughs are used a further distinction need to be made between crossbeams with and without cope holes. When no cope hole is applied, the trough will pass the crossbeam through cut-outs. The connection is fully welded all around the crossbeam and a crack starts most likely at the weld toe at the location of the trough soffit, see Figure 2.9a. This crack is due to the longitudinal stresses in the trough and may further propagate into the crossbeam. Those longitudinal stresses are caused by local wheel loading, which is located above a trough, next to the crossbeam, plus out-of-plane bending of the crossbeam (Kolstein, 2007). This causes longitudinal bending moments in the trough. When a crack has initiated in the trough, it may further grow into the crossbeam, because of out-of-plane bending and shear stresses, which are present in the crossbeam. Also for the cracks which start at the location of the weld end adjacent to a cope hole, which are shown in Figure 2.9b and Figure 2.9c, the maximum stress range occurs when a load is applied on the trough web next to the crossbeam. This statement is also supported by a research performed by (Yokozeki & Miki, 2016), in which they investigated the critical loading positions for the trough to crossbeam connection with cope hole.

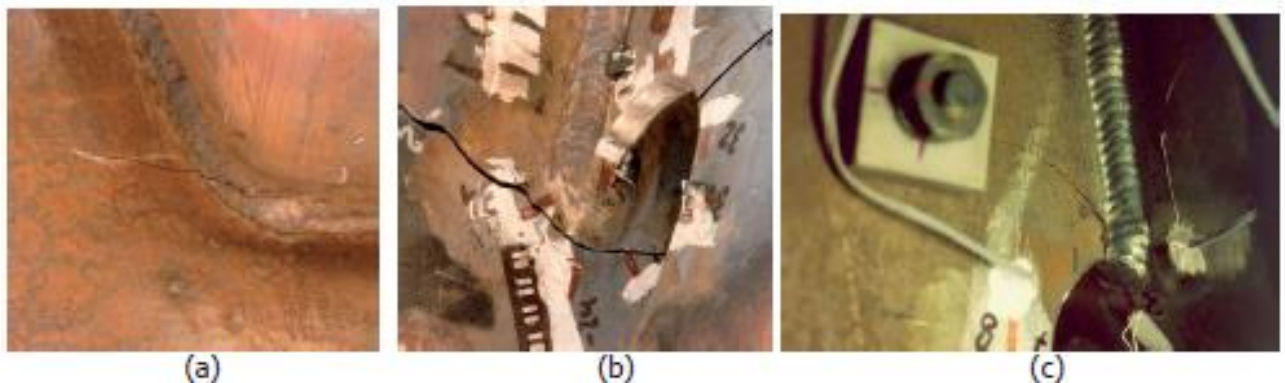


Figure 2.9 Failure modes continuous trough to crossbeam connection (Kolstein, 2007)

If a cope hole is applied three other different cracks are likely to occur in the connection (Kolstein, 2007):

- A crack starting from the weld toe located vertically in the trough;
- A crack starting from the weld end at the weld toe adjacent to a cope hole which propagates; longitudinally in the trough, Figure 2.9b;
- A crack starting from the same weld ends located in the crossbeam, Figure 2.9c.

It is also possible that a crack occurs at the edge of a cope hole and propagates into the crossbeam which is shown in Figure 2.9b. All the above mentioned crack locations are visible during inspection. The height and stiffness of the crossbeam will have a significant effect on the stress at the rib-to-crossbeam connection.

### 2.3.3. Effect of OSD elements on fatigue resistance

#### Deck plate

In the past OSD's were designed based on the static resistance and not designed based on the fatigue resistance. In new bridges the fatigue resistance is taken into account and the main difference, between the old and new OSD design bridges is the thickness of the deck plate. In the past the thickness of the deck plate was 10-12mm, depending if it was a movable or fixed bridge. New bridges have a deck plate thickness of 18-22mm. Several studies have shown that increasing the deck plate thickness will improve the fatigue life (Murakoshi, Hirano, & Harada Hideaki) (Nassif & Linzell, 2013).



In EN1993-2 (EN1993-2, 2011), minimum values for the deck plate thickness can be found which are depending on the traffic category. For traffic category 1 the deck plate thicknesses are between 18 and 22mm. In general, the plate thickness of the rib is 6-8mm and the thickness of the crossbeam is 10-16mm.

### Trough and crossbeam

In a research performed by (Nassif & Linzell, 2013) a parametric study was performed to determine the influence of the trough and crossbeam thickness on the fatigue life. Several different fatigue details were investigated: the connection of the rib-to-deck plate joint and rib-to-crossbeam joint with and without a cope hole. The thickness of the crossbeam, trough and deck plate was varied to investigate the influence on the stress range. The following conclusions can be drawn based on their research:

- 1) Out of the three investigated parts, increasing the thickness of the trough web had the least effect on the peak stresses at the critical locations;
- 2) Increasing the thickness of the crossbeam will have a positive effect on the fatigue resistance at the connection of the crossbeam, trough and deck plate, but limited effects were observed at the location of the weld toe connection of the trough and crossbeam with cope hole.

#### 2.3.4. Relevant detail categories OSD EN3

In the EN1993-1-9 (EN1993-1-9, 2011), several different detail categories are listed for different details in the OSD. Since the focus of this thesis is on the rib-to-crossbeam connection only the detail categories of these details will be stated.

For the rib-to-crossbeam connection several detail categories are possible depending on the configuration of the structural elements. EN1993-1-9 (EN1993-1-9, 2011) proposes a detail category of 80 for the continuous longitudinal stringer with an additional cut-out in cross girder, when the thickness of the crossbeam is less or equal than 12mm. When the thickness of the crossbeam is larger than 12mm, EN1993-1-9 (EN1993-1-9, 2011) gives a detail category of 71. When the critical section in the web of the crossbeam with cut-outs is considered, the detail category is equal to 71. These detail categories can be used when assessment is based on the direct stress range ( $\Delta\sigma$ ). An overview of the detail categories from EN1993-1-9 (EN1993-1-9, 2011) can be seen in Figure 2.10.

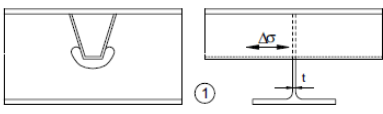
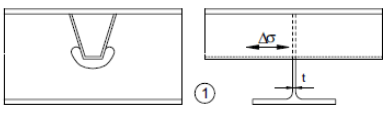
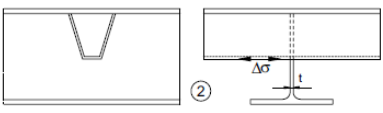
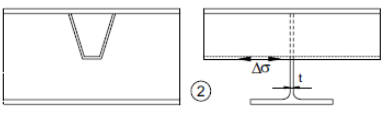
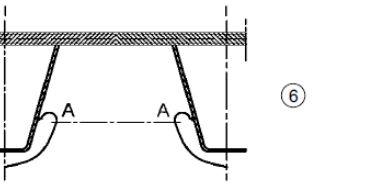
Detail category	Constructional detail		Description	Requirements
80	$t \leq 12\text{mm}$		1) Continuous longitudinal stringer, with additional cutout in cross girder.	1) Assessment based on the direct stress range $\Delta\sigma$ in the longitudinal stringer.
71	$t > 12\text{mm}$			
80	$t \leq 12\text{mm}$		2) Continuous longitudinal stringer, no additional cutout in cross girder.	2) Assessment based on the direct stress range $\Delta\sigma$ in the stringer.
71	$t > 12\text{mm}$			
71			6) Critical section in web of cross girder due to cut outs.	6) Assessment based on stress range in critical section taking account of Vierendeel effects.  NOTE In case the stress range is determined according to EN 1993-2, 9.4.2.2(3), detail category 112 may be used.

Figure 2.10 Detail category for stringer to crossbeam connection (EN1993-1-9, 2011)



The national annex of EN 1993-2 (EN1993-2-NB, 2011) proposes different detail categories when the fatigue assessment is based on the hot spot stress approach based on a 3D FE model calculation. Detail category 100 may be used when a crossbeam with cope hole is used. For the connection of the trough and crossbeam, the detail categories from Figure 2.11 should be used.

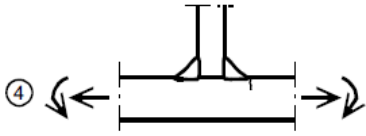
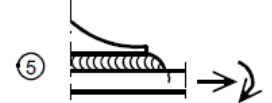
100		4) Non load-carrying fillet welds.	4) - Weld toe angle $\leq 60^\circ$ . - See also NOTE 2.
100		5) Bracket ends, ends of longitudinal stiffeners.	5) - Weld toe angle $\leq 60^\circ$ . - See also NOTE 2.

Figure 2.11 Detail categories hot spot stress approach (EN1993-1-9, 2011)

Detail category 125 may be used when no cope hole is present. There is no distinction made between the thickness of the crossbeam. In a research performed by (Kolstein, 2007) the same characteristic detail categories are proposed for the direct stress range approach. Kolstein also investigated the detail categories for different crack locations in the structural member. An overview of these results can be seen in Figure 2.12.

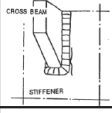
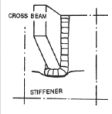
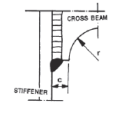
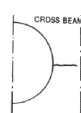
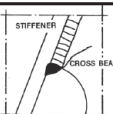
80		$t \leq 12\text{mm}$	<b>3) Continuous trough to crossbeam joint with cope holes – trough failures</b>	3a) Assessment based on the direct stress range $\Delta\sigma$ in the trough web at the crossbeam.
71		$t > 12\text{mm}$	3a) Failure of the trough web along the vertical weld	$t$ is thickness of crossbeam
125			3b) Failure of the trough web at the lower end of the weld	3b and 3c) Assessment based on the geometric stress range extrapolated to the weld toe in the web of the trough. 3b) The joint is loaded in one direction only.
56			3c) See 3b)	3c) The joint is loaded in two directions.
125	All types of cope holes		<b>4) Continuous trough to crossbeam joint with cope holes – crossbeam failures</b>	4a and 4b) Assessment based on the geometric stress range at the free edge of the cope hole.
80			4a) Cracks starting at the free edge of the cope hole	4) The joint is loaded in one direction only.
71			4b) See 4a)	4b) The joint is loaded in two directions.
71			4b) Cracks starting at the weld toe in the cope hole	4b) Assessment based on the geometric stress range inside the cope hole at the weld toe

Figure 2.12 Detail category for stringer to crossbeam connection (Kolstein, 2007)

### 2.3.5. Performed experiments on trapezoidal stiffeners and crossbeam connection

In the past years a lot of research has been performed on the trough to crossbeam connection. The different types of loading of these experiments can be divided in three different cases: three-point bending test, in-plane bending and out-of-plane bending.

#### Three point bending tests

Most of the time, the three-point bending tests were performed on a single trough and crossbeam. These tests were performed in the 70's and 80's of the last century. An overview of a test set-up and dimensions which was performed by (Nunn, 1974) is shown in Figure 2.13. The total length of the trough is equal to 1.37m and the throat thickness is 6mm.

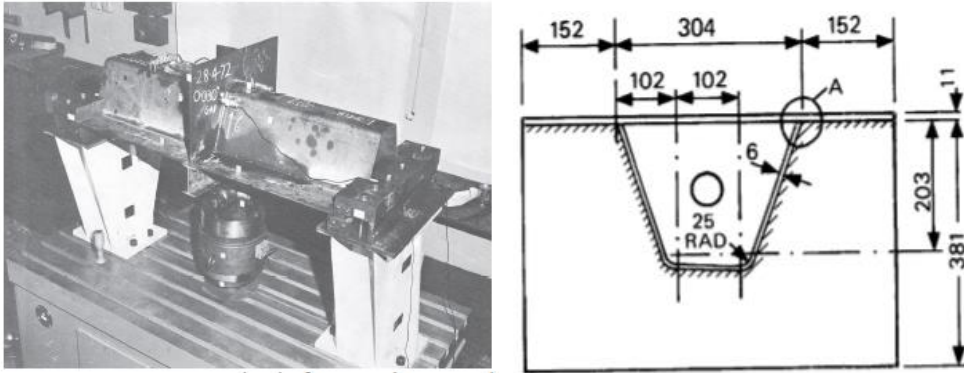


Figure 2.13 Overview three-point bending test (left), dimensions trough (right) (Nunn, 1974)

In this full scale experiment the trough is fitted between the crossbeam, which corresponds with detail category 36 in (EN1993-2-NB, 2011). The crossbeam is supported at both ends and the load is applied directly above the crossbeam by an actuator, and distributed over the full width of the trough by an I-section. Half of the tested specimens had a gap, 0.5mm, between the crossbeam and trough, while for the other half there was no gap. During this experiment a sinusoidal load with a frequency of 45 Hertz was applied with a load range of -45kN to 45kN for the batches with no gap and a load range of -35kN to 35kN for the batches with a gap. The focus of this research was on the edge of the trough soffit and all cracks occurred at the weld root which propagated through the weld almost parallel to the crossbeam. The out-of-plane bending of the crossbeam is not taken into account in the test program. (Hänsch & Müller, 1961) performed an experiment on a backing strip in which both full penetration butt welds and fillet welds with a throat thickness of 5mm were tested. The results of both research programs are shown in Figure 2.14 in which it can be seen that the butt welded connection has a higher fatigue resistance than the fillet weld. The obtained stress range of the experiment performed by (Nunn, 1974) is the stress range at 14mm measured with strain gauges, which were placed on the soffit of the trough, 14mm from the crossbeam.

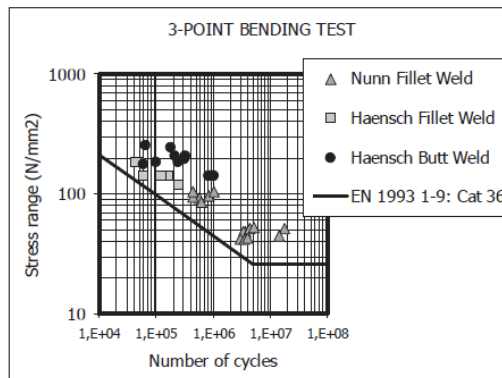


Figure 2.14 Results research programs trough fitted between crossbeam (Kolstein, 2007)

### In-plane bending

The fatigue resistance of a crossbeam which is loaded by in-plane loading is investigated by (Lehrke, 1990). An overview of a test set-up and geometry is shown in Figure 2.15. The test set-up consists of six continuous troughs with a total length of 2300mm and the span of the crossbeam is equal to 3900mm. The crossbeam is supported at both ends and is loaded by a concentrated force of 200kN, which causes shear forces and bending moments. Both the “normal” cope hole, with a radius of 40mm, and “Haibach” cope hole were tested during these experiments. (Lehrke, 1990) concluded that, for both tested cope hole configurations, the highest stresses are found at the free edge. This is caused by bending of the crossbeam between the cutouts which causes tension and compression

stresses which can be seen in Figure 2.16. As can be seen from the figure, the maximum tensile and compressive stresses at the edge of the cope hole, are almost the same for both cope holes, but also some differences occur. The maximum stress at the location of the connection where the cope hole is fillet welded to the trough is lower for the “Haibach” cope hole. Furthermore, the area of the highly stressed surface is larger for “normal” used cope hole when compared with the “Haibach” cope hole.

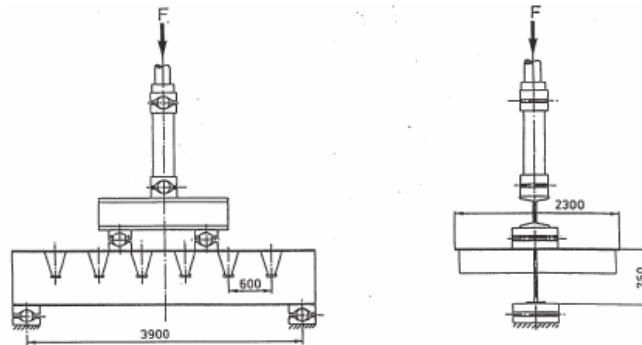


Figure 2.15 Test set-up in-plane bending crossbeam (Lehrke, 1990)

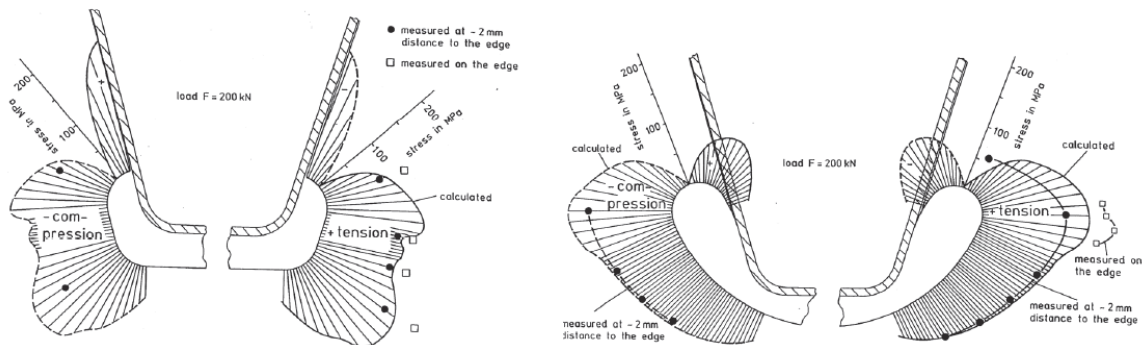


Figure 2.16 Distribution of stresses along cope hole edges, normal cope hole (left), and Haibach cope hole (right) (Lehrke, 1990)

During the experiment cracks occurred at two different locations. The first location is at the edge of cope hole, which was the case for both the “normal” and “Haibach” cope hole. The second location is at the end of the weld where the cope hole is welded to the trough. This latter crack only occurred for the “Haibach” cope hole. In Figure 2.16 it can be seen that the stresses which occur at this location are lower for the “Haibach” cope hole when compared with the “normal” cope hole. An explanation for this crack is that at the end of the weld the residual stresses are locally higher, due of the heat-flux caused by welding. Another observation which indicated residual stresses is the fact that the cracks which occurred at the free edge, which was in compression, remained open after removing of the load. Based on the performed experiment it was concluded that the fatigue resistance of the “Haibach” cope hole when looking at the free edge is 3 to 5 times higher than the “normal” cope hole.

In a research performed by (Zhang, Cui, Bu, Liu, & Ye, 2015) a full scale bridge deck was tested and modelled in which different loads were applied at the crossbeam on the trough web. Different loading cases were investigated: loaded above the trough web and loaded between the troughs. The location of interest was the rib-to-crossbeam connection with cope hole. During the experiment cracks occurred at the rib-to-crossbeam connection at the bottom of the weld toe. Three different fatigue assessment methods were investigated: nominal stress-, effective notch- and hot spot stress method. When the results for nominal stress method were compared with the recommended detail category 71, the results were not consistent with the recommended detail category. The results of the effective

notch- and hot spot stress method were in agreement with the detail categories from E1993-1 (EN1993-1-9, 2011) or IIW recommendations (Hobbacher, 2009). The hot spot stress range is calculated based on the linear extrapolation method recommended by IWW (Niemi, Fricke, & Maddox, 2018) and the results of the research are shown in Figure 2.17.

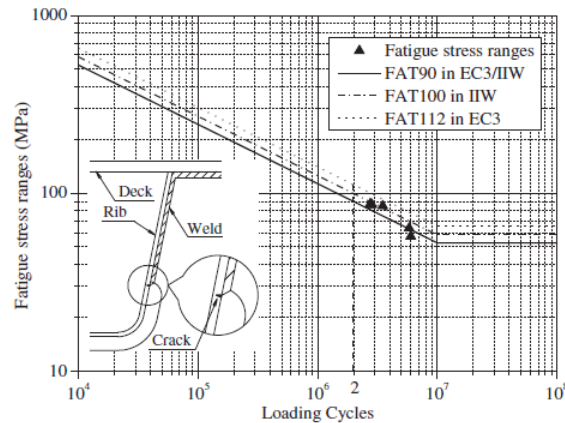


Figure 2.17 Test results based on hot spot stress method (Zhang, Cui, Bu, Liu, & Ye, 2015)

### Out-of-plane bending

In a research performed by (Beales, 1990) a full scale orthotropic steel deck specimen which has a total length of 1500mm was tested. The test consists of a single trough and a fully supported crossbeam. The force is applied, at the end of the trough, with a hydraulic actuator with a frequency of 3 to 6 Hertz. A typical test set-up is shown in Figure 2.18.

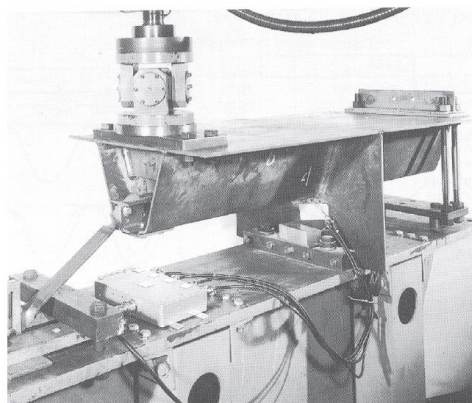


Figure 2.18 Test set-up in-plane bending crossbeam (Beales, 1990)

In different experiments performed by (Kolstein & Leendertz, 1989) and (Kolstein, 1997), which has a similar loading and type of specimen as shown in Figure 2.18, the continuous trough and crossbeam connection was investigated with out-of-plane loading. Trapezoidal troughs were used during the experiment. A distinction can be made between a crossbeam with and without a cope hole in which the “normal” cope hole, with a radius of 40mm and “Haibach” cope hole were used, which is shown in Figure 2.19. The total height of the trough is 325mm, the bottom width is 105mm and the thickness is equal to 6mm.

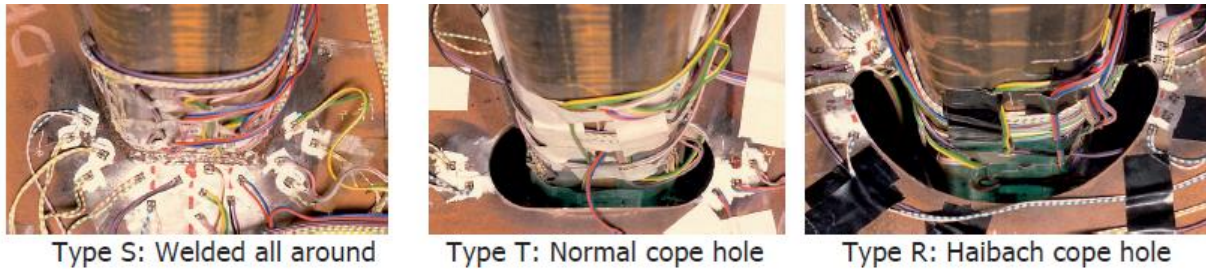


Figure 2.19 Tested joints between crossbeam and continuous troughs (Kolstein H. , 2007)

Depending on the type of configuration: continuous trough, with or without cope hole, the following cracks occurred during the experiment (Kolstein & Leendertz, 1989), (Kolstein, 1997):

- At the end of the weld in the trough web;
- At the end of the weld in the crossbeam;
- At the edge of the trough soffit, at the weld toe;
- At the free edge of the cope hole.

In section 2.3.2, Figure 2.9, a graphical representation of those cracks are shown. For the trapezoidal stiffener which is welded all around, cracks occurred at the edge of the trough soffit, at the weld toe, see Figure 2.19 type S, the results are shown in Figure 2.20a. In this subfigure the longitudinal stresses are shown, which are based on the strain gauges which were placed 15mm away from the weld toe. For the troughs including a crossbeam with cope hole, see Figure 2.19 type T and R, the cracks occurred at two different locations: at the end of the weld in the trough web and at the free edge of the cope hole. The stress range which is shown in Figure 2.20b is obtained by placing strain gauges in perpendicular direction to the crack growth. It can be concluded that the fatigue strength of the “normal” cope hole is slightly lower when compared with the “Haibach” cope hole, based on the measured longitudinal stress in the trough web, which can be seen in Figure 2.20b. The results of the experiment in which the cracks occurred at the free edge of the cope hole are shown in Figure 2.20c. The obtained stress range is measured at the free edge of the cope hole, and a large scatter in results can be seen, in which the fatigue strength of both cope hole shapes is more or less similar.

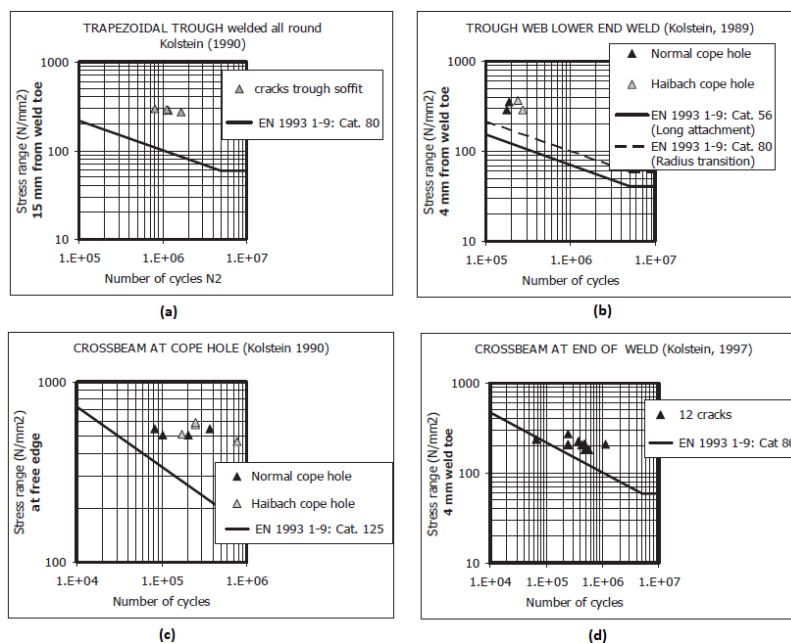


Figure 2.20 Overview results performed experiment by (Kolstein & Leendertz, 1989)



### Palmgren-Miner rule

The Palmgren-Miner rule is a cumulative damage model in which the total damage (D) of load cases with different amplitudes can be calculated. This damage is defined with the following formula:

$$D = \sum \frac{n_i}{N_r} = \frac{n_1}{N_1} + \frac{n_2}{N_2} + \frac{n_3}{N_3} + \dots \leq 1.0$$

In which  $n_i$  is the number of cycles with the specified stress range ( $S_i$ ) and  $N_r$  is the amount of load cycles to failure, for the detail category, at the specified stress range ( $S_i$ ) (Zhao, Wilkinson, & Hancock, 2005). If the calculated fatigue damage for the detail is larger than one, it is expected that failure will occur.

## 2.4. Fatigue strength assessment methods

There are different fatigue strength assessment methods to determine the stress range which can be used for the estimation of the fatigue life: (modified) nominal stress method, effective notch method and hot spot stress method (Hobbacher, 2014). The hot spot stress method and (modified) nominal stress method are described in EN1993-1-9 (EN1993-1-9, 2011). Generally, when a simple detail calculation needs to be performed, the nominal stress method is used. For details with a more complex geometry, it is recommended to use the hot spot stress method. Another fatigue strength assessment method which it not included in EN1993-1-9 (EN1993-1-9, 2011), but is included in the International Institute of Welding recommendations (Hobbacher, 2014) is the effective notch method. An overview of the nominal stress, notch stress and hot spot stress is shown in Figure 2.21.

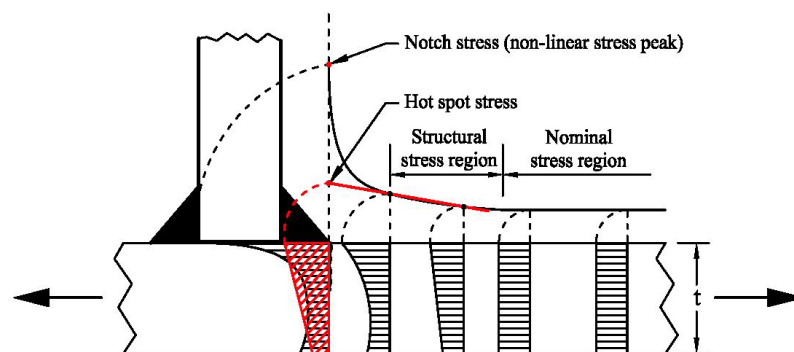


Figure 2.21 Different stresses for fatigue assessment methods (Aygül, 2012)

### 2.4.1. (modified) Nominal stress method

With the nominal stress method, only the nominal stresses are used for the determination of the fatigue life. This method does not take the weld imperfections and geometry of the weld into account, those stress concentrating effects should be considered in the corresponding detail category. In the cases that a stress concentration needs to be considered, a modification factor,  $k_f$ , can be applied. This method is also called modified nominal stress method. The stress concentration factor takes into account the stress concentrating effects like geometric discontinuities, misalignments or eccentricities. By multiplying the nominal stress with the stress concentration factor,  $k_f$ , the modified nominal stress is determined.

### 2.4.2. Hot spot stress method

The hot spot stress method is applied to study the stress states at the hot spot positions where cracks may initiate. The hot spot stress method is based on the stress range at the hot spot location in the vicinity of the weld. An overview of the stresses is shown in Figure 2.22. A distinction can be made between three types of stresses: the membrane stress ( $\sigma_m$ ), the bending stresses ( $\sigma_b$ ) and the

nonlinear peak stress ( $\sigma_{nlp}$ ). A nonlinear stress concentration due to the notch effect of the weld is present at the weld toe (Niemi, Fricke, & Maddox, 2018). The membrane stresses are constant throughout the thickness and can be seen as the average stress in the member without taking geometrical discontinuities and the weld geometry into account. The bending stresses are linear through the thickness. The non-linear stress peak, which results from the weld geometry, is depending on the weld form, the weld toe geometry and the size of the weld (Akhlaghi, 2009). With the hot spot stress method this latter part, the nonlinear peak stress, is not taken into account.

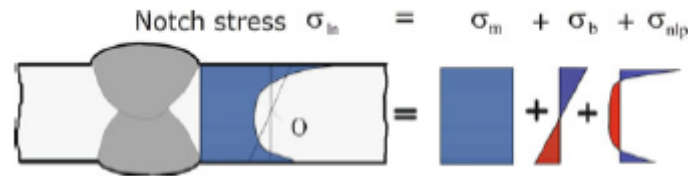


Figure 2.22 Hot spot stress: summation of membrane stress and bending stress (Niemi, Fricke, & Maddox, 2018)

The hot spot stress method is a method in which stresses at the weld toe are extrapolated. This method is only appropriate when cracks initiate from the weld toe. If the crack initiates from the weld root and propagates in the weld throat, the hot spot stress method is not applicable. With the hot spot stress method geometric discontinuities are taken into account. The local weld geometry is not considered with this method, but the weld geometry is considered in the S-N curve. The hot spot stresses can be obtained based on codes and recommendations, like EN1993 (EN1993-1-9, 2011) and IIW (Niemi, Fricke, & Maddox, 2018), or when FE modelling is performed by extrapolating the stress from specific reference points.

When the finite element analysis is used for the calculation of the stresses, those stresses will be influenced by the notch effect, the welds local geometry. This notch effect, which occurs at the weld toe, will result in very high stresses due to a singularity that will occur at that location. In reality this singularity is not present at the weld toe. To disregard this very high peak stress, extrapolation at specific points at a distance from the notch is used to calculate the hot spot stress. The notch effect will “disappear” at approximately 0.3-0.4 times the plate thickness. An overview of the notch stress and hot spot stress can be seen in Figure 2.23. The nominal stress is the stress which is not affected by the weld- and global geometry.

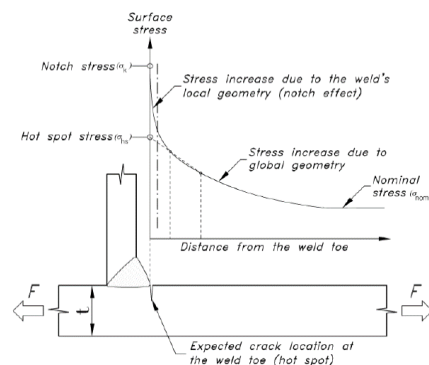


Figure 2.23 Overview hot spot stress and notch stress (Niemi, Fricke, & Maddox, 2018)



### Types of hot spot

A distinction can be made between two different types of hot spots: type a and type b. Those two types are shown in Figure 2.24. With a type a hot spot the weld toe is located on the plate surface, while with a type b hot spot the weld toe is located on the plate edge. For a type a hot spot the reference points, and thus the stress distribution which approaches the weld toe, are depending on the thickness of the plate. For type b hot spot reference points are not depending on the thickness of the plate (Niemi, Fricke, & Maddox, 2018). This is because for a type b hot spot the thickness of the plate is not a relevant parameter for the reference point and thus reference points with a fixed value are proposed.

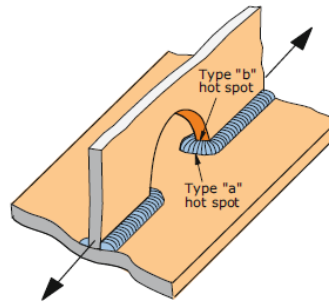


Figure 2.24 Type a and type b hot spot (Hobbacher, 2014)

### Hot spot stress extrapolation methods

There are different types of methods to determine the hot spot stress range. One method is by extrapolation of the stress on the plate surface while the second method is by extrapolation of the stress through the thickness of the plate.

### HSS extrapolation based on experimental results

In an experimental set-up the hot spot stress can be determined using strain gauges which are placed at specific locations. When the structural stress is calculated based on the strain gauges, the linear extrapolation is sufficient to obtain the stress. With linear extrapolation the strain should be extrapolated at  $0.4t$  and  $1.0t$  the thickness of the plate and the hot spot strain can be calculated with the following formula:

$$\varepsilon_{hs} = 1.67\varepsilon_{0.4t} - 0.67\varepsilon_{1.0t}$$

During experimental set-ups often multi-strip strain gauges are placed in which their locations does not exactly match with the extrapolation point which are mentioned above. In such cases sufficient strain gauges should be placed to calculate the strain at the specific locations based of interpolation. The structural stress can be calculated from the structural strain with the following formula in uniaxial stress state, in which  $E$  is the Young's modulus:

$$\sigma_{hs} = \varepsilon_{hs} * E$$

### HSS extrapolation based on finite element modelling

As mentioned previously, to calculate the hot spot stress extrapolation points are needed. The IIW (Niemi, Fricke, & Maddox, 2018) gives recommendations about those extrapolation points depending of the mesh size, coarse or fine, and the type of hot spot, a or b. In Figure 2.25 those recommendations are shown. To obtain the hot spot stress when a coarse mesh is applied, linear extrapolation is used. When a fine mesh is applied, both the quadratic or linear extrapolation can be used depending on the hot spot type, a or b.

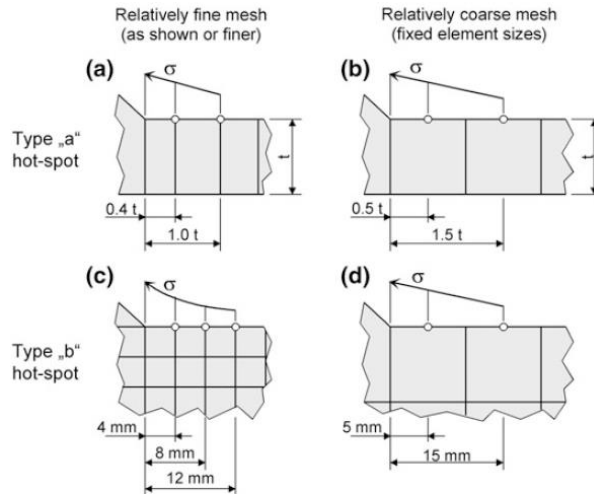


Figure 2.25 Structural stress evaluation guideline for surface stress extrapolation (Niemi, Fricke, & Maddox, 2018)

A further distinction can be made based on the element types used: solid or shell elements. The IIW recommendation (Niemi, Fricke, & Maddox, 2018) also gives a guideline for the different type of elements. Based on the mesh size and element type the table shown below gives reference points for the location of the extrapolation points.

Table 2-1 Guideline on stress evaluation and meshing (Niemi, Fricke, & Maddox, 2018)

Types of model and weld toe:		Relatively coarse models		Relatively fine models	
		Type a	Type b	Type a	Type b
Element Length × Width	Shells:	$\leq t \times t$ and $t \times w/2^a$	10 mm × 10 mm	$\leq 0.4t \times t$ and $0.4t \times w/2^a$	$\leq 4 \text{ mm} \times 4 \text{ mm}$
	Solids:	$\leq t \times t$ and $t \times w^a$	10 mm × 10 mm	$\leq 0.4t \times t$ and $0.4t \times w/2^a$	$\leq 4 \text{ mm} \times 4 \text{ mm}$
Extrapol. Points	Shells:	0.5t/1.5t (mid-side pts.) <sup>b</sup>	5 mm/15 mm (mid-side points)	0.4t/1.0t (nodal points)	4 mm/8 mm/12 mm (nodal points)
	Solids:	0.5t/1.5t (surface centre)	5 mm/15 mm (surface centre)	0.4t/1.0t (nodal points)	4 mm/8 mm/12 mm (nodal points)

<sup>a</sup>w = attachment width (attachment thickness +2 weld leg lengths), see also 4.4

<sup>b</sup>surface centre at transverse welds, if the weld below the plate is not modelled, see Fig. 4.4c, d

The IIW recommendations (Niemi, Fricke, & Maddox, 2018) recommends using elements with a higher order when a coarse mesh is applied, since the read out values are at mid points of the elements. In the case of a relatively fine meshed model, 0.4t and 1.0t are used as the extrapolation points. With relatively fine meshed models it is also possible to obtain the stresses through quadratic extrapolation. Quadratic extrapolation is advised for thick-walled structures, when the applied force has a sharp change in direction, or when, due to structural discontinuity, a large nonlinear stress increase, at the location of the hot spot is expected (Niemi, Fricke, & Maddox, 2018).

As mentioned before, when a relatively fine mesh is used the extrapolation points are at 0.4t and 1.0t. The hot spot stress value can then be calculated, based on the values of the extrapolation points, with the following formula:

$$\sigma_{hs} = 1.67\sigma_{0.4t} - 0.67\sigma_{1.0t}$$

From Table 2-1 it can be concluded that the hot spot stress method using surface stress extrapolation is depending on the: element type (solid or shell), element size (relatively coarse or fine) and the type of hot spot (type a or b). In a study performed by (Al-Emrani & Aygül, 2014) the same conclusion is stated.

#### 2.4.2.1. Other structural stress determination approaches

##### One-point hot spot stress method

Another extrapolation technique is proposed by (Fricke, 2002) and is called the one-point hot spot stress method. With this method the hot spot stress at a specific location,  $0.5t$ , is directly read out from this point. The results from the experiments, performed by Fricke, look promising and the scatter in test results was smaller when compared with the other extrapolation methods. However, to match the experimental results, the hot spot stress based on the reference point of the one-point-determination need to be multiplied with a factor 1.12. The stress at the reference point,  $0.5t$ , can be directly read out from the FE model when quadratic elements, with an element size of  $t \times t$ , are used.

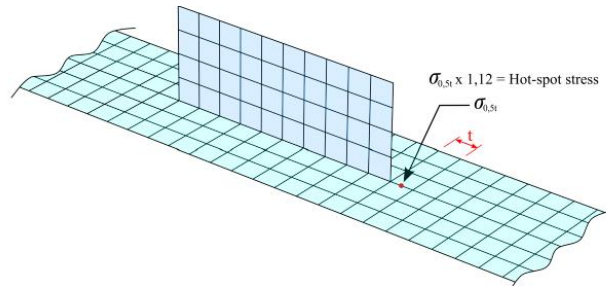


Figure 2.26 Determination one-point hot spot stress (Al-Emrani & Aygül, 2014)

##### Sub surface (one-millimeter) stress method (Xiao and Yamada)

The one-millimeter stress method is proposed by (Xiao & Yamada, 2004), and is a method in which the determination of the structural stress is done 1 mm below the surface of the weld toe. The advantage of this method is that it is relatively easy and gives a better representation of the thickness and size effect. The results from this research are in agreement with the linear surface extrapolation method. For this method, since the reference point is 1mm below the surface, the thickness of the elements is of importance. As a result, this approach is only applicable to solid elements and cannot be used for shell elements. A graphical representation of this method is shown in Figure 2.27. A limitation of this method is that it is not suitable for a combination of normal and bending stresses, it is only applicable if solely normal stresses are present. The bending stresses will result in a linear stress distribution over the thickness while normal stresses have a constant distribution. Due to this limitation this method cannot be used.

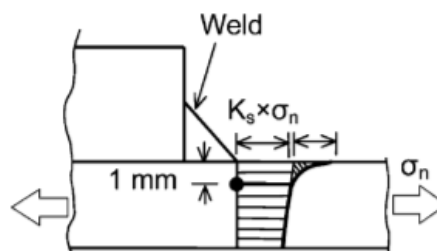


Figure 2.27 1mm stress method (Xiao & Yamada, 2004)

##### Structural stress method proposed by Dong

Another structural stress method is proposed by (Dong, 2001). To obtain the through thickness linear stress distribution a special procedure needs to be used. Different procedures exist for solid and shell element modelling. For solid elements this method requires two different planes which need to be defined: one at the location of the weld toe, and another at some distance ( $\delta$ ) from plane A-A: plane B-B. This plane B-B is chosen because of the stress singularity which might occur at the location of the weld toe. A graphical representation of this principle can be seen in Figure 2.28. As aforementioned, the structural stress is a combination of bending stress and membrane stress. Based on equilibrium

conditions in the stress resultants between both planes, the linear part of the structural stress can be derived. The bending ( $\sigma_b$ ) and membrane ( $\sigma_m$ ) component must satisfy the equations shown below in which the first equation is for plane A-A while the latter one is for plane B-B.

$$\sigma_m * \frac{t^2}{2} + \sigma_b * \frac{t^2}{6} = \int_0^t \sigma_x(y) * y * dy + \delta * \int_0^t \tau_{xy}(y) * dy$$

$$\sigma_m = \frac{1}{t} \int_0^t \sigma_x(y) * dy$$

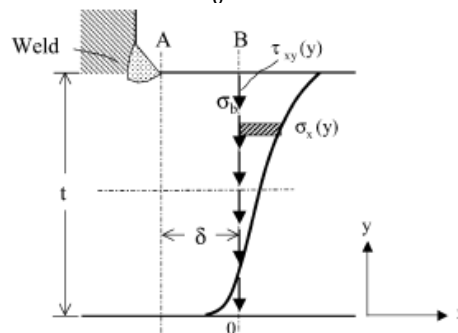


Figure 2.28 Through thickness procedure plane A-A and B-B

The hot spot stress can be directly evaluated at the location of the hot spot, which is along the weld toe, when shell elements are used. This is because the elements already assume the stress distribution to be linear. It is further preferred to use the element nodal forces for the calculation of the line moments and line forces. The membrane and bending stresses can be calculated from these line forces and moments. This procedure will result in a higher accuracy when compared with the procedure based on element stresses.

#### 2.4.3. Effective notch method

In the effective notch method both the geometry of the joint and the geometry of the weld are taken into account. At the location of the weld toe and root in the FE model stress singularities may occur. To omit those stress singularities a notch is applied at those locations. As stated before, in EN3 the effective notch method is not included, but recommendations can be found in the IIW recommendations (Hobbacher, 2014). This method can be used for cracks which occur both at the weld toe and at the weld root. At the location of the weld toe or weld root, a fictitious rounding, a notch with a radius of 1mm, is applied, see Figure 2.29. For the fatigue strength assessment only one S-N curve is needed.

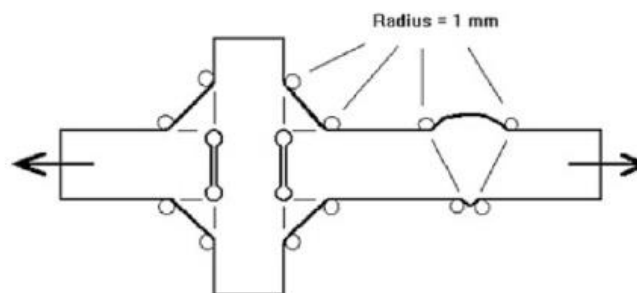


Figure 2.29 Effective notch radius (Hobbacher, 2014)

#### 2.4.4. Comparison of fatigue strength assessment methods

Several researchers performed experiments in combination with finite element modelling to investigate the accuracy of the fatigue strength assessment methods. In a study performed by (Beld, 2019) the connection of the rib-to-deck joint at the location of the crossbeam was investigated in which the specific detail was modelled with both solid and shell elements. Specific attention was given to the crack which initiate and propagates at the weld root. The experimental results of two rib-to-deck joints were compared with the results from FE modelling. In this research the nominal stress method, effective notch method and the hot spot stress method were compared. The nominal stress method gave the lowest fatigue life of all three fatigue life assessment methods. A reason for this is that the nominal stress method is most simple assessment method and the least factors, like the weld geometry and weld discontinuity, are taken into account with this method. The effective notch method resulted in only 10% of the fatigue life when compared with the fatigue life obtained with the hot spot stress method. When the results from the finite element model are compared with the corresponding detail category, 125, all models show a slight conservative result when compared with the experimental results. The results of the hot spot stress method are shown in Figure 2.30 in which the results are plotted with the recommended S-N diagram. The hot stress fatigue assessment method gave the highest fatigue life when all three assessment methods are compared, and furthermore still gave conservative results when compared with the experimental results.

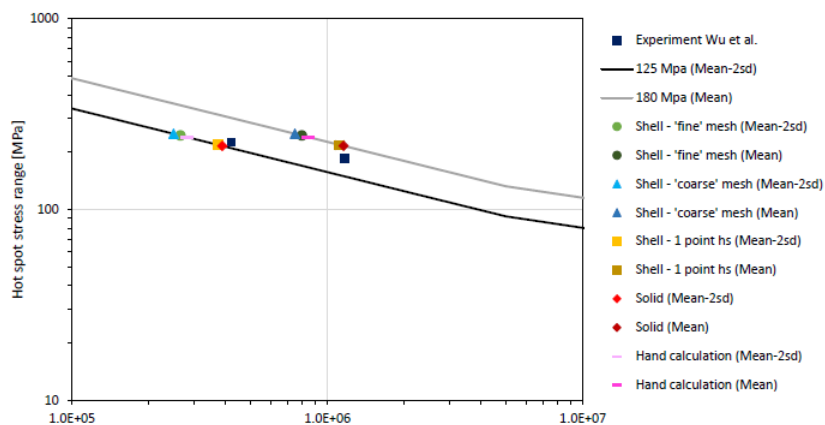


Figure 2.30 Comparison hot spot stress method and cycles to failure (Beld, 2019)

In another research, performed by (Aygül, Al-Emrani, & Urushadze, 2012), also the nominal stress method, effective notch method and hot spot stress method were compared. This research focused on the open stiffener and crossbeam with cut-outs connection. A constant loading with a magnitude of 200kN to 400kN was applied during the experiments and the boundary conditions chosen in such a way to simulate a simply supported beam. The nominal stress method only gives good results when the normal stress and shear stress distribution are considered correctly, otherwise it would result in non-conservative results when compared with the relevant detail category in EN3.

The hot spot stress which was obtained from finite elements models showed good agreement with the results from the static test. For obtaining the hot spot stress quadratic surface stress extrapolation was used. FE models consisting of only solid elements were used for the effective notch method, while for the hot spot stress method, both a shell and solid FE model was made. The fatigue life estimation based on the effective notch method showed conservative results when compared with the representative detail category 225. A detail category of 300 was proposed in this research for the effective notch method. The calculated fatigue life based on the effective notch method was 50%

lower when compared with the hot spot stress method. An overview of the fatigue assessment methods with the recommended design S-N curves is shown in Figure 2.31.

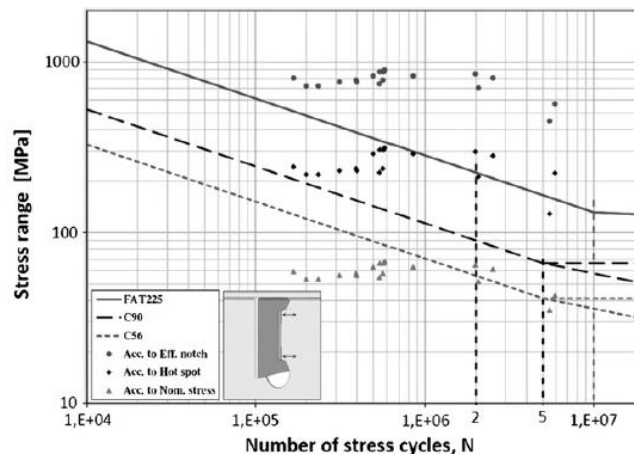


Figure 2.31 S-N curves for different fatigue assessment methods (Aygül, Al-Emrani, & Urushadze, 2012)




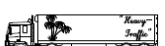

## 2.5. Fatigue load models (FLM)

According to EN1991-2 (EN1991-2, 2011) there are five different types of fatigue load models which can be used for bridges. EN1991-2 (EN1991-2, 2011) gives recommendations when to use which fatigue load model. For the determination of the unlimited fatigue life with constant amplitude loading fatigue load model 1 and 2 need to be applied. These two load models are not relevant and thus are disregarded in this report. When a safe life of the bridge needs to be designed fatigue load models 3, 4 and 5 need to be applied. Fatigue load model 3 is based on a single vehicle model with a maximum and minimum stress with a constant stress range. Fatigue load model 4 is based 5 different types of standard lorries. This means that different types of lorries are used in this model which will result in a stress range spectrum. The last fatigue load model is FLM 5 in which data from real life measurements are used for the loading. This fatigue load model is not taken into account. A guideline made by Rijkswaterstaat (RWS) (Ministerie van Infrastructuur en Milieu, 2017) prescribes to make use of FLM4 at all time. Furthermore EN1991-2 (EN1991-2, 2011) states that FLM 4 gives more accurate results when compared with FLM3 based on the assumption that it can be neglected that more than one vehicle is present on the bridge. Based on the above mentioned points fatigue load model 4 is used for this thesis.

### Fatigue load model 4 (FLM 4)

In fatigue load model 4, a distinction is made between 5 different types of trucks. Those 5 different types have to be considered separately. In Table 2-2 an overview of the different types of commonly used trucks are shown.

**Table 2-2 Overview different types of trucks for fatigue load model 4a (EN1991-2, 2011) and (Beld, 2019)**

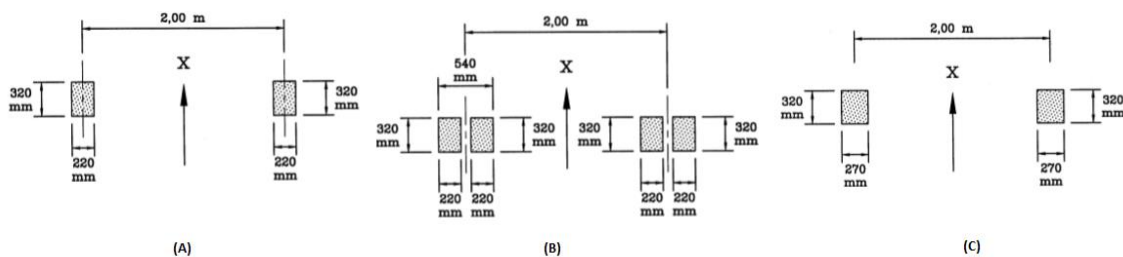
Type	Type		Traffic type			Wheel type
	Axle spacing m	Axle load kN	Long distance % <sup>a</sup>	Medium distance % <sup>a</sup>	Local traffic % <sup>a</sup>	
	4,5	70 130	20,0	50,0	80,0	A B
	4,20 1,30	70 120 120	5,0	5,0	5,0	A B B
	3,20 5,20 1,30 1,30	70 150 90 90	40,0	20,0	5,0	A B C C
	3,40 6,00 1,80	70 140 90 90	25,0	15,0	5,0	A B C C
	4,80 3,60 4,40 1,30	70 130 90 80 80	10,0	10,0	5,0	A B C C C

<sup>a</sup> percentage of lorries

As can be seen from the table, for each truck type several different specifications are mentioned: the wheel type, traffic type, axle load and the distance between the axles. These specifications can be used for the different types of loading in the finite element models.

**Axle types**

A distinction can be made between the different axle types: A, B and C. An overview of these axle types is shown in Figure 2.32 in which axle type A corresponds with subfigure (a), axle type B with subfigure (b) and axle type C with subfigure (c). Axle type A is the single wheel with shape 220mm\*320mm. The type B is the double wheel with shape 220mm\*320mm, and the type C is single wheel with shape 270mm\*320mm.



**Figure 2.32 Definitions of different axle types (EN1991-2, 2011)**

**Traffic categories**

In the design of bridges, the volume of the traffic can be classified into different categories based on the function and the position of the bridge. In (EN1991-2, 2011), there are 4 different categories: low flow rates (local and main roads), medium flow rates and high flow rates. An overview of these traffic categories is obtained from (EN 1991-2 NB, 2011) and is shown in the Table 2-3. In which N is the indicative number of heavy vehicles expected per year per slow lane which should be used to calculate the total fatigue damage.

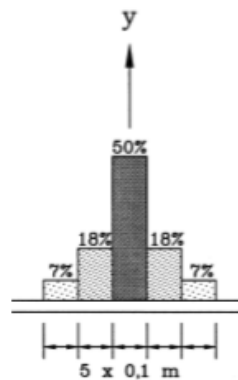


**Table 2-3 Traffic categories (EN1991-2, 2011)**

Traffic categories		$N_{\text{obs}}$ per year and per slow lane
1	Roads and motorways with 2 or more lanes per direction with high flow rates of lorries	$2,0 \times 10^6$
2	Roads and motorways with medium flow rates of lorries	$0,5 \times 10^6$
3	Main roads with low flow rates of lorries	$0,125 \times 10^6$
4	Local roads with low flow rates of lorries	$0,05 \times 10^6$

### Statistical distribution of transverse wheels

The position of the transverse wheels is an important aspect in the fatigue life when an orthotropic steel deck bridge is taken into account (EN1991-2, 2011). A statistical distribution of the transverse wheel position must be taken into account with respect to the center line of the vehicle. This statistical distribution of the wheel is shown in Figure 2.33. There are in total  $5 \times 0.1\text{m}$  parts in the model. Half of the traffic volume is in the centerline of the vehicle, 18% locates within 0.1m from the center parts, and 7% is at the outer side.



**Figure 2.33 Statistical distribution of transverse location of center line of vehicle (EN1991-2, 2011)**

## 2.6. Finite element analysis

### 2.6.1. Introduction

Finite element analyses are performed to obtain an approximation of a physical phenomenon. These so-called physical phenomena are solved by the finite element program using partial differential equations. Solving these differential equations is needed in order to compute desired quantities like strains, stresses or displacements. For this thesis the finite element software “Abaqus 2019” is used to perform the finite element analysis. The orthotropic steel deck is modelled with a 3D model with different element types to perform the analysis. The different element types which are used in these models are solid and shell elements. As mentioned in section 2.4.2, it is extremely important to take into account the different types of elements and element sizes to obtain reasonable results for the hot spot stress using surface extrapolation. In this section shell and solid elements will be investigated and differences will be stated.

### 2.6.2. Shell elements

Shell elements are 2D elements and give an accurate approximation of the results if the thickness is substantially smaller than the width and length of the element. When modelling a structure with shell elements, the mid-planes of this structure are modelled. The thickness of the element is given as a property. Usually, when shell elements are used, the welds are not modelled, but in some cases, it can

be important to do so. For instance between two discontinuities, where high local bending occurs, the welds can be modelled with different modelling techniques: rigid links, increased thickness or oblique shell elements (Hobbacher, 2014).

### Rigid links

With rigid links the rigidity of the weld is modelled by linking the two adjacent shell elements to each other with rigid links. This method is proposed by (Fayard, Bignonnet, & Dang, 1996). Those rigid links are defined by nodes which are along the full length of the weld. It is important to choose the length of two adjacent shell elements, E1 and E2, as accurately as possible, since this represents the rigidity of the weld. The hot spot stress can be directly read from the center of gravity, and thus no need for any extrapolation technique is required.

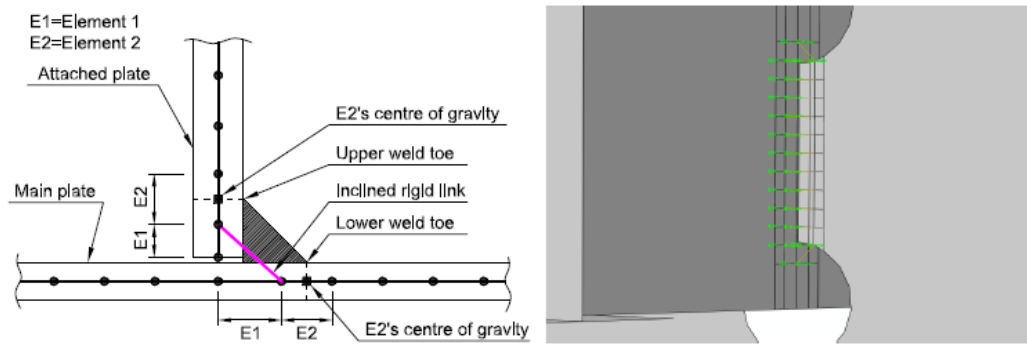


Figure 2.34 Shell modelling weld making use of rigid links (Aygül, 2012)

### Increased thickness

Another method to model the weld with shell elements is by using the increased thickness. (Niemi E., 1995) proposed this method to locally increase the thickness at the location of the weld. The principle of the increased thickness weld modelling is shown in Figure 2.35. The thickness is locally increased by the plate thickness plus the throat thickness of the weld. The length of the locally increased thickness is equal to half the plate thickness, due to midplane modelling, plus the weld leg length. When a cruciform joint is considered, (Eriksson, Lignell, Olsson, & Spennare, 2003) suggested to use two rows of shell elements in which the local thickness is increased, for both plates.

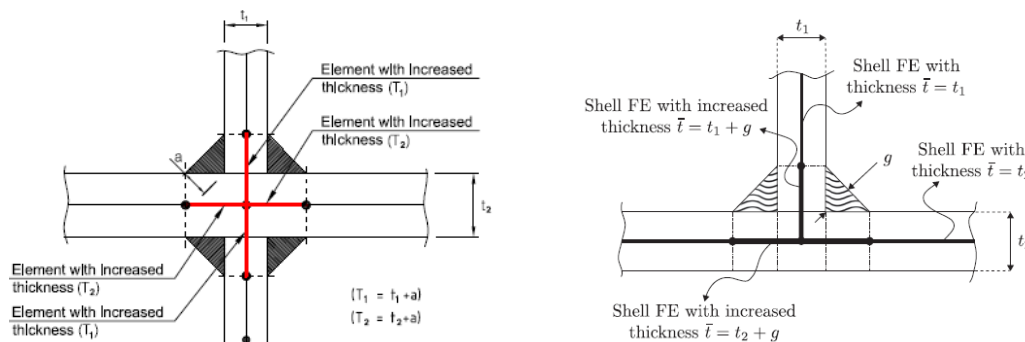


Figure 2.35 Shell modelling weld making use of increased thickness (Aygül, 2012), left, and (Echer & Marczak, 2017), right

### IIW approach (local increased thickness and weld tip included)

Another weld modelling technique can be found in the IIW recommendations regarding the hot spot stress approach (Niemi, Fricke, & Maddox, 2018). A graphical representation of this method is shown in Figure 2.36. With this method the weld ends are modelled and furthermore the thickness is locally increased, which is a similar procedure as with the increased thickness method proposed by (Eriksson, Lignell, Olsson, & Spennare, 2003). An element with increased thickness, which is equal to the

thickness of the plate plus the weld leg length, is applied at the location of the weld. The height of the increased thickness region is equal to half the plate thickness plus the weld leg length.

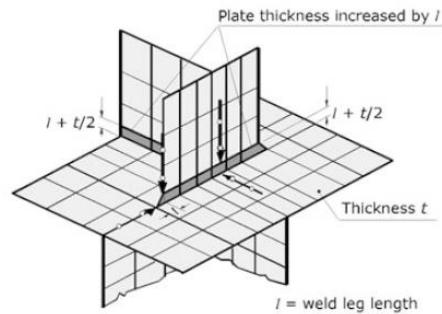


Figure 2.36 Weld modelling technique reinforced plate strips with inclined ends (Hobbacher A. , 2009)

### Oblique shell elements

The weld modelling making use of oblique shell elements is proposed by (Niemi E. , 1995). With this method both the stiffness and the geometry of the weld can be modelled in an accurate way. The main plate should be connected with the attached plate at the common node which is shown in Figure 2.37. The thickness of the oblique shell elements is equal to the throat thickness of the weld.

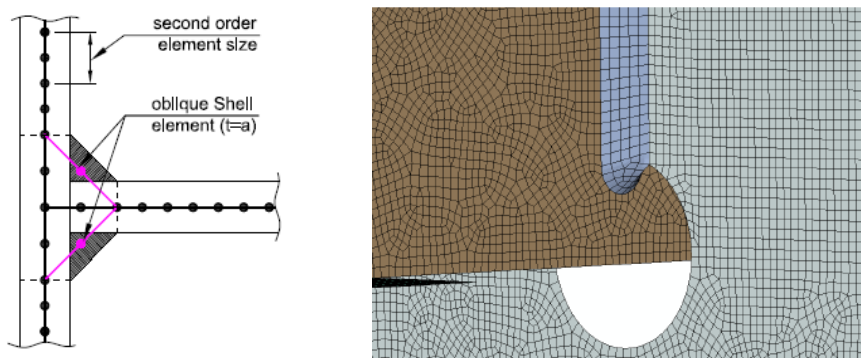


Figure 2.37 Shell modelling weld making use of oblique shell elements (Niemi E. , 1995) and (Aygül, 2012)

Without the modelling of the weld, the plate stiffness is underestimated between two adjacent discontinuities. With shell elements, a distinction can be made between different geometrical shapes: triangular or rectangular. The elements which have a triangular shape are beneficial when the geometry is curved or irregular. At the nodes of an element the degrees of freedom are defined. Linear triangular elements and linear rectangular elements have 3 and 4 nodes, respectively. Elements with a rectangular shape have more nodes and thus more degrees of freedom when compared with elements with a triangular shape. In general this will result in results which have a more accurate approximation.

Besides to the linear elements, higher order elements can also be used. The quadratic elements have additional nodes: 6 for the triangular and 8 for the rectangular elements. When using the quadratic elements the computational time will increase, but also higher accuracy is achieved. Prior to the finite element modelling it should be determined if the higher order elements are required for the analysis. A graphical representation of a shell element model is shown in Figure 2.38. When shell elements are used for analyzing the hot spot stresses, the hot spot is at the location where the different plates intersect, i.e. the structural intersection point. Shell elements have 5 degrees of freedom per node which are three translational and two rotational.

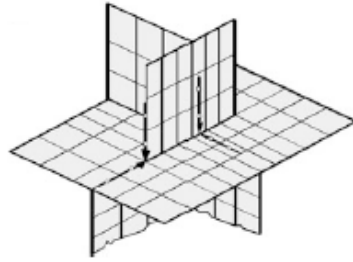


Figure 2.38 Shell element model without the weld modelled (Hobbacher A. , 2009)

#### Limitations shell element modelling hot spot stress

There are two different situations in which the hot spot stress cannot be captured well with shell elements. One situation is a cruciform joint or welded transverse stiffener connection, where a transverse stiffener is welded to the main plate, is loaded in tension. In this case no stress flow in the transverse stiffener will occur in the shell element in which the transverse stiffener is only represented by a line. As a consequence, the obtained hot spot stress range is equal to the nominal stress range. Another situation occurs in the case of simple butt-welded joints, also loaded in tension. In this case no stress concentration will occur and the obtained hot spot stress range is equal to the nominal stress range. When the S-N curve for the hot spot stress range is used in those situations, non-conservative results are obtained. In those cases it is recommended to use the nominal stress method (DNV GL, 2016).

#### 2.6.3. Solid elements

Solid elements are elements which give a 3D representation of the structure. Solid elements give the most accurate approximation of the results since they are closest to the real life situation. With solid elements a distinction can be made between two different geometrical elements: 4-noded tetrahedral, or 8-noded hexahedral elements. These elements are similar as the shell elements, but in the case of solid elements they are a three dimensional representations. Also higher order elements are possible with solid elements. A graphical representation of a solid element model is shown in Figure 2.39. With a solid FE model the geometry of the weld can be modelled and this will result in more precise results when compared with a FE model which consists of shell elements. The degrees of freedom (DOF) per node in the solid elements is equal to three translational DOF's. Solid elements take the variation throughout the thickness of the element into account.

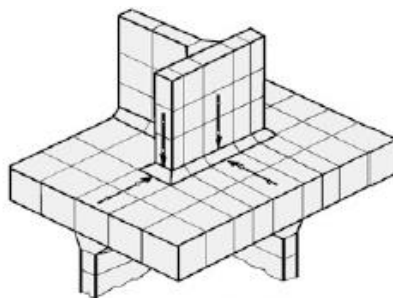


Figure 2.39 Solid element model with weld modelled (Hobbacher A. , 2009)

#### 2.6.4. Differences between shell and solid elements

When the solid and shell elements are compared, different results can be expected. The mid-surface of the structure is modelled with shell elements, and the thickness of the element is given as a property. An approximation is that the results will not be influenced by the thickness. This approximation may, in some cases, give inadequate results. Solid element takes the variation throughout the thickness into account and will this give more precise results.

Solid elements require more modelling and computational time when compared with shell elements, but the results are closer to reality. Depending on the required accuracy of the results one could choose which element type is most suitable for the analysis. Another difference is that the weld can be fully modelled with solid elements, while with shell elements only an approximation based on the stiffness can be done.

When the bending behavior of the shell and solid elements are compared another difference can be found. In a research performed by (Osawa, et al., 2011) the accuracy of the hot spot stress based on a shell model and solid model is compared for a specific connection. When a connection is made between a flange plate and web plate with only shell elements the different parts are only supported by a line. If the same connection is made with solid elements, the flange plate is supported over the plate thickness. This principle is represented in Figure 2.40. The transverse bending of the flange plate is close to zero over the thickness of the web plate in the case of solid elements. This is not the case for shell elements since the web plate is modelled as a line and thus will have a different influence on the longitudinal stresses. Consequently, the curvature of the shell element model is larger than the solid element model.

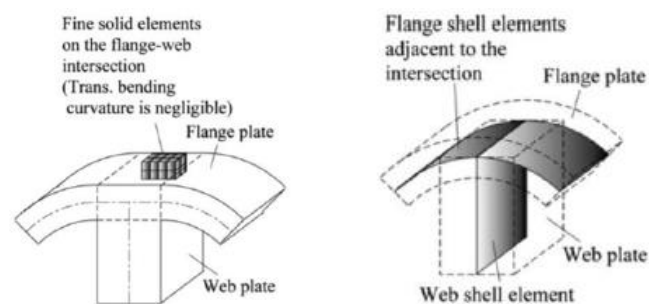


Figure 2.40 Comparison curvature solid (left) and shell element (right) (Osawa, et al., 2011)

### 2.7. Performed research on different modelling techniques (shell and solid)

In several researches both solid and shell elements were used for the finite element modelling. In this subchapter the most important conclusions and remarks are summarized to get an idea which differences to expect between FE modelling with both elements.

In a research performed by (Aygül, Al-Emrani, & Urushadze, 2012) the differences in modelling techniques for a connection which consists of an open stiffener to crossbeam connection with a cope hole were investigated. An overview of the investigated detail is shown in Figure 2.41.

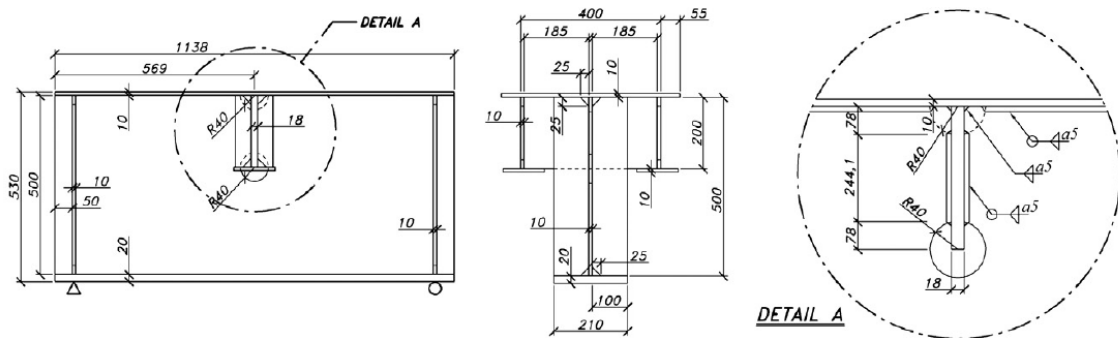


Figure 2.41 Overview investigated test specimen (Aygül, Al-Emrani, & Urushadze, 2012)

The research focused on the modelling of the detail with solid and shell elements. Several different techniques of modelling the shell model were investigated: no weld modelled, weld end modelled with same thickness as the crossbeam, see Figure 2.42(a), weld modelled by using oblique elements, see Figure 2.42(b), weld modelled by increasing the thickness in the region of the weld, see Figure 2.42(c) and weld modelling with oblique rigid links, see Figure 2.42(d).

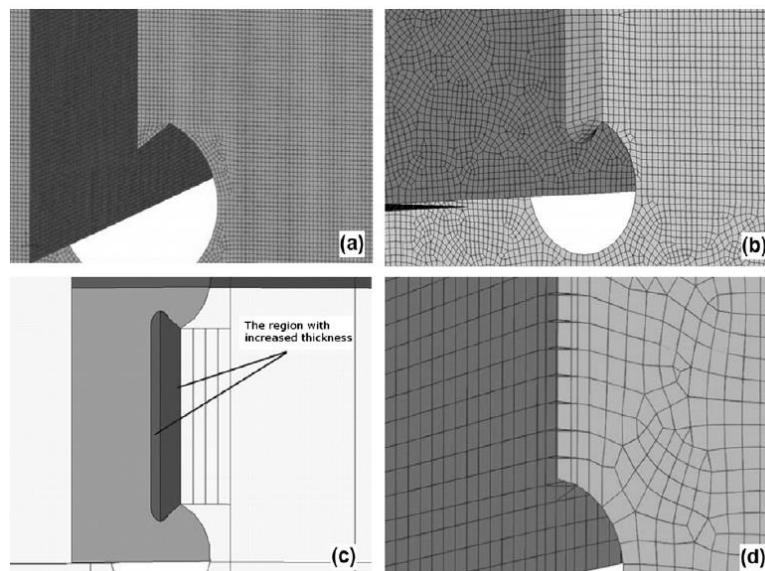


Figure 2.42 Different modelling techniques weld modelling shell elements (Aygül, Al-Emrani, & Urushadze, 2012)

Two different hot spot locations were investigated: HS1, which is at the bottom cope hole, and HS2, which is at the top cope hole. The hot spot stress method is used for the fatigue life assessment. Furthermore, the differences in the linear and quadratic surface stress extrapolation, in which the recommendations from IIW were followed were investigated. Also, a non-extrapolation method where the stress at 0.5t was extracted was used. The results of this research for both hot spot locations are shown in Figure 2.43, in which the ratio of the adapted shell model and the solid model is calculated and a large scatter in results is observed. When making use of quadratic extrapolation the scatter in results is reduced. It can be concluded that the ratio between the solid and shell hot spot stresses is depending on how the detail is modelled. When a regular shell FE model, in which the weld is not modelled, is used, the scatter in results is the largest and overconservative. For the shell model without weld modelling the structural intersection point, which is the shared node of the crossbeam and stiffener at the location of interest, is taken as the extraction point. When modelling techniques for the welds are used for the shell FE model, the ratio between the differences is smaller. Care should be taken, because for some modelling techniques the shell model will underestimate the stresses which result in non-conservative results.

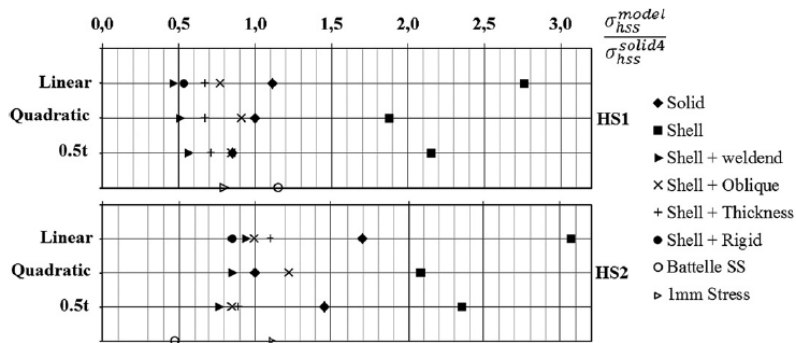


Figure 2.43 Results FEM models for hot spot locations (Aygül, Al-Emrani, & Urushadze, 2012)

In a recent research performed by (Beld, 2019), the focus was on the connection of the rib-to-deck joint at the location of the crossbeam of an OSD. Special attention was given to the weld root failure. This specific detail was modelled with both shell and solid elements. Quadratic elements were used for the shell model, while for the solid FE model both types of elements: linear and quadratic, were used. The weld was modelled in the solid FE model, while for the shell FE models the weld was disregarded. First a mesh sensitivity study was performed to investigate for which element size the results are not depending on the element size anymore. It was concluded that an element size of 4mm for the shell model, and an element size of 2mm for the solid model, gave a stable element size, in with quadratic elements were used. In Figure 2.44 the strain range versus distance from weld root is shown, and some differences in results are observed. The difference in results for quadratic and linear solid element models is approximately 10% and the trendline of the graph is a bit different. When the results from the quadratic solid element model, are compared with the results from the quadratic shell element model, with an element size of 4mm, the shell model is overestimating the strains at the location close to the weld root. After 20mm the results for both the shell and solid elements are still approximately 10% different. Furthermore, the shell model with an element size of 4mm matches the experimental results within 10%, except at the first location which is at 4mm from the weld root.

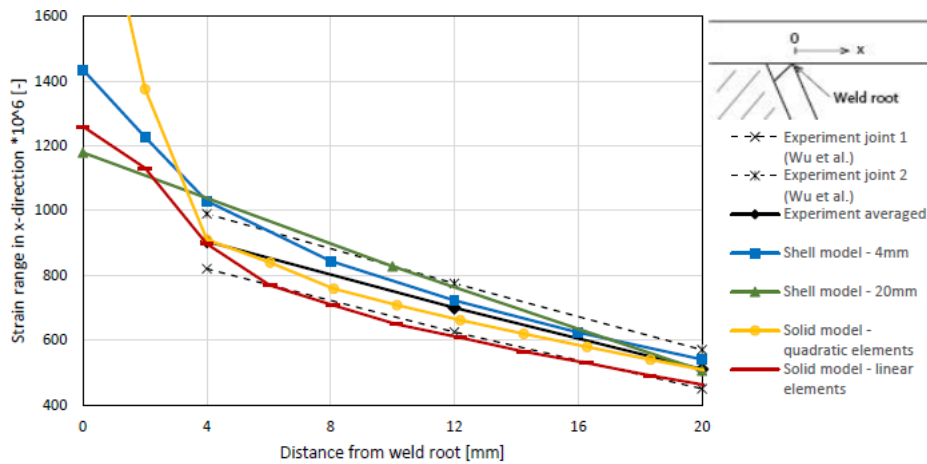


Figure 2.44 Comparison of results shell and solid models (Beld, 2019)

In a research performed by (Liu, Huang, Gao, & Li, 2011), the comparison between the differences of shell and solid elements is made for four different specimens. In Figure 2.45 an overview of these specimens is given. Specimen 1 consists of a plate of which a gusset is welded with fillet welds, for specimen 2 a hopper corner is used, specimen 3 consists of a welded connection between transverse and longitudinal frames and specimen 4 is welded T-joint.



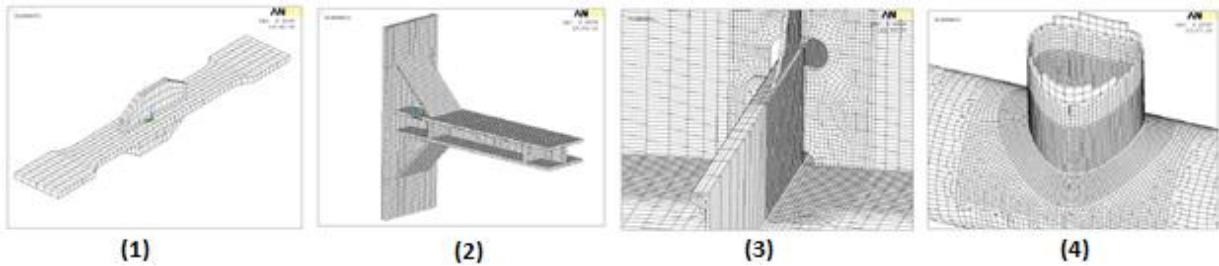


Figure 2.45 Overview investigated specimens (Liu, Huang, Gao, & Li, 2011)

Both quadratic solid and shell elements were used for the comparison and an overview of the results can be seen in Table 2-4. Linear surface extrapolation is used for obtaining the hot spot stresses at the weld toe. For the shell models the structural intersection point is used as reference point. Specimen 1 is loaded with a uniform tension load of 0.67MPa, which results in a nominal stress equal to 1.0MPa. Specimen 2 is loaded with a vertical force of 244N, which results in a nominal stress range at the weld toe which is equal to 1.0MPa. Specimen 3 is loaded with a uniform tension load which is equal to 368.84kN. For specimen 4 two different load cases were examined: load case one in which an axial force of 10kN is applied in the brace, and load case two in which a shear force of 50kN is applied to the brace, to simulate in-plane bending of the brace.

As can be seen the difference in hot spot stress results of the shell and the solid models for both specimen 1 and 2 are quite small. This is because the stresses of specimen 1 and 2 are mainly membrane- and bending stresses which can be described accurately with shell elements. For specimen 3 the difference in results is 35% which is caused by the eccentric connection and the torsional stiffness which are not well captured by the shell elements. This is because the shell element does not have any stiffness in the rotational degree of freedom, which is normal to the element, also called the drilling rotation, in the local axis system. When elements which are non-planar, not on the same line, join at a node, a very small stiffness, in the drilling rotation, may occur due to the transformation from local to global axis system when the element size is sufficiently small. This small torsional rotational stiffness may cause problems in the evaluation of the stiffness matrix and thus may give erroneous results. This problem can be solved by applying a torsional spring with a small fictitious stiffness in the normal rotation direction (Krishnamoorthy, 1994). For both load cases of specimen 4 a large difference in hot spot stresses for the solid and shell model is obtained, i.e. 31 and 26%. Even though the T-joint connection seems rather simple, at the intersection of the joint a complex stress distribution occurs which cannot be accurately described with the shell elements.

Table 2-4 Comparison of results shell and solid models for hot spot stress approach (Liu, Huang, Gao, & Li, 2011)

FE models		Hot spot stress (MPa)	$\frac{\text{Shell-Solid}}{\text{Solid}} \times 100\%$
Specimen 1	Shell	1.223	-6.35%
	Solid	1.306	
Specimen 2	Shell	2.245	3.12%
	Solid	2.177	
Specimen 3	Shell	11.648	-35.41%
	Solid	18.034	
Specimen 4	Shell	15.580	31.05%
	Solid	11.889	
Specimen 4	Shell	30.840	26.25%
	Solid	24.428	

### 3. VALIDATION OF FEM MODELS

In this chapter, Finite Element models are created using solid and shell elements to study the effect of these to different modelling techniques on the hot spot stress calculation by the surface extrapolation approach. First a single sided fillet welded longitudinal attachment joint is investigated to analyze the hot spot stress under tension and bending moment. Afterwards, FE models based on the OSD test specimen which is currently being tested in Stevinlab II laboratory of Delft University of Technology is built and validated with measured results. A comparison between shell element and solid elements is also given.

#### 3.1. Validation: single sided fillet welded longitudinal attachment connection

To see the differences in results for the FE models based on solid and shell elements a simple and straightforward connection is investigated. This simple connection consists of a main plate and gusset plate which are welded all around by fillet welds. In this study both tension and bending load will be applied. Since this study is based on the differences between the solid and shell elements, and the influence of the different parameters, tension and bending is applied to obtain the ratio between the different elements. The validation of the model is based on tension loading and when the results are in good compliance with the experimental results, the model will be adapted to a bending load.

##### 3.1.1. Description of the model

In a research performed by (Śledziwski, 2018) the fatigue life assessment of a longitudinal non-load carrying attachment is carried out and the results for different specimens are given. An overview of the tested specimen is shown in Figure 3.1. The tested specimens are subjected to uniform tension.

##### 3.1.1.1. Dimensions and geometry

The connection consists of two plates, one main and one attachment, which are connected by fillet welding. An overview of the geometry and dimensions can be seen in Figure 3.1. The steel plates both have a thickness of 16mm, and the longitudinal attachment has a height of 50mm and a length of 60mm. The total length of the main steel plate is 300mm and the throat thickness of the welds is 5mm.

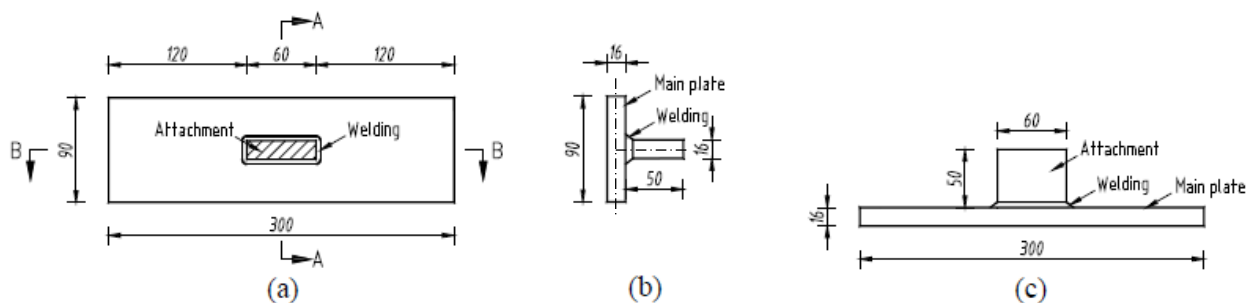


Figure 3.1 Overview dimensions tested specimen (Śledziwski, 2018)

##### 3.1.1.2. Boundary conditions

Since the tested specimen is symmetrical over plane A-A, which can be seen in Figure 3.1(a), only half of the specimen is modelled. An overview of the boundary conditions for both the tension and bending loading is shown in Figure 3.3. At the symmetry plane the translation in X-direction is constrained. To prevent kinematic movement the translational degrees of freedom in Y- and Z-direction are constrained at one location in the finite element model. For the shell model, also the rotational degrees of freedom are constraint in the symmetry plane. The boundary conditions are shown in Figure 3.3.

### 3.1.1.3. Material properties and loading

Steel with a Young's modulus of 210.000 MPa and a poisson ratio of 0.3 is used. During the experiment loads with a magnitude of 144 to 260kN were applied on the specimen. Since it is a linear elastic calculation, the validation is done based on one load case which is equal to 144kN.

### 3.1.1.4. Elements used and mesh size

#### Shell

For the shell elements use is made of 4-noded, S4(R), and 8-noded elements, S8R, which uses linear and quadratic interpolation. Different element sizes will be investigated: 0.5mm, 1mm, 2mm, 4mm, and 8mm. Both plates are modelled making use of mid-surface modelling, see dashed lines in Figure 3.1b. This means that the height of the stiffener plate is equal to  $50\text{mm} + 0.5 \cdot t_p = 58\text{mm}$ . The mesh sensitivity analysis is performed based on the difference in hot spot stress range between the different element sizes. If the difference, of the hot spot stress range, between one mesh refinement is smaller than 1%, it is concluded that convergence occurred.

#### Solid

The solid elements which are used for the FE model consists of 8-noded and 20-noded elements in which interpolation is done linearly and quadratically: C3D8(R), and C3D20(R). For both the linear and quadratic elements, also the element type in which full integration is used, C3D8 and C3D20, is investigated, to see the differences between the two elements. As with the shell model, also for the solid model a mesh sensitivity study is performed. The investigated elements sizes are: 1mm, 2mm, 4mm and 8mm. Furthermore, a seam is applied to model the gap between the gusset plate and the main plate.

In Table 3-1 an overview of the integration points for each element type is shown. With the reduced integration elements less integration points are used to solve the integral when compared with the full integration elements. More integration points will result in a higher accuracy of the results, but it will also increase the computational time. In Figure 3.2 an overview of a linear shell element is shown in which a distinction is made between full (S4) and reduced (S4R) integration.

Table 3-1 Overview integration points investigated elements

Element type	Integration points
C3D8	2 x 2 x 2
C3D8R	1 x 1 x 1
C3D20	3 x 3 x 3
C3D20R	2 x 2 x 2
S4	2 x 2
S4R	1 x 1
S8R	2 x 2

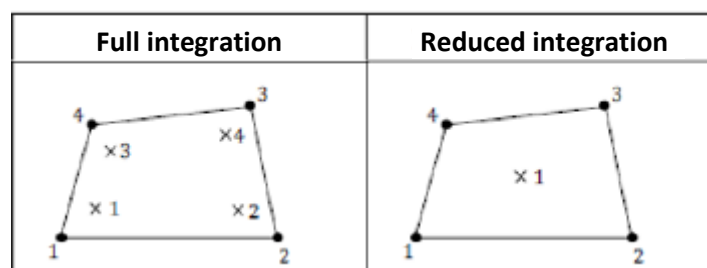


Figure 3.2 Overview integration points linear shell element full and reduced integration (SIMULIA, 2011)

### 3.1.2. Overview solid and shell FE models

An overview of both the shell and the solid model for tension loading is shown in Figure 3.3 and an overview for the bending loading is shown in Figure 3.4. The uniform tension load is applied on the edge of the main plate. The uniform bending load is applied by constraining the edge of the plate to the reference point and applying the bending load to this reference point.

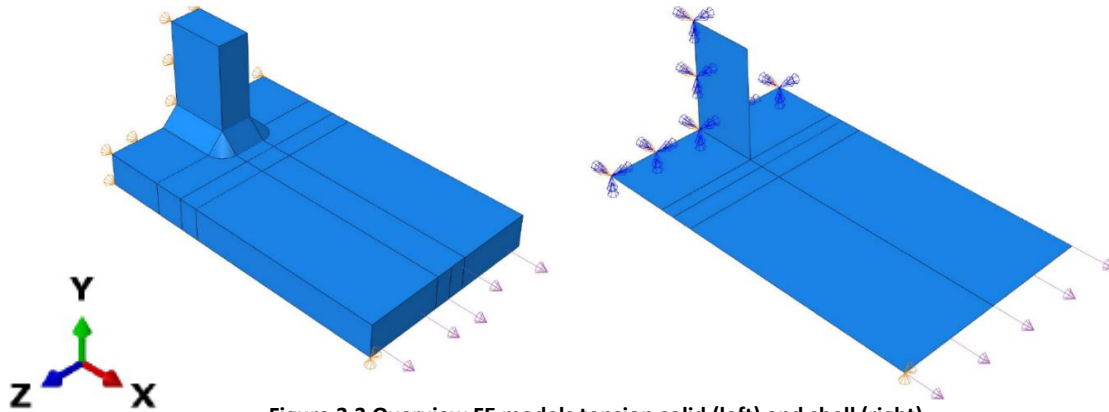


Figure 3.3 Overview FE models tension solid (left) and shell (right)

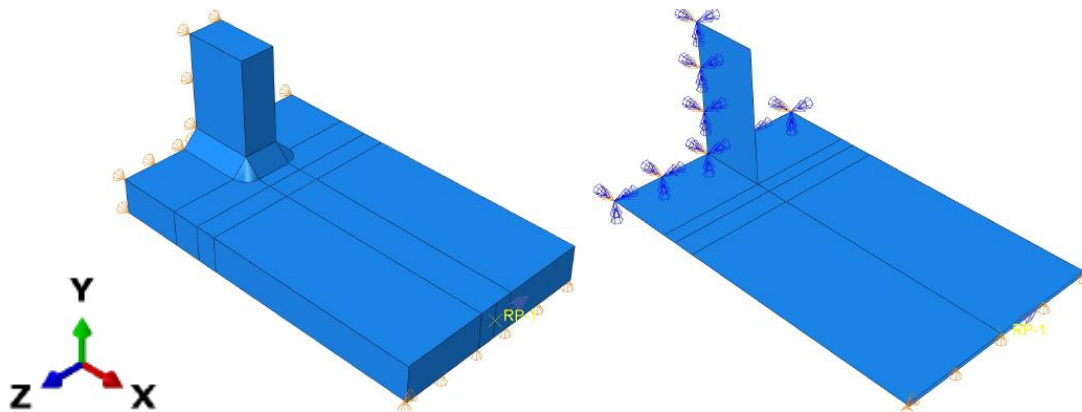


Figure 3.4 Overview FE models bending solid (left) and shell (right)

### 3.1.3. Analysis of element type and element size for shell and solid FE models

An element size sensitivity study is carried out for both load cases to obtain results which are not depending on the element size anymore. Furthermore, four different types of elements are investigated for the solid FE model. Linear and quadratic elements with full integration (C3D8 and C3D20), and linear and quadratic with reduced integration (C3D8R and C3D20R). An overview of the applied mesh for both the shell and solid model is shown in Figure 3.5 in which an element size of 2mm is used. In Figure 3.6 an overview of the mesh around the weld is shown.

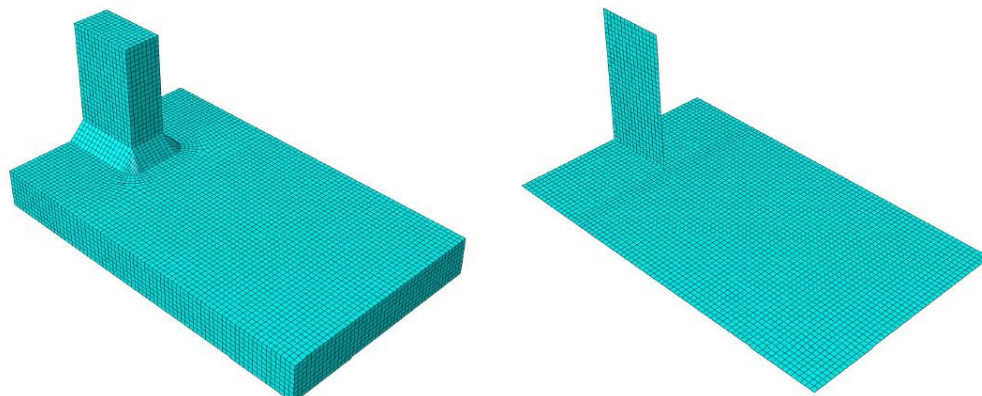
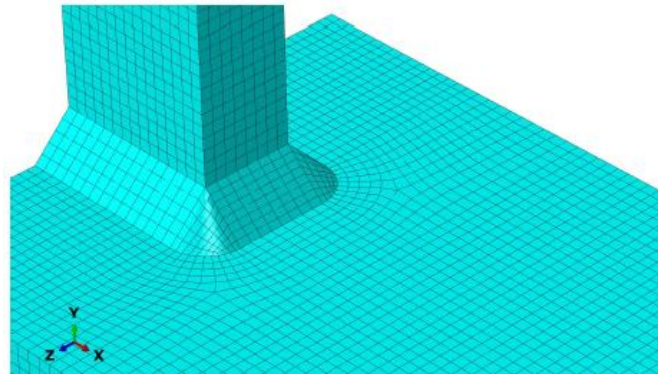
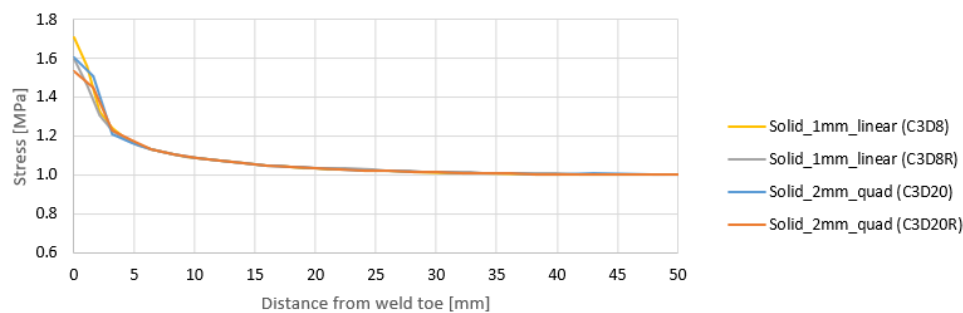


Figure 3.5 Overview FE model mesh solid (left) and shell (right)



**Figure 3.6 Local mesh around weld solid model**

The results of the mesh refinement study, including graphs and tables, for both the solid and shell FE models, loaded in tension, can be found in Annex A1. In Figure 3.7 the result of the element sensitivity for different type of solid elements types is shown.



**Figure 3.7 Overview result solid 2mm quadratic (C3D20R) and 1mm linear (C3D8R) loaded in tension**

In this section only the conclusions of the study are stated. With the mesh refinement study the ratio of the obtained hot spot stress and nominal stress is calculated.

The quadratic solid element, C3D20(R), converges with an element size of 2mm, in which the difference between the reduced integration and full integration is small, i.e. less than 1%. For the linear solid element, C3D8(R) convergence occurs for an 1mm element size.

The quadratic shell element, S8R, converges with an element size of 1mm, and for the linear elements, S4(R), convergence occurs at an element size of 0.5mm. If the 2mm quadratic solid elements, C3D20(R), are compared with the 1mm linear solid elements, C3D8(R), the results also almost the same. The scatter in results between the four investigated element types, for the solid elements, is the largest for the larger element size. If a sufficiently small element size is chosen, the results of the elements with and without reduced integration are almost the same. This same observation is valid for the shell elements.

Since the computational time without reduced integration will increase significantly, the elements with reduced integration can be used if the mesh size is sufficiently small, which is in this case equal or smaller than 2mm for quadratic solid elements, and 1mm for quadratic shell elements. With the element size which is not larger than 1 mm, first order element and second order elements show close results in both solid and shell type elements. The sensitivity of the element size and element type is not high for the studied cases.

### 3.1.4. Validation of solid element model loaded in tension and shell results comparison

For the validation of the built finite element model consisting of solid elements use is made of the results which can be found in (Śledziewski, 2018). Different load ranges were used on different specimens, and for the validation the results of the FE model are compared with the results of the stresses which occurred at a tension loading of 144kN. The obtained hot spot stress range from the experiment, making use of linear surface extrapolation, is 118.4MPa.

In Figure 3.8 the results from the solid FE model are shown in which quadratic elements with an element size of 2mm are used. The weld toe is taken as the origin for the horizontal axis. The nominal stress range is equal to 100.3MPa and the hot spot stress range is obtained using linear extrapolation. The stress range at 0.4t, which is 6.4mm, is equal to 113.7MPa and the stress range at 1.0t, which is 16mm, is equal to 105.4MPa. This results in a hot spot stress which is equal to 119.4MPa. The results for the hot spot stress obtained from the FE model and experiment are very close to each other, the difference is smaller than 1% and thus it can be concluded that the solid FE model is reliable. The ratio between the obtained hot spot stress and nominal stress is equal to 1.18 in the experiment. Linear surface extrapolation is used for obtaining the hot spot stresses at the weld toe. In Figure 3.8 an overview of the stress range versus weld toe distance is shown.

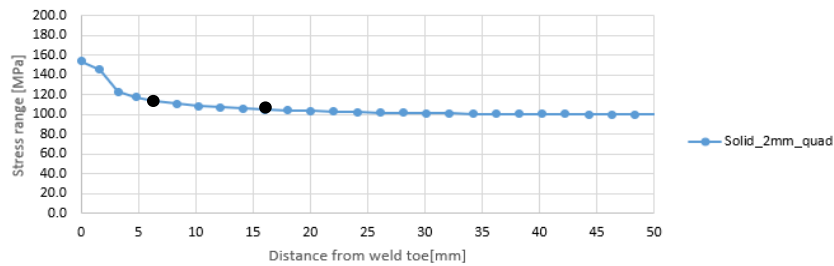


Figure 3.8 Stress range obtained from solid FE model under tension load:144kN

### 3.1.5. Investigation of influence of different parameters on stresses

To investigate the behavior of both the solid and shell elements a parametric analysis is performed in which the geometry is changed. To make the graphical representation more clear, the ratio between the hot spot stress and nominal stress, versus the weld toe distance will be shown, which can be found in Annex A1. Furthermore, an 1MPa pressure will be applied for the tension load case. The influence of different parameters on the stress range will be investigated and the different parameters are:

- Weld shape;
- Weld throat thickness;
- Main plate thickness;
- Stiffener plate thickness.

The first two points can only be taken into account by the solid model since for the shell model the weld is not modelled. The other two points are relevant for both the shell and solid model. In Table 3-2 an overview of the investigated sensitivity parameters and the variation cases are shown.

Table 3-2 Overview sensitivity analysis parameters

Sensitivity parameters	Variation cases
Weld shape	Round and sharp corners (solid)
Throat thickness [mm]	4,5 and 6 (solid)
Main plate thickness [mm]	12, 16 and 20 (solid and shell)
Stiffener plate thickness [mm]	12, 16 and 20 (solid and shell)



### Weld modelling with shell FE model

To investigate if the differences between the different elements can be reduced, the weld is modelled in the shell FE model with a method which can be found in the IIW recommendations regarding the hot spot stress approach (Niemi, Fricke, & Maddox, 2018), see section 2.6.2. The results of this approach should be closer to the results from the solid elements, since the weld is modelled, but it still is approximation of reality. A further advantage of modelling the weld end in the shell model is that the weld toe can be taken as the origin, instead of the structural intersection point. Thus, both the adapted shell model and the solid model have the same starting point for the read out of the strain range and this will make the comparison more straightforward. An overview of the weld modelling approach is shown in Figure 3.9. The thickness of the stiffener plate is locally increased by the weld leg length. This will result in a total thickness of  $16+7.07=23.07\text{mm}$  for the reference model.

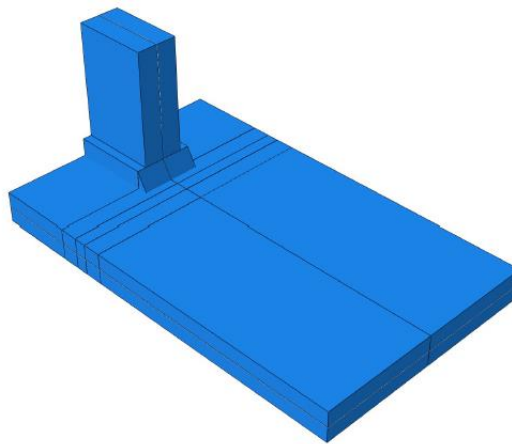


Figure 3.9 Overview shell FE model with weld included

#### 3.1.5.1. Loaded in tension

The results of the performed sensitivity study are shown in Table 3-3 for both the solid elements and shell elements. The reference case is when both plate thicknesses are equal to 16mm. For the solid FE model C3D20R elements are used, and for the shell FE model S8R, elements are used. The corresponding graphs can be found in Annex A1. In Table 3-4 the differences of the parametric analysis are shown as an percentage.

Table 3-3 Overview results sensitivity analysis solid and shell element model loaded in tension

Sensitivity parameters	Variation cases	Calculated ratio $\frac{\sigma_{HSS}}{\sigma_{nom}}$ solid	Calculated ratio $\frac{\sigma_{HSS}}{\sigma_{nom}}$ shell	$\frac{\sigma_{HSS\_shell}}{\sigma_{HSS\_solid}}$	$\frac{\sigma_{HSS\_shell\_weld}}{\sigma_{HSS\_solid}}$
Weld shape	Round corners	1.192	-	-	-
	Sharp corners	1.185	-	-	-
Throat thickness	4mm	1.199	-	-	-
	5mm	1.190	-	-	-
	6mm	1.185	-	-	-
Main plate thickness	12mm	1.227	1.340	1.09	1.16
	16mm	1.190	1.219	1.02	1.09
	20mm	1.160	1.152	0.99	1.04
Stiffener plate thickness	12mm	1.201	1.177	0.98	1.04
	16mm	1.190	1.219	1.02	1.10
	20mm	1.180	1.256	1.06	1.12

Table 3-4 Overview difference in percentage solid and shell models

Sensitivity parameters	Variation cases	Difference ratio $\frac{\sigma_{HSS}}{\sigma_{nom}}$ solid [%]	Difference ratio $\frac{\sigma_{HSS}}{\sigma_{nom}}$ shell [%]	Difference ratio $\frac{\sigma_{HSS}}{\sigma_{nom}}$ shell with weld [%]
Main plate thickness	12mm	+3.5	+9.9	+9.7
	16mm	-	-	-
	20mm	-2.5	-5.5	-6.7
Stiffener plate thickness	12mm	+0.9	-3.4	-2.8
	16mm	-	-	-
	20mm	-0.8	+3.0	+2.4

For the reference case, in which both plate thicknesses are 16mm, the hot spot stress obtained from the shell FE model is higher when compared with the solid FE model, but this is not the case for all variation cases. Increasing main plate thickness to 20mm and decreasing the stiffener plate thickness to 12mm will result in a higher hot spot stress for the solid FE model, when compared with the shell FE model. The obtained ratios are equal to 0.98 and 0.99 respectively. As can be seen from Table 3-4, the behavior of the solid and shell FE models is similar in terms of signs, both models will increase or decrease at the same time when the thickness of the main plate is adapted. When the main plate thickness is increased or decreased, the ratio of the hot spot stress will increase and decrease, respectively, for both the solid and shell FE model. The ratio between the obtained hot spot stress of the shell and solid FE models will also differ if the thickness is increased or decreased, which can be seen in Table 3-3.

When the thickness of the stiffener plate is adapted, the behavior between the shell and solid element models is different. When the thickness of the stiffener plate is decreased from 16mm to 12mm, this results in an increase in hot spot stress for the solid FE model, while it decreases for the shell model. The opposite is observed when thickness of the stiffener plate is increased from 16mm to 20mm. The ratio between the obtained hot spot stress of the solid and shell FE models will also change if the thickness of the stiffener plate is adapted.

As can be seen from Table 3-3, the behavior of the adapted shell FE models is not becoming any closer to the solid FE model. The ratio between the solid and shell with weld FE models becomes larger when the weld modelling technique is applied. For this tension load, the shell element models with weld modelled by a local thicker plate don't show an improvement compared with shell without weld modelled.

#### 3.1.5.2. Loaded in bending

For the specimen loaded in bending, an uniform bending moment is applied at the edge of the main plate. To obtain a nominal stress which is equal to 1MPa, a load which is equal to 3840Nmm is applied. As with the tension loading, also for this loading type an element sensitivity study is performed in which the results are shown in Annex A1.

The difference between linear, C3D8(R) and quadratic, C3D20(R) solid elements, with a coarse mesh size, i.e. 8mm, is large, the difference is 40%. When the element size is decreased also the differences in results between the quadratic and linear elements will decrease. Another observation is that the difference between the quadratic elements with full integration and reduced integration is only a few percent, and when the element size is smaller than 2mm the differences are neglectable. Even for an element size of 1mm the difference between the linear solid elements with full and reduced integration is 2.5%. For the shell elements the difference between the linear elements with reduced



and full integration is smaller when compared with the solids. With an element size equals 8mm the difference is only 8% and for an element size of 2mm the difference is less than 1%. A quadratic solid element converges with an element size of 2mm, in which the difference between the reduced integration and full integration is less than 1%. This is a similar observation as for the tension loading. For the linear solid element convergence occurs for an 1mm element size, since the difference with the smaller element size is smaller than 1%. For the shell element model the quadratic elements will converge with an element size of 1mm, and for the linear elements convergence occurs at an element size of 0.5mm.

The results of the performed sensitivity study are shown in the Table 3-5 for both the shell and solid elements. The corresponding graphs can be found in Annex A1.

**Table 3-5 Overview results sensitivity analysis solid elements loaded in bending**

Sensitivity parameters	Variation cases	Calculated ratio $\frac{\sigma_{HSS}}{\sigma_{nom}}$ solid	Calculated ratio $\frac{\sigma_{HSS}}{\sigma_{nom}}$ shell	$\frac{\sigma_{HSS\_shell}}{\sigma_{HSS\_solid}}$	$\frac{\sigma_{HSS\_shell\_weld}}{\sigma_{HSS\_solid}}$
Weld shape	Round corners	1.262	-	-	-
	Sharp corners	1.257	-	-	-
Throat thickness	4mm	1.269	-	-	-
	5mm	1.262	-	-	-
	6mm	1.253	-	-	-
Main plate thickness	12mm	1.310	1.219	0.93	0.95
	16mm	1.262	1.102	0.87	0.91
	20mm	1.210	1.050	0.87	0.89
Stiffener plate thickness	12mm	1.275	1.083	0.85	0.88
	16mm	1.262	1.102	0.87	0.90
	20mm	1.242	1.113	0.90	0.93

**Table 3-6 Overview difference in percentage solid and shell models**

Sensitivity parameters	Variation cases	Difference ratio $\frac{\sigma_{HSS}}{\sigma_{nom}}$ solid [%]	Difference ratio $\frac{\sigma_{HSS}}{\sigma_{nom}}$ shell [%]	Difference ratio $\frac{\sigma_{HSS}}{\sigma_{nom}}$ shell with weld [%]
Main plate thickness	12mm	+3.8	+10.6	+8.5
	16mm	-	-	-
	20mm	-4.1	-4.8	-5.7
Stiffener plate thickness	12mm	+1.1	-1.7	-1.2
	16mm	-	-	-
	20mm	-1.6	+1.0	+0.9

### Conclusions

Similar observations as with the tension loading are also observed for the bending loading. As can be seen from Table 3-6, the behavior of the solid and shell element models is similar in terms of signs, the hot spot stress of both models will increase or decrease at the same time when the thickness of the main plate is adapted. If the thickness of the stiffener plate is adapted the behavior of the solid and shell FE models is opposite. The ratio between the obtained hot spot stress of the solid and shell FE models will also differ if the thickness is increased or decreased, which can be seen in Table 3-5. For all investigated variation cases the shell FE model is underestimating the hot spot stress when compared with the solid FE model. This underestimation is due the fact that the weld is not modelled with the shell FE model, and thus the bending stiffness of this model is smaller when compared with the solid FE model. This will result in lower stresses and thus a lower hot spot stress.

In Table 3-5 it can be seen that the shell FE models with the weld modelled show a small improvement in the ratio  $\frac{\sigma_{HSS\_shell\_weld}}{\sigma_{HSS\_solid}}$ , but this improvement is very limited since it is only 2 a 3%. The behavior of the adapted shell FE model is still closer to the original shell FE model, than the solid FE model. As with the tension loading, the difference in percentage, which is shown Table 3-6, is still similar to the shell model. The behavior when the stiffener plate thickness is adapted did not change. When looking at the results of the weld modelling technique for the shell FE models, it can be concluded that the improvement for the bending load is very limited, while for the tension load results no improvement is found.

### 3.1.6. Shell modelling using top/bottom-surface approach

Usually shell structures are modelled making use of mid-surface modelling. Another possibility is to model the structure making use of shell offset by using the top-surface or bottom-surface approach. In this approach the reference surface is shifted from the mid-surface which can be seen in Figure 3.10, in which Figure 3.10b represents the bottom-surface offset, while Figure 3.10c represents the top-surface offset. With this first approach the geometry of the shell model is closer to the solid model, since the overlap due to mid-surface modelling is eliminated. However, it is not clear what the difference in stress distribution will be for both modelling techniques. Hence, a comparison between the models using center line shell elements and shifted shell elements is given in this sub-section. The shell element degrees of freedom are associated to the reference surface and kinematic quantities are calculated from this location. Shifting the reference surface thus influences the results and it is investigated how much it will differ in results based on the investigated welded transverse stiffener specimen. An overview of both modelling approaches for the investigated detail can be seen in Figure 3.11, in which the shell render thickness option is used.

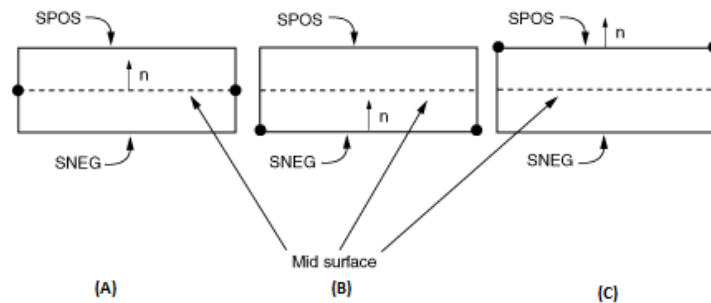


Figure 3.10 Offset shell elements positive (top) and negative (bottom) approach

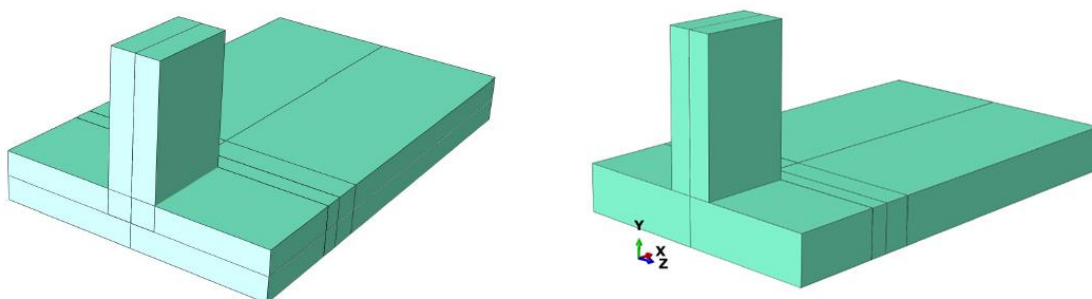


Figure 3.11 Modelling approaches shell elements, left mid-surface, right bottom-surface

Applying the bottom-surface offset approach will cause an eccentricity for the tension loading, since the uniform loading is applied at the nodes which are shifted from the mid-surface. Due to this eccentricity secondary stresses occur which will influence the results, both for the nominal stress range and the hot spot stress range. A similar observation was found by (Klarholm, 2016) in which the FE software Nastran was used for offset modelling of a C-bar, which is used in airplanes. The calculated hot spot stress for the reference model, making use of mid-surface modelling is 1.22, while this value is equal to 6.00 for the bottom-surface approach. The results of the tension loading are shown in Figure 3.12. It can be concluded that the bottom-surface approach is not suitable if the specimen is loaded in tension, it will cause huge secondary stresses due to the eccentric which occurs with this type of modelling. For the bending load a similar observation can be seen, but the influence is much less.

The results of the bending loading type are shown in Figure 3.13. The calculated hot spot stress for the reference model, making use of mid-surface modelling is 1.102 while this value is equal to 1.491 for the bottom-surface approach. As can be seen from the graph, the bottom-surface offset modelling approach will only influence the results in the first 15mm, the nominal stress for both approaches is the same. The stress concentration at the structural intersection point for the bottom-surface approach is twice the value of the stress concentration due to the mid-surface modelling. This can be explained by looking at the amount of material which is at the structural intersection point. For the bottom-surface approach, it is on the edge of the main plate and stiffener plate, while for the mid-surface modelling it is the main plate plus a part of the stiffener plate, since it is mid-surface modelled. The latter method will result in more material at the structural intersection point, and thus in a lower stress. Also for the bending load, the bottom-surface approach will influence the results, and thus it this approach is also not suitable to use. All the outputs regarding the displacements can be found in Annex A2.

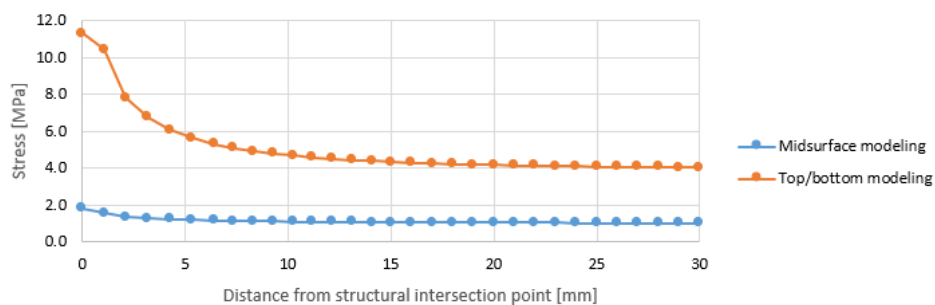


Figure 3.12 Stress range obtained from shell FE model with different modelling approaches loaded in tension

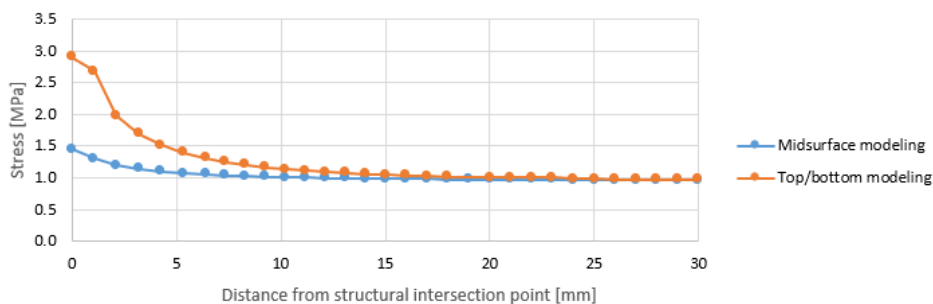


Figure 3.13 Stress range obtained from shell FE model with different modelling approaches loaded in bending

## 3.2. Validation: OSD in Stevinlab II

### 3.2.1. Description of the model

A full scale OSD which is tested at the Delft University of Technology forms the bases for the different FE models. All data regarding the geometry and location of strain gauges is obtained from (Wu & Kolstein, 2020). Furthermore, some real life measurements are performed for obtaining the exact geometry of weld at location of the trough and cope hole, and exact locations of the strain gauges.

#### 3.2.1.1. Dimensions and geometry

The OSD consists of three crossbeams, eight continuous troughs (closed stiffeners) and a deck plate. For the troughs a distinction can be made between troughs which cross the crossbeam with and without cope holes, which can be seen in Figure 3.14b. Half of the troughs, four, includes a cope hole with a specific shape: "Haibach" cope hole. The other four troughs pass the crossbeam through cut-outs and are welded all around the crossbeam. The deck plate of the OSD has a total length of 9375mm, a width of 5100mm and a thickness of 20mm. The center to center distance between the crossbeams is 3000mm. An overview of the dimensions of the deck plate can be seen in Figure 3.14a.

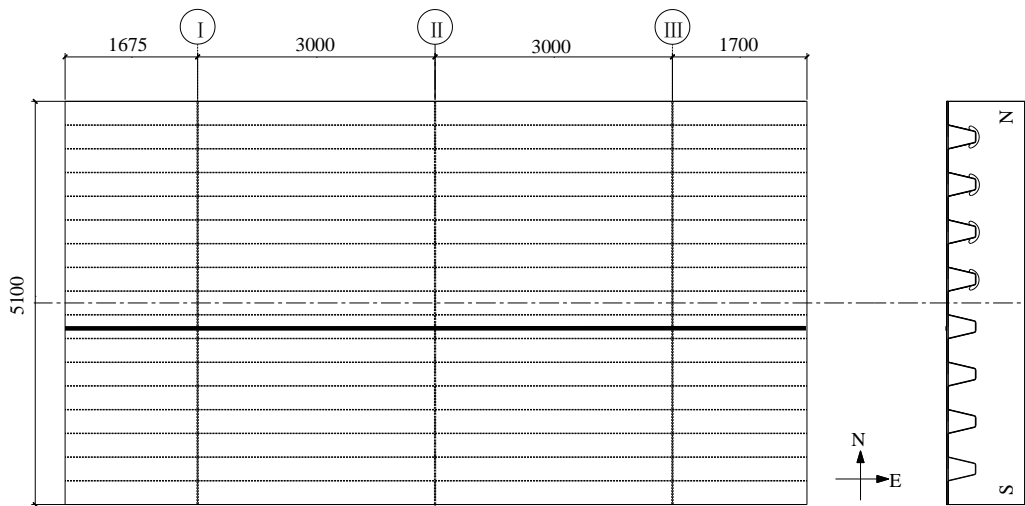


Figure 3.14 (a) Top view of dimensions deck plate (b) distinction crossbeam with and without cope hole (Wu & Kolstein, 2020)

The total height of the crossbeam, including the bottom flange and the deck plate is 1000mm. The web of the crossbeam has a thickness of 16mm, and the thickness of the bottom flange is 12mm. The troughs have a center to center distance of 600mm and the bottom flange has a width of 200mm. The dimensions of the crossbeam are shown in Figure 3.15. Troughs which are labeled with number 1,3,5 and 7 are automatic welded to the deck plate while troughs which are labeled with number 2,4,6 and 8 are manually welded.

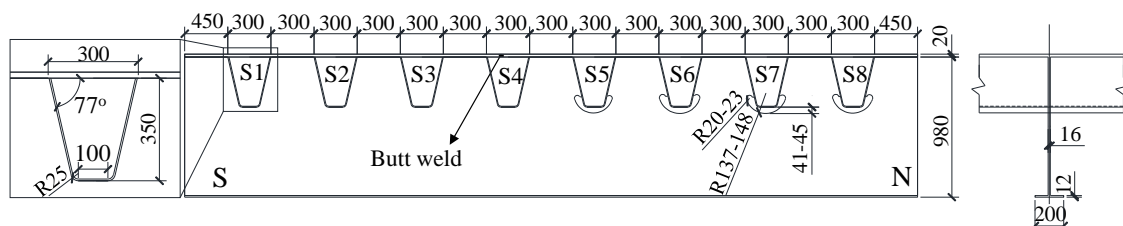


Figure 3.15 Dimensions crossbeam (Wu & Kolstein, 2020)

Note: the detailed values are measured in the lab and the model is built following the detailed information.

The troughs have a height of 350mm, and the thickness is equal to 6mm. The distance between the webs of the troughs is 140mm at the bottom, and 300mm at the top of the trough. As stated before, half of the troughs includes a cope hole in the crossbeam. An overview of the dimensions of the trough with a “Haibach” cope hole are shown in Figure 3.15. The troughs and crossbeam are connected through fillet welding.

### 3.2.1.2. Boundary conditions

During the performed experiments the crossbeam is fully supported over the whole length by an “I”-shape beam. This is taken into account in the finite element model by constraining the translational degree of freedom, in Y-direction, of the bottom flange. To prevent kinematic movement the translational degrees of freedom in X- and Z-direction are constraint at one position of the bottom flange, which is shown in Figure 3.18.

### 3.2.1.3. Material properties

Steel with a Young’s modulus of 210.000 MPa and a poisson ratio of 0.3 is used. An elastic calculation is performed, so only those two material properties are needed. The elastic calculation is sufficient since fatigue occurs at a stress range which is lower than the Yield strength of the material (Lee, et al., 2010).

### 3.2.1.4. Load

A static load is applied at two different locations at the same time, which is used for the validation of the model. The load range has a magnitude of 2 times 100kN and is distributed over an area of 270 x 320mm. This will result in a distributed load with a magnitude of 1.16N/mm<sup>2</sup>. The load is applied on the right web of trough 5 with an offset of 600mm from crossbeam I. The load positions are shown in Figure 3.16.

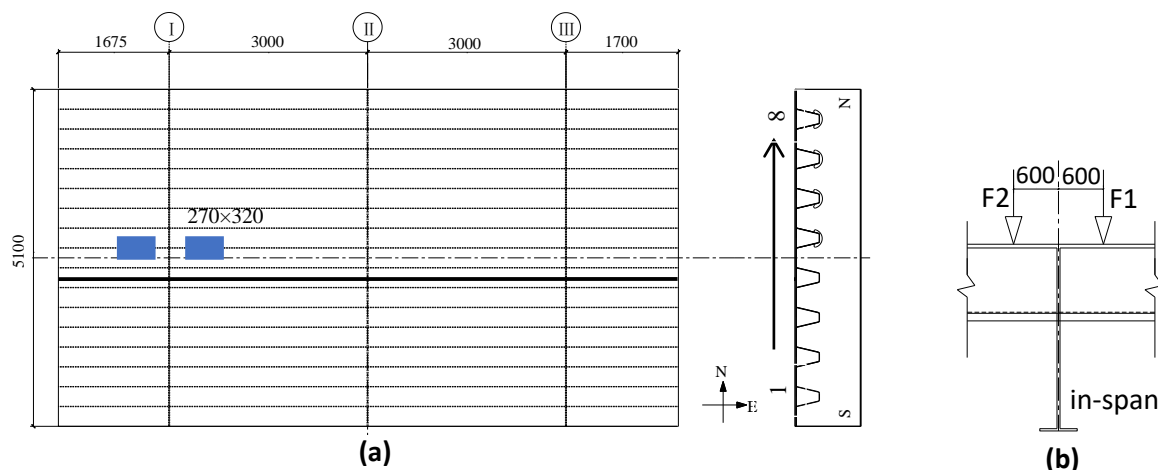


Figure 3.16 Location of static load, subfigure a: top view, sub figure b: size view (Wu & Kolstein, 2020)

### 3.2.1.5. Modelling approach for shell model

For the shell model different modelling techniques are possible to model the structure. The shell model can be divided in the following parts: deck plate, crossbeam I, II and III, troughs 1-8 and the bottom flange of the crossbeam. In Figure 3.17 a graphical representation of the modelling approach is shown. In the left figure an overview of the connection is shown and in the right figure the render shell thickness option is on to show the thickness of the shell elements. Mid-surface modelling is used for the shell element models, since in section 3.1.6 it was concluded that the bottom-surface approach is not a suitable method. With the mid-surface modelling approach, the mid-surface is taken as the

reference. With this method a slight overlap, which is equal to  $0.5t$  the plate thickness, will occur where different parts intersect which can be seen in the right figure. All geometric information can be found in section 3.2.1.1. To see if the same observations occur as with the simple fillet welded transverse stiffener connection, the OSD is modelled with the bottom-surface offset approach. The results of this modelling technique can be found in Annex B.

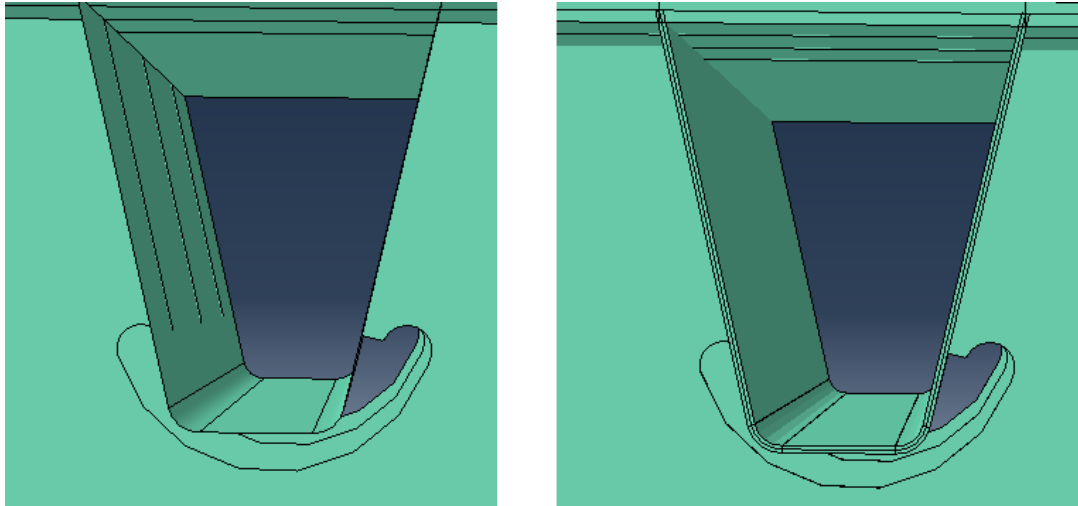


Figure 3.17 Overview modelling approach shell model

#### 3.2.1.6. Elements used and mesh size

##### Shell

The shell element model consists of 8-noded reduced integration elements which are named “S8R” in Abaqus in which quadratic interpolation is done. Use is made of a global and local mesh size. This is done to obtain more accurate results at the region of interest. The global mesh size is 100 mm, while at the region of interest, a local mesh refinement is applied in which a distinction is made between a coarse and fine local mesh refinement.

##### Solid

The solid elements which are used in the sub-solid element model consists of 8-noded reduced integration elements which are named “C3D8R” and 20-noded elements which are named “C3D20R” in Abaqus. The 8-noded element uses linear interpolation, while in the latter one, interpolation is done quadratically. Since the solid element is a small sub-model of the whole structure, the global and local mesh sizes of the shell element model remain the same. The local sub-model has an element size of 2mm, which means that the element is  $2 \times 2 \times 2 [\text{mm}^3]$ . The solid elements will give a better approximation of the strain ranges when compared with shell elements. Due to the relatively small solid sub-model the computational time will not increase in a significant manner. The edges of the shells and the surfaces of the solid elements are connected with each other through the “tie” constraint. With the sub-solid model also the weld geometry is modelled. Furthermore, a seam is applied at the location of the at the rib-to-crossbeam connection. This seam is applied to model the gap between the crossbeam and the trough, because in reality this connection is only connected with fillet welds and thus all the forces are transferred through the welds.

An overview of the used element types and sizes, for both the solid and shell FE models, are given in Table 3-7.

Table 3-7 Overview used elements and mesh size

Element type	Global mesh size [mm]	Local mesh size [mm]
Shell: S8R	100	8
Shell: S8R	100	2
Solid: C3D8R	-	2
Solid: C3D20R	-	2

3.2.2. Overview global shell element and solid sub-model

An overview of the global shell model is shown in Figure 3.18 and Figure 3.19, an overview of the sub-solid model is shown in Figure 3.20, and in Figure 3.21 the weld detail is shown.

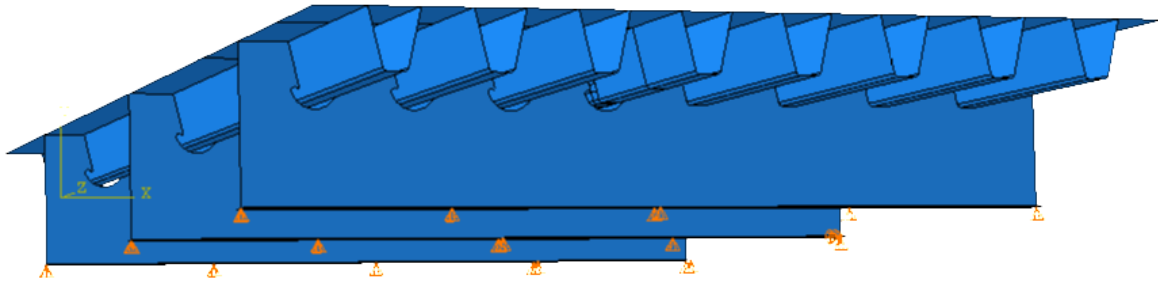


Figure 3.18 Overview global shell model

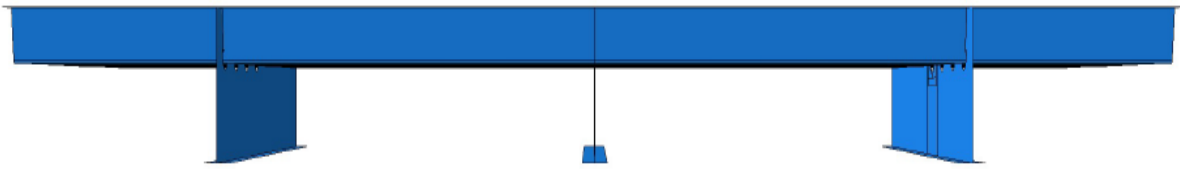


Figure 3.19 Side view global shell model

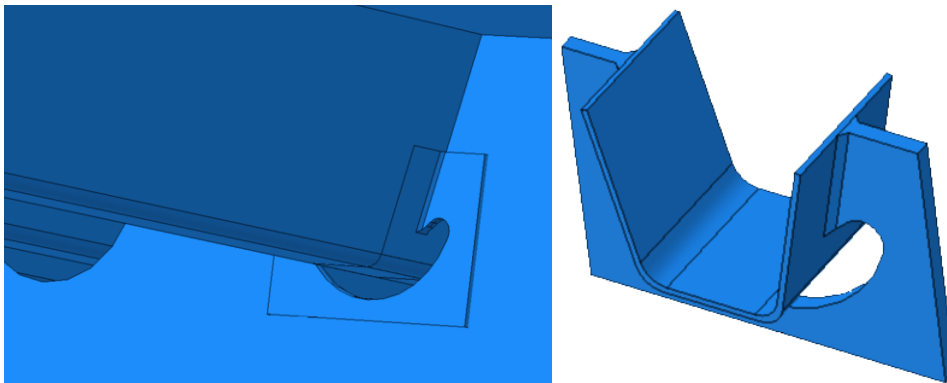


Figure 3.20 Overview sub solid model

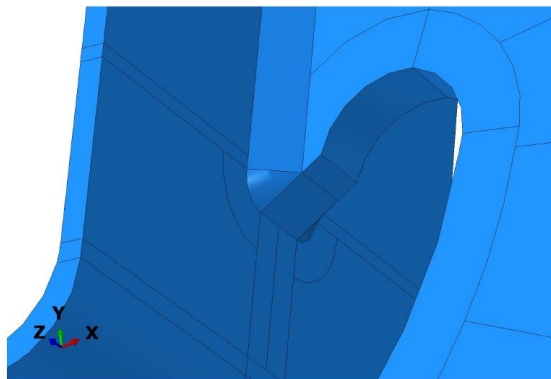


Figure 3.21 Overview detail location solid model



In Figure 3.22 a top view of the global shell model mesh is shown in which half of the total length of the OSD is shown. The local mesh is shown in Figure 3.23 in which a local element size of 2mm is used. To create a smooth transition between the global mesh size of 100mm and the local element size of 2mm, several transition zones are applied. The several transition zones are: from 100 to 50mm, from 50mm to 10mm and from 10mm to 2mm, in which one transition zone can be seen in Figure 3.23.

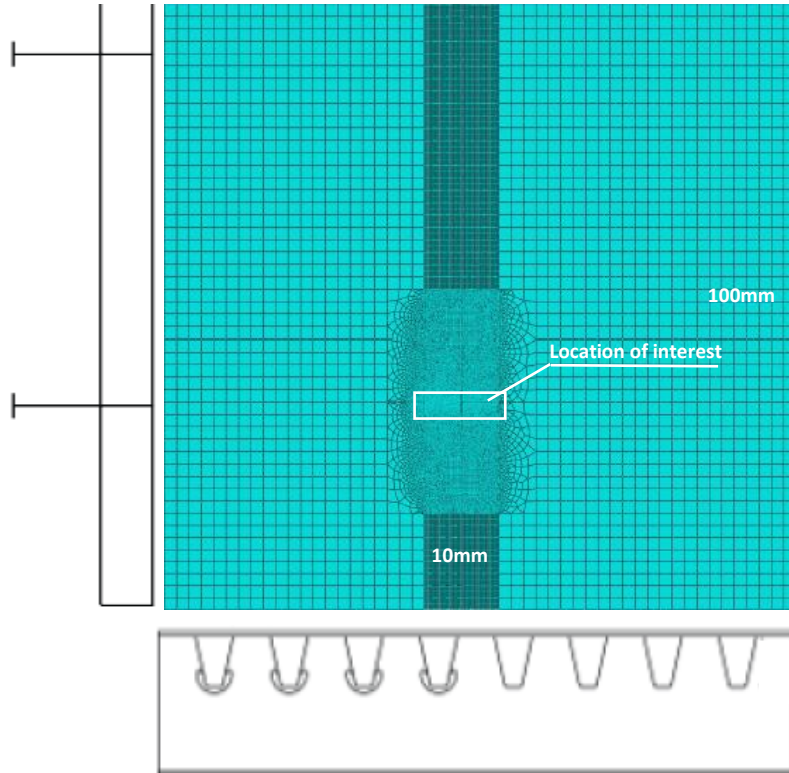


Figure 3.22 Top view global mesh size model

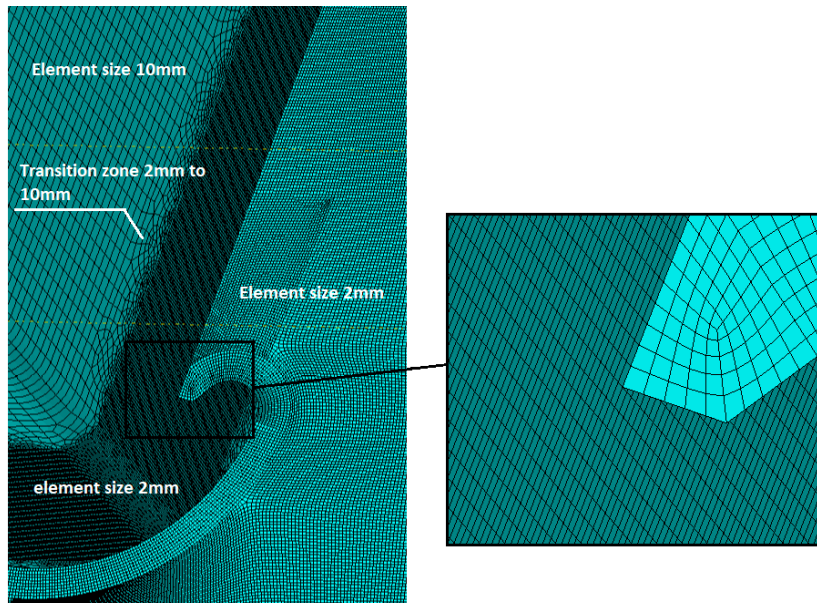


Figure 3.23 Overview local element size of 2mm and transition zone to 10mm



An overview of the sub-solid mesh is shown in Figure 3.24 in which also a zoomed in detail of the weld is shown.

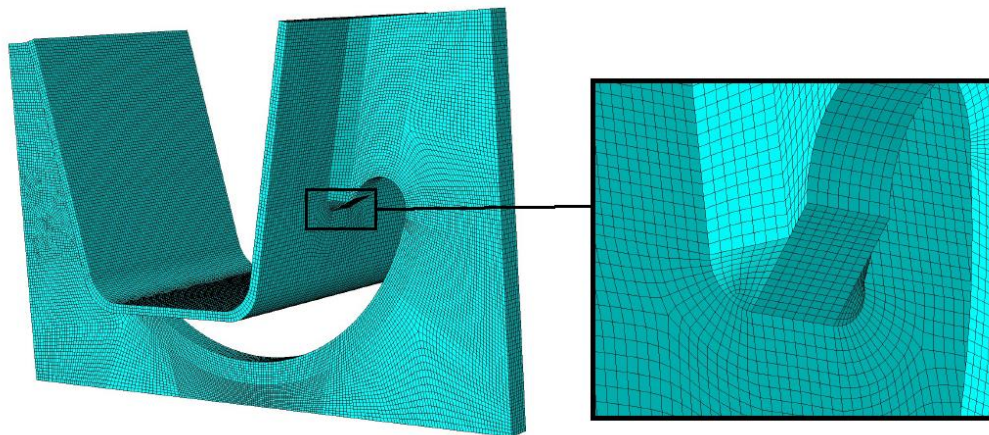


Figure 3.24 Overview global mesh sub solid model (left) and weld detail (right)

### 3.2.2.1. Strain analysis and validation

The validation of the finite element models is based on the strain range values which were measured during the experiment of (Wu & Kolstein, 2020). The measurement of the strain range is performed by strain gauges and different locations of the strain gauges are used for the validation. A distinction can be made between three locations of interest:

- X-direction from weld toe: free edge (strain gauges 61-57, 401 and 402);
- X-direction from weld toe: in-span (strain gauges 67-71, 405 and 406);
- Y-direction from weld toe (strain gauges 66-62, 403 and 404);

These locations are shown in Figure 3.25. The free edge direction is in the direction of the cantilever part, left to crossbeam I, while the in-span direction is in the direction of crossbeam II, which is shown in Figure 3.16. The trough of interest is trough number 5, and the shown strain gauges are placed on the right web of this trough.

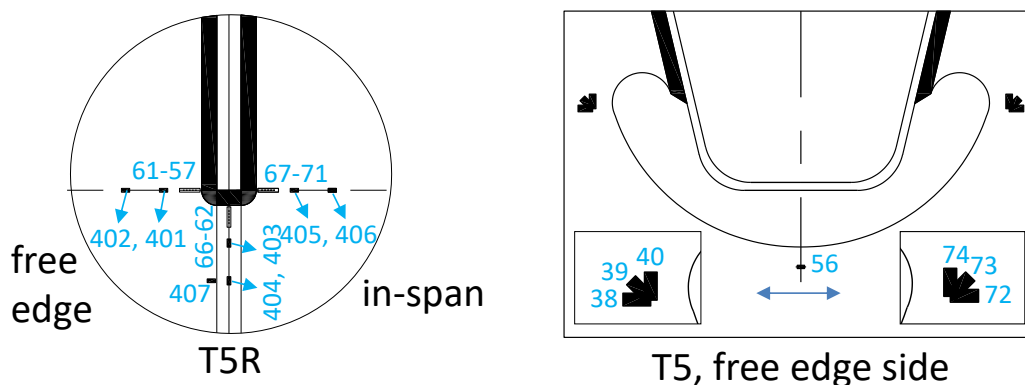


Figure 3.25 Overview locations strain gauges experiment OSD TUD (Wu & Kolstein, 2020)

In theory the strain gauges are at fixed location from the weld toe: 2,4,6,8,10,25 and 50mm. To obtain the exact location of all the relevant strain gauges, the locations are measured in the lab and an overview of the distances from weld toe are shown in Table 3-8. In the first column the predefined values are shown, while in the second, third and fourth column the exact measured values are shown.

Table 3-8 Overview strain gauges distance from weld toe

Predefined value	Y-direction	X-direction free edge	X-direction in span
4mm	4.5mm	6.3mm	6.1mm
6mm	6.5mm	8.3mm	8.1mm
8mm	8.5mm	10.3mm	10.1mm
10mm	10.5mm	12.3mm	12.1mm
12mm	12.5mm	14.3mm	14.1mm
25mm	26.8mm	26.8mm	26.3mm
50mm	51.1mm	51.7mm	51mm

As can be seen from Table 3-8, small differences occur between the theoretical and measured values. The results from the finite element modelling are compared with the experimental results in which the as-measured values for the location of the strain gauges is used.

### 3.2.3. Analysis and validation of solid-sub model and shell FE model

#### 3.2.3.1. Analysis of element size

##### Solid FE model

A study of the influence of the element size on the strain range, in the web of the trough, is performed to obtain a stable element size for the solid element. Three different local element sizes are investigated: 1mm, 2mm and 4mm for which the results are given in the following figures. For obtaining the strain range values, the average element output at the nodes is used in Abaqus. An element size of 2mm means that the strain range is extracted every 2mm in Abaqus, and for an 1mm element size, every 1mm. This is not shown in the graphs below, because otherwise it becomes difficult to read the results. Furthermore only the results of the mesh refinement study of the solid and shell FE model for the Y-direction in the web of the trough is shown. The results of the solid and shell X-direction path can be found in Annex C.

##### Y-direction (vertical)

In the Figure 3.26 the results for the strain range in Y-direction for the quadratic solid element models with different element sizes are shown, while in Figure 3.27 the results of the linear solid elements are shown.

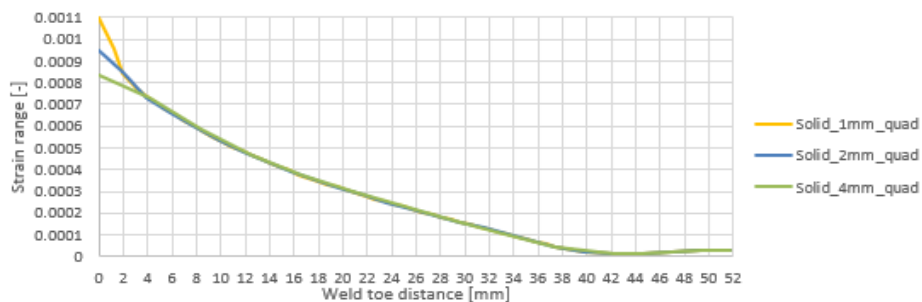


Figure 3.26 Strain range in Y-direction for different quadratic element sizes

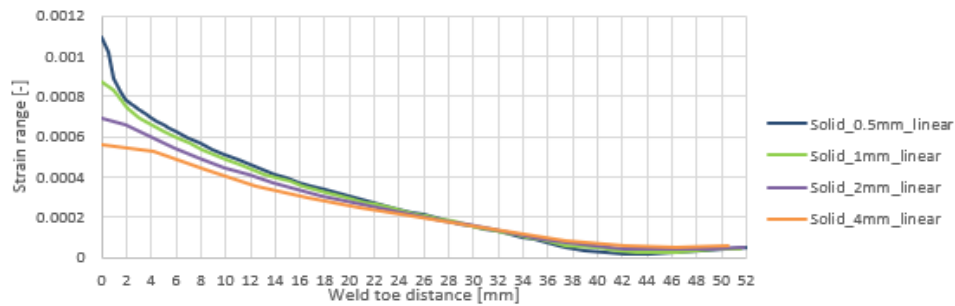


Figure 3.27 Strain range in Y-direction for different linear element sizes

As can be seen from Figure 3.26 and Figure 3.27, the smaller the element size, the higher the strain range will be at the weld toe. This is due to the singularity which occurs at that location. The quadratic element sizes of 1 and 2 millimeter have a more or less similar strain range at the location which is 2mm from the weld toe. At the location between 2 and 4mm the results with a 4mm element size differ from the smaller element sizes. The first hot spot stress extrapolation point is at  $0.4t$  from the weld toe, which is equal to 2.4mm ( $0.4 \cdot 6\text{mm}$ ). Thus it is advised to use an element size of 2mm for the quadratic solid elements, since there is a difference between the 2mm and 4mm elements size in the first 4mm. When the hot spot stress results of the solid 2mm element size and the solid 1mm element size are compared, the difference is 1%, so it can be concluded that the 2mm quadratic solid elements are converged. All the investigated quadratic element sizes will converge to the same value after a length which is equal to the element size.

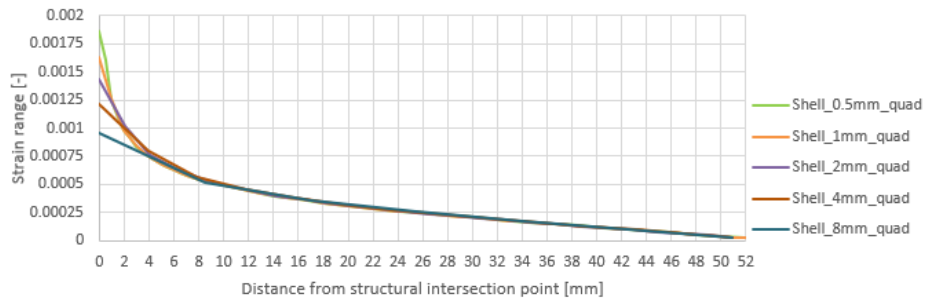
As can be seen from Figure 3.27, there is quite a scatter in the first 20mm between the investigated linear elements. The difference in results between the 0.5mm and 1mm linear elements in the first 10mm from the weld toe is still around 7%, while the difference between larger element sizes is even larger. The difference in hot spot stress range between the 0.5mm and 1mm linear element size is 5%. Elements smaller than the 0.5mm, are not feasible because it will increase the computational time in a significant way when compared with the 2mm quadratic elements. Overall the linear solid elements cannot simulate the bending behavior very well.

#### Shell FE model

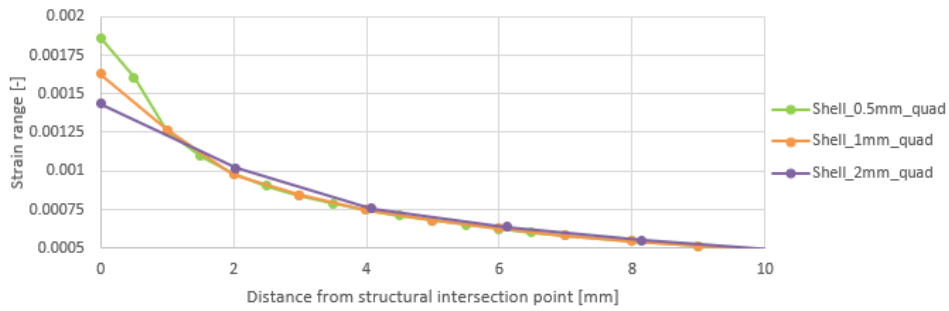
A similar study as with the sub solid element model is performed to investigate the influence of the element size on the strain range. Five different local element sizes are investigated: 0.5, 1mm, 2mm, 4mm and 8mm for which the results are given in the following figures.

#### **Y-direction (vertical)**

In the Figure 3.28 the results for the strain range in Y-direction for the shell models with different element sizes is shown, and in Figure 3.29 a zoomed in graph of the first 10mm from the structural intersection point is shown. The structural intersection point is taken as the starting point, since the weld is not modelled with the shell elements.



**Figure 3.28 Strain range in vertical direction for different element sizes**



**Figure 3.29 Zoomed in results strain range in vertical direction for different element sizes**

As can be seen from Figure 3.28, the smaller the element size, the higher the strain range will be at the structural intersection point. This is due to the singularity which occurs at that location. The element sizes of 0.5 and 1mm have a more or less similar strain range at the location which is 2mm from the structural intersection point. The element sizes of 2mm and 4mm show comparable results 4mm and 8mm from the structural intersection point. The element size of 8mm will show comparable results at 8mm from the structural intersection point. The first hot spot stress extrapolation point is at  $0.4t$  from the weld toe, which is equal to 2.4mm.

As can be seen in Figure 3.29, the results of the 2mm elements size at this location are higher when compared with the 1mm and 0.5mm element size. The difference in the hot spot stress range between the 0.5mm element size, 238.73 MPa, and 1mm element size, 236.75MPa, is 0.8%, while this difference is 5% between the 1mm and 2mm element size. Thus it can be concluded that the results of the 1mm element size are converged. All the investigated element sizes will converge to the same value after some distance, but to obtain more precise results, close to the structural intersection point, it is advised to use an element size of 1mm. For obtaining the strain range at a larger distance away from the weld toe a larger element size can be used.

### 3.2.3.2. Strain analysis and validation

For the validation of the FE models use is made of the strain gauges which were placed for the experiments of (Wu & Kolstein, 2020). For the solid FE model quadratic elements with an element size of 2mm and linear elements with an element size of 0.5mm are compared with the experimental results. For the shell FE model a coarse element size of 8mm and a fine elements size of 1mm are compared with the experimental results. For the shell element models the structural intersection point of the crossbeam and trough is taken as the starting point. This point is different for the solid elements, in which the weld toe is taken as the starting point, but the IIW recommendations (Niemi, Fricke, & Maddox, 2018) states to use the structural intersection point as a starting point for shell elements when the weld is not modelled.

### Y-direction (vertical)

In the Figure 3.30 the results for the strain range in Y-direction for the four different FE models are shown. Furthermore the experimental results are shown in the figure.

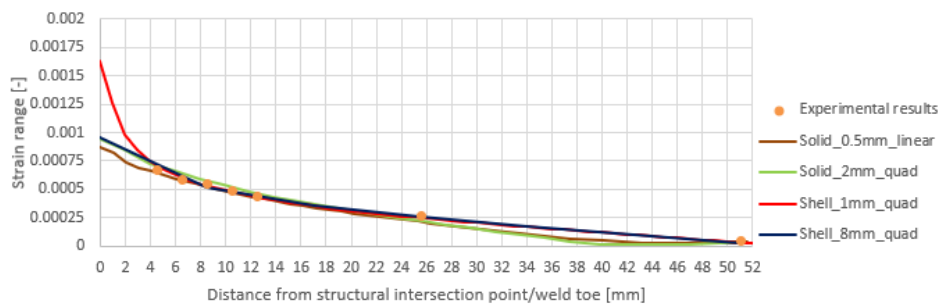


Figure 3.30 Strain validation solid and shell FE model Y-direction trough

### X-direction (horizontal)

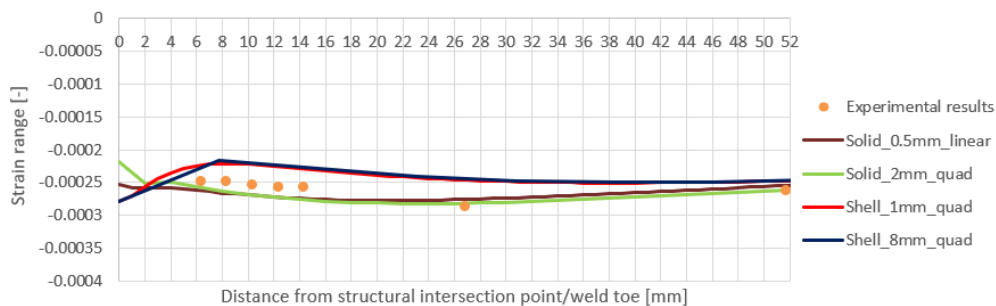


Figure 3.31 Strain validation solid and shell FE model X-direction trough, free edge

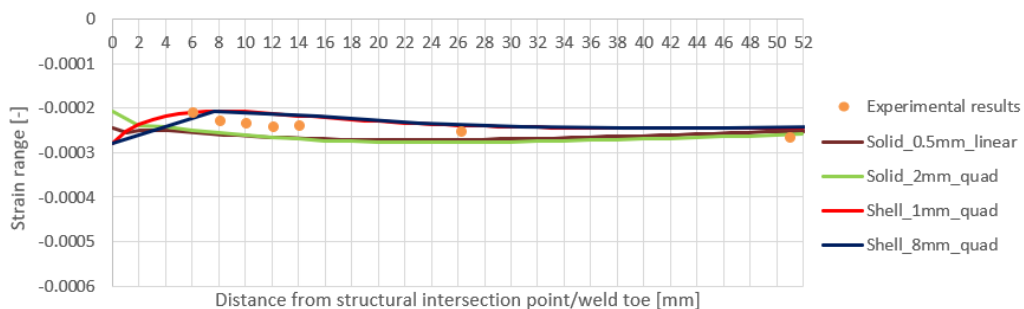


Figure 3.32 Strain validation solid and shell FE model X-direction trough, in span

#### 3.2.4. Conclusions based on validation of the different models

##### Solid FE model

For the strain ranges in Y-direction, the results of the first 5 strain gauges matches quite well with the experimental results, for both the linear and quadratic solid elements. The average difference with the experimental results of the first five strain gauges is 6%, for the quadratic elements, and 2.5% for the linear elements. A side note should be placed here is that the difference in hot spot stress range between the 0.5mm and 1mm linear element size is 5%. Elements smaller than the 0.5mm are not applied because it will increase the computational time in a significant way when compared with the 2mm quadratic elements.

At 25.6mm the difference, for both element types, with the experimental results, is around 15-20%, but at the location of the last strain gauge, which is at 51mm, the difference is 6%. The larger difference in results between the FE model and experimental results at 25.6mm can be due to a locally smaller thickness of the trough at that location due to fabrication tolerances.

The strain range in X-direction on the free edge side, shows good compliance with the experimental results, the average difference is 4% and furthermore the results are conservative. The results in X-direction on in-span side are also within 10% difference on average. Only the first measured point has a larger difference which is 16%. For all the three investigated validation paths the results of the FE models are conservative at almost all locations. Only at the location of the last 2 strain gauges in horizontal direction, which are at 25 and 50mm from the weld toe, non-conservative results occur, but the difference in percentage is only 1 and 3%. Based on the performed element refinement study it can be concluded that an element size of 2mm gives stable results.

### **Shell FE model**

From the strain range in Y-direction it can be concluded that the results close to the structural intersection point are depending on the elements size. The smaller the element size, the larger the strain range at the location of the structural intersection point. The average difference for the first 6 strain gauges is only 4.2%, while for the last strain gauge the difference is 30%, but since the measured strain range at that location is relatively small, a small difference in obtained stress will result in a large difference in percentage.

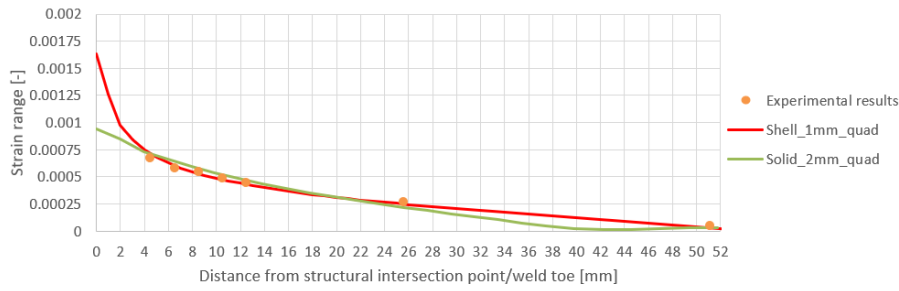
The strain range in X-direction on the free edge side, has an average difference between the FE model and experimental results of 9%. The trendline of the FE model is also in compliance with the trendline from the experiments. All results from the FE model are non-conservative. At the in-span direction also all results obtained from the FE model are non-conservative and the average difference between the experiment and FE model is 9%. Based on the performed element refinement study it can be concluded that an element size of 1mm gives stable results using shell elements.

#### *3.2.5. Comparison results shell and solid models*

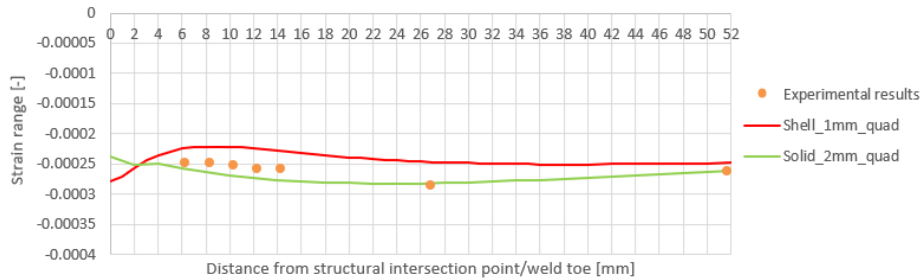
Now that the element sizes in which convergence occurs are known a comparison between the solid and shell FE model can be made. The results for all 3 investigated locations is shown in Figure 3.33 to Figure 3.35.

As can be seen from Figure 3.33, the results obtained from the quadratic solid and shell elements are quite similar. In the first 4mm there is an overestimation of the strain range by the shell model, this is due to the large stress concentration which occurs at the structural intersection point. The stress concentration at the structural intersection point of the shell model, is 1.95 times larger than the stress concentration which occurs at the weld toe in the solid model. From 5 to 15mm the trendlines of both elements are close to each other. After 25mm a larger difference between the shell and solid model occurs, but it should be noted that at 51mm both elements show a strain range which is almost the same.

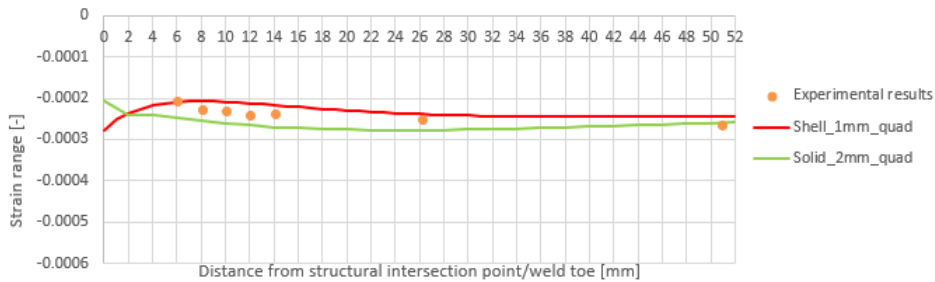
In Figure 3.34 the results for the X-direction free edge are shown and larger differences between both type of elements occur for this case. The shell elements are underestimating the strain range, while the solid elements are overestimating the strain range when compared with the experimental results. As with the results in Y-direction, also for this direction a stress concentration occurs at the structural intersection point. The trendline of both elements is more or less the same from 8 to 25mm, but in the first 8mm the trendlines are opposite to each other. Similar observations are also valid for X-direction in-span for which the results are shown in Figure 3.35. A comparison between the obtained hot spot stress range for both element types will be performed in chapter 4.



**Figure 3.33 Y-direction: comparison 1mm quadratic shell element with 2mm quadratic solid element**



**Figure 3.34 X-direction free edge: comparison 1mm quadratic shell element with 2mm quadratic solid element**



**Figure 3.35 X-direction in-span: comparison 1mm quadratic shell element with 2mm quadratic solid element**

### 3.2.6. Comparison of measured geometry versus ideal geometry

For the validation of the model, the geometry of the cope hole and weld is measured as precisely as possible. Engineering firms use the ideal geometry to model the OSD so a comparison is made between those two situations to see if large differences occur. Three differences with the ideal geometry were measured and those differences are: radius of the cope hole, see “X” in Figure 3.36a, the length from the trough to the curved part of the cope hole, i.e. soft toe, see “Y” in Figure 3.36a, and the weld geometry at the location of the trough and cope hole, see Figure 3.36b.

The ideal radius of the of the small curved part of the cope hole is equal to 20, while the measured radius is equal to 21mm. A larger difference is found with the measured length soft toe, 16mm, since the ideal length is equal to 10mm. The ideal throat thickness of the welds is 5mm, while the throat thickness of the vertical weld at the web of the trough is measured as 6.1mm, see “a” in Figure 3.36b. The ideal weld leg length is 7.07, see “X1” in Figure 3.36b, while the measured one is equal to 12mm. All differences are summarized in Table 3-9.

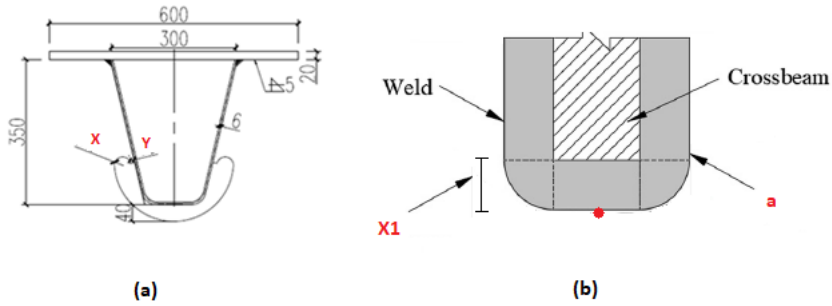


Figure 3.36 Overview differences between ideal and as-measured geometry

Table 3-9 Overview as-measured and ideal geometry

Variable	Theoretical value [mm]	As-measured value [mm]
Length soft toe (Y)	10	16
Radius cope hole (X)	20	21
Throat thickness weld web trough (a)	5	6.1
Weld leg length (X1)	7.07	12

In Figure 3.37, Figure 3.38 and Figure 3.39 the results for the vertical and horizontal direction are shown.

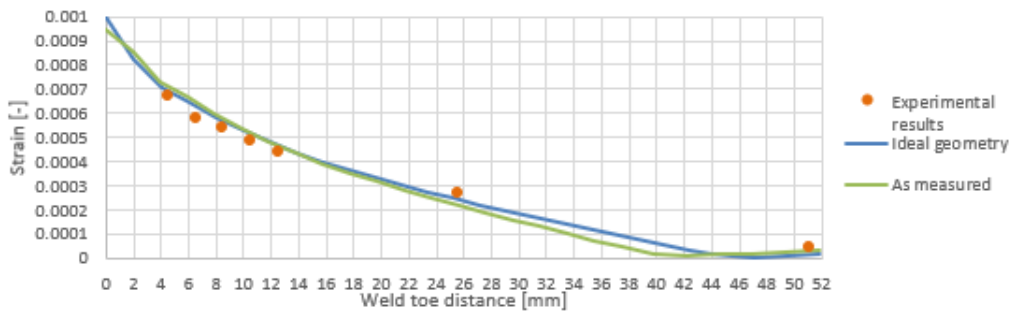


Figure 3.37 Comparison ideal geometry and as-measured Y-direction , strain in Y-direction

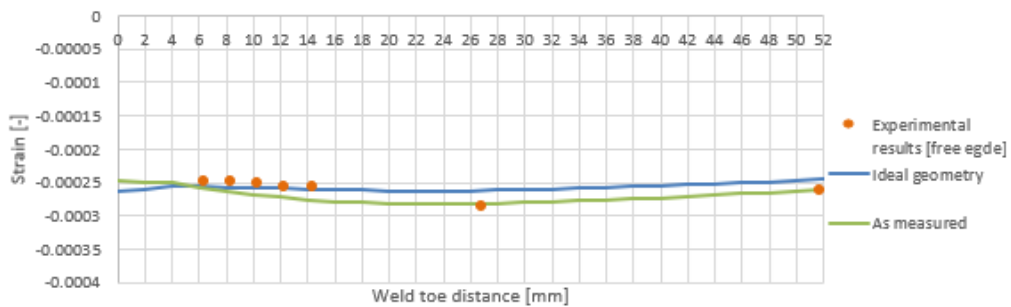


Figure 3.38 Comparison ideal geometry and as-measured X-direction free edge, strain in X-direction

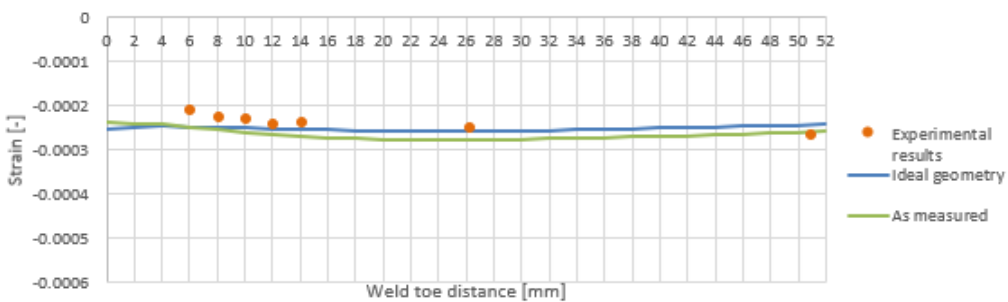


Figure 3.39 Comparison ideal geometry and as-measured X-direction in span, strain in X-direction



As can be seen from Figure 3.37, the graphs of the ideal and as-measured geometry are almost the same for the first 22mm. After 22mm a difference can be seen until approximately 42mm. Since the weld leg length in the as-measured model is equal to 12mm, while the ideal weld leg length is equal to 7.07mm, the location of the weld toe for both models is not the same, a difference of 5mm occurs between both models. When the results of both FE models are compared with the experimental results, the values are similar for the first 5, and last strain gauge. Only at the strain gauge, which is 26.8mm away from the weld toe a difference occurs.

The vertical distance between the strain gauges in X-direction from the lower edge of weld toe, see red dot in Figure 3.36b, is equal to 20mm. Since this value is related to the weld leg length, X1, also the read out point for the strain ranges is different in both models in X-direction. For both the horizontal free edge and in-span direction the strain range is constant over the measured length of 50mm, for the ideal geometry. The as-measured strain range shows a trendline which is similar with the experimental results. The results of the obtained strain ranges from the ideal geometry FE model are a bit closer to the experimental results, but the trendlines are clearly different. The difference between the ideal and as-measured geometry remains more or less constant over the measured length.

Overall it can be concluded that the differences in results between the ideal geometry and the as-measured geometry is around 6% in this specific case. Even with a relatively large difference in geometry, weld leg length 12mm instead of 7.07mm and the length of the soft toe equal to 16mm instead of 10mm, the difference in results is not significant. Applying the ideal geometry instead of the as-measured geometry is a good approximation, since the differences are small. The ideal geometry is much faster and easier to model. Furthermore obtaining the exact geometry is very time consuming and thus expensive and at some locations, for instance the throat thickness of the weld, still difficult to measure very accurately. Moreover in case of the design of an OSD bridge measuring the as built measurements is not possible, since the bridge is not build yet.

## 4. FATIGUE ASSESSMENT BASED ON HSS METHOD REFERENCE MODELS

In this chapter the fatigue strength assessment method based on the hot spot stress method will be performed using the solid and shell reference FE model of the orthotropic steel deck. Different extrapolation types will be used: linear and quadratic. Furthermore, a “fine” and “coarse” element size will be used for the FE models. A detail category of 100 is used for the calculation of the fatigue assessment as was concluded in section 2.4.2. The fatigue assessment is based on the crack in the trough at the lower end of the weld flank.

### 4.1. HSS results from experiments

Based on the results of the experiments performed by (Wu & Kolstein, 2020), the hot spot stress can be determined based on the strain measurements. The IIW recommendations are followed for obtaining the hot spot stress at the weld toe. Since the weld toe is located on the surface of the plate this type of hot spot is classified as type a. Since the first strain gauge is located at a distance which is larger than 0.4t, a trendline is used to determine the required value at 0.4t. For obtaining this trendline the results of the multistrip strain gauges which are at 4.5 to 12.5mm from are used. First the strain range at the specific location is calculated and multiplied with the Young’s modulus, of 210GPa, to obtain the hot spot stress at the weld toe.

#### Hot spot stress vertical direction

When a series of strain gauges are attached, the linear extrapolation trend line can be applied. After multiplying the  $\epsilon_{ns}$  with the Young’s modulus a hot spot stress of 183.75 MPa is obtained.

### 4.2. HSS results from Finite element models

The hot spot stress is obtained from the different FE models and calculated based on linear and quadratic extrapolation. In section 3.2.3.1 it is concluded that a singularity will occur at the weld toe. this singularity is not taken into account in the fatigue analysis, since extrapolation points which are at a certain distance from the weld toe are used for the calculation of the hot spot stress method.

Based on the IIW recommendations both linear and quadratic extrapolations methods can be used. For linear surface stress extrapolation the strains at 0.4t and 1.0t are required, while for quadratic extrapolation the strains at 0.4t, 0.9t and 1.4t are required. The formulas for obtaining the hot spot stresses can be found in section 2.4.2. A further distinction is made between the “fine” and “coarse” element sizes. An overview of the results can be found in Table 4-1 in which a distinction is made between the different type of extrapolation and element sizes.

Table 4-1 Overview results HSS extrapolation vertical direction

	HSS extrapolation points	HSS solid [MPa]	HSS shell [MPa]	$\frac{\sigma_{HSS\_shell}}{\sigma_{HSS\_solid}}$
<b>Vertical direction</b>				
<b>coarse mesh type a</b>	0.5t and 1.5t	180.24	224.83	1.25
<b>fine mesh type a linear</b>	0.4t and 1.0t	195.93	236.28	1.21
<b>fine mesh type a quadratic</b>	0.4t, 0.9t and 1.4t	203.34	257.55	1.27

The hot spot stress results are depending on the size of the element and on which type of extrapolation is used. The coarse meshed models, with an element size equal to 4mm, 0.67t, give a bit lower hot spot stress results, when compared with fine meshed models, which have an element size of 1mm, 0.167t, for the shell elements and 2mm, 0.33t, for the solid elements. Also the type of extrapolation, linear or quadratic, will influence the results. Since the stress concentration at the weld toe is smaller for the solid FE model, the difference between the linear and quadratic hot spot stress extrapolation is less. With the fine meshed models the stress concentration, and thus the trendline of the stress, which occurs at the structural intersection point can be better approximated by the FE model. This will result in more accurate results when compared with the relatively coarse meshed models. The performed study based on the element size shows that a refined solid element model with global size of 2mm show higher values than the 4mm one. An refined model with element size of 1mm is applied for the shell FE model.

#### Comparison results shell and solid FE models

As can be seen from Table 4-1, the obtained hot spot stress with shell elements is higher in all cases when compared with the hot spot stress results from the solid model. The ratio between the coarse element models is 1.25, while the ratio for the fine element models the ratio is 1.21 with linear extrapolation, and 1.27 with quadratic extrapolation. The overestimation of the hot spot stress is 25% when compared with the results obtained from the solid FE models.

### 4.3. Comparison FE model solid and experimental results

The hot spot stresses for both the experiment and finite element modelling, with solid elements, were calculated and an overview of the results in shown in Table 4-2.

Table 4-2 Overview experimental and FE model results HSS

	HSS extrapolation points	HSS solid model [MPa]	Experiment [MPa]	$\frac{\sigma_{HSS\_solid}}{\sigma_{HSS\_exp}}$	$\frac{\sigma_{HSS\_shell}}{\sigma_{HSS\_exp}}$
<b>Vertical direction</b>					
<b>Linear extrapolation</b>	0.4t and 1.0t	195.93	183.75	1.07	1.29
<b>Quadratic extrapolation</b>	0.4t, 0.9t and 1.4t	203.34	-	1.10	1.40

As can be seen from Table 4-2, the results of the hot spot stress of the solid FE model are close to the experimental results, the difference is 7% for the linear extrapolation and 6% for the quadratic extrapolation. In both cases the hot spot stress obtained from the FE model are higher than the experimental results and thus the results are conservative. The solid FE element model includes the geometry of the joint and the geometry of the weld, while the shell FE model only includes the former one and thus the solid FE model gives a better approximation of reality. With the shell FE model a larger overestimation of the hot spot stress is obtained which is equal to 29-40%.

## 5. TRANSVERSE STIFFENER CONNECTION: WELD MODELLING TECHNIQUES SHELL FE MODEL

In this chapter it is investigated if different weld modelling techniques for the shell FE models are valid for a simple connection. This is investigated for a single sided fillet welded transverse attachment joint. In total 4 different models are compared: solid, shell without weld, shell weld IIW and shell weld Eriksson. The comparison will be made for both the obtained stresses and the deformations. The latter is done to see if the bending stiffness of the adapted shell models is in compliance with the solid FE model bending stiffness. Furthermore different type of load cases are applied to simulate in-plane and out-of-plane behavior of the specimen.

The investigated joint is similar to the trough to crossbeam connection in the OSD. An overview of the specimen is shown in Figure 5.1. In total two geometrical variants will be investigated in which the plate thicknesses are the same as the thickness of the trough and crossbeam in the old and new OSD design. As was concluded in section 2.3.3 the old and new OSD designs have different plate thicknesses. The thickness of the trough is equal to 6mm for the old OSD design and equal to 8mm for the new OSD design which is matching with the thickness of the main plate. The thickness of the crossbeam is equal to 12mm and 16mm for the old and new OSD design respectively which is similar with the stiffener plate, see Table 5-1. The throat thickness of the fillet weld is equal to 5mm.

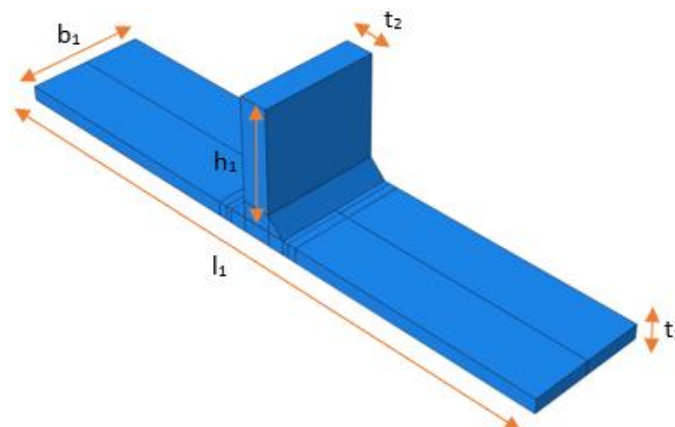


Figure 5.1 Overview geometry FE model

Table 5-1 Overview dimensions specimen

Length ( $l_1$ )	250mm
Width ( $b_1$ )	50mm
Height ( $h_1$ )	50mm
Thickness main plate ( $t_1$ )	6mm or 8mm
Thickness stiffener plate ( $t_2$ )	12mm or 16mm

### Boundary conditions

The specimen is constrained at one end by a pinned constraint and at the other end by a roller constraint which is shown in Figure 5.2.

### Material properties and applied loading

Steel with a Young's modulus of 210.000 MPa and a poisson ratio of 0.3 is used. Four different load cases will be applied which are shown in Figure 5.2. For load case 1 (LC1) an uniform in-plane load of 1N/mm<sup>2</sup> is applied while for LC2 a bending moment of 0.12kNm is applied over the width direction of the stiffener. For the new design variant this bending moment is scaled by the plate thickness of the

stiffener plate and a uniform bending moment of 0.21kNm is applied which will result in similar stresses as with the old variant. For LC3 the same load is applied, but applied at the thickness direction of the stiffener, which will result in torsion. The fourth load case is a combination of LC1 and LC2: uniform tension load and out-of-plane bending.

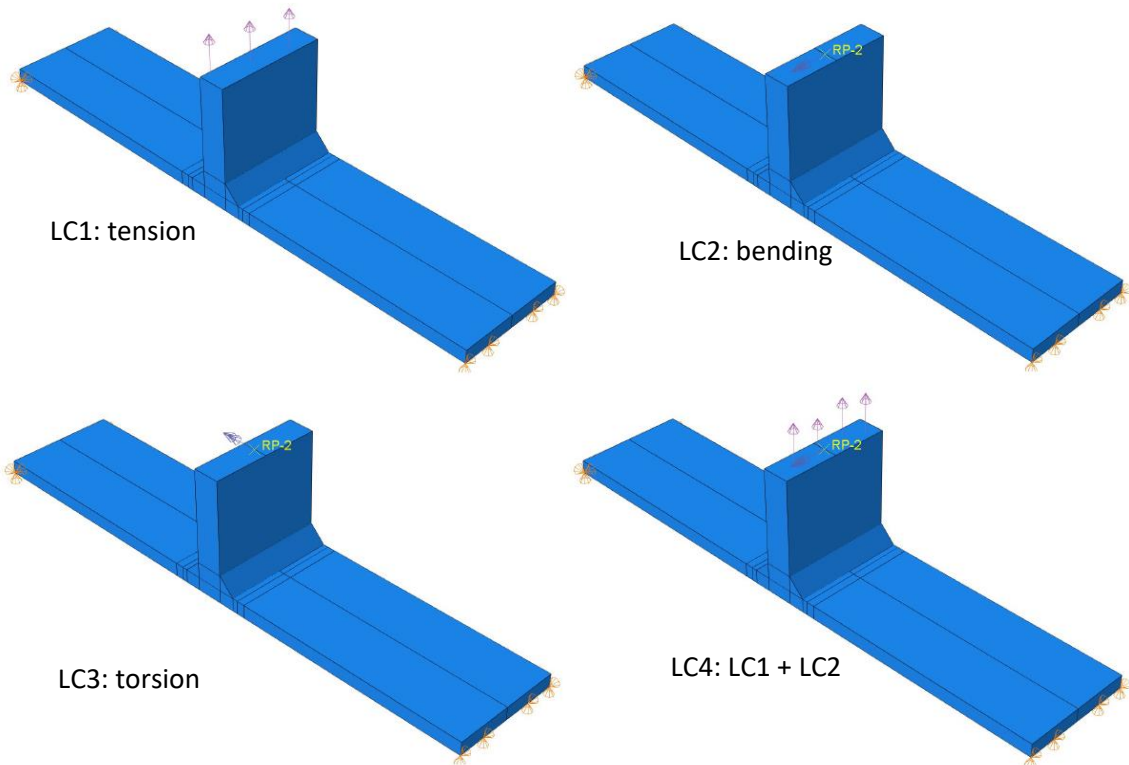


Figure 5.2 Overview different loading cases

#### Elements used and mesh size

For the shell elements use is made of 8-noded quadratic elements, S8R, while for the solid elements use is made of 20-noded quadratic elements, C3D20R. An element size of 2mm is used for the solid FE model and an element size of 1mm is used for the shell FE model. Furthermore the shell FE models are modelled based on mid-surface modelling. An overview of the mesh for both the shell and solid FE model is shown in Figure 5.3.

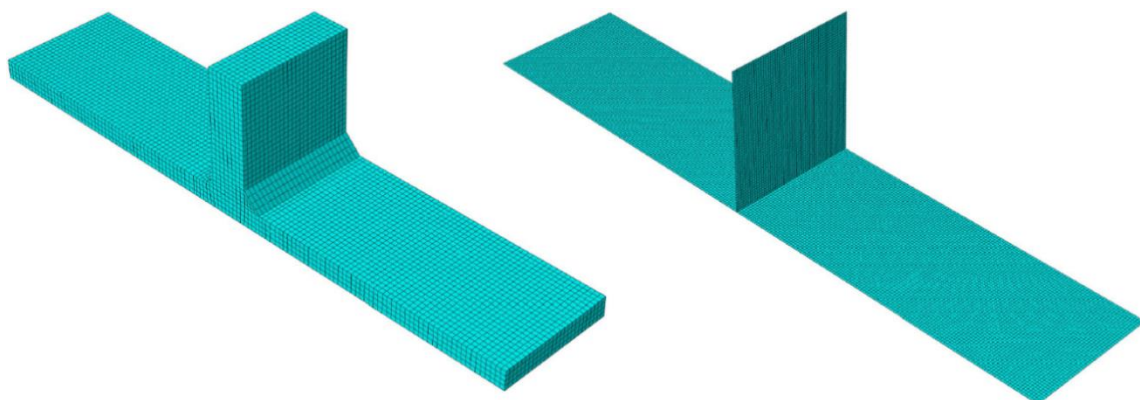


Figure 5.3 Overview meshed FE models. Left: solid FE model and right: shell FE model

### Weld modelling techniques shell FE models

Two different types of weld modelling techniques are investigated which are similar to the weld modelling techniques for the OSD. On the left side of Figure 5.4 the IIW approach is shown in which only the thickness of the stiffener plate is locally increased by the weld leg length. In the right figure the Eriksson approach is shown in which both the main plate and the stiffener plate are increased by the weld throat thickness. Both adapted shell FE models and the shell model without weld are compared with the solid FE results. The weld modelling techniques are discussed in section 2.6.2.

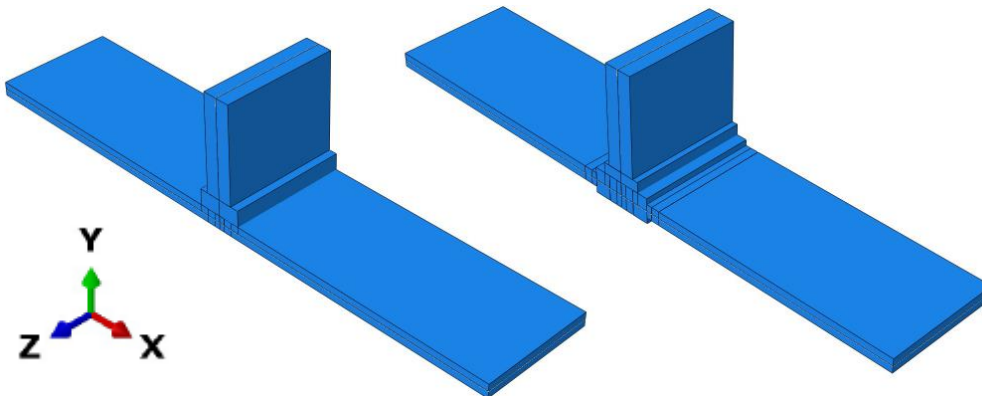


Figure 5.4 Different weld modelling techniques: IIW (left) and Eriksson (right)

The Eriksson weld modelling approach is based on a cruciform joint and for this type of joint the thickness of both plates is locally increased with:  $t+a$ . Since the investigated joint is similar to a T-joint geometry, which is basically half of cruciform joint, an additional model will be made in which the thickness of the main plate is increased with  $t+0.5a$ , instead of  $t+a$ . The model in which the thickness of the main plate is locally increased with  $t+a$  is named: Eriksson I, while the model in which the main plate is increased with  $t+0.5a$  is named: Eriksson II.

### Results

As was stated earlier, both the results of the stress and the deformations are compared. For the stress extrapolation the results of the path which is shown in Figure 5.5 (left) are compared. The deformations in X, Y and Z-direction at the top of the stiffener are compared for the comparison of the bending stiffness, which is shown in Figure 5.5 (right). Also the path for the deformation extrapolation is shown in this figure.

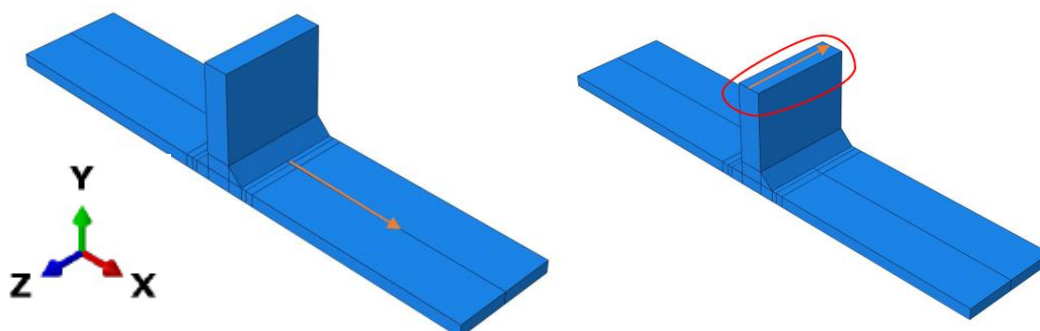


Figure 5.5 Stress extrapolation path (left) and deformation extrapolation path (right)

In Figure 5.6 the comparison of the stress is made for the old OSD dimensions, thickness main plate 6mm, thickness stiffener 12mm, for LC4. The other load cases and the graphs of the new OSD variant can be found in Annex J.

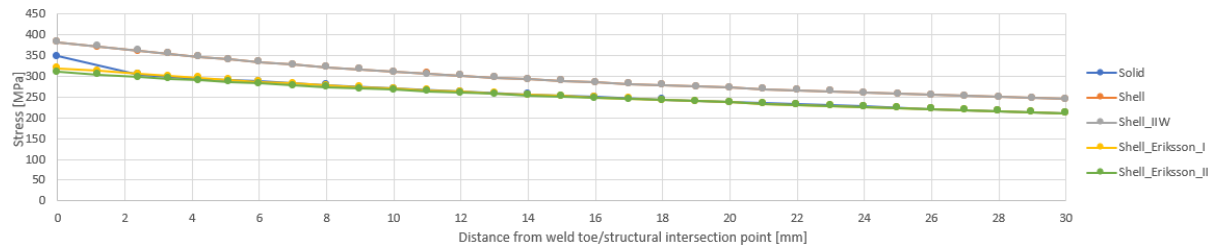


Figure 5.6 Stress range load case IV: combination in-plane and out-of-plane I, old variant

As can be seen from the figure, the shell without weld and the shell weld with the IIW approach show very similar results. For those two FE models the structural intersection point of the two plates is taken as the starting point. For the solid and shell weld with the Eriksson approach the weld toe is taken as the starting point. The shell with the Eriksson weld modelling approach give results which are very similar to the solid FE model results. An overview of the obtained hot spot stress results is shown in Table 5-2 for both the old and new OSD design variants. An overview of the ratios is shown in Table 5-3.

Table 5-2 Overview obtained hot spot stress results old OSD variant thicknesses

		Solid [MPa]	Shell [MPa]	Shell weld IIW [MPa]	Shell weld Eriksson I [MPa]	Shell weld Eriksson II [MPa]
LC1: in-plane-uniform load	Old OSD	118.89	144.69	144.52	120.95	117.62
	New OSD	86.96	106.27	106.32	85.87	84.02
LC2: out-of-plane bending I	Old OSD	195.32	233.83	234.72	196.92	191.15
	New OSD	189.59	229.70	230.10	187.86	183.18
LC3: out-of-plane bending II	Old OSD	0.00	0.00	0.00	0.00	0.00
	New OSD	0.00	0.00	0.00	0.00	0.00
LC4: combination LC1 and LC2	Old OSD	314.33	378.53	379.26	317.87	308.77
	New OSD	276.51	335.97	336.43	274.42	267.80

Table 5-3 Overview ratios HSS different FE models

		$\frac{\sigma_{HSS\_shell}}{\sigma_{HSS\_solid}}$	$\frac{\sigma_{HSS\_shell\_IIW}}{\sigma_{HSS\_solid}}$	$\frac{\sigma_{HSS\_shell\_Eriksson\_I}}{\sigma_{HSS\_solid}}$	$\frac{\sigma_{HSS\_shell\_Eriksson\_II}}{\sigma_{HSS\_solid}}$
LC1: in-plane-uniform load	old OSD	1.22	1.22	1.02	0.99
	new OSD	1.22	1.22	0.99	0.97
LC2: out-of-plane bending I	old OSD	1.20	1.20	1.01	0.98
	new OSD	1.21	1.21	0.99	0.97
LC3: out-of-plane bending II	old OSD	1	1	1	1
	new OSD	1	1	1	1
LC4: combination LC1 and LC2	old OSD	1.20	1.21	1.01	0.98
	new OSD	1.22	1.22	0.99	0.97

For the old design variant, thickness main plate 6mm, thickness stiffener 12mm, the results of the obtained hot spot stress of the solid FE model and shell weld Eriksson I FE model, in which both plate thicknesses are locally increased with  $t+a$ , are within 1.5%. The shell weld Eriksson I hot spot stress

results are a bit higher when compared with the solid. Both the shell model without weld and the shell model with the IIW weld will result in an overestimation of the hot spot stress of 20%. For the new design variant, thickness main plate 8mm, thickness stiffener 16mm, the obtained hot spot stress results of the solid and Eriksson I FE models are also within 1%. In this case the obtained hot spot stress of the shell weld Eriksson I is lower, i.e. 0.70%, when compared with the solid FE results. Applying the IIW weld modelling technique will hardly influence the results for this investigated detail. If the Eriksson II weld modelling approach is applied, in which the thickness of the main plate is locally increased with  $t+0.5a$  instead of  $t+a$ , the hot spot stress is underestimated for both the new and old OSD design variant. The results of the Eriksson I weld modelling approach are better matching with the solid FE results. Based on the obtained hot spot stresses this method is preferable.

### Comparison deformations

A similar study as was performed with obtaining the hot spot stress is also performed for the deformations. The four different load cases will all result in a deformation which is predominantly in one or two directions. The in-plane load (LC1) will result in deformation in predominantly Y-direction, while the out-of-plane load I (LC2) will result in deformation predominantly in X-direction. The out-of-plane-load II (LC3) will result in both deformation in Y- and Z-direction, respectively. Load case 4 (LC4), which is a combination of the in-plane load and out-of-plane loading will result in both deformations in X- and Y-direction. The deformations in the other directions are smaller than  $10^{-3}$ mm and not taken into account.

In Figure 5.7 to Figure 5.9 the deformations for load case four (LC4) are shown. The results for the other load cases and the results of the new OSD variant are shown in Annex J.

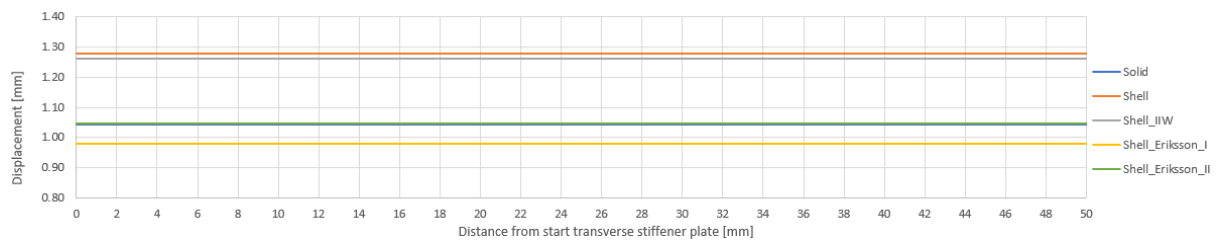


Figure 5.7 Total deformation U, load case IV: combination in-plane and out-of-plane I, old variant



Figure 5.8 Deformation U1 (X-direction), load case IV: combination in-plane and out-of-plane I, old variant

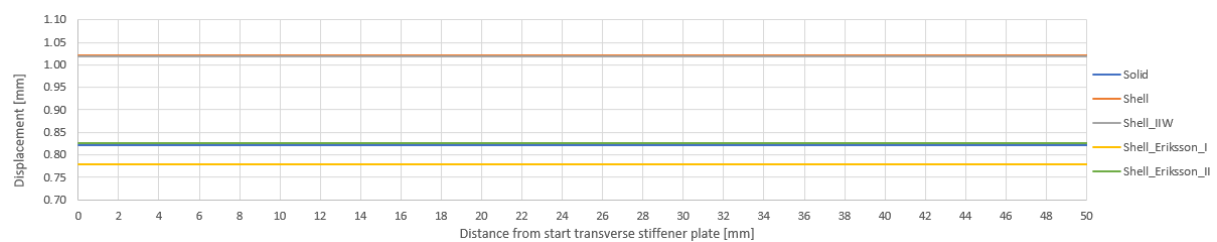


Figure 5.9 Deformation U2 (Y-direction), load case IV: combination in-plane and out-of-plane I, old variant



The weld modelling approach proposed by (Eriksson, Lignell, Olsson, & Spennare, 2003) shows good results for all four investigated load cases when the deformation is compared with the solid FE results. The results are plus and minus 3% for the individual load cases, and depend on the loading type. Applying LC1 and LC2 at the same time, the difference between the solid FE model and shell weld Eriksson I is equal to 6%. It can be concluded that for this simple specimen the weld modelling approach proposed by Eriksson is a good method to simulate the weld with the shell FE model.

#### **Overall conclusions differences t+a and t+0.5a Eriksson weld modelling technique**

When the differences in deformation between the Eriksson I and Eriksson II weld modelling techniques concluded that the deformations of the Eriksson II weld modelling technique are higher when compared with the solid FE model, while the Eriksson I weld modelling technique give slightly smaller deformations, i.e. 6% for the investigated load cases, expect load case 3 (torsion load case). With this load case the deformations are 4% larger when compared with the solid FE results. With the Eriksson II weld modelling technique, in which the main plate thickness is locally increased with t+0.5a the deformation are a bit higher, i.e. within 5%, when compared with the solid deformations. Based on this observation the bending stiffness of the Eriksson II approach is lower compared with the solid FE models.

For the hot spot stress extrapolation, the Eriksson II weld modelling technique gives a hot spot stress which is lower than the obtained hot spot stress of the solid FE model. This will result in a non-conservative hot spot stress. The Eriksson I weld modelling technique is overestimating the hot spot stresses for all the investigated load cases of the old OSD variant. With the new OSD variant the Eriksson I weld modelling technique is underestimating the hot spot stress, by only 0.70%.

When the hot spot stresses are compared the Eriksson I weld modelling technique give results which are closer to the solid FE model when compared with the Eriksson II technique. The Eriksson II weld modelling technique gives non-conservative hot spot stresses. Since the main task of this thesis is to perform the comparison of the hot spot stress of different FE models, the Eriksson I weld modelling technique is preferable since the results are better matching and conservative when compared with the solid FE model.

#### **Hot spot stress results in transverse attachment plate**

Furthermore the comparison between the obtained hot spot stress in the stiffener is made for the solid FE model and the shell weld Eriksson I FE model. The extrapolation is performed in the middle of the stiffener plate, as was also the case with the main plate. This investigation is performed for load case 2 and 4 for which the results are shown in Table 5-4. The corresponding graphs with the stress in the stiffener can be found in Annex J. As can be seen from Table 5-4, the obtained hot spot stress with the shell Eriksson I weld modelling approach is lower when compared with the solid FE hot spot stress results. The obtained ratio is equal to 0.95-0.99.

**Table 5-4 Overview obtained hot spot stress results stiffener**

		<b>Solid [MPa]</b>	<b>Shell Eriksson I [MPa]</b>	$\frac{\sigma_{HSS\_shell\_Eriksson\_I}}{\sigma_{HSS\_solid}}$
<b>LC2: out-of-plane bending I</b>	<b>Old OSD</b>	108.57	103.80	0.96
	<b>New OSD</b>	106.92	102.00	0.95
<b>LC4: combination LC1 and LC2</b>	<b>Old OSD</b>	109.03	107.75	0.99
	<b>New OSD</b>	107.50	105.08	0.98

## 6. PARAMETRIC STUDIES

In this chapter, a comparison of the FE models using shell and solid element is carried out with different geometric variants and load cases. First both the parametric studies will be explained in detail. The solid FE model will be used as reference for the analysis as good agreement was found in section 3.2. The results of the shell FE model are compared with the results from the solid FE model. The following two crack locations are studied in this chapter: longitudinally in the trough starting from the weld end at the lower weld toe adjacent to the cope hole and in the crossbeam parallel to the weld toe at some distance from the soft toe. Both cracks were shown in section 1.3. Different geometrical variants will be investigated in this chapter: the thickness of the different parts of the OSD, i.e. trough, deck plate and crossbeam, and furthermore one axle loading from fatigue load model 4 (FLM4) will be used: axle type C.

### 6.1. General information of parametric studies

#### 6.1.1. Geometric information FE model

The basis of the FE model which is used for the parametric studies is different on several points when compared with the FE model which was used for the validation of the OSD in section 3.2. This validation of the FE model was based on the as-measured dimensions. To make the results of the parametric analysis more general, the nominal dimensions of the trough, cope hole and weld are used. Furthermore, since the focus of this thesis is on the crossbeam with a cope hole, all troughs will pass the crossbeam through a cut-out with cope hole. Another point of attention is that in the validation of the OSD, the full bottom flange of the crossbeam was supported, and thus in-plane deformation was fully prevented. To make the FE model more realistic, other boundary conditions are applied which will also result in in-plane deformation of the crossbeam. To simulate the main girder, both ends of the crossbeam are constraint in X,Y and Z-direction over the full height, as can be seen in Figure 6.3.

Since the point of interest is the local behavior of the connection of the crossbeam and trough at the location of the cope hole, a smaller part of the overall global FE model can be modelled. This model consists of three crossbeams in which the crossbeam of interest is the middle one. The height of the web of the crossbeam is equal to 1200mm and the length is equal to 12.5m. The web of the crossbeam has a thickness of 12 or 16mm, depending on the old or new design of the OSD. The thickness of the bottom flange is equal to 25mm and the width of the bottom flange of the crossbeam is 350mm. The troughs have a center to center distance equal to 600mm, thus 19 troughs are modelled for the crossbeam which is shown in Figure 6.1. The distance from the outer side of the crossbeam to the web of the first trough is equal to 700mm. The dimensions of the crossbeam are determined in cooperation with Rijkswaterstaat.

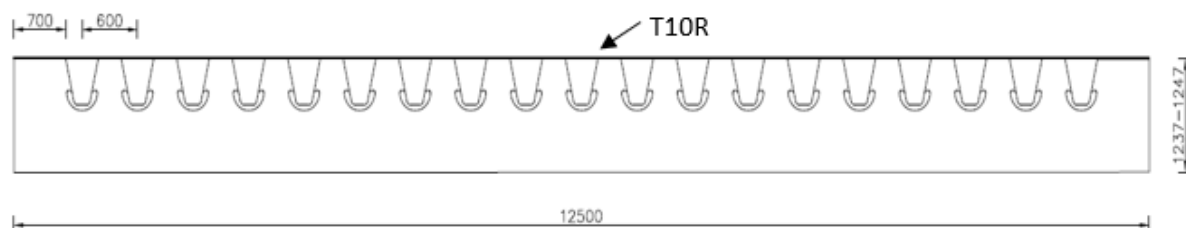
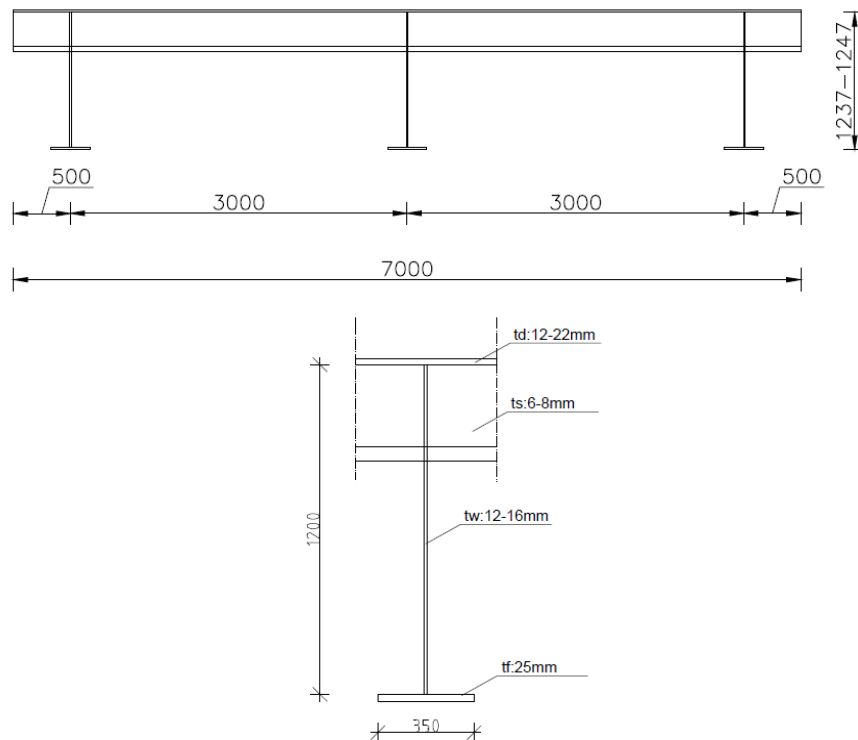


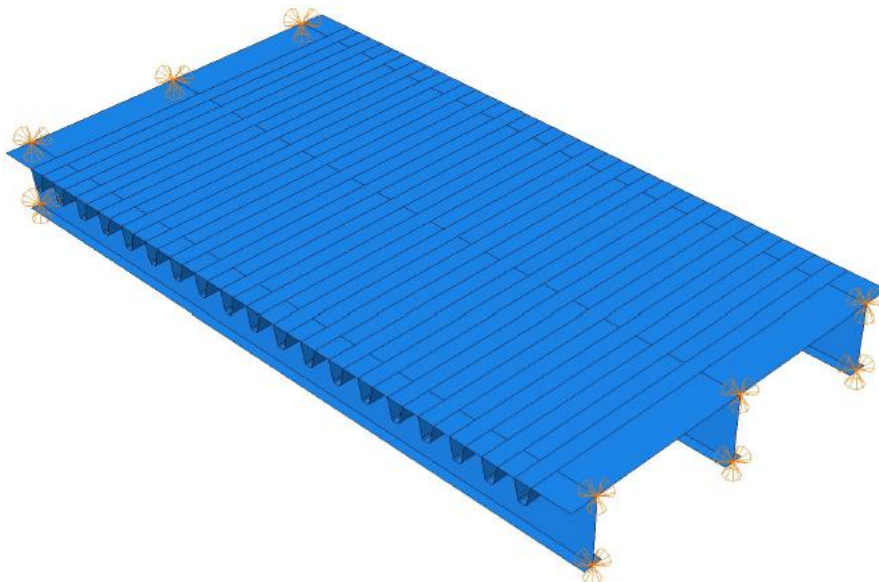
Figure 6.1 Overview dimensions crossbeam [mm]

A sideview of the bridge is shown in Figure 6.2 in which the considered ranges in thickness of the deck plate and web of the crossbeam are shown. At both sides of the outer crossbeams the deck plate is extended by 500mm and thus the overall dimensions of the FE model, are 12.5m by 7m.



**Figure 6.2 Side view dimensions bridge and variation dimensions [mm]**

An overview of the global shell FE model is shown in Figure 6.3.



**Figure 6.3 Overview global shell FE model**

#### 6.1.2. Old and new OSD dimensions

As stated in section 2.3.3, a distinction need to made between the thicknesses of different parts of the OSD for the old and new design. The main difference between the old and new OSD design are the thicknesses of the deck plate, crossbeam and trough. In Table 6-1 an overview of those differences

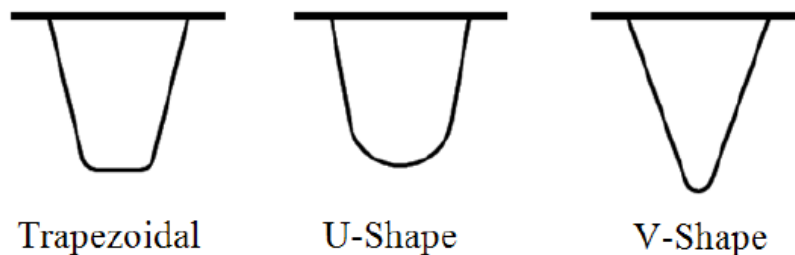
is shown, and these thicknesses form the basis for the variation cases. As with the dimensions of the crossbeam, the different thicknesses are also determined in cooperation with Rijkswaterstaat.

**Table 6-1 Overview investigated thicknesses parts OSD**

	Old OSD [mm]	New OSD [mm]
<b>Trough</b>	6	8
<b>Crossbeam</b>	12	16
<b>Deck plate</b>	12	22

### 6.1.3. Shape of the trough

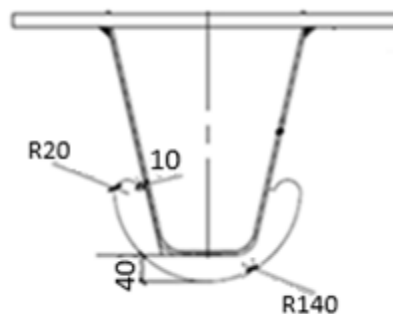
There are three different types of trough shapes which are used in OSD's: trapezoidal, V-shape and the U-shape, which are shown in Figure 6.4. The most commonly used shape is the trapezoidal (Federal highway administration, 2012) and this shape will form the starting point of this study. The geometric dimensions of this trapezoidal trough are the same as the dimensions which are used for the reference model and can be found in section 3.2.1.1. The troughs have a center to center distance of 600mm which is the same as for the reference models.



**Figure 6.4 Investigated trough shapes (Federal highway administration, 2012)**

### 6.1.4. Cope hole geometry

The Haibach cope hole will be investigated which is shown in Figure 6.5. Also the geometrical dimensions are shown in this figure.



**Figure 6.5 Overview geometrical variant cope hole**

### 6.1.5. Overview variants

Based on the above mentioned geometric variants the following variants will be investigated which are shown in Table 6-2.

**Table 6-2 Overview variants parametric study**

	Description	Shape trough	Shape cut-out	Deck plate [mm]	Trough [mm]	Crossbeam [mm]
<b>VARIANT 1</b>	Old variant 1	Trapezoidal	Haibach	12	6	12
<b>VARIANT 2</b>	New variant 1	Trapezoidal	Haibach	22	8	16

## 6.2. Small Parametric analysis

To get a better understanding about the differences in behavior between the shell and solid FE model, several loading positions are investigated first. This small study is performed for both the old and new OSD variant with a Haibach cope hole. Furthermore the differences in results between the new and old OSD variant will also be determined. The different loading positions will result in pure in-plane or pure out-of-plane rotation of the crossbeam which is shown in Figure 6.6. Three different types of loading will be investigated:

- pure in-plane global deformation crossbeam;
- pure in-plane local deformation crossbeam;
- pure out-of-plane rotation.

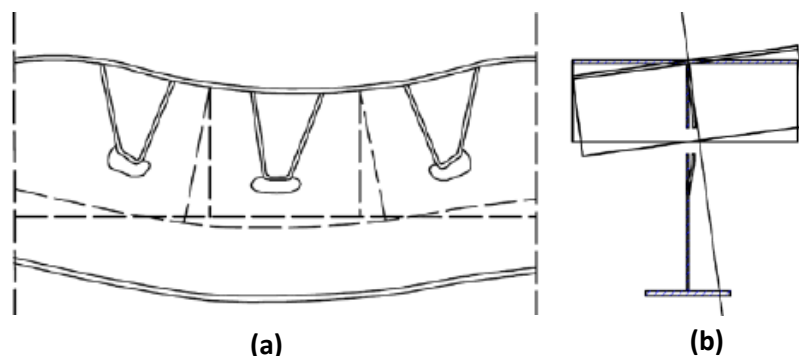


Figure 6.6 (a) In-plane rotation crossbeam and (b) out-of-plane rotation crossbeam (EN1993-2, 2011)

The wheel patch, which was used in section 3.2, is also used for this study: 270mm x 320mm and the total applied force equal to 100kN. For global pure in-plane deformation, the load will be applied at locations (1A')+(1A''), see Figure 6.7a, in which the load is applied on both sides of the crossbeam. The offset from the center of the load to the crossbeam is equal to 500mm and the loads are positioned between the webs of the trough, see position 1 in Figure 6.7b. For the pure out-of-plane rotation the same loading position, (1A')+(1A''), is used, but instead of placing both loads facing downwards, one load is placed upward and the other one downwards. This will result in pure out-of-plane rotation of the crossbeam, see Figure 6.6b. The last loading position is the local in-plane deformation of the crossbeam at the location of the cope hole. For this case the loads are placed at three different positions on top the crossbeam: between the webs of the trough, position 1 in Figure 6.7b, between the troughs, position 2 in Figure 6.7b, and on the web of the trough, position 3 in Figure 6.7b.

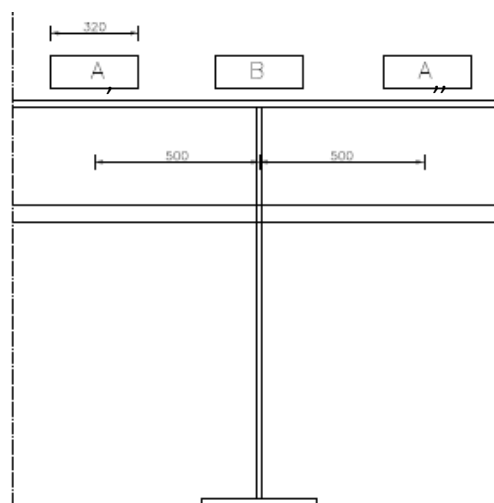
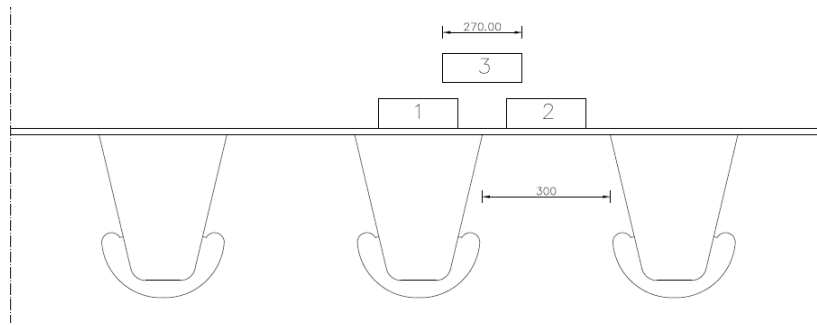


Figure 6.7a Loading positions longitudinal direction



**Figure 6.7b Loading positions transverse direction**

All five investigated loading positions are summarized below:

- Loading position 1 (LP1): 500mm offset from crossbeam, loaded between webs in-plane, (1A')+(1A'');
- Loading position 2 (LP2): 500mm offset from crossbeam, loaded between webs out-of-plane loading, (1A')+(1A'');
- Loading position 3 (LP3): on top of crossbeam, loaded between webs, local in-plane, 1B;
- Loading position 4 (LP4): on top of crossbeam, loaded outside webs, local in-plane, 2B;
- Loading position 5 (LP5): on top of crossbeam, loaded on web trough, local in-plane, 3B.

In the main part of the report only the results of loading position 1 and 2 for the old OSD variant are shown. The other loading positions and the similar study for the new OSD variant can be found in Annex E.

#### 6.2.1. Mesh sensitivity analysis

A study of the influence of the element size on the stress range, in the web of the trough and the crossbeam, is performed to obtain a stable element size for the solid and shell elements. In section 3.2.3.1 a similar mesh sensitivity analysis is performed for the OSD from the Stevinlab. Three different loading positions are investigated: loading position 1,2 and 3 which will result in different types of behavior of the crossbeam.

A similar mesh lay-out as was used in section 3.2.2 is also used for the mesh of this FE model. For both the solid and shell elements the results for the three investigated loading positions can be found in Annex D. Furthermore the local mesh for both FE models is shown. It is concluded that quadratic solid elements, C3D20R, with an element size of 2mm and quadratic shell elements, S8R, with an element size of 1mm, give converged results.

#### 6.2.2. Crack in trough (crack 1)

An overview of the investigated path for the crack in the web of the trough is shown in Figure 6.8. This path starts at the lower weld toe and continues perpendicular to the weld toe.

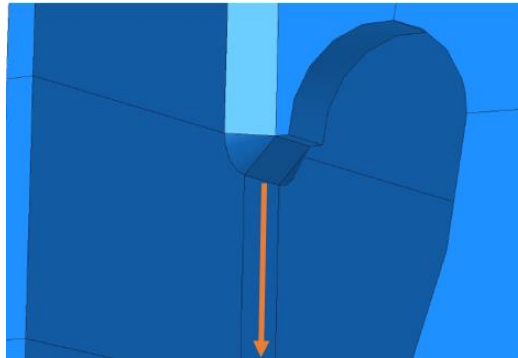


Figure 6.8 Overview path in web trough

### 6.2.3. Crack in crossbeam (crack 2)

#### 6.2.3.1. Critical crack location crossbeam

In an orthotropic steel deck in which a “Haibach” cope hole is used different types of crack can occur in which two cracks are shown in Figure 6.9 by the orange and blue lines. The blue crack initiates directly at the weld end of the crossbeam, see black dot (X=0) in Figure 6.9, while the orange crack occurs at some distance away from the soft toe, wherever the stress in the orange path is the largest.

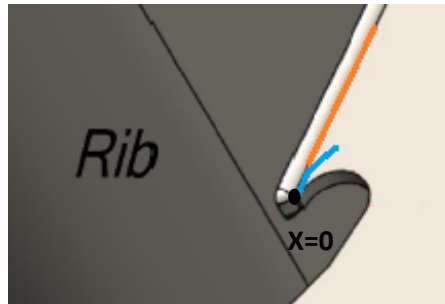


Figure 6.9 Different cracks which can occur in the crossbeam which Haibach cut-out (Kitner, 2016)

In an OSD with a regular “Haibach” cope hole the crack will initiate at X=0mm which is shown with the blue crack. If the improved “Haibach” cope hole is used it is not expected that a crack can occur, since there will be no stiffness which is because the crossbeam stops abruptly over there. To investigate this, both cracks are investigated to check which crack is the critical one. The local geometries of both types of cope holes is shown in Figure 6.10.

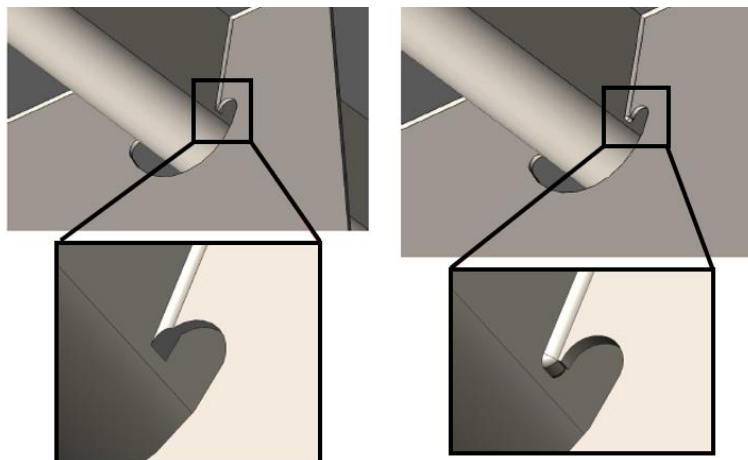


Figure 6.10 Overview local geometry cope with regular “Haibach” cope hole and cope hole with improved “Haibach” cope hole (Kitner, 2016)

The principal stress and the stress perpendicular to the weld toe will be compared for the following 2 cases: the red path (Path 1) with the green path (P1 TT) and the yellow path (Path 2) with the purple path (P2 TT), which is shown in Figure 6.11. In which TT stands for through thickness. The black dot, which is shown in Figure 6.11 is a singular point. Due to this reason this point is not taken into account in the comparison of the different stresses. The yellow path (Path 2) has an offset from the red path (Path 1) which is equal to 1.46mm, which is half of the length from the weld toe to the curved part of the cut-out. For the through thickness stresses the  $X=0\text{mm}$  is at the location of the black dot in the figure below.

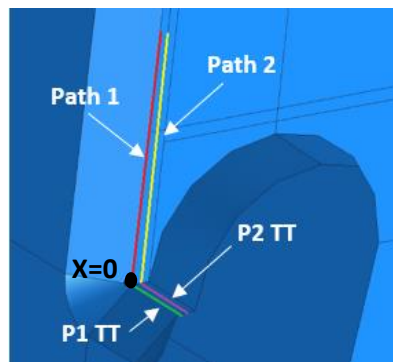


Figure 6.11 Overview investigated paths

This investigation is performed for the five loading positions are shown in section 6.2 and the results for those loading positions can be found in Annex F.

For all investigated load positions a high value occurs at  $X=0\text{mm}$ , due to the singularity, in both the red (Path 1) and green (Path 2) path from Figure 6.11. If the results of  $X=0\text{mm}$  are disregarded, the absolute maximum principal stress and stress perpendicular to the weld toe of the red path (Path 1) show higher stress values at the maximum location, i.e. approximate  $X=30\text{mm}$ , when compared with those same stresses through the thickness of the crossbeam, green path (P1 TT).

The stresses through the thickness of path 2, see purple line (P2 TT), in Figure 6.11, are very low which is because this path is at the end of the crossbeam and thus zero stiffness is at that location. The maximum obtained principal stress in this path is approximately 2MPa which occurs with loading position 6. The stress perpendicular to the weld toe is close to zero for the investigated load cases.

The highest stress in the path parallel to the vertical weld of the crossbeam occur at approximately  $X=30\text{mm}$  and those stress values are higher when compared with the stress through the thickness at  $X=0\text{mm}$  for all investigated load cases. **Based on this it can be concluded that the crack which initiates at some distance from the soft toe, is the governing crack.**

#### 6.2.3.2. Crack in crossbeam at some distance from soft toe

For a regular linear hot spot stress extrapolation, the stress need to be extrapolated at a distance of  $0.4t$  and  $1.0t$  from the weld toe. Depending on where the crack which initiate in the crossbeam, this regular hot spot stress extrapolation may not be possible. As can be seen from Figure 6.12, the distance from the trough to the rounded part of the cope hole, i.e. soft toe, is only 10mm which is marked with the red circle. This 10mm is without the weld modelled, which has a leg length of 7.07mm. This will result in an available path of only 2.93mm in which the thickness of the crossbeam is 12mm and the thickness of the trough 6mm. This 2.93mm is not sufficient to perform a regular hot spot stress extrapolation. If the crack will initiate at a height which is larger than 20mm, which is equal



to the radius of the small circle of the cope hole, see Figure 6.13, a regular hot spot stress extrapolation is possible.

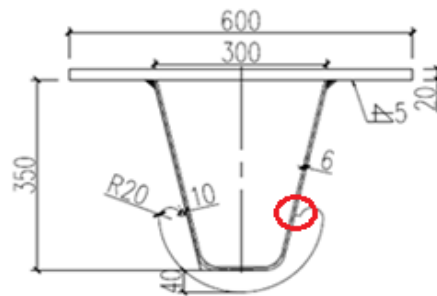


Figure 6.12 Overview dimensions trough and Haibach cope hole

Four different paths are investigated to see how the stress behavior is locally. The four different paths are shown in Figure 6.13. Path 1 is parallel to the weld toe, path 2 is also parallel to the weld toe with an offset of 1.47mm, which is  $0.5 \times 2.93\text{mm}$ , and path 3 has an offset from the weld toe which is equal to 2.93mm. Path 4 is chosen in the direction perpendicular to the crack initiation and the location of path 4 is where the stress perpendicular to the weld toe in path 1, 2 and 3 is maximum. This critical location in path 1, 2 and 3, forms the starting point of path 4. The starting point of path 1, 2 and 3 is the soft toe of the cut-out.

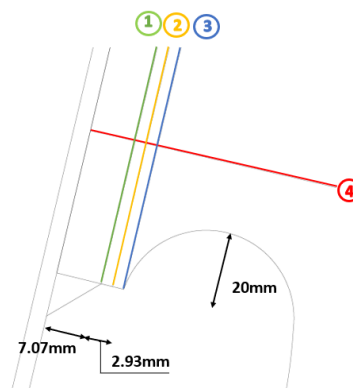


Figure 6.13 Overview path location crossbeam (left) and starting positions path 1,2 and 3 (right)

### Biaxial/multiaxial stress state

In the case of an uniaxial stress, the direction of the principal stress is more or less perpendicular to the weld toe, as shown in Figure 6.14, thus the maximum principal stress can be directly taken for the hot spot calculation (Niemi, Fricke, & Maddox, 2018). If the stress state is multiaxial, or biaxial, the angle of the maximum principal stress is inclined relative to the weld toe and thus a problem arises. Which strategy to choose to determine the hot spot stress is not clear and the recommendations of different authors will be stated. A brief of the summary of the main approaches in literature will be given in the following sections.

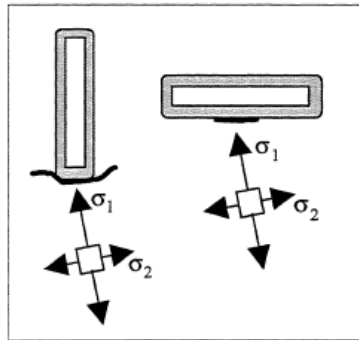


Figure 6.14 principal stress predominantly perpendicular to weld toe (Niemi, Fricke, & Maddox, 2018)

**Structural Hot spot Stress Approach to Fatigue Analysis of Welded Components Designer's Guide (Niemi, Fricke, & Maddox, 2018)**

In the IIW recommendations for the structural hot spot stress approach (Niemi, Fricke, & Maddox, 2018) it is stated that a distinction need to be made between the principal stress and the stress perpendicular to the weld toe. In many practical cases the direction of the maximum principal stress is approximately perpendicular to the weld toe and thus this stress can be directly taken as the hot spot stress (Niemi, Fricke, & Maddox, 2018). If the angle between the maximum principal stress and the normal to the weld toe is smaller or equal than 60 degrees, the maximum principal stress should be taken. While if this angle is larger than 60 degrees, the stress perpendicular to the weld toe, or the minimum principal stress, whoever is the largest, should be taken for the hot spot stress.

In Figure 6.15 a graphical visualization is shown in which both principal stresses are tensile. In case of doubt which stress component to use, especially when the direction of the maximum and minimum principal stress is changing during a load cycle, which is the case with moving loads on a bridge, the partial load factor should be increased sufficiently. It is not stated in which order this partial factor should be increased.

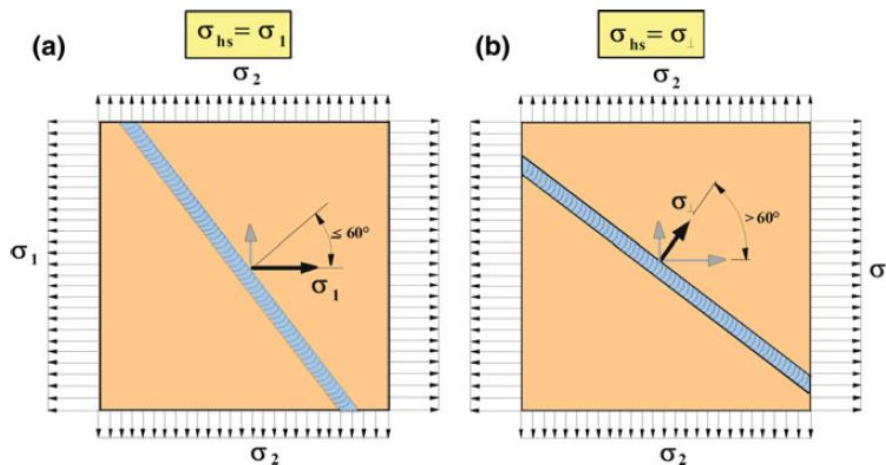


Figure 6.15 Definition of stress components for hot spot calculation (Niemi, Fricke, & Maddox, 2018)

**Fatigue design of offshore steel structures DNVGL-RP-C203 (DNV GL, 2016)**

In the DNVGL standard (DNV GL, 2016) a different methodology is proposed in which the detail category is depending on the angle of the principal stress with the normal to the weld toe. When using the hot spot stress methodology a distinction is made between category D and C2 which is shown in Figure 6.16, in which D corresponds with detail category 90, while C2 corresponds with detail category 100. If the angle of the principal stress and the normal to the weld toe is smaller than 60 degrees, detail category D should be used, while if the angle is larger than 60 degrees detail category C2 should

be used. This distinction at an angle of 60 degrees can also be found in the IIW recommendation for the structural hot spot stress approach (Niemi, Fricke, & Maddox, 2018), but there it is recommended to take the stress perpendicular to the weld toe, or the minimum principal stress whoever is the largest, instead of increasing the detail category. Furthermore it is stated that: "In general the stress range in both the two principal directions shall be assessed with respect to fatigue" and thus both the maximum and minimum principal stress should be used.

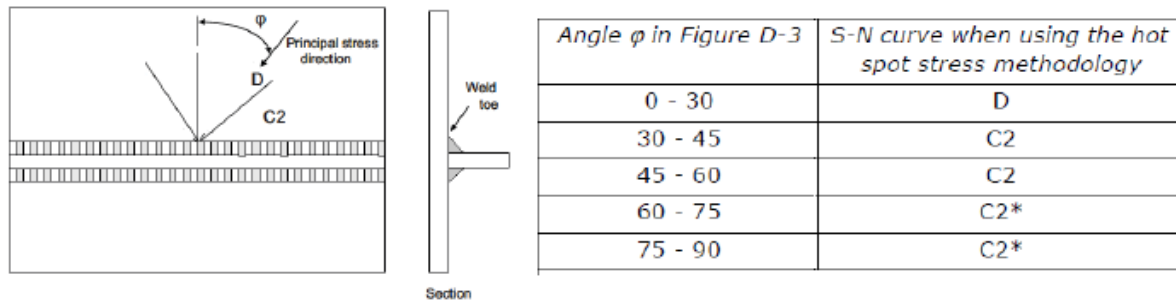


Figure 6.16 Classification detail category joint with respect to angle principal stress (DNV GL, 2016)

### Fatigue design of welded joints and components (Hobbacher A., 2016)

In the IIW recommendations for welded joints and components (Hobbacher A., 2016) it is stated that the maximum principal stress should be calculated and used for the hot spot stress determination. No distinction is made between the minimum and maximum principal stress and furthermore the stress perpendicular to the weld toe is not mentioned at all. No further description is given in this document.

### Multiaxial fatigue in welded details (Gustafsson & Saarinen, 2007)

As stated in (Gustafsson & Saarinen, 2007), the detail categories in EN-1993-1-9 (EN1993-1-9, 2011) are based on experiments in which the stress perpendicular to the weld toe is used. If the principal stress has an angle with the normal to the weld toe, problems may arise with the detail category. In such a case the principal stress is the combination of the stress perpendicular and parallel to the weld toe and this will result in an angle with the weld toe. The S-N curves in EN3 assume the stress perpendicular to the weld toe. Whether and how it can be applied to the multiaxial stress states is not clear in the current version of EN1993-2 (EN1993-2, 2011).

### Stress Determination for Fatigue Analysis Of Welded Components (Niemi E. , 1995)

In case of a multiaxial stress state, Niemi (Niemi E. , 1995) stated that if the direction of the maximum principal stress is acting more or less parallel to the weld toe, this maximum principal stress is not the governing stress, and the minimum principal stress, which is perpendicular to weld toe in this case, should be taken for the hot spot calculation. Not a clear distinction is given when to take the maximum and when to take the minimum principal stress as the governing stress. It is stated that in case of doubt, the fatigue life should be calculated based on both the maximum and minimum principal stress. If the angle of the principal stress is more or less perpendicular to the weld toe, the maximum principal stress should be taken for the hot spot calculation. Furthermore it is stated that in the case of non-proportional loading, i.e. moving loads on a bridge, the stress is depending on the time and the direction of the principal stress will also vary in time. This non-proportional loading can result in non-conservative fatigue life calculation when the calculation is based on the maximum principal stress. In many structural applications, it is sufficient to only calculate the stress perpendicular to the weld toe and use this stress for the hot spot stress calculation (Niemi E. , 1995).

## Review of literature

As can be concluded from the investigated codes, recommendations and papers, different authors have different opinions for which stress component to take in case of biaxial/multiaxial stress. Even two different authors (Hobbacher A. , Fatigue design of welded joints and components, 2016) and (Niemi E. , 1995) from the same institute, the International Institute of Welding (IIW), have different opinions for which stress component to take. Hobbacher stated that the maximum principal stress should be used in all cases, while Niemi stated that the stress perpendicular to the weld toe is more suitable. Furthermore it is stated that in case of non-proportional loading, which is the case for moving loads on a bridge, the direction of the principal stress is varying with time. The principal stress can result in non-conservative results in the case of non-proportional loading. No clear recommendations are given what to do in this case.

**In this study both the principal stresses and the stress perpendicular to the weld toe are investigated.** This study is performed for load positions 1,2 and 3 which are: global in-plane deformation, global out-of-plane deformation and local in-plane deformation of the crossbeam. The results for load position 1 are shown in the figures below. The results for the other 2 load cases can be found in Annex D.

### 6.2.3.2.1. Results solid loading position 1 (LP1)

In Figure 6.17 the results of the absolute maximum principal stress in path 1,2 and 3 are shown while in Figure 6.18 and Figure 6.19 the maximum and minimum principal stress are shown. In Figure 6.20 the results of the stress perpendicular to the weld toe are shown. The absolute maximum principal stress is the largest principal value when the absolute value of all principal values is compared.

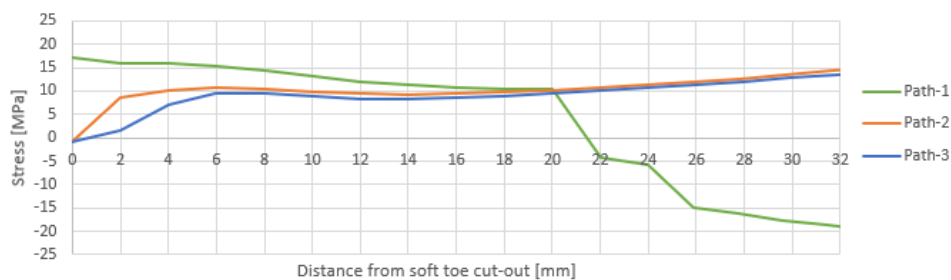


Figure 6.17 LP1: absolute maximum principal stress for path 1,2 and 3 solid FE model

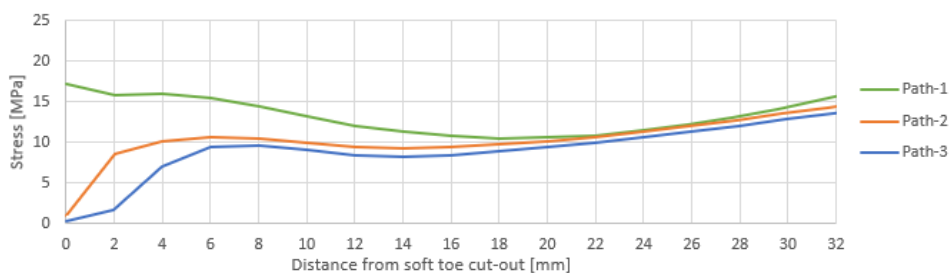


Figure 6.18 LP1: maximum principal stress for path 1,2 and 3 solid FE model

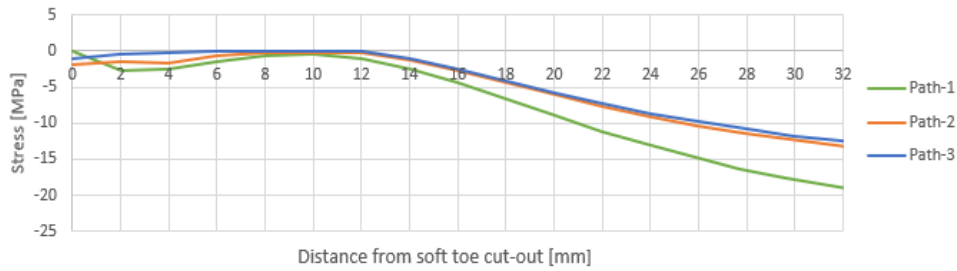


Figure 6.19 LP1: minimum principal stress for path 1,2 and 3 solid FE model

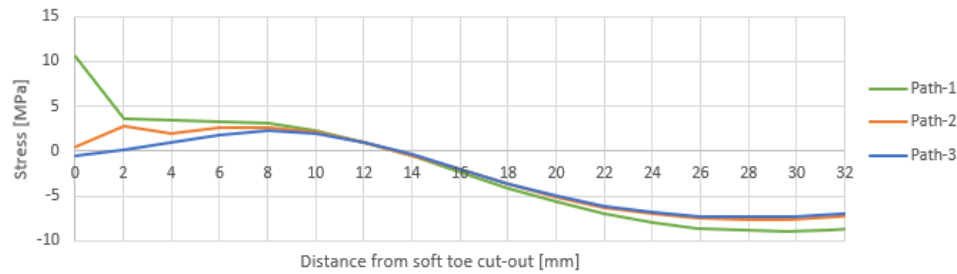


Figure 6.20 LP1: stress perpendicular to weld toe for path 1,2 and 3 solid FE model

As can be seen from the figures, the results of path 2 and 3 are similar, while a larger difference with path 1 is observed, which is due to the singularity at the weld toe. When the results of Figure 6.18, the maximum principal stress, and Figure 6.20, the stress perpendicular to the weld toe, are compared with each other, the maximum principal stress and stress perpendicular to the weld toe are clearly different. As can be seen from Figure 6.20, the stress perpendicular to the weld toe shows a more or less constant value at 26-32mm. The maximum stress occurs at 30mm from the soft toe of the cut-out, which can be seen in Figure 6.13. This 30mm is the critical location for path 1,2 and 3 and which forms the starting position for path 4.

Those stable stress results, in the range of 26-32mm, are not observed in the principal stress cases (absolute, maximum and minimum). Since the principal stress in the crossbeam is not the same as the stress perpendicular to the weld toe this is further investigated, and the direction is shown in Figure 6.21. As can be seen from the figure, the direction of the principal stress is rather parallel than perpendicular to the weld toe. The angle between the normal to the weld toe, and the maximum principal stress is equal to approximately 75° and 70° at the positions with distances 0mm and 25mm away from the end point at the bottom, respectively. In Figure 6.21 the direction of the principal stress is shown.

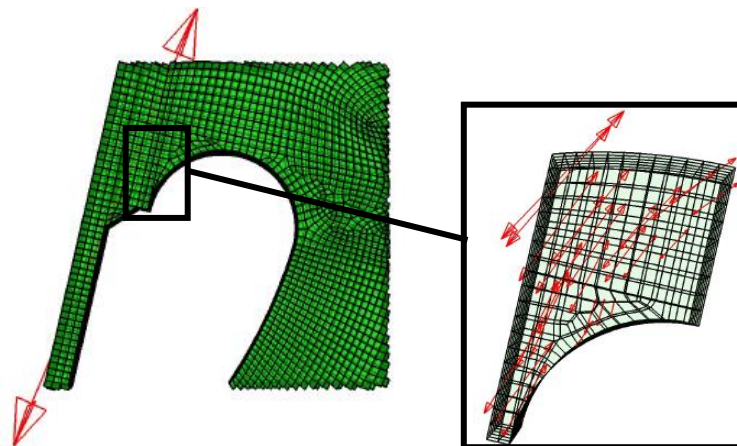


Figure 6.21 LP1: direction maximum principal in the crossbeam global (left) and local in crossbeam (right)

### Results of path 4 for LP1

As stated before, for the stress perpendicular to the weld toe, the maximum stress occurs at 30mm. Since this height, 30mm, is larger than the radius of the small circle of the cope hole, which is equal to 20mm, it is possible to perform a hot spot extrapolation at path 4. To make the graphical visualization more clear, the dimensions are shown in Figure 6.22.

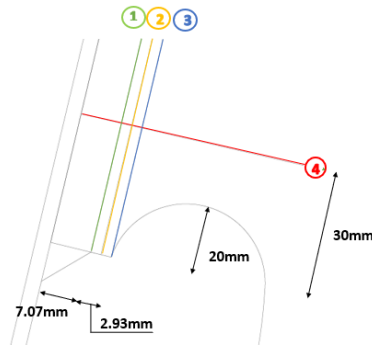


Figure 6.22 Overview path location crossbeam with dimensions and starting positions path 1,2 and 3 (right)

To investigate the stress behavior for both the principal stresses and the direct stresses of path 4, the results are shown in Figure 6.23. As with the results for path 1,2 and 3, also with the results for path 4 a difference is observed between the minimum/maximum principal stress and the stress perpendicular to the weld toe. As was stated earlier, the angle between the maximum principal stress and the normal to the weld toe is larger than 60 degrees, and thus by following the IIW recommendations (Niemi, Fricke, & Maddox, 2018) the stress perpendicular to the weld toe, or the minimum principal stress whoever is the largest, should be taken for the hot spot stress. When those two stresses are compared it can be seen that the minimum principal stress is larger, and thus the minimum principal stress should be used for the hot spot stress calculation.

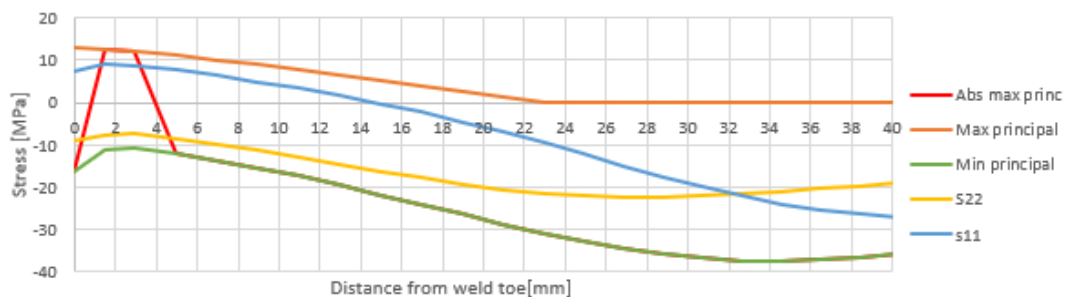


Figure 6.23 LP1: results principal and direct stresses path 4 at 30mm

#### 6.2.3.2.2. Results shell loading position 1 (LP1)

In Figure 6.25 the results of the principal stress in paths 1,2 and 3 are shown while in Figure 6.26 and Figure 6.27 the maximum and minimum principal stress is shown. In Figure 6.28 the results of the stress perpendicular to the weld toe are shown. The structural intersection point of the trough and the crossbeam is taken as the starting point for path 1. The locations of paths 1,2 and 3 in the shell FE model are shown in Figure 6.24.

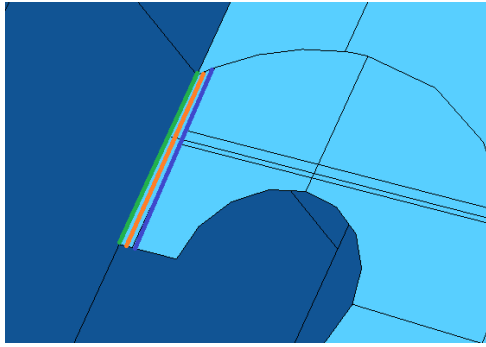


Figure 6.24 Location path 1,2 and 3 shell FE model

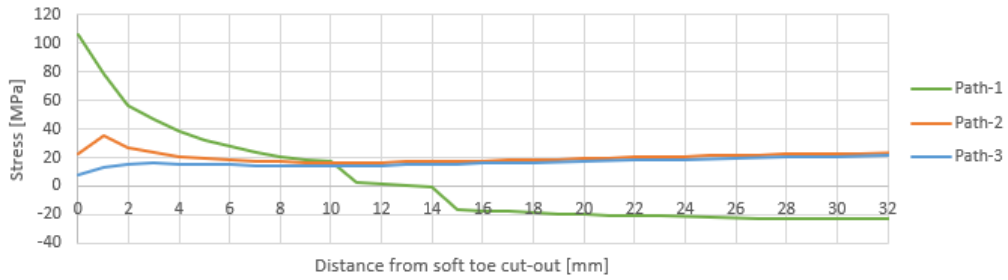


Figure 6.25 LP1: absolute maximum principal stress for path 1,2 and 3 shell FE model

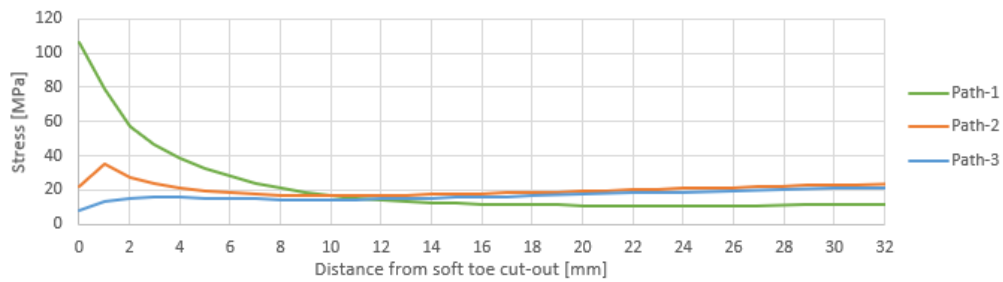


Figure 6.26 LP1: maximum principal stress for path 1,2 and 3 shell FE model

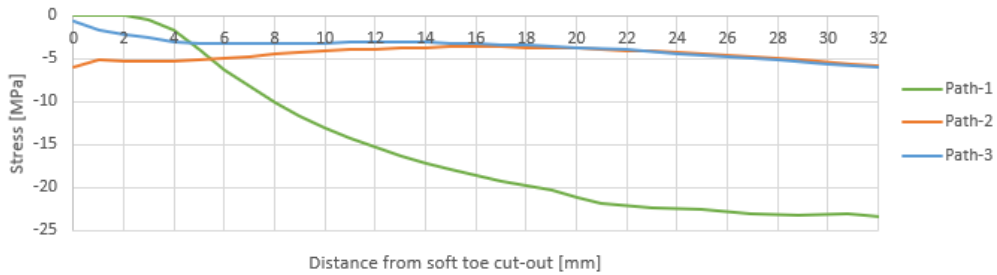


Figure 6.27 LP1: minimum principal stress for path 1,2 and 3 shell FE model

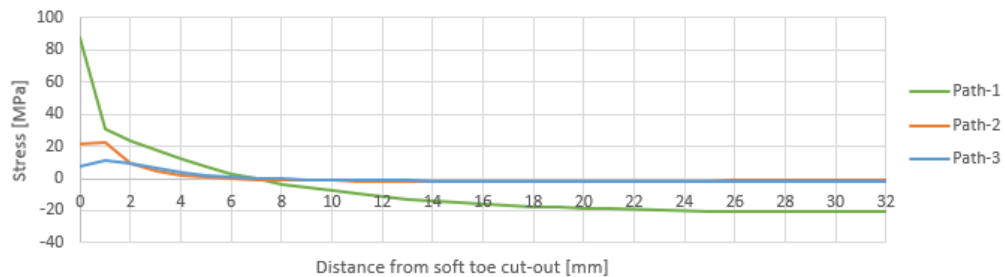


Figure 6.28 LP1: stress perpendicular to weld toe for path 1,2 and 3 shell FE model

As can be seen from Figure 6.25 to Figure 6.28, the results from path 2 and 3 for all five stress components are of the same order for every stress component, while path 1 shows large differences with the other 2 paths. Those large differences at the start of path 1 are due to the singularity which occurs at the structural intersection point. For the comparison of the results, path 1 is disregarded and

only the results from path 2 and 3 are taken into account. The stress perpendicular to the weld toe, see Figure 6.28, is close to zero and constant after approximately 6mm. If the results of the solid FE model, see Figure 6.20, and the results of Figure 6.28 are compared, it can be seen that the regular shell FE model does not capture the stresses perpendicular to the weld toe well. Thus it can be concluded that this FE model is not suitable for calculation of the this investigated crack.

The same procedure is followed for the other investigated loading positions and new OSD variant for which only the results are shown over here. The full investigation can be found in Annex E.

#### 6.2.3.2.3. *Angle of principal stress for other loading positions*

##### **Angle of principal stress and normal to weld toe LP2 and LP3 in solid FE model**

For LP3, local in-plane loading between the web of the trough, similar observations are also valid for the solid FE results for the crossbeam location. The angle between the normal to the weld toe and the maximum principal stress is equal to approximately 80 degrees at the starting point of the path, which is directly at the soft toe. The angle is approximately 60 degrees 25mm away from the starting point.

For LP2, global out-of-plane loading between the web of the trough, the angle between the normal to the weld toe, and the maximum principal stress is equal to approximately 35 degrees at the starting point of the path, which is directly at the soft toe. The angle is approximately 0 degrees 25mm away from the starting point

As can be concluded from the three investigated loading positions, the angle of the maximum principal stress is depending on the loading position. Furthermore the angle of the principal stress is changing over the length of path 1,2 and 3. For loading position 1 and 3, which will result in global and local in-plane deformation of the crossbeam, the angle between the maximum principal stress and the normal to the weld toe is the largest and is larger than 60 degrees. Based on this value the stress perpendicular to the weld toe, or the minimum principal stress whichever is the largest, should be used for the hot spot stress determination. For load position 2 this angle is between 0 and 35 degrees and thus the maximum principal stress should be used based on the IIW recommendations (Niemi, Fricke, & Maddox, 2018).

##### **Results of path 4 under LP1, LP2 and LP3 in solid FE model**

To investigate the stress behavior for both the maximum/minimum principal stress and the stress perpendicular to the weld toe, both stress components are used for the hot spot stress calculation. Since it was determined that the angle of the principal stress and the normal to the weld toe is larger than 60 degrees for load position 1 and 3, the comparison is made with the minimum principal stress. For load position 2 this angle is smaller than 60 degrees and thus the maximum principal stress is used.

##### **Comparison of hot spot stress calculated by principal stress and direct stress**

The results of the hot spot stress extrapolation of the three load cases are shown in Table 6-3. The height from the soft toe of the cut-out to path 4 for load position 1 and 3 is equal to 30mm, which can be seen in Figure 6.22, while this height is equal to 24mm for loading position 2. Linear surface extrapolation is performed for the determination of the structural stress in the crossbeam. As was concluded in section 6.2.1 the required element size for the quadratic solid elements is equal to 2mm, and for the quadratic shell elements equal to 1mm.



**Table 6-3 Results comparison hot spot stress path 4 solid FE model for principal stress and stress perpendicular to weld toe**

	HSS absolute principal stress [MPa]	HSS stress perpendicular to weld toe [MPa]	$\frac{\sigma_{HSS\_solid\_principal\_stress}}{\sigma_{HSS\_solid\_stress\_perpendicular}}$
<b>Load position 1</b>	-7.32	-4.65	1.57
<b>Load position 2</b>	+8.71	+8.74	1.00
<b>Load position 3</b>	-6.30	-4.42	1.43

As can be seen from Table 6-3, the hot spot stress obtained with the principal stress is higher when the same calculation is performed with the stress perpendicular to the weld toe. The results from the principal stress are more conservative.

As was observed previously, the angle of the principal stress in the crossbeam is depending on the loading position. When an uniaxial stress state occurs, which is the case in the web of the trough, the angle of the maximum principal stress is more or less equal to the normal of the weld toe and thus no distinction need to be made between the angle of the principal stress. When a biaxial stress is present, the angle of the principal stress and the normal to the weld toe is depending on the loading position. Based on the above mentioned observations, and taking the IIW recommendations for the hot spot stress (Niemi, Fricke, & Maddox, 2018) into account, the angle of the principal stress should be calculated for every loading position.

This dependency, of the angle of the principal stress and the loading position, makes it difficult to base a stress range on. The direction is changing for every loading position, so the direction should be fixed for every loading position individually which is a tedious job to do. Another possibility is to study the shear stress in the weld, and the stress perpendicular to the weld toe. Those stress components have a fixed direction and thus are not depending on the loading position. But this will result in two different stress components for the hot spot stress calculation. This method is proposed by (Susmel & Tovo, 2006), and is only possible for the solid FE model since in this case the weld is modelled. With the shell FE model this is not the case and thus no comparison can be made between the FE models.

Different authors have different recommendations which procedure to choose in case of a biaxial stress state. Even in the IIW recommendations different authors have different recommendations which stress component to take. In the case of non-proportional loading, i.e. moving loads on a bridge, the stress is depending on the time and the direction of the principal stress will also vary in time. This non-proportional loading can result in non-conservative fatigue life calculation when the calculation is based on the maximum principal stress (Niemi, Fricke, & Maddox, 2018).

Furthermore the detail categories in EN1993-1-9 (EN1993-1-9, 2011) are based on experiments in which the stress perpendicular to the weld toe is used. If the principal stress has an angle with the normal to the weld toe, i.e. it is not perpendicular to the weld toe, problems may arise with the detail category. In such cases the principal stress is the combination of the stress perpendicular and parallel to the weld toe and this will result in an angle with the weld toe. The S-N curves in EN3 assume the stress perpendicular to the weld toe and thus this criterion is not fulfilled with the principal stress in case of a multiaxial stress. No detail categories are given in EN1993-1-9 (EN1993-1-9, 2011) for the principal stress.

### 6.2.3.3. Weld modelling shell FE model

To investigate if the results of the shell FE model can be improved, two weld modelling techniques are used for this analysis. One modelling technique is the increased thickness method, proposed by (Eriksson, Lignell, Olsson, & Spennare, 2003) and the other is the IIW method (Niemi, Fricke, & Maddox, 2018). A detailed description of both weld modelling techniques can be found in section 2.6.2. An overview of those modelling techniques is shown in Figure 6.29.

With the IIW weld modelling technique (Figure 6.29 left) the thickness of the crossbeam is locally increased and furthermore the tip of the weld is also modelled. The thickness of the crossbeam is increased over a height which is equal to the leg length of the weld plus half of the thickness of the trough, which is equal to  $7.07+3=10.07\text{mm}$  for the old OSD variant. The locally increased thickness of the crossbeam is equal to the thickness of the crossbeam plus the weld leg length, which is equal to  $12+7.07=19.07\text{mm}$  for the old OSD variant. With the increased thickness method (Figure 6.29 right), both the thickness of the trough and crossbeam is increased locally. This increased thickness is equal to the thickness of the trough or crossbeam plus the throat thickness of the weld which is equal to 5mm.

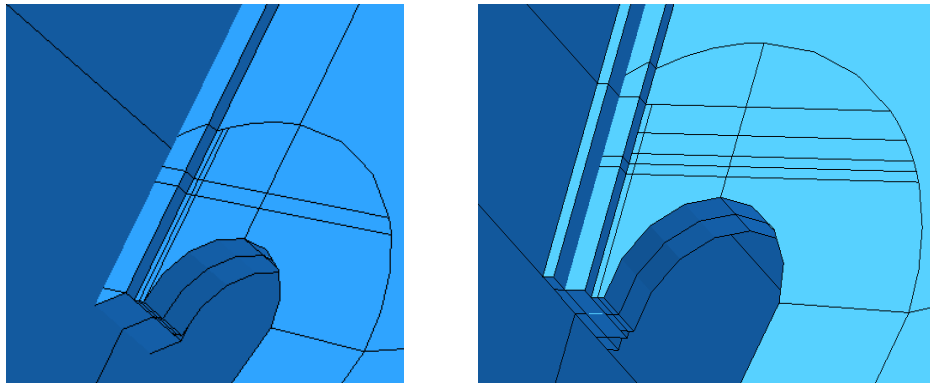


Figure 6.29 IIW weld modelling method (left) and increased thickness method (right)

The read out location of stresses for path 1 is the weld toe and not the structural intersection point of the trough and crossbeam anymore. This will result in the same read out location for both the solid and the shell with weld FE models.

### 6.2.3.4. Comparison results different models

For the comparison of the results between the three different models the results of path 2 are compared. In Figure 6.30 the results of the maximum principal stress path 2 are shown while in Figure 6.31 the results of the stress perpendicular to the weld toe are shown.

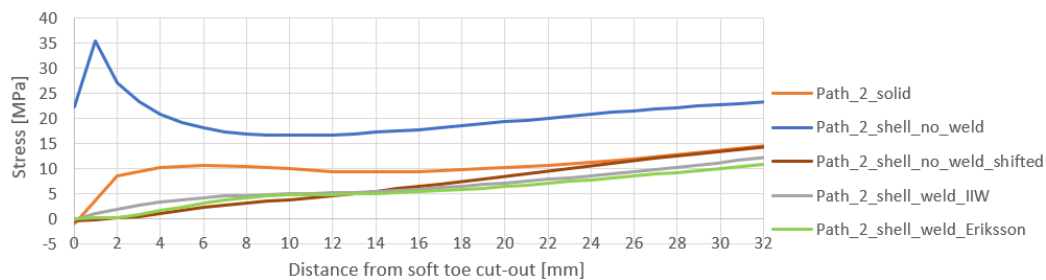
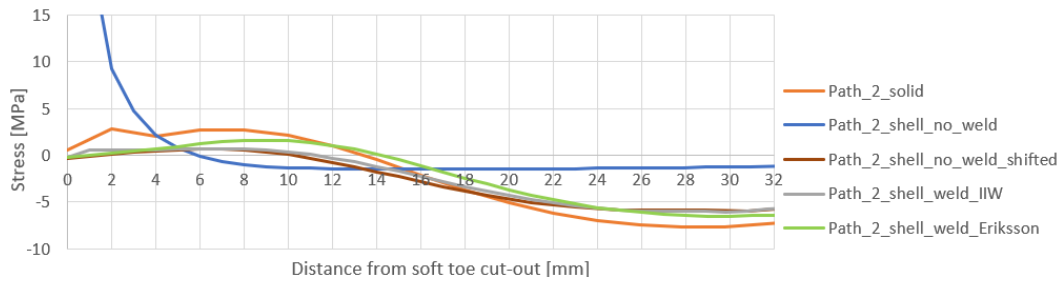


Figure 6.30 LP1: comparison maximum principal stress, path 2 for different FE models



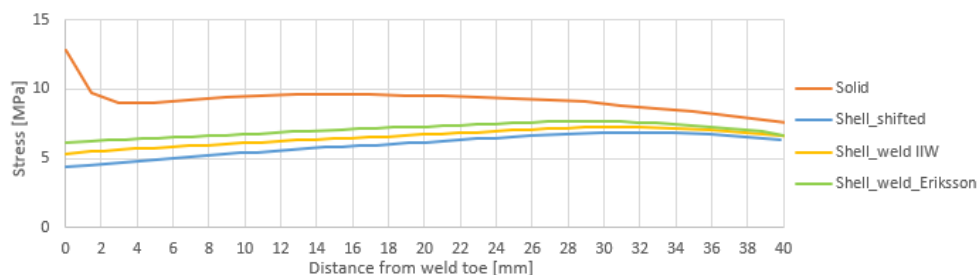
**Figure 6.31 LP1: comparison stress perpendicular to weld toe, path 2 for different FE models**

As can be seen from Figure 6.30, the singularity which occurs at the structural intersection point in the shell FE model almost fully disappeared when the weld modelling is applied for the shell FE model. Furthermore the trendline of the solid FE model and shell model with weld is closer the trendline of the shell model without weld. The maximum principal stress of the shell FE models with weld is lower throughout the whole length of the path when compared with the solid results. As can be seen from Figure 6.31, the weld modelling improved the results for the stresses perpendicular to the weld toe a lot and also the singularity is almost fully disappeared. The results improved in a qualitative way, i.e. the trendline of the solid and shell with weld FE models is matching, but in a quantitative way since some differences still exist when compared with the solid FE model.

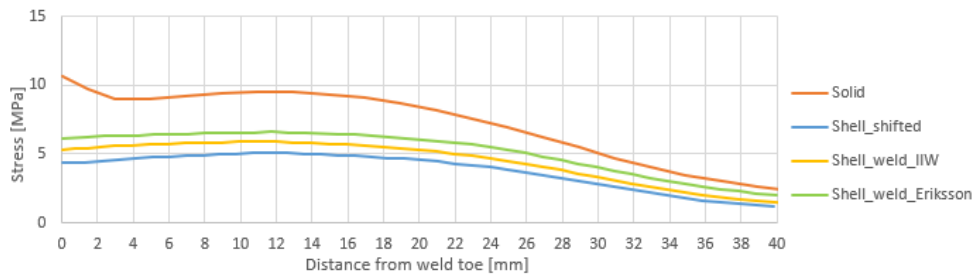
Furthermore shifting the extraction positions of the shell FE model from the structural intersection point of the trough and crossbeam to the imaginary weld toe will have a huge influence on the results. This shifting is only done to see how much the weld modelling techniques improve the results when compared to the original shell model. The differences between the shifted shell FE model and the shell weld FE models results is limited. The weld modelling thus has limited influence for this in-plane loading type. As can be seen from the figure, all FE models, solid and shell with weld, have their maximum value for path 2 at the same location in the crossbeam, at approximately 30mm.

### Results LP2

For LP2, in which the crossbeam is under out-of-plane loading, the difference in stress results between the shell FE models and solid FE model is still quite large. The results for the absolute principal stress are shown in Figure 6.32 and for the stress perpendicular to the weld toe in Figure 6.33.



**Figure 6.32 LP2: comparison absolute maximum principal stress path 4**



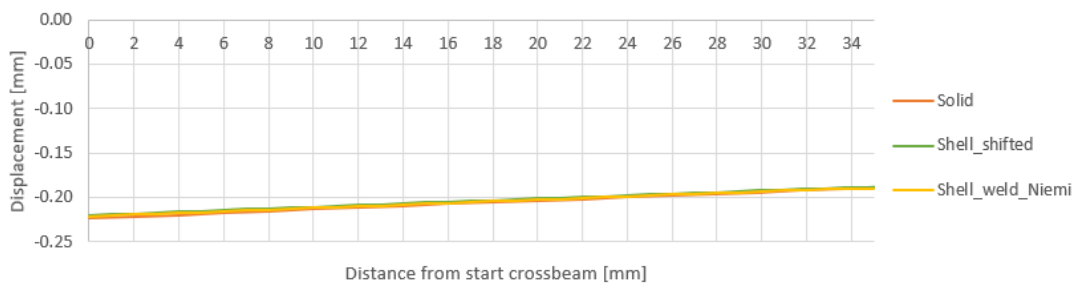
**Figure 6.33 LP2: comparison stress perpendicular to weld toe path 4**

As can be seen from both figures, the results from the shell FE models are non-conservative when compared with the solid. The Eriksson weld modelling technique in the shell FE model shows results closest to the solid FE model. When a linear extrapolation is performed to obtain the hot spot stress, the hot spot stress for the solid FE model is equal to +8.71MPa, and for the shell FE model with Eriksson weld modelling technique equal to +6.26MPa. This is an underestimation of a factor 0.70.

### Deformations crossbeam for LP2

Since a large difference occurs between the solid and shell FE model this difference will be further investigated to see what causes this large difference. The global and local deformations between the solid and shell FE model will be investigated and furthermore the influence of the weld modelling with the solid FE model is investigated.

In Annex G, the contour plots and graphs of the deformation are shown at the location of the crossbeam and trough. Furthermore the deformed mesh figures can be found in this annex. With LP2 the crossbeam will deform solely out-of-plane and for the comparison the out-of-plane deformation in path 2 is shown in Figure 6.34. As can be seen from the figure, hardly any difference between the solid and shell FE models occur for the out-of-plane deformation.



**Figure 6.34 LP2: out-of-plane deformation (U3) path 2 different FE models**

Another possible explanation for the differences is the way in which the forces are transferred in the shell and solid FE models. In the shell model the connection of the crossbeam and trough can be seen as a fully penetrated connection and thus the load is directly transferred from the trough to the crossbeam. For the solid FE model a seam is applied between the trough and crossbeam and thus the load is transferred from the trough, through the weld, to the crossbeam. In the shell FE model the load is transferred directly to the crossbeam, which has a thickness of 12mm, while in the solid FE model the load is transferred to two times the throat thickness of the weld which is equal to  $5 \times 2 = 10\text{mm}$ .

To see how the results are affected two additional solid models are created. One in which the seam is removed and one in which the seam and the weld are both removed. The three solid FE models with and without seam are shown in Figure 6.35. In which the left figure is the original FE model, the middle figure when the seam is removed and the right figure when both the seam and weld are removed. The

results of path 4 are shown in Figure 6.36. Furthermore the obtained hot spot stress values for all three solid FE models and the shell model without weld are shown in Table 6-4.

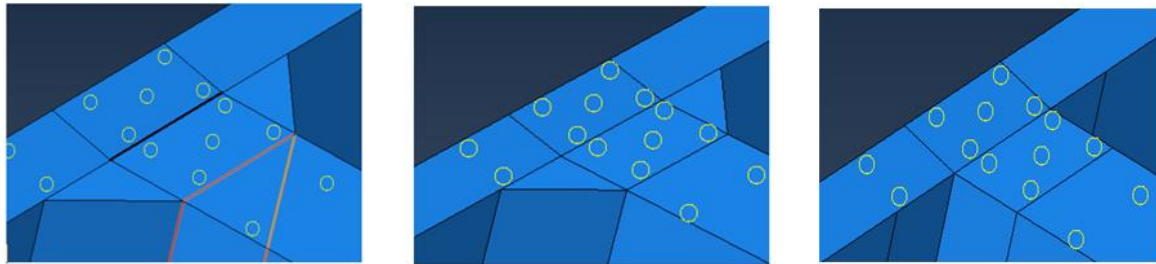


Figure 6.35 Solid FE model with seam (left), without seam (middle) and without seam and weld (right)

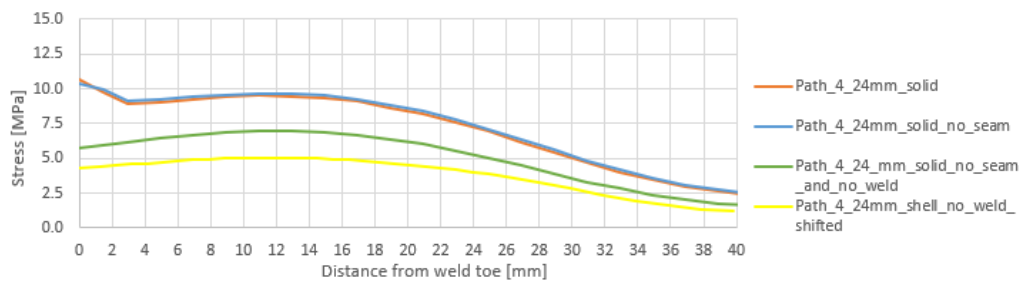


Figure 6.36 Comparison solid with and without seam modelled stress perpendicular to weld toe path 4

Table 6-4 Overview obtained hot spot stress values adapted solid models

	Obtained HSS [MPa]	$\frac{\sigma_{HSS\_shell\_original}}{\sigma_{HSS\_solid\_XXX}}$
<b>Solid original</b>	8.71	0.52
<b>Solid no seam</b>	8.98	0.50
<b>Solid no seam and no weld</b>	6.09	0.74
<b>Shell original</b>	4.50	-

Applying a seam will hardly influence the results in the crossbeam. The obtained stress in path 4 is almost similar for the case with and without a seam applied which is shown in Figure 6.36. The solid FE model with no seam and no weld is as close as possible to the shell FE model, but the ratio is still a factor 0.74.

#### 6.2.3.5. Result variant 2: new OSD thicknesses

For this small parametric analysis also the results are obtained for variant 2 which is the new OSD variant. In this variant the thickness of the trough, deck plate and crossbeam are adapted and in Table 6-5 the differences are shown.

Table 6-5 Overview differences in thickness between new and old OSD variant

	Old OSD [mm]	New OSD [mm]
<b>Trough</b>	6	8
<b>Crossbeam</b>	12	16
<b>Deck plate</b>	12	22

The same strategy as with the old variant, which was investigated previously, is also followed for this variant.

First a mesh sensitivity study is performed to determine the appropriate element size, this mesh sensitivity analysis is performed for loading position 1 and 2. Similar conclusions as with the old OSD variant are also valid for this new variant.

The next step is to investigate at what height in path 2 and 3 the maximum value of the stress occurs. This height forms the starting location of path 4. The third step is to calculate the hot spot stress in the trough and the crossbeam for all five load cases and make the comparison with the variant 1, which is the old OSD.

### Maximum values path 2 and 3

As was concluded in section 6.2.3.2.3, when the results of paths 2 and 3 are compared, of both the solid and shell FE models, the maximum value in path 2 occurred at the same location for all investigated load cases. Also for the new variant the maximum value for paths 2 and 3 occurred at the same distance from the soft toe of the cut-out and thus only the results for path 2 are shown in Figure 6.37. In this figure the stress perpendicular to the weld toe is shown.

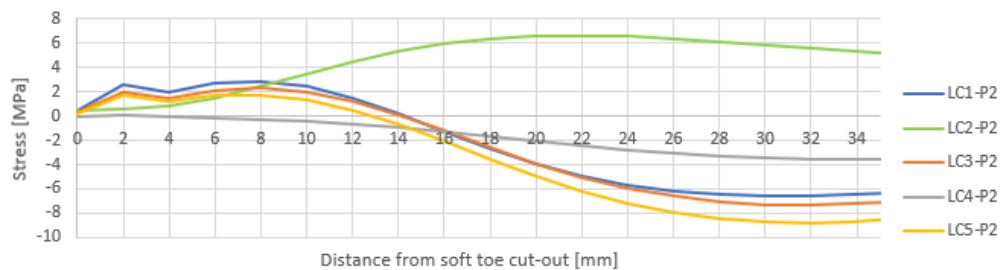


Figure 6.37 Results path 2 for investigated load cased solid FE model, new OSD variant (stress perpendicular to weld toe)

As can be seen from Figure 6.37, the maximum value in path 2, occurs at 32mm away from the soft toe of the cut-out for loading positions 1,3,4 and 5. Only for loading position 2 the maximum value occurs at 22mm. The maximum value in path 2 forms the starting location of path which is perpendicular to the weld toe. In Table 6-6 the comparison for the location of the maximum is summarized. As can be seen from the table, for the old OSD variant the maximum stress occurs at 30mm, while for the new OSD variant this maximum occurs at 32mm. Since path 4 has another starting height in the old OSD variant when compared with the new OSD variant, it is not possible to make an exact comparison for the hot spot stresses in the crossbeam.

Table 6-6 Overview locations with maximum value path 2 for new and old OSD variant

	New OSD		Old OSD	
	Solid [mm]	Shell [mm]	Solid [mm]	Shell [mm]
LC1	32	32	30	30
LC2	22	22	24	24
LC3	32	32	30	30
LC4	32	32	30	30
LC5	32	32	30	30

Note: the distance from weld end to the maximum stress perpendicular to the weld toe stress is shown.

#### 6.2.4. Hot spot stress results in old and new OSD variants

##### Results in trough

In Table 6-7 the hot spot stress results in the web of the trough are shown for both the old and new OSD variant, while in Table 6-8 the ratio between the solid and the two different shell models is shown. The ratio between the obtained hot spot stress of the old and new OSD is shown in Table 6-9.

**Table 6-7 Overview obtained hot spot stress results old and new OSD variant trough (stress perpendicular to weld toe)**

	Old OSD variant				New OSD variant			
	$\sigma_{HSS\_solid}$ [MPa]	$\sigma_{HSS\_shell}$ [MPa]	$\sigma_{HSS\_shell\_IIW}$ [MPa]	$\sigma_{HSS\_shell\_Eriksson}$ [MPa]	$\sigma_{HSS\_solid}$ [MPa]	$\sigma_{HSS\_shell}$ [MPa]	$\sigma_{HSS\_shell\_IIW}$ [MPa]	$\sigma_{HSS\_shell\_Eriksson}$ [MPa]
<b>LP 1</b>	+57.90	+65.93	+64.78	+60.67	+34.29	+39.01	38.47	+38.08
<b>LP 2</b>	+0.00	+0.00	+0.00	+0.00	+0.00	+0.00	+0.00	+0.00
<b>LP 3</b>	+39.35	+48.08	+45.40	+43.67	+26.43	+30.87	+29.92	+29.62
<b>LP 4</b>	+3.21	+3.43	+3.40	+2.86	+5.64	+6.14	+6.01	+5.76
<b>LP 5</b>	+35.50	+41.09	+40.48	+38.04	+26.68	+29.27	+29.09	+28.63

**Table 6-8 Overview obtained ratio hot spot stress results solid and shell models for old and new OSD variant trough**

	Old OSD variant			New OSD variant		
	$\frac{\sigma_{HSS\_shell}}{\sigma_{HSS\_solid}}$	$\frac{\sigma_{HSS\_shell\_IIW}}{\sigma_{HSS\_solid}}$	$\frac{\sigma_{HSS\_shell\_Eriksson}}{\sigma_{HSS\_solid}}$	$\frac{\sigma_{HSS\_shell}}{\sigma_{HSS\_solid}}$	$\frac{\sigma_{HSS\_shell\_IIW}}{\sigma_{HSS\_solid}}$	$\frac{\sigma_{HSS\_shell\_Eriksson}}{\sigma_{HSS\_solid}}$
	<b>Loading position 1</b>	1.14	1.12	1.05	1.14	1.12
<b>Loading position 2</b>	1	1	1	1	1	1
<b>Loading position 3</b>	1.22	1.15	1.11	1.17	1.13	1.12
<b>Loading position 4</b>	1.07	1.06	0.89	1.09	1.07	1.02
<b>Loading position 5</b>	1.16	1.14	1.07	1.10	1.09	1.07

**Table 6-9 Ratio hot spot stress old and new OSD variant in web trough**

	$\frac{\sigma_{HSS\_solid\_new}}{\sigma_{HSS\_solid\_old}}$	$\frac{\sigma_{HSS\_shell\_new}}{\sigma_{HSS\_shell\_old}}$	$\frac{\sigma_{HSS\_shell\_IIW\_new}}{\sigma_{HSS\_shell\_IIW\_old}}$	$\frac{\sigma_{HSS\_shell\_Eriksson\_new}}{\sigma_{HSS\_shell\_Eriksson\_old}}$
	<b>Loading position 1</b>	0.59	0.59	0.59
<b>Loading position 2</b>	1	1	1	1
<b>Loading position 3</b>	0.67	0.64	0.66	0.68
<b>Loading position 4</b>	1.76	1.79	1.77	2.01
<b>Loading position 5</b>	0.68	0.71	0.72	0.75

As can be seen from Table 6-7, the new OSD variant is behaving better in all load positions, except for loading position 4. The ratio between the results of the solid FE model and both shell FE models is shown in Table 6-8 and the scatter in results between the solid and shell without weld FE model has a maximum of 1.22 for loading position 3. When the weld is modelled with the shell FE model the scatter is decreased to a factor 1.15. Modelling the weld will reduce the scatter between the solid and shell FE models and will thus improve the results of the shell FE model. For all five investigated load positions the shell FE results are overestimating the hot spot stress when compared with the solid FE model and are conservative.

From Table 6-9 it can be seen that the ratio between the hot spot stress of the old and new OSD variant is quite constant for all the three FE models for the individual load positions. For loading positions 1,3 and 5 this ratio is equal to 0.59-0.75 for the solid and different shell FE models. The

critical loading position, which gives the highest hot spot stress in the trough, is loading position 1, followed by loading position 3 and 5.

In Annex H a further investigation of the differences between the old and new OSD variant is performed for loading position 4. With this loading position the hot spot stress of the new OSD variant is higher when compared with the old OSD variant. The difference between the new and old OSD variant is only the thickness of the trough, crossbeam and deck plate. One of those parameters is adapted at the time to see which parameter will result in this stress concentration for the new OSD. This can be easily done with a shell FE model, thus this model is used for the comparison. Increasing the thickness of the trough from 6mm to 8mm, will result in a higher stress concentration at the structural intersection point. This stress concentration results in a hot spot stress which is 3.50 higher when compared with the original old OSD variant. A side node which should be placed by loading position 4 is that the obtained hot spot stress is very low when compared with the other load cases. The obtained hot spot stress for load position 4 is only 3MPa, while for load case 1,3, and 5 it is more than 40MPa. And thus it is not a critical position.

#### Results in crossbeam

In Table 6-10 the hot spot stress results of the crack in the crossbeam, with path 4 at 30mm and 32mm from the soft toe for the old and new variant, respectively, are shown for both the old and new OSD variant. In Table 6-11 the ratio between the solid and the two different shell models is shown. The ratio between the obtained hot spot stress for the old and new OSD variant is shown in Table 6-12.

Table 6-10 Overview obtained hot spot stress results old and new OSD variant crossbeam

	Old OSD variant				New OSD variant			
	$\sigma_{HSS\_solid}$ [MPa]	$\sigma_{HSS\_shell\_shift}$ [MPa]	$\sigma_{HSS\_shell\_IIW}$ [MPa]	$\sigma_{HSS\_shell\_Eriksson}$ [MPa]	$\sigma_{HSS\_solid}$ [MPa]	$\sigma_{HSS\_shell\_shift}$ [MPa]	$\sigma_{HSS\_shell\_IIW}$ [MPa]	$\sigma_{HSS\_shell\_Eriksson}$ [MPa]
LP 1	-4.65	-4.32	-4.52	-4.97	-3.73	-3.33	-3.60	-3.88
LP 2	+8.71	+4.50	+5.57	+6.26	+5.46	+2.78	+3.34	+3.75
LP 3	-4.42	-4.11	-4.17	-4.42	-3.99	-3.31	-3.65	-3.79
LP 4	-1.69	-1.52	-1.57	-1.76	-1.62	-1.34	-1.45	-1.59
LP 5	-5.30	-4.71	-5.07	-5.20	-4.60	-3.91	-4.25	-4.59

Table 6-11 Overview obtained ratio hot spot stress results old and new OSD variant crossbeam

	Old OSD variant			New OSD variant		
	$\frac{\sigma_{HSS\_shell\_shifted}}{\sigma_{HSS\_solid}}$	$\frac{\sigma_{HSS\_shell\_IIW}}{\sigma_{HSS\_solid}}$	$\frac{\sigma_{HSS\_shell\_Eriksson}}{\sigma_{HSS\_solid}}$	$\frac{\sigma_{HSS\_shell\_shifted}}{\sigma_{HSS\_solid}}$	$\frac{\sigma_{HSS\_shell\_IIW}}{\sigma_{HSS\_solid}}$	$\frac{\sigma_{HSS\_shell\_Eriksson}}{\sigma_{HSS\_solid}}$
LP 1	0.93	0.97	1.07	0.89	0.96	1.04
LP 2	0.51	0.64	0.72	0.51	0.61	0.69
LP 3	0.93	0.94	1.00	0.83	0.91	0.95
LP 4	0.90	0.93	1.04	0.83	0.89	0.98
LP 5	0.89	0.96	0.98	0.85	0.92	1.00



Table 6-12 Ratio hot spot stress old and new OSD variant in crossbeam

	$\frac{\sigma_{HSS\_solid\_new}}{\sigma_{HSS\_solid\_old}}$	$\frac{\sigma_{HSS\_shell\_shifted\_new}}{\sigma_{HSS\_shell\_shifted\_old}}$	$\frac{\sigma_{HSS\_shell\_IIW\_new}}{\sigma_{HSS\_shell\_IIW\_old}}$	$\frac{\sigma_{HSS\_shell\_Eriksson\_new}}{\sigma_{HSS\_shell\_Eriksson\_old}}$
Loading position 1	0.80	0.77	0.80	0.78
Loading position 2	0.63	0.56	0.60	0.60
Loading position 3	0.90	0.81	0.87	0.86
Loading position 4	0.96	0.92	0.92	0.90
Loading position 5	0.87	0.87	0.84	0.88

From Table 6-10 it can be seen that the new OSD variant has lower hot spot stress values for all investigated loading positions. A side note which should be placed over here is for the old OSD variant the maximum stress occurs at a height of 30mm from the soft toe, while for the new OSD variant this maximum occurs at 32mm. Since path 4 has another position in the old OSD variant when compared with the new OSD variant, it is not possible to make an exact comparison for the hot spot stresses in the crossbeam. As can be seen from Table 6-11, the shell FE models are underestimating the hot spot stresses when compared with the solid FE model and thus result in non-conservative results. The scatter between the solid and shell FE model is the largest for loading position 2, in which an out-of-plane torsional load is applied.

Applying the weld with the shell FE model will reduce the scatter for all investigated load cases and thus will reduce the scatter between the solid and shell FE results. For the in-plane load case the ratio between the obtained hot spot stress of the solid and shell weld Eriksson approach is equal to 0.93-1.04, while for the out-of-plane loading this ratio is equal to 0.69-0.72. As with the results from the web of the trough, also the difference in results between the individual load cases for all four FE models is quite constant as can be seen from Table 6-12..

### 6.3. Parametric study I and II: loading positions and different geometries

In this subchapter the critical loading positions of the OSD will be determined for both the old and new OSD variants based on influence lines. One axle load from fatigue load model 4 (FLM4) is used. As was stated in section 2.5., in fatigue load model 4, a distinction is made between 5 different types of trucks. Those 5 different types need to be considered in a separate manner from each other. For each truck type, several different specifications are mentioned: the wheel type, traffic type, axle load and the distance between the axles. With FLM4 the different type of trucks move over the bridge deck in transversal and longitudinal direction, in this parametric study only axle type C is taken into account. An overview of the wheel patch dimensions and the center to center distance is shown in Figure 6.38. The axle load for type C is equal to 80-90kN, for this analysis the highest load is chosen which result in an axle load of 90kN.

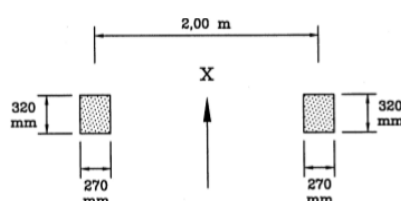


Figure 6.38 Definition of axle type C (EN1991-2, 2011)

For the parametric analysis the trough of interest is the right web of the middle trough, which is named T10R and shown in Figure 6.1 and Figure 6.39. The loads will be placed in three different positions in transverse direction, which is similar to the loading positions of the small parametric analysis. For

position 1 the load is placed between the webs of the trough, with position 2 the load is placed on the web of the trough and with position 3 the load is placed in between two troughs. In Figure 6.40 an overview of the three transverse loading positions is given.

To obtain the critical locations in longitudinal direction use is made of a DLOAD subroutine. The load is moved from crossbeam 1 (CB1) to crossbeam 3 (CB3) with step sizes of 250mm which is shown in Figure 6.39. This will result in 25 steps for every transverse loading position. The two loading positions, in longitudinal direction, which result in the minimum and maximum stress will be determined and used to study the comparison of the solid and shell FE model.

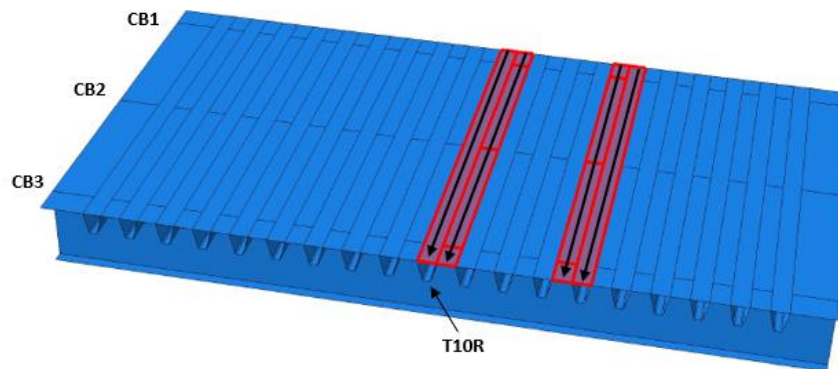


Figure 6.39 Loading position longitudinal direction

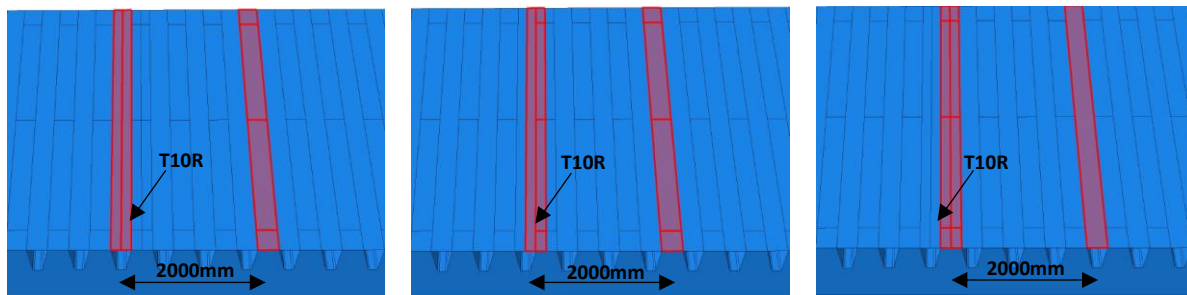


Figure 6.40 Overview loading positions, left: between web of trough, middle: on web of trough, right: between troughs

A distinction is made between the influence lines for both investigated crack locations: crack in web of trough at lower weld end, and the crack in the crossbeam at some distance from the soft toe, respectively. For every influence line the comparison is made between five different FE models: solid, shell without weld, and three shell models with the weld modelled. Those weld modelling techniques are: IIW approach (Niemi, Fricke, & Maddox, 2018), Eriksson approach (Eriksson, Lignell, Olsson, & Spennare, 2003) and the combined approach which is a combination of the two weld modelling techniques. With the combined approach both the thickness of the trough and crossbeam are increased locally based on the increased thickness method of Eriksson (Eriksson, Lignell, Olsson, & Spennare, 2003). Furthermore the weld tip is modelled based on the IIW method (Niemi, Fricke, & Maddox, 2018) with the thickness equal to the increased thickness of the crossbeam. This combined weld modelling technique is shown in Figure 6.41.

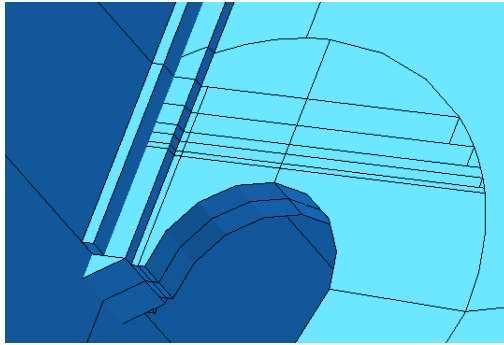


Figure 6.41 Combined weld modelling technique: increased thickness and weld tip modelled

6.3.1. Crack in web of trough at lower weld end (crack 1)

In Figure 6.42 to Figure 6.47 the results of the crack in the web of the trough are shown for the old and new OSD dimensions in which axle type C with a load of 90kN is applied. The thickness of the different parts can be found in Table 6-1. For the shell model without weld and the shell with the Eriksson weld modelling approach (Eriksson, Lignell, Olsson, & Spennare, 2003) the structural intersection point is taken as the starting point for the read out of the stresses, while for the solid, shell with weld I/W approach and the combined modelling technique the weld toe is taken as the starting point. The hot spot stress calculation is based on the stress perpendicular to the weld toe.

Old OSD variant

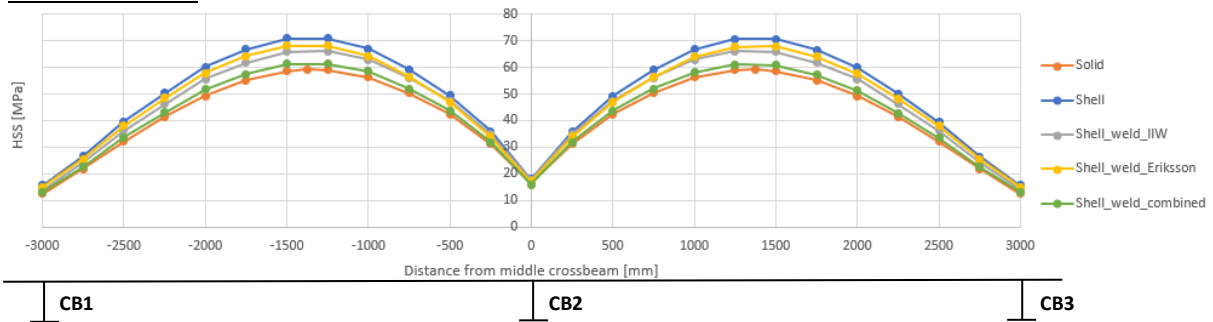


Figure 6.42 Influence line crack in web of stiffener, loaded on top of web of trough, old OSD variant

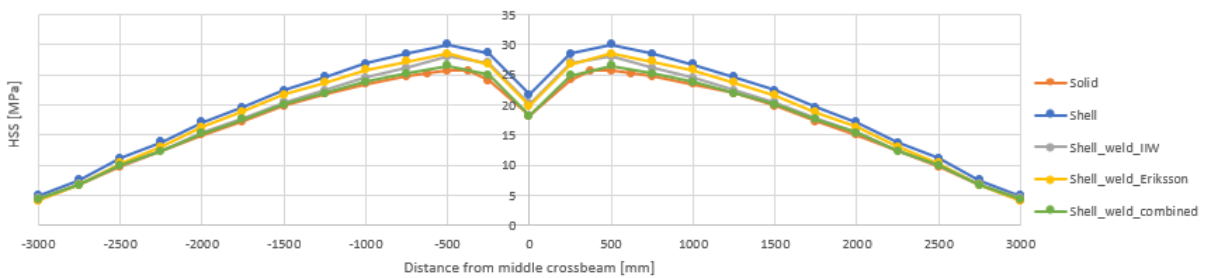


Figure 6.43 Influence line crack in web of stiffener, loaded between webs of trough, old OSD variant

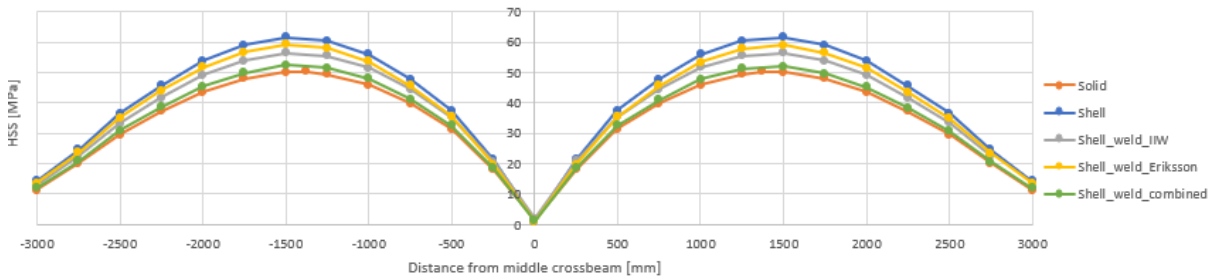


Figure 6.44 Influence line crack in web of stiffener, loaded between troughs, old OSD variant

## New OSD variant

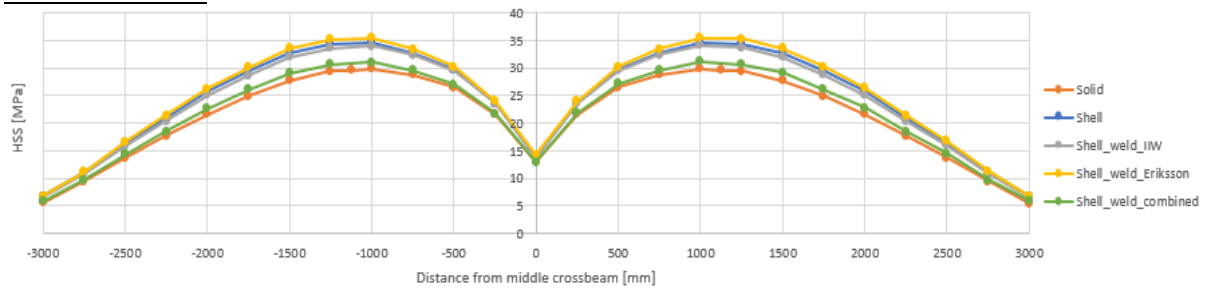


Figure 6.45 Influence line crack in web of stiffener, loaded on top of web of trough, new OSD variant

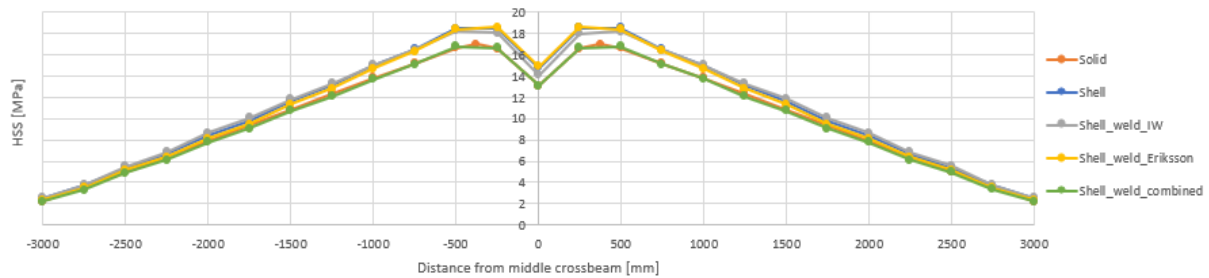


Figure 6.46 Influence line crack in web of stiffener, loaded between webs of trough, new OSD variant

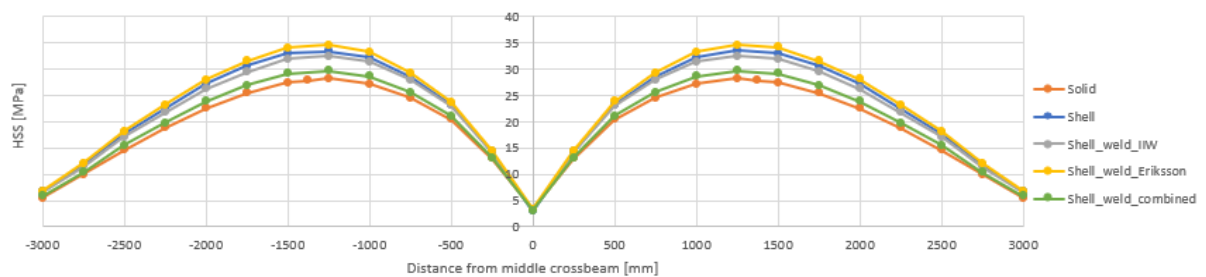


Figure 6.47 Influence line crack in web of stiffener, loaded between troughs, new OSD variant

As can be seen from Figure 6.42 to Figure 6.47, the influence line is symmetric as it can be mirrored around  $X=0$ . All five investigated FE models have their maximum hot spot stress value at the same loading position. In Table 6-13 the maximum hot spot stress values with their locations are shown for the solid FE model for the crack initiating from lower weld end in the web of the trough.

Table 6-13 Overview maximum HSS values trough for solid FE model old and new OSD variant

		Loaded on top of web trough	Loaded between webs	Loaded between troughs
Maximum HSS value [MPa]	old OSD	+59.25 MPa	+25.65 MPa	+50.39 MPa
	new OSD	+29.86 MPa	+17.00 MPa	+28.19 MPa
Location maximum value [mm]	old OSD	+/-1375mm	+/-375mm	+/-1375mm
	new OSD	+/-1000mm	+/-375mm	+/-1250mm

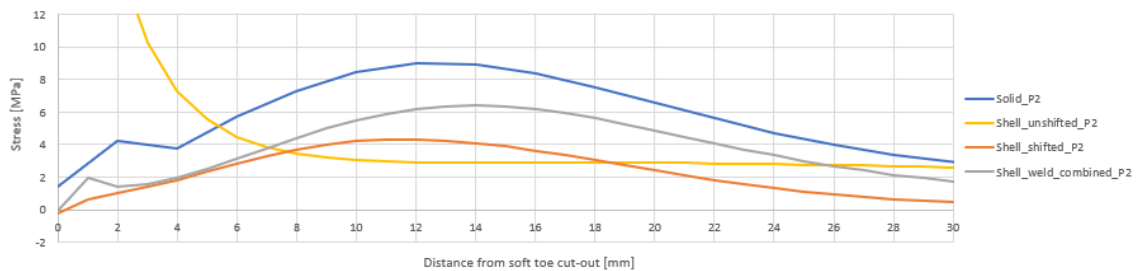
As can be seen from Table 6-13, placing the load on top of the web results in the highest hot spot stress. Placing the load between the webs of the trough results in the lowest hot spot stress out of the three investigated transverse load positions. In this FE model only three crossbeams are modelled and thus the negative part of the influence line is not taken into account, i.e. only positive hot spot stress values are obtained. Due to this limitation the minimum value of the hot spot stress is chosen to be equal to 0 MPa.

### 6.3.2. Crack in crossbeam (crack 2)

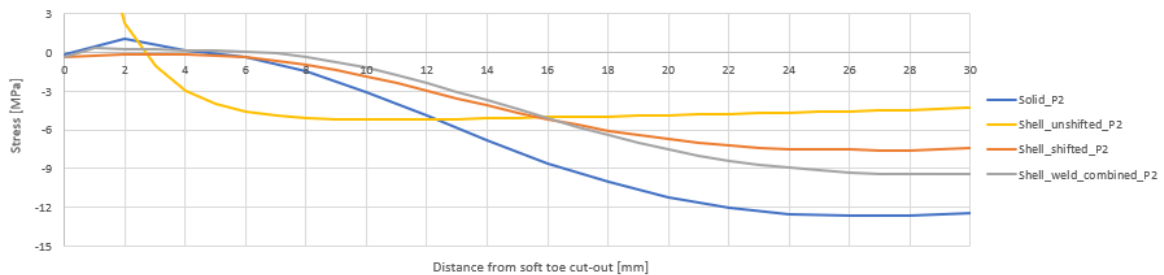
As was concluded from the small parametric analysis in section 6.2.3, the maximum value in path 2 is depending on the type of loading. For in-plane deformation its maximum value occurs at 30mm from the soft toe of the cut-out, while for out-of-plane deformation of the crossbeam this is equal to 24mm for the old OSD variant. For the new OSD variant those values are equal to 32mm and 22mm respectively. Since the applied wheel axle will result in both in-plane and out-of-plane deformation, the location should occur between those values.

The weld toe is taken as the starting location for the stress extrapolation for the solid FE model, while for the shell FE model the structural intersection point is taken as the starting location (Niemi, Fricke, & Maddox, 2018). In Figure 6.48 and Figure 6.49 the stresses in path 2, which is 1.47mm away from the weld toe, or structural intersection point, are shown. The location of the maximum stress in path 2 forms the starting location of path 4, which is perpendicular to the weld toe. For a graphical representation of path 2 and 4, see Figure 6.22. Figure 6.48 and Figure 6.49 are based on the critical loading position loaded on top of the web of the trough. As can be seen from the figures, the unshifted shell FE model, in which the structural intersection point is taken as the starting point, is giving stresses which are off when compared with the solid FE model. It shows constant values after 8mm. The stress in path 2 cannot be captured well with this shell model and thus the location of path 4 cannot be determined. Due to this the shell FE model is not suitable for the determination of this crack.

When the starting point of the shell FE model is changed from the structural intersection point to the imaginary weld toe, the absolute values are still off when compared with the solid FE model. The results improved in a qualitative way, i.e. the trendline of the solid and shell with weld FE models is matching, but in a quantitative way since some differences still exist when compared with the solid FE model. Furthermore the location of the maximum stress in path 2 is the same. For the sake of comparison of the different FE models the shifted shell FE results are included in the investigation to see how much the weld modeling techniques will improve the results.



**Figure 6.48 Results path 2, loaded on top of web, comparison FE models, old OSD variant, maximum stress path 2 at 12/14mm (stress perpendicular to weld toe)**



**Figure 6.49 Results path 2, loaded on top of web, comparison FE models, old OSD variant, maximum stress path 2 at 28mm (stress perpendicular to weld toe)**

### Critical loading position old OSD variant crack in crossbeam

First it is investigated at what height in path 2 the maximum stress occurs for all five FE models. In Figure 6.50 the stress perpendicular to the weld toe in path 2 for the critical locations is shown for the solid FE model of the old OSD variant. In this figure a distinction is made between the transverse loading positions and a further distinction is made between the minimum and maximum stresses which are obtained. The largest minimum value of the stress occurs at a height of 26-28mm in path 2, while the largest maximum value occurs at a height of 12-14mm in path 2. As was shown Figure 6.22 a regular hot spot stress extrapolation is not possible at a height of 12mm, since there is not sufficient material present.

The same check is also performed for the new OSD variant for the solid model. As can be seen from the figure, the largest minimum stress occurs at 28-30mm, while for the largest maximum stress this is at 12-14mm. Those locations are the same as with the old OSD variant. The differences in obtained stress for the minimum values in path 2 at 26-30mm are very small. For the solid FE model, with an element size of 2mm, smaller than 1%, and smaller than 0.5% for the shell FE models with an element size of 1mm.

For all three shell FE models the same procedure is followed and a summary of the old OSD variant is given in Table 6-14, while for the new OSD variant the results are given in Table 6-15.

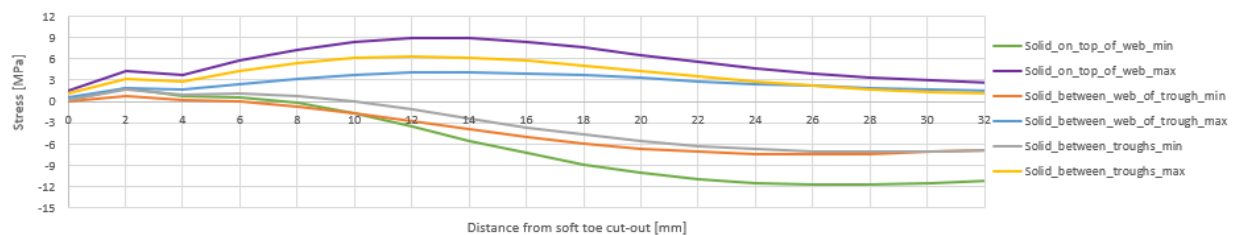


Figure 6.50 Results path 2 critical locations crossbeam solid FE model, old OSD variant (stress perpendicular to weld toe)

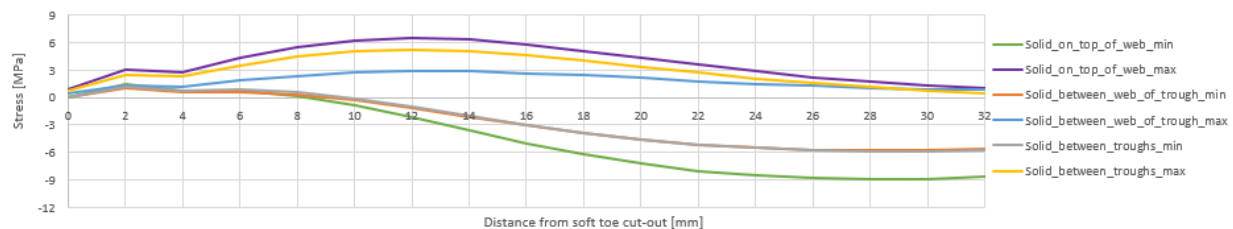


Figure 6.51 Results path 2 for critical locations crossbeam solid FE model, new OSD variant (stress perpendicular to weld toe)

Table 6-14 Location of maximum stress in path 2 for investigated transverse loading positions, old OSD variant

	Solid	Shell (shifted)	Shell IIW	Shell Eriksson	Shell combined weld
<b>Loaded on top of web trough</b>	12/28mm	12/28mm	12/28mm	14/28mm	14/28mm
<b>Loaded between webs</b>	14/26mm	12/26mm	13/26mm	14/28mm	14/28mm
<b>Loaded between troughs</b>	12/28mm	11/28mm	11/28mm	13/29mm	13/29mm

Table 6-15 Location of maximum stress in path 2 for investigated transverse loading positions, new OSD variant

	Solid	Shell (shifted)	Shell IIW	Shell Eriksson	Shell combined weld
<b>Loaded on top of web trough</b>	12/28mm	12/28mm	12/28mm	14/28mm	14/28mm
<b>Loaded between webs</b>	12/28mm	12/28mm	13/28mm	14/30mm	14/30mm
<b>Loaded between troughs</b>	12/30mm	12/30mm	12/30mm	13/31mm	13/31mm

As can be seen from both tables, the location of the minimum and maximum stress perpendicular to the weld toe in path 2 is depending on the transverse loading position. When the load is placed on top of the web or between the troughs the maximum location is at 12mm from the soft toe, while when the load is placed between the webs the maximum location is at 14mm from the soft toe. Furthermore some minor differences in the location of the maximum and minimum stress between the solid and four shell FE models can be seen. Those differences are a maximum of 2mm.

The governing transverse loading position, i.e. in which the highest stress range is obtained in the crossbeam, is when the load is placed on top of the web of the trough. The location for the minimum and maximum stress of this transverse loading position will also be used for the other two transverse loading positions. This will result in a minimum stress at 28mm and a maximum stress at 12/14mm from the soft toe. The stress range can be determined based on those two locations.

In Figure 6.52 to Figure 6.57 the influence lines for the crossbeam are shown for both the old and new OSD variants. Path 4 is at a height of 28mm and is the same for all five FE models. As was concluded in the previous section, for longitudinal locations  $X=-3000\text{mm}$  to  $X=0\text{mm}$  (CB1 to CB2), the maximum value in path 4 occurs at 12-14mm, and no regular hot spot stress extrapolation is possible. To make it possible to obtain an influence line, the stresses are extracted at P4\_28mm for the whole length of the influence line, i.e. for longitudinal locations  $X=-3000\text{mm}$  to  $X=+3000\text{mm}$  (CB1 to CB3). Linking the stress of P4\_12/14mm with the stress of P4\_28mm will be performed later on in this report.

### Old OSD variant

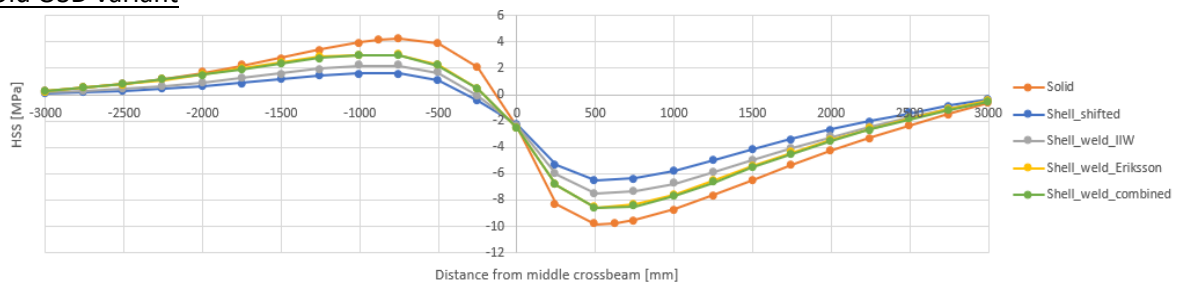


Figure 6.52 Influence line crack in crossbeam, loaded on top of web of trough, old OSD variant

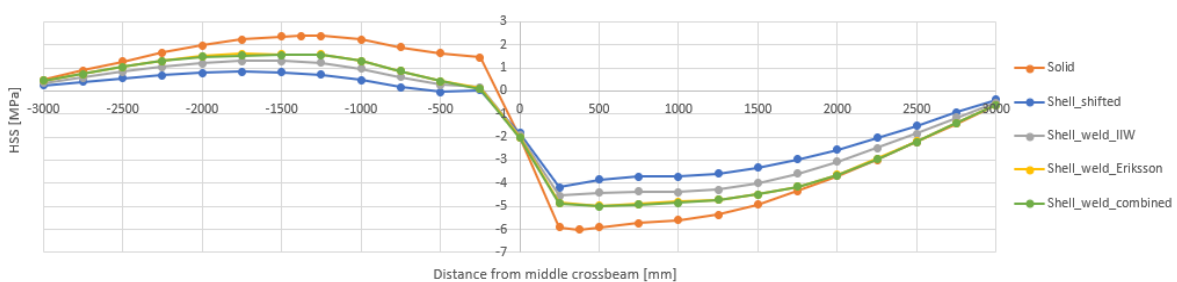


Figure 6.53 Influence line crack in crossbeam, loaded between webs of trough, old OSD variant

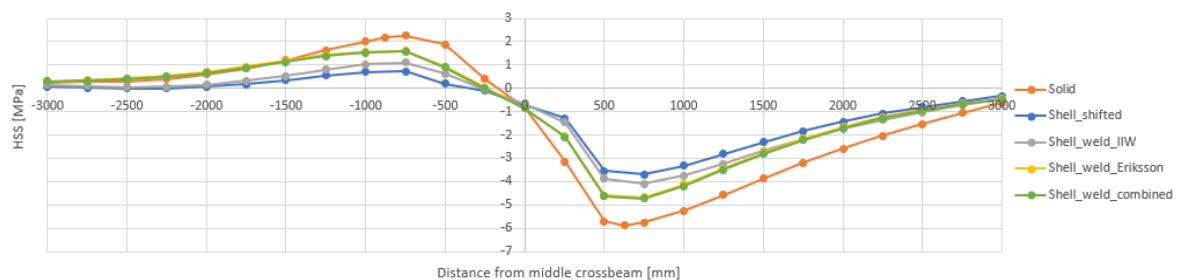


Figure 6.54 Influence line crack in web of stiffener, loaded between troughs, old OSD variant



## New OSD variant

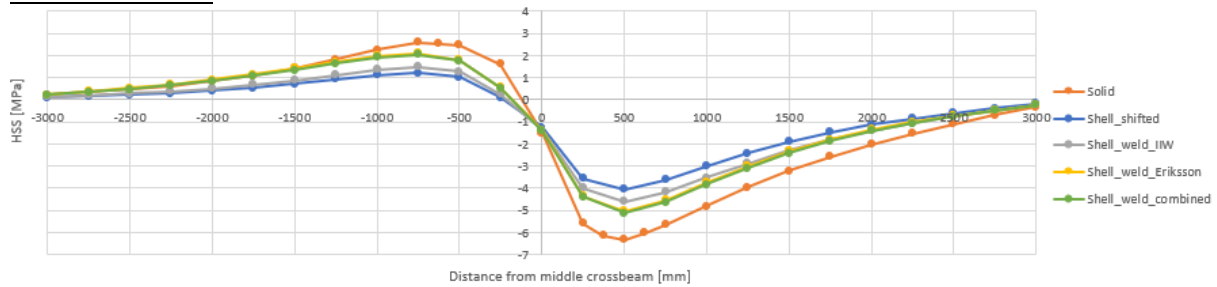


Figure 6.55 Influence line crack in crossbeam, loaded on top of web of trough, new OSD variant

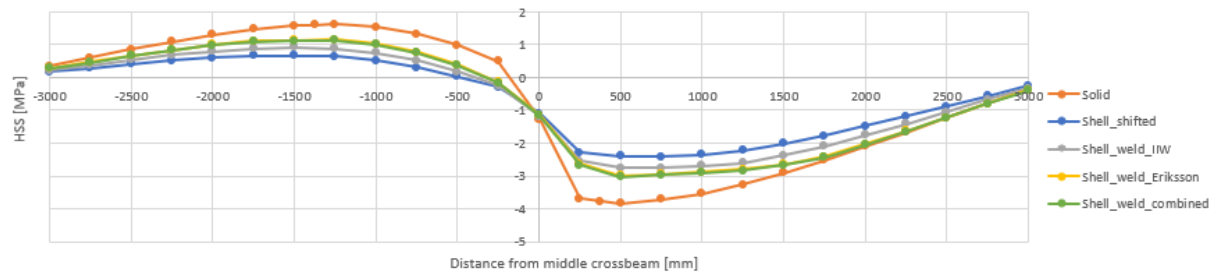


Figure 6.56 Influence line crack in crossbeam, loaded between webs of trough, new OSD variant

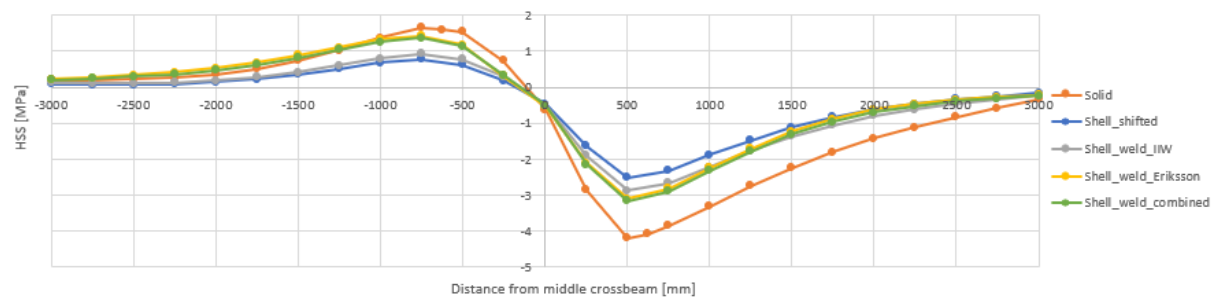


Figure 6.57 Influence line crack in web of stiffener, loaded between troughs, new OSD variant

As can be seen from Figure 6.52 to Figure 6.57, the influence line consists of both positive and negative hot spot stress values. Without the weld modelling of the shell FE model a large difference in results can be seen when compared with the solid FE model. Including the weld in the shell FE model will improve the results and the weld modelling technique proposed by (Eriksson, Lignell, Olsson, & Spennare, 2003), the increased thickness method, gives the largest improvement. The differences between the Eriksson weld modelling approach and the combined approach are negligible in those cases, i.e. the difference is smaller than 1%. The obtained hot spot stresses of the solid FE model are higher for all loading positions when compared with the four shell FE models.

An overview of the obtained hot spot stress for the solid FE model of the both the old and new OSD variant is shown in Table 6-16.

Table 6-16 Overview maximum and minimum HSS values crossbeam, old OSD variant

	Loaded on top of web trough		Loaded between webs		Loaded between troughs	
	Old OSD	New OSD	Old OSD	New OSD	Old OSD	New OSD
Maximum HSS value [MPa]	+4.21	+2.58	+2.39	+1.61	+2.26	+1.66
Minimum HSS value [MPa]	-9.84	-6.35	-6.02	-3.85	-5.88	-4.16



As can be seen from Table 6-16, placing the load on top of the web of the trough will result in the highest hot spot stress range. Placing the load between the webs of the trough or between the troughs will result in almost the same stress range. A side note which should be placed is that for the determination of the maximum hot spot stress value the path at 28mm is taken, while from Figure 6.50 it can be seen that the maximum value occurs at 12mm. A further investigation to obtain the hot spot stress from path 4 at a height of 12/14mm will be performed in section 6.4.

### 6.3.3. Conclusions based on parametric studies I and II

In this subchapter the results of parametric study I and II are shown. A distinction is made between the crack in the web of the trough and the crack in the crossbeam.

#### Results of crack in trough

The critical loading positions for the crack location in the web of the trough for both the old and new OSD variant are shown in Table 6-17.

Table 6-17 Location of minimum and maximum hot spot stress for crack in web trough

	Old OSD variant		New OSD variant	
	Min [mm]	Max [mm]	Min [mm]	Max [mm]
<b>Loaded on top of web trough</b>	-	+1375	-	+1000
<b>Loaded between webs</b>	-	+375	-	+375
<b>Loaded between troughs</b>	-	+1375	-	+1250

The obtained hot spot stress for the critical loading positions is shown in Table 6-18. The ratios between the shell and solid FE models are shown in Table 6-19 for the old OSD and new OSD variant. This ratio is more or less constant for the total influence line.

Table 6-18 Obtained hot spot stress solid and shell FE models, web of trough, at critical loading position

		$\sigma_{HSS\_solid}$ [MPa]	$\sigma_{HSS\_shell}$ [MPa]	$\sigma_{HSS\_shell\_IIW}$ [MPa]	$\sigma_{HSS\_shell\_Eriksson}$ [MPa]	$\sigma_{HSS\_shell\_combined}$ [MPa]
<b>Loaded on top of web trough</b>	<b>old OSD</b>	+59.25	+72.18	+65.86	+68.12	+61.66
	<b>new OSD</b>	+29.86	+34.58	+33.90	+35.39	+30.93
<b>Loaded between webs</b>	<b>old OSD</b>	+25.65	+30.04	+27.10	+27.86	+26.28
	<b>new OSD</b>	+17.00	+18.51	+18.09	+18.47	+17.04
<b>Loaded between troughs</b>	<b>old OSD</b>	+50.39	+62.16	+56.00	+58.78	+52.40
	<b>new OSD</b>	+28.19	+33.51	+32.54	+34.60	+29.67

Table 6-19 Overview obtained ratios HSS solid and shell FE models, web of trough, at critical loading position

		$\frac{\sigma_{HSS\_shell}}{\sigma_{HSS\_solid}}$	$\frac{\sigma_{HSS\_shell\_weld\_IIW}}{\sigma_{HSS\_solid}}$	$\frac{\sigma_{HSS\_shell\_weld\_Eriksson}}{\sigma_{HSS\_solid}}$	$\frac{\sigma_{HSS\_shell\_weld\_combined}}{\sigma_{HSS\_solid}}$
<b>Loaded on top of web trough</b>	<b>old OSD</b>	1.15-1.25	1.10-1.15	1.15	1.05
	<b>new OSD</b>	1.10-1.20	1.15	1.15-1.20	1.05
<b>Loaded between webs</b>	<b>old OSD</b>	1.10-1.20	1.05-1.10	1.10	1.00-1.05
	<b>new OSD</b>	1.05-1.15	1.05-1.15	1.05-1.15	1.00
<b>Loaded between troughs</b>	<b>old OSD</b>	1.20-1.25	1.10-1.15	1.15	1.05
	<b>new OSD</b>	1.15-1.20	1.10-1.20	1.15-1.25	1.05

Three different weld modelling techniques for the shell FE model were investigated: IIW, Eriksson and a combination of the two approaches. As can be seen from Table 6-19, the shell with the combined weld modelling technique gives the best results when compared with the hot spot stress of the solid FE model. Applying this weld modelling technique for the shell reduces the scatter in results from a factor 1.20-1.25 to a factor 1.05 for both the old and new OSD variant.

The obtained hot spot stress for the new OSD variant is lower for all load cases when compared with the old variant. The reduction in calculated hot spot stress is a factor 1.50-2.00, depending on the transverse loading position.

**CV (coefficient of variation) for shell weld model**

Based on the above mentioned critical loading positions for the investigated transverse positions, the coefficient of variation will be determined based on the following formula:

$$COV = \frac{\textit{standard deviation}}{\textit{mean}}$$

This calculation is done only for the shell with combined weld modelling since this method showed the best results when compared with the solid FE model. The mean value is equal to **1.04** for both the old and new OSD variant. A coefficient of variation of **0.8%** is obtained for the old OSD variant, while a CV of **2.2%** is obtained for the new OSD variant. The standard deviation is equal to 0.01 and 0.02 respectively.

Results of crack in crossbeam

The critical loading positions for the crack location in the crossbeam for both the old and new OSD variant are shown in Table 6-20.

**Table 6-20 Location of minimum and maximum hot spot stress for crack in crossbeam**

	Old OSD variant		New OSD variant	
	Min [mm]	Max [mm]	Min [mm]	Max [mm]
<b>Loaded on top of web trough</b>	+500	-750	+500	-750
<b>Loaded between webs</b>	+375	-1375	+500	-1250
<b>Loaded between troughs</b>	+625	-750	+500	-750

The obtained hot spot stress in the crossbeam for the different FE models can be found in Table 6-21. The ratio of the solid hot spot stress and the shell hot spot stress is differing for investigated transverse load positions. Only the ratio of the solid and shell FE models is compared at the location of the maximum and minimum hot spot stress. The ratio is shown in

Table 6-22 and Table 6-23 in which the hot spot stress results are obtained at 28mm from the soft toe of the “Haibach” cope hole, i.e. P4\_28mm.

Table 6-21 Obtained hot spot stress solid and shell FE models, crossbeam, at critical loading position, for P4\_28mm

	$\sigma_{HSS\_solid}$ [MPa]	$\sigma_{HSS\_shell\_shifted}$ [MPa]	$\sigma_{HSS\_shell\_IIW}$ [MPa]	$\sigma_{HSS\_shell\_Eriksson}$ [MPa]	$\sigma_{HSS\_shell\_combined}$ [MPa]
<b>Loaded on top of web trough old OSD</b>	Min: -9.84 Max: +4.21	Min: -6.54 Max: +1.60	Min: -7.49 Max: +2.21	Min: -8.55 Max: +3.02	Min: -8.59 Max: +2.97
<b>Loaded between webs old OSD</b>	Min: -6.02 Max: +2.39	Min: -4.07 Max: +0.75	Min: -4.47 Max: +1.26	Min: -4.99 Max: +1.63	Min: -5.07 Max: +1.62
<b>Loaded between troughs old OSD</b>	Min: -5.88 Max: +2.26	Min: -3.75 Max: +0.73	Min: -3.99 Max: +1.12	Min: -4.81 Max: +1.61	Min: -4.90 Max: +1.57
<b>Loaded on top of web trough new OSD</b>	Min: -6.35 Max: +2.58	Min: -4.06 Max: +1.21	Min: -4.61 Max: +1.49	Min: -5.05 Max: +2.10	Min: -5.13 Max: +2.04
<b>Loaded between webs new OSD</b>	Min: -3.85 Max: +1.61	Min: -2.40 Max: +0.63	Min: -2.75 Max: +0.91	Min: -2.98 Max: +1.15	Min: -3.02 Max: +1.13
<b>Loaded between troughs new OSD</b>	Min: -4.16 Max: +1.66	Min: -2.50 Max: +0.78	Min: -2.87 Max: +0.93	Min: -3.10 Max: +1.43	Min: -3.16 Max: +1.39

Table 6-22 Overview obtained ratios HSS solid and shell FE models old OSD variant, for P4\_28mm

	$\frac{\sigma_{HSS\_shell\_shifted}}{\sigma_{HSS\_solid}}$	$\frac{\sigma_{HSS\_shell\_weld\_IIW}}{\sigma_{HSS\_solid}}$	$\frac{\sigma_{HSS\_shell\_weld\_Eriksson}}{\sigma_{HSS\_solid}}$	$\frac{\sigma_{HSS\_shell\_weld\_combined}}{\sigma_{HSS\_solid}}$
<b>Loaded on top of web trough</b>	Min: 0.66 Max: 0.38	Min: 0.76 Max: 0.52	Min: 0.87 Max: 0.72	Min: 0.87 Max: 0.70
<b>Loaded between webs</b>	Min: 0.68 Max: 0.32	Min: 0.76 Max: 0.53	Min: 0.83 Max: 0.68	Min: 0.84 Max: 0.68
<b>Loaded between troughs</b>	Min: 0.63 Max: 0.34	Min: 0.70 Max: 0.50	Min: 0.82 Max: 0.71	Min: 0.83 Max: 0.70

Table 6-23 Overview obtained ratios HSS solid and shell FE models new OSD variant, for P4\_28mm

	$\frac{\sigma_{HSS\_shell\_shifted}}{\sigma_{HSS\_solid}}$	$\frac{\sigma_{HSS\_shell\_weld\_IIW}}{\sigma_{HSS\_solid}}$	$\frac{\sigma_{HSS\_shell\_weld\_Eriksson}}{\sigma_{HSS\_solid}}$	$\frac{\sigma_{HSS\_shell\_weld\_combined}}{\sigma_{HSS\_solid}}$
<b>Loaded on top of web trough</b>	Min: 0.64 Max: 0.47	Min: 0.73 Max: 0.58	Min: 0.81 Max: 0.80	Min: 0.81 Max: 0.79
<b>Loaded between webs</b>	Min: 0.62 Max: 0.39	Min: 0.71 Max: 0.57	Min: 0.78 Max: 0.71	Min: 0.79 Max: 0.70
<b>Loaded between troughs</b>	Min: 0.60 Max: 0.47	Min: 0.69 Max: 0.56	Min: 0.82 Max: 0.74	Min: 0.83 Max: 0.73

A large scatter in results between the solid and shell FE models can be seen from Table 6-22. For the part of the influence line which will result in the maximum hot spot stress the ratio is close to 0.30-0.50. While for the part of the influence line which will result in the minimum hot spot stress value the ratio is around 0.60-0.70. Including the weld modelling will improve the results of the shell FE model and the scatter in results is reduced. With the increased thickness weld modelling technique, proposed by (Eriksson, Lignell, Olsson, & Spennare, 2003), the difference in results is around 0.72 for the maximum critical position and around 0.83 for the minimum critical position. Combining both the weld modelling approaches will give results which are similar to the Eriksson weld modelling technique results. The hot spot stress results of all shell models are underestimating the hot spot stress when

compared with the solid FE results. The combined weld modelling technique give the best results when compared with the solid FE results.

The obtained hot spot stress for the new OSD variant is lower for all load cased when compared with the old variant. The reduction in calculated hot spot stress is a factor 1.40-1.70, depending on the transverse loading position.

In the crossbeam, the stress perpendicular to the weld toe cannot be captured in a good way with the regular shell model. Due to this it is not possible to determine the location of the maximum stresses perpendicular to the weld toe in path 2. The shell FE model is not suitable for the calculation of this type of crack.

#### 6.4. Further investigation parametric studies

In this section the differences between the solid and shell FE models for the critical loading positions from section 6.3 are further investigated and a comparison between the different FE models is made. Furthermore an investigation to obtain the hot spot stress from path 4 at a height of 12/14mm from the soft toe of the cut-out is performed. As was concluded in section 6.3.3, the combined weld modelling technique shows results which are closest to the solid FE results. Based on this only the results of this weld modelling technique are shown

In the next figures a comparison between the solid, original shell and shell with weld FE models are shown for the critical loading positions. First the results of the crack in the web of the trough are shown for the critical loading position in transverse direction, i.e. in which the highest stress range is observed. Next to that the results in the crossbeam are shown in which a distinction is made between the maximum stress at a height of 28mm and 12/14mm from the soft toe. The former results in the minimum hot spot stress, while the latter results in the maximum hot spot stress.

##### 6.4.1. Crack in web of trough at lower weld end (crack 1)

In Figure 6.58 and Figure 6.59 the results for the transverse loading position in which the load is applied on the web are shown for the old and new OSD variant. This transverse loading position results in the highest hot spot stress. The other graphs of the other critical transverse loading positions of the old OSD and new OSD variants can be found in Annex I.

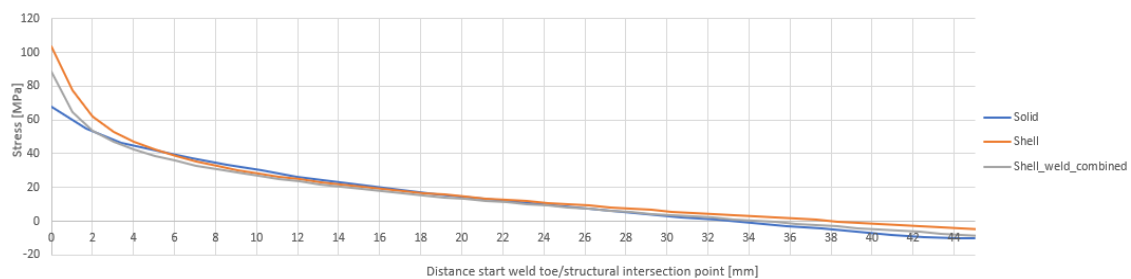
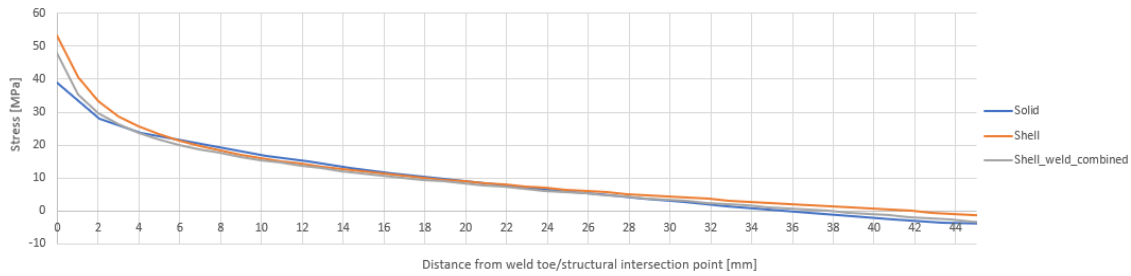


Figure 6.58 Comparison for critical loading position X=+1375mm, loaded on top of web, crack in web trough, old OSD variant (stress perpendicular to weld toe)



**Figure 6.59 Comparison for critical loading position X=+1000mm, loaded on top of web, crack in web trough, new OSD variant (stress perpendicular to weld toe)**

From the above figures it is observed that the trendlines of the investigated FE models are in good compliance. Both the original shell and the shell with the combined weld modelling techniques are overestimating the hot spot. The regular shell FE models are underestimating the stress perpendicular to the weld toe with a few percent from 5mm to approximately 18mm from the weld toe/structural intersection point. The shell with combined weld modelling approach is also underestimating the stress a bit from 2mm to 18mm from the weld toe/structural intersection point. The underestimation of the stress is larger with the shell with combined weld modelling, but the obtained hot spot stress is closer to the solid FE results. This also occurs for the other loading positions which are not critical, i.e. the shell with weld is underestimating from 5mm to 18mm from the weld toe/structural intersection point, but the obtained hot spot stress is only 5% higher. Furthermore, it can be seen from the figures that the stress at 45mm from the weld toe, of the solid FE model and shell with weld FE model is of the same order. An overview of the obtained hot spot stress and stress at 45mm from the weld toe/intersection point for the critical transverse loading positions of the old and new OSD variant is shown in Table 6-24 and Table 6-25.

**Table 6-24 Overview hot spot stress and stress at 45mm for critical loading positions, web of trough, old OSD variant**

	Loaded on top of web trough		Loaded between webs		Loaded between troughs	
	HSS [MPa]	Stress at 45mm [MPa]	HSS [MPa]	Stress at 45mm [MPa]	HSS [MPa]	Stress at 45mm [MPa]
<b>Solid FE model</b>	+59.25	-9.96	+25.65	-0.58	+50.19	-9.30
<b>Shell FE model</b>	+72.18	-4.93	+30.04	+0.82	+62.16	-4.74
<b>Shell combined weld FE model</b>	+61.66	-8.74	+26.28	-0.45	+52.40	-7.93

**Table 6-25 Overview hot spot stress and stress at 45mm for critical loading positions, web of trough, new OSD variant**

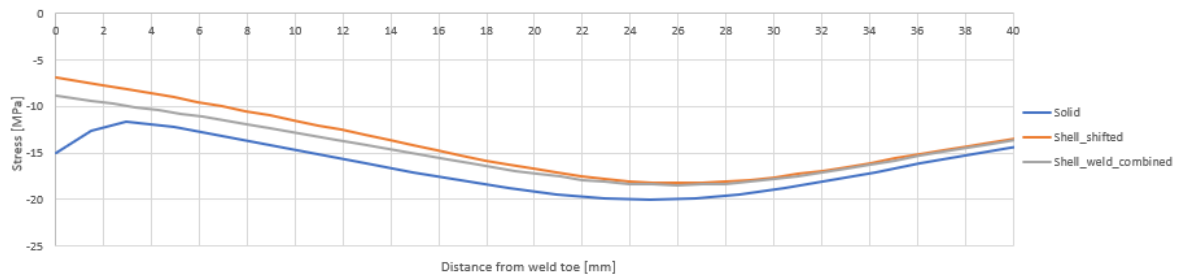
	Loaded on top of web trough		Loaded between webs		Loaded between troughs	
	HSS [MPa]	Stress at 45mm [MPa]	HSS [MPa]	Stress at 45mm [MPa]	HSS [MPa]	Stress at 45mm [MPa]
<b>Solid FE model</b>	+29.86	-3.76	+17.00	-0.18	+28.19	-4.86
<b>Shell FE model</b>	+34.69	-1.49	+19.07	+1.12	+33.51	-2.71
<b>Shell combined weld FE model</b>	+31.14	-3.19	+17.36	-0.07	+29.67	-4.26

#### 6.4.2. Crack in crossbeam (crack 2)

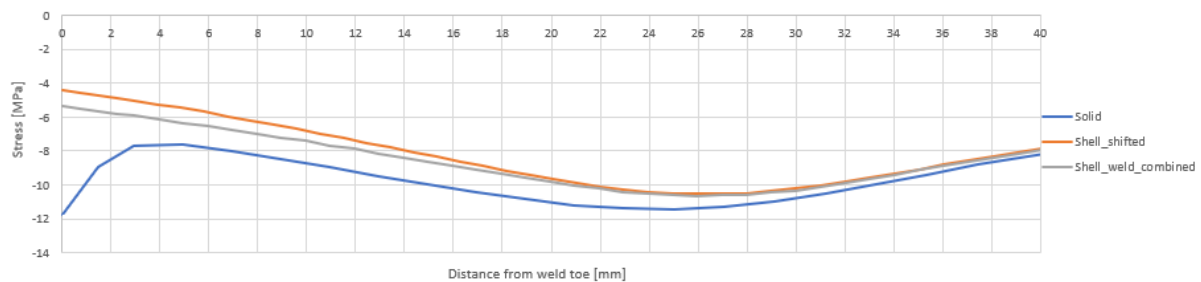
For the crack in the crossbeam, initiating from the weld toe at some distance from the soft toe of the cut-out, a distinction need to be made between the minimum and maximum obtained hot spot stress values. As was stated earlier, the minimum hot spot stress occurs at a height of 28mm from the soft toe, for longitudinal locations: X=0mm to X=3000mm (CB2 to CB3), while the maximum hot spot values

occur at height of 12mm from the soft toe, for longitudinal locations  $X=-3000\text{mm}$  to  $X=0\text{mm}$  (CB1 to CB2). First the results of the minimum hot spot stress are shown.

In Figure 6.60 and Figure 6.61 the results for the transverse loading position in which the load is applied on the web of the trough are shown for the old and new OSD variant. The other graphs of the other critical transverse loading positions of the old OSD and new OSD variants can be found in Annex I. In those figures the critical locations are shown which result in the minimum hot spot stress. The results of the shell original FE model are shifted to the weld toe to make the comparison between the different models, since in section 6.3.2 it was concluded that the original shell FE model cannot capture the stresses in a good manner. This is done only for the sake of comparison.



**Figure 6.60 Comparison stress P4\_28mm, for critical loading position  $X=+500\text{mm}$ , loaded on top of web, crack in CB, old OSD variant (stress perpendicular to weld toe)**



**Figure 6.61 Comparison stress P4\_28mm, for critical loading position  $X=+500\text{mm}$ , loaded on top of web, crack in CB, new OSD variant (stress perpendicular to weld toe)**

In Figure 6.60 and Figure 6.61 the stress perpendicular to the weld toe at a height of 28mm are shown. It is clearly visible that the shell FE models are underestimating the hot spot stress in the crossbeam. This underestimation is directly at the weld toe where a stress concentration occurs. At 40mm away from the weld toe the stresses perpendicular to the weld toe of all three FE models are of the same order again. Furthermore it can be seen that modelling the weld with the shell FE model will reduce the scatter in results when compared with the solid FE model.

An overview of the obtained hot spot stress and stress at 40mm from the weld toe for the critical loading positions of the old and new OSD variant is shown in Table 6-26 and Table 6-27. In Table 6-28 an overview of the ratio between the hot spot stress of the shell combined weld and solid FE model is given.

**Table 6-26 Overview hot spot stress and stress at 40mm for critical loading positions, crossbeam, old OSD variant**

	Loaded on top of web trough		Loaded between webs		Loaded between troughs	
	HSS [MPa]	Stress at 40mm [MPa]	HSS [MPa]	Stress at 40mm [MPa]	HSS [MPa]	Stress at 40mm [MPa]
<b>Solid FE model</b>	-9.84	-14.41	-6.02	-10.95	-5.88	-8.06
<b>Shell FE model (shifted)</b>	-6.54	-13.48	-4.07	-10.36	-3.75	-7.57
<b>Shell combined weld FE model</b>	-8.59	-13.66	-5.07	-10.67	-4.90	-7.60

**Table 6-27 Overview hot spot stress and stress at 40mm for critical loading positions, crossbeam, new OSD variant**

	Loaded on top of web trough		Loaded between webs		Loaded between troughs	
	HSS [MPa]	Stress at 40mm [MPa]	HSS [MPa]	Stress at 40mm [MPa]	HSS [MPa]	Stress at 40mm [MPa]
<b>Solid FE model</b>	-6.35	-7.86	-3.85	-5.86	-4.16	-5.13
<b>Shell FE model (shifted)</b>	-4.06	-7.62	-2.40	-5.79	-2.50	-4.93
<b>Shell combined weld FE model</b>	-5.13	-7.71	-3.02	-5.82	-3.16	-4.95

**Table 6-28 Overview ratio HSS shell combined weld and solid for critical loading positions (minimum hot spot stress)**

		$\frac{\sigma_{HSS\_shell\_combined\_weld}}{\sigma_{HSS\_solid}}$
<b>Loaded on top of web trough</b>	<b>old OSD</b>	0.87
	<b>new OSD</b>	0.81
<b>Loaded between webs</b>	<b>old OSD</b>	0.84
	<b>new OSD</b>	0.79
<b>Loaded between troughs</b>	<b>old OSD</b>	0.83
	<b>new OSD</b>	0.76

For both the old and new OSD variant the largest scatter in results, i.e. the smallest ratio, is observed when the load is placed between the troughs. For the old OSD variant this ratio is equal to 0.83, while for the new OSD variant this ratio is equal to 0.76.

**Investigation to obtain the hot spot stress from path 12/14mm and link to HSS path 28mm**

As stated earlier, for the crossbeam it is found that for the negative hot spot stress values of the influence line, i.e. for longitudinal locations: X=0mm to X=3000mm (CB2 to CB3), path 4 is at a height of 28mm from the soft toe, i.e. the maximum stress in path 2 occurs at 28mm. For the positive hot spot values of the influence line, i.e. for longitudinal locations: X=-3000mm to X=0mm (CB1 to CB2), path 4 is at a height of 12/14mm from the soft toe, and no regular HSS extrapolation is possible since there is not sufficient material. To see how the trendlines of P4\_28mm and P4\_12mm or P4\_14mm are, the results of the stress perpendicular to the weld toe are extracted. The different paths are shown in Figure 6.62. Also the results from an additional path, P4\_22mm, are extracted which is in between the two other paths.

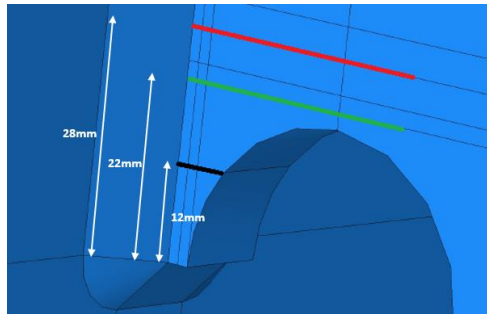


Figure 6.62 Overview different paths perpendicular to weld toe

In Figure 6.63 the stress perpendicular to the weld toe is shown for the three paths at the critical loading position: loaded on top of web  $X=-750\text{mm}$ , see Figure 6.52. As can be seen from the figure, the trendline of all three paths is approximately parallel to each other.

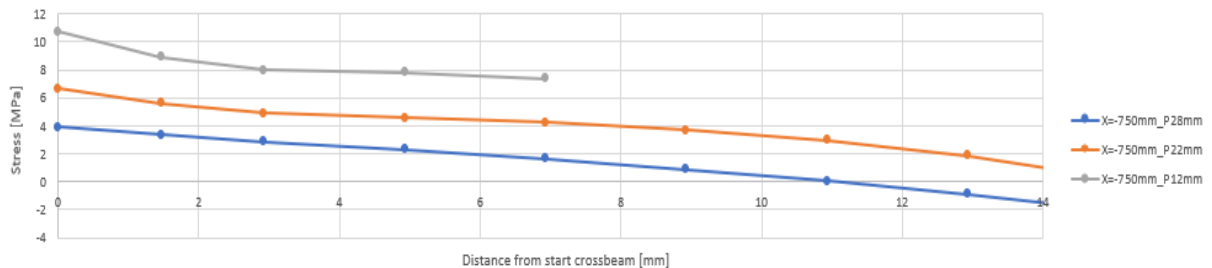


Figure 6.63 Stress perpendicular to weld toe in P4\_12mm, P4\_22mm and P4\_28mm critical loading position  $X=-750\text{mm}$ , loaded on top of web, solid FE model

Stress path critical locations for crack in crossbeam P4 12/14mm old OSD variant:

From Table 6-14 and Table 6-15 it was concluded that the location of the maximum stress is both depending on the transverse loading position and the FE model. For the solid and regular shifted shell FE model the maximum stress occurs at a height of 12mm from the soft toe, while for the shell combined weld FE model the maximum stress occurs at 14mm from the soft toe.

The stress perpendicular to the weld toe is shown in Figure 6.64 and Figure 6.65 for the transverse loading position, in which the load is applied on the web of the trough, for the old and new OSD variant. The other graphs of the other critical transverse loading positions of the old OSD and new OSD variants can be found in Annex I. Also the stress at those critical locations at a height of 28mm from the soft toe can be found in Annex I.

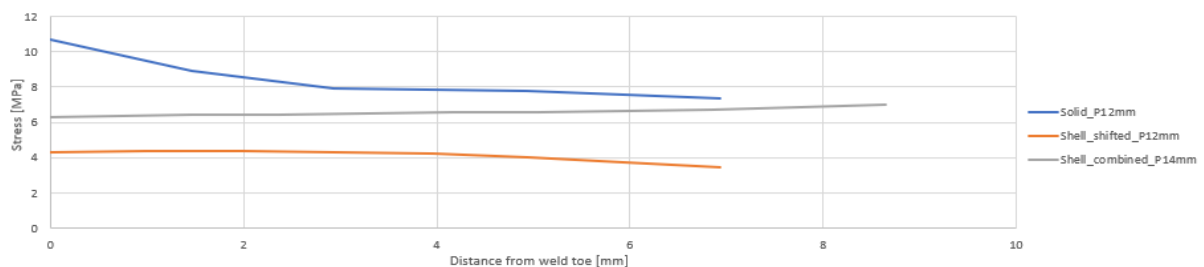
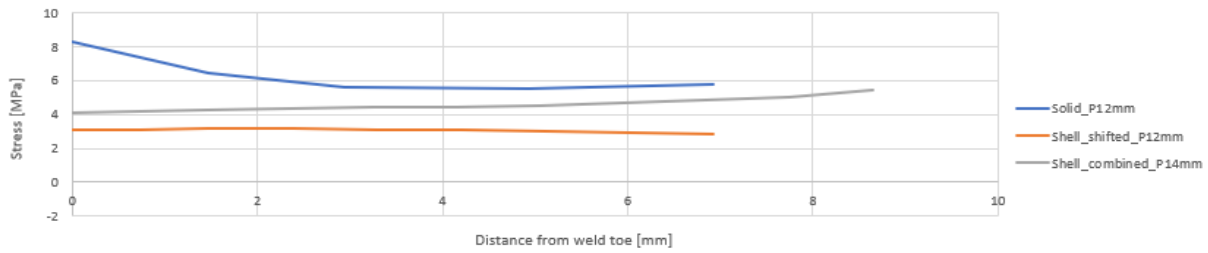


Figure 6.64 Comparison stress perpendicular to weld toe, P4\_12/14mm, for critical loading position  $X=-750\text{mm}$ , loaded on top of web, crack in CB, old OSD variant





**Figure 6.65 Comparison stress perpendicular to weld toe, P4\_12/14mm, for critical loading position X=-750mm, loaded on top of web, crack in CB, new OSD variant**

As was investigated previously, when the combined weld modelling technique is applied for the shell FE model, the maximum stress occurs at 14mm from the soft toe instead of the 12mm for the solid FE model. Due to this the trendline of this shell combined weld FE model is bit different when compared with the solid FE model. Furthermore the stress in both shell FE models is quite constant at the measured path. A similar observation is also valid for the solid FE model after approximately 3mm from the weld toe. From 0mm to 3mm from the weld toe a stress concentration occurs due to the weld toe.

#### Approximation method I: direct stress read out

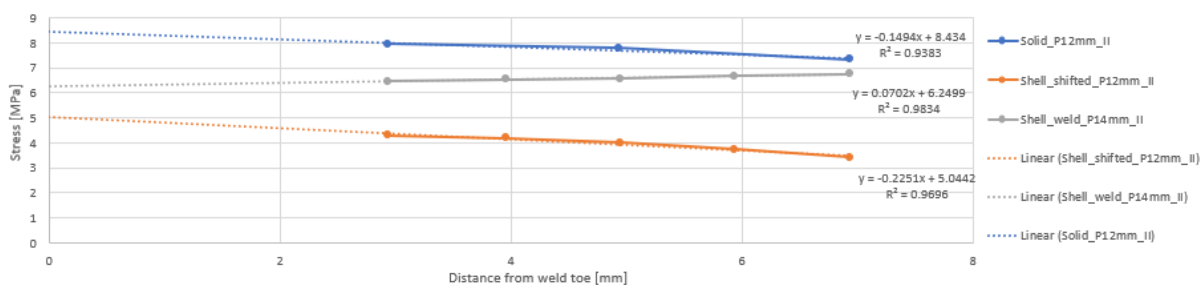
Since a regular hot spot stress extrapolation is not possible for this location an approximation need to be made. As stated, for the solid FE model the stress at 3mm from the weld toe is quite constant, or the graph has a slight slope. For the shell FE models the stress is almost constant so the stress at X=0mm is taken as the hot spot stress. For the solid FE model the stress at 2.93mm away from the weld toe is taken as the hot spot stress. The obtained hot spot stress can be found in Table 6-29.

**Table 6-29 Obtained hot spot stress at P4\_12/14mm, crack is crossbeam, old and new OSD variants (approx. method I)**

	Loaded on top of web trough		Loaded between webs		Loaded between troughs	
	Old OSD HSS [MPa]	New OSD HSS [MPa]	Old OSD HSS [MPa]	New OSD HSS [MPa]	Old OSD HSS [MPa]	New OSD HSS [MPa]
<b>Solid FE model</b>	+8.2	+5.6	+3.8	+2.4	+5.8	+4.4
<b>Shell FE model (shifted)</b>	+4.2	+3.1	+1.6	+1.1	+3.1	+2.6
<b>Shell combined weld FE model</b>	+6.2	+4.2	+2.8	+1.7	+4.4	+3.4

#### Approximation method II: linear curve fitting of results

Another procedure is also followed to determine the hot spot stress. This method is based on linear curve fitting of the results. As can be seen from Figure 6.64, the stress of the solid FE model is quite constant after approximately 3mm from the weld toe. Based on this the trendline is linearly curve fitted for the solid and shell FE models. The same distance from the weld toe: 2.93mm to 6.93mm, is chosen to make the comparison and an overview of this procedure is shown in Figure 6.66.



**Figure 6.66 Linear curve fitted results different FE models, loaded on top of web, old OSD variant**

The results of the linear curve fitting procedure for the other investigated locations are shown in Table 6-30.

Table 6-30 Obtained hot spot stress at P4\_12/14mm, crack is crossbeam, old and new OSD variants (approx. method II)

	Loaded on top of web trough		Loaded between webs		Loaded between troughs	
	Old OSD HSS [MPa]	New OSD HSS [MPa]	Old OSD HSS [MPa]	New OSD HSS [MPa]	Old OSD HSS [MPa]	New OSD HSS [MPa]
<b>Solid FE model</b>	+8.34	+5.52	+4.10	+2.80	+5.56	+4.43
<b>Shell FE model (shifted)</b>	+5.04	+3.35	+2.00	+1.27	+3.47	+2.78
<b>Shell combined weld FE model</b>	+6.25	+4.06	+2.85	+1.95	+4.23	+3.21

Based on the results from both approximation methods the ratio between the hot spot stress of the shell FE models and solid FE model can be calculated for which the results are shown in Table 6-31.

Table 6-31 Overview ratios obtained hot spot stress crack in crossbeam for different approximation methods

		Approximation method I		Approximation method II	
		$\frac{\sigma_{HSS\_shell\_shifted}}{\sigma_{HSS\_solid}}$	$\frac{\sigma_{HSS\_shell\_weld\_comb}}{\sigma_{HSS\_solid}}$	$\frac{\sigma_{HSS\_shell\_shifted}}{\sigma_{HSS\_solid}}$	$\frac{\sigma_{HSS\_shell\_weld\_comb}}{\sigma_{HSS\_solid}}$
<b>Loaded on top of web trough</b>	<b>old OSD</b>	0.51	0.76	0.60	0.75
	<b>new OSD</b>	0.55	0.75	0.61	0.74
<b>Loaded between webs</b>	<b>old OSD</b>	0.42	0.74	0.49	0.70
	<b>new OSD</b>	0.45	0.71	0.45	0.70
<b>Loaded between troughs</b>	<b>old OSD</b>	0.53	0.76	0.62	0.76
	<b>new OSD</b>	0.59	0.76	0.63	0.73

As can be seen from Table 6-31, the ratio between the hot spot stress of the shell FE model with combined weld and the solid FE is quite constant for the critical transverse loading positions and equal to approximately 0.70-0.76 for both the old and new OSD variant. The results of the shell FE model are shifted from the structural intersection point to the weld toe, this is not the standard procedure but is done for the sake of comparison of the improvement of the applied weld modelling technique.

#### Link hot spot stress from path 28mm to hot spot stress path 12/14mm

With the above mentioned approximation methods the hot spot stress at P4\_12/14mm is determined. The next step is to investigate a link between the hot spot stress of P4\_28mm and P4\_12/14mm. The obtained hot spot stresses of P4\_28mm are shown in Table 6-21, while the results of P4\_12/14mm are shown in Table 6-29 and Table 6-30. The ratio between the hot spot stress at P4\_28mm and P4\_12/14mm is calculated to see what factor is obtained and the results are shown in Table 6-32.

Table 6-32 Overview ratio HSS P4\_28mm and P4\_12/14mm for critical loading positions (maximum hot spot stress)

		$\frac{\sigma_{HSS\_solid\_P12mm}}{\sigma_{HSS\_solid\_P28mm}}$	$\frac{\sigma_{HSS\_shell\_weld\_P14mm}}{\sigma_{HSS\_shell\_weld\_P28mm}}$
<b>Loaded on top of web trough</b>	<b>old OSD</b>	1.98	2.10
	<b>new OSD</b>	2.10	1.99
<b>Loaded between webs</b>	<b>old OSD</b>	1.72	1.76
	<b>new OSD</b>	1.73	1.73
<b>Loaded between troughs</b>	<b>old OSD</b>	2.14	1.99
	<b>new OSD</b>	2.66	2.34

Based on the results from Table 6-32 the link between the hot spot stress at P4\_12/14mm and P4\_28mm can be directly made. To obtain the maximum hot spot stress for the crack in the crossbeam a distinction can be made between the following three levels:

**Level 1:** extract the stress at P4\_28mm in the shell weld FE model and calculate the hot spot stress of P4\_12/14mm based on the scaling factors from Table 6-32 to obtain the hot spot stress range of the critical loading positions. To link the hot spot stress of the shell combined weld FE model and the solid FE model use can be made of Table 6-31. From Table 6-31 the minimum ratio, i.e. most conservative, is equal to 0.70, while in Table 6-32 the maximum ratio is equal to 2.66. To link the hot spot stress in P4\_14mm from the shell combined weld FE model with the hot spot stress range in P4\_28mm of the solid model a scaling factor of  $\frac{2.66}{0.70} = 3.80$ , is proposed. Due to the applied approximations a factor of 4 is advised to be conservative.

**Level 2:** repeat the exact same procedure to calculate everything manually once again for the shell combined weld FE model. Make a distinction between the different locations of the maximum stresses and calculate the scaling factor for obtaining the maximum hot spot stress. As with level 1, use Table 6-31 to link the hot spot stress of the shell combined weld FE model with the solid FE model.

**Level 3:** repeat the procedure of level 2 also for the solid FE model and again make a distinction between the different locations of the maximum stress. Use the obtained hot spot stress of the solid and shell combined weld FE models to calculate the scaling factor.

The hot spot stress range is calculated based on the maximum hot spot stress from Table 6-30 and the minimum hot spot stress from Table 6-26 and Table 6-27. The result is shown in Table 6-33 and the calculated ratio between the solid and shell combined weld FE models is shown in Table 6-34.

**Table 6-33 Obtained hot spot stress range crack in crossbeam**

	Loaded on top of web trough		Loaded between webs		Loaded between troughs	
	Old OSD HSS range [MPa]	New OSD HSS range [MPa]	Old OSD HSS range [MPa]	New OSD HSS range [MPa]	Old OSD HSS range [MPa]	New OSD HSS range [MPa]
<b>Solid FE model</b>	18.18	11.87	10.12	6.65	11.44	8.49
<b>Shell FE model (shifted)</b>	11.58	7.41	6.07	3.67	7.22	5.28
<b>Shell combined weld FE model</b>	14.84	9.19	7.92	4.97	9.13	6.47

**Table 6-34 Overview ratios obtained hot spot stress range crack in crossbeam solid and shell combined weld FE model**

		$\frac{\sigma_{HSS\_shell\_weld\_combined}}{\sigma_{HSS\_solid}}$
<b>Loaded on top of web trough</b>	<b>old OSD</b>	0.82
	<b>new OSD</b>	0.78
<b>Loaded between webs</b>	<b>old OSD</b>	0.79
	<b>new OSD</b>	0.75
<b>Loaded between troughs</b>	<b>old OSD</b>	0.80
	<b>new OSD</b>	0.76

As can be seen from Table 6-34, the ratio is almost constant for the critical loading positions of the three investigated transverse loading positions. For the old OSD variant the most conservative ratio is equal to 0.79, while for the new OSD variant this ratio is equal to 0.75.

### CV (coefficient of variation) for shell combined weld model

Now that the hot spot stress range is determined, the coefficient of variation is calculated based on the results from Table 6-34. The mean value is equal to **0.80** and **0.76** for the old and new OSD variant, respectively. The coefficient of variation is equal to **1.9%** for the old OSD variant, while a CV of **2.0%** is obtained for the new OSD variant. The standard deviation is equal to 0.02 for both the old and new OSD variant.

### Element size dependency minimum/maximum stress path 2

In section 6.2.1 a mesh sensitivity study was performed in which the obtained hot spot stress was taken as the convergence criterium. It was concluded that for the quadratic solid elements, C3D20R, with an element size of 2mm and for the quadratic shell elements, S8R, with an element size of 1mm showed converged results. In section 6.3.3 it was concluded that the minimum value of path 2 occurs at 28mm from the soft toe for both the solid and shell combined weld FE Model. The maximum stress in path 2 occurs at 12mm from the soft toe for the solid FE model and at 14mm for the shell combined weld FE model.

In this section it is investigated if the minimum and maximum stress locations in path 2 are influenced by the element size. For the shell FE model two additional element sizes are investigated: 2mm and 4mm, while for the solid FE model 4mm and 8mm are investigated. This investigation is performed for the critical load cases when the load is applied on the web of the trough of both the old and new OSD variant, since this resulted in the largest stress range. In Table 6-35 the results of this element size study are shown.

Table 6-35 Overview minimum/maximum stress in path 2 for different element sizes loaded on top of web trough,

	Element size	Old OSD variant		New OSD variant	
		Min [mm]	Max [mm]	Min [mm]	Max [mm]
Solid FE model	2mm	28	12	28	12
	4mm	28	12	28	12
	8mm	24	16	32	16
Shell combined weld FE model	1mm	28	14	28	14
	2mm	28	14	28	14
	4mm	28	12	28	12

For the shell with combined weld FE model the minimum value is not depending on the investigated element sizes. All three element sizes have a node at 28mm. For the maximum stress the shell element size of 4mm has its maximum value at 12mm, since no node is at 14mm. For the solid FE model similar observations are valid. The element size of 2mm and 4mm give the same results, while the elements size of 8mm has its minimum and maximum values at a different location, since no nodes are present at 12mm and 28mm. Furthermore the element size of 8mm give distorted elements and is not recommended to use. The location of the minimum and maximum stress in path 2 is hardly influenced by the element size, the differences are limited and equal to 2mm.

**Additional research to limit the differences of the shell and solid FE models: adaptation local geometry cope hole shell FE model**

As was concluded previously, after applying the combined weld modelling approach for the shell FE model (i.e. IIW and Eriksson), the ratio between the shell and solid hot spot stress results is a factor 0.75-0.80. It is investigated if the scatter in results can be reduced by adapting the local geometry of the cope hole in the shell FE model.

In Figure 6.67 an overview of the local geometry of the “Haibach” cut-out is shown for both the solid and shell FE models. As can be seen from the figure, the length of the soft toe in the solid FE model is equal to 10mm (left), while in the shell FE model (right) this is equal to 10mm + half the thickness of the trough, due to mid-surface modelling. For the old OSD variant this length is equal to 13mm and equal to 14mm for the new OSD variant. The results of the solid FE model, the shell combined weld with a soft toe of 13mm (old OSD variant) and the shell combined weld with a soft toe of 10mm are compared in this report. The critical loading positions of all three transverse positions will be further investigated. The critical loading positions can be found in Table 6-20. The comparison is made for the stress perpendicular to the weld toe of path 2 and 4.



Figure 6.67 Local geometry soft toe, solid (left) and shell (right)

In Table 6-36 an overview of the obtained ratios based on hot spot stress of the different transverse loading positions for the solid and shell FE model is shown. The hot spot stresses are obtained at 28mm from the soft toe, i.e. P4\_28mm. The stress graphs can be found in Annex K.

As can be seen from Table 6-36, the critical loading positions which results in the largest positive hot spot stress (HSS) value, the adapted local geometry of the cope hole will improve the results of the hot spot stress. The results of this FE model are closer to the solid FE model results. For the critical loading positions which result in the largest negative hot spot stress value, the opposite occurs. The adapted shell FE model will give results which are further away of the solid FE model when compared with the original shell combined weld FE model.

Table 6-36 Overview obtained HSS path 4 28mm of different FE models for shell combined weld FE model

		$\frac{\sigma_{HSS\_shell\_combined\_weld\_original}}{\sigma_{HSS\_solid}}$	$\frac{\sigma_{HSS\_shell\_combined\_weld\_adapted}}{\sigma_{HSS\_solid}}$
Loaded on top of web trough	Min HSS	0.88	0.81
	Max HSS	0.70	0.81
Loaded between webs trough	Min HSS	0.84	0.74
	Max HSS	0.67	0.81
Loaded between troughs	Min HSS	0.83	0.79
	Max HSS	0.70	0.77

Furthermore the hot spot stress range is calculated for the different FE models for which the results are shown in Table 6-37. The obtained hot spot stress range for the adapted geometry is even lower than the original shell FE model with combined weld, although the difference is very small.

Table 6-37 Overview obtained HSS range with path 4 at 28mm from soft toe (P4\_28mm) of different FE models

	Loaded on top of web trough	Loaded between webs trough	Loaded between troughs
	HSS range [MPa]	HSS range [MPa]	HSS range [MPa]
Solid FE model	14.05	8.41	8.14
Shell comb. weld soft toe 13mm	11.60	6.68	6.47
Shell comb. weld soft toe 10mm	11.44	6.42	6.41

Although the adaptation of the local geometry of the soft toe of the cope hole has some influence on the hot spot stress values of the investigated critical locations, see Table 6-36, the obtained hot spot stress range remains almost the same, see Table 6-37. This local adaptation of the cope hole will not reduce the scatter in results between the solid and shell FE models.

**Additional research to limit the differences of the shell and solid FE models: adaptation local thickness weld shell FE model**

Since the adaptation of the cope hole did not reduce the scatter in results, the stiffness of the connection of the trough and crossbeam is investigated. The local increased thickness for the shell with combined weld model is equal to  $t+a$ . Two additional models are created in which the thickness is locally increased with  $t+1.5a$  and  $t+2a$  respectively. Also for this investigation the load is applied on the web of trough. The results of the critical loading position  $X=-750\text{mm}$  are shown in Figure 6.68.

Increasing the local thickness to  $t+1.5a$  and  $t+2a$  will have a positive effect on the scatter between the shell combined weld and solid FE model if the fixed location of P4\_28mm is compared. The obtained ratio between the shell and solid hot spot stress is improved from 0.82 to 0.91. For the same the transverse loading position of the new OSD variant the ratio is improved from 0.80 to 0.90. However, the maximum stress in path 2 is again shifted by changing the local thickness of the connection. The maximum stress with both increased thicknesses,  $t+1.5a$  and  $t+2a$ , occurs at 30-31mm from the soft toe, instead of 28mm with the  $t+a$  local increased thickness.

If the obtained hot spot stress of the shell FE model with local increased thickness of  $t+2a$ , which occurs at a height of 30mm from the soft toe, is compared with the hot spot stress of the local increased thickness of  $t+a$ , which occurs at 28mm from the soft toe, the improvement is almost complete vanished. Which is also visible in Figure 6.68 in which the results of shell combined  $t+2a$  P4\_30mm are almost matching with shell combined  $t+a$  P4\_28mm for the first 15mm from the weld toe. Furthermore, as can be seen from Figure 6.68, the stress at 32mm from the weld toe is also quite different, since the comparison is not made on the same location in both FE models. Locally increasing the thickness with  $t+2a$  will not improve the ratio in hot spot stress results between the solid and shell weld FE models, since the location of the maximum stress is also changing. The bending stiffness of the connection is improved which was observed by comparing the result of P4\_28mm for both models. Similar observations are also valid for the other critical loading positions.

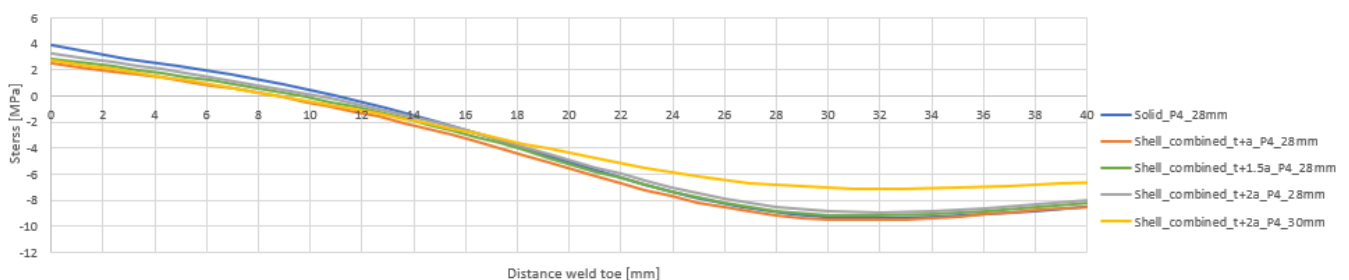


Figure 6.68 Results local increased thickness shell FE model, loaded on top of web  $X=-750\text{mm}$ , old OSD variant

## 7. RESULTS AND DISCUSSION

In this chapter the results of the performed research are summarized and furthermore the results will be discussed. The calculation of the hot spot stress is based on the stress perpendicular to the weld toe.

In **chapter 3** two different types of connections are investigated and validated: a single sided fillet welded plate connection with a longitudinal attachment and a full OSD specimen.

- **Single sided fillet welded plates with a longitudinal attachment**

This type of joint is loaded in tension and bending. A parametric study is performed in which the thickness of the main plate and attachment plate is increased or decreased. With the uniform tension load the obtained hot spot stress from the shell FE model is higher when compared with the hot spot stress of the solid FE model for all investigated geometries. The obtained ratio of the hot spot stress of the shell FE model divided by hot spot stress solid FE model is equal to **1.05-1.15**. When the uniform bending load is applied the obtained hot spot stress from the shell FE model is lower than the hot spot stress of the solid FE model. The ratio is equal to **0.85-0.95**.

It is furthermore investigated whether the weld modelling technique proposed by the IIW (Niemi, Fricke, & Maddox, 2018) reduces the scatter in results between the two FE models. For the uniform tension load the weld modelling technique increases the scatter in results between the shell and solid FE models, while for the uniform bending this scatter reduces by a few percent.

Moreover an extensive study for different type of elements is investigated in which a distinction is made between linear and quadratic elements with full or reduced integration. The elements with full integration have more integration points when compared with the reduced integration, thus are more accurate, but the computational time also increases significantly. If the element size is sufficiently small, the difference between the full and reduced quadratic elements is neglectable small. Based on this study it is concluded that quadratic solid elements, C3D20R, with an element size of 2mm ( $t/8$ ) are recommended. The linear elements need a refined mesh of 0.5mm ( $t/32$ ), which resulted in a large computational time. For the shell elements, quadratic elements, S8R, with an element size of 1mm ( $t/16$ ) are recommended.

- **Full OSD specimen**

A full OSD specimen which is being tested at Stevinlab II at the Delft University of Technology is numerically modelled and validated. This validation is based on strain gauges which are placed at different locations at the OSD. Three different locations are validated: vertically from the weld toe at the lower weld end adjacent to the cope hole and two horizontally in the trough, at 20mm distance from the same lower weld toe end.

On average, the differences between the solid FE model and the experimental results are within **7%**. A possible explanation for the differences between the experimental results and the FE results are a locally smaller thickness of the plate elements due to fabrication tolerances. After the validation of the reference solid FE model, the shell FE model is also compared with the solid FE- and experimental results. The shell FE model results in a large strain concentration directly at the structural intersection point, but at 40mm from the weld toe/structural intersection point the obtained strains for both FE models are of the same order.

Furthermore the influence of the differences between the as-measured weld geometry and ideal weld geometry is investigated. In general the differences between the as-measured and ideal weld geometry FE models are within 5%. Based on this result it is concluded that using the ideal weld geometry is sufficient, even though in reality the throat thickness of the weld is not uniform.

In **chapter 4** the fatigue assessment of the OSD specimen is performed based on the hot spot stress method. First the comparison with the experimental results and solid FE model results is made and the difference is equal to 6%, in which the solid FE model shows larger hot spot stress values. The obtained hot spot stress of the shell FE model is 25% higher than the results of the solid FE model.

In **chapter 5** a single sided fillet welded transverse attachment joint is investigated for both the deformations and the hot spot stress. Two different weld modelling techniques for the shell FE model are investigated: the IIW approach (Niemi, Fricke, & Maddox, 2018) and the increased thickness method (Eriksson, Lignell, Olsson, & Spennare, 2003). With the increased thickness method a further distinction is made between a local increased thickness of the base plate of  $t+a$  and  $t+0.5a$ . Furthermore four different load cases are investigated which result in in-plane and out-of-plane deformation of the specimen.

The hot spot stress ratio of the shell over solid FE models is equal to a factor 1.20. A similar factor is also obtained in chapter 4. The structural intersection point is taken as the origin for the extraction of the stresses for the original shell FE model, while for the shell FE model with the weld modelling techniques the weld toe is taken as the origin. By applying the weld modelling technique using the Eriksson approach the scatter in results between the shell and solid FE models is reduced to a factor **0.97-1.02**. The local increased thickness of the main plate by  $t+0.5a$  (Eriksson II) results in slightly non-conservative results, while the locally increased thickness  $t+a$  (Eriksson I) showed slight conservative results.

Furthermore the deformations of the different FE models are compared. As is the case with the hot spot stress, also for the deformation the weld modelling technique proposed by Eriksson shows results which are closest to the solid FE model. Depending on which Eriksson local increased thickness is applied, the deformations at the top of the transverse plate are lower, and higher, than the solid FE results for Eriksson I and II, respectively.

In conclusion, the weld modelling technique proposed by Eriksson shows good results based on both the hot spot stress, nominal stress, and the deformations when compared with the solid FE model. This is because of the additional stiffness which is created at the location of the weld.

In **chapter 6** the parametric analysis for both the old and new geometrical OSD variants is performed. The main difference between the old and new OSD variants is the thickness of the different components. The two weld modelling techniques from chapter 5 are also used for this analysis and furthermore an additional weld modelling technique is created. This additional weld modelling technique is a combination of the IIW (Niemi, Fricke, & Maddox, 2018) and Eriksson (Eriksson, Lignell, Olsson, & Spennare, 2003) weld modelling techniques. The focus of this parametric analysis is of the following two crack locations:

- Crack in trough: initiating from the weld end at the lower weld toe adjacent to a cope hole;
- Crack in crossbeam: initiating from the weld toe in the crossbeam at some distance from the soft toe.



- **Crack in trough**

The shell FE model results in an overestimation of the hot spot stress which is equal to a factor 1.15-1.25. Applying the combined weld modelling approach: IIW (Niemi, Fricke, & Maddox, 2018) and Eriksson (Eriksson, Lignell, Olsson, & Spennare, 2003), results in an overestimation of the hot spot stress by a factor of approximately 1.05. This overestimation is constant for all obtained hot spot stress values of the influence line. The mean value of the hot spot stress ratios is equal to **1.04** (range: 1.00-1.05). The coefficient of variation (CV) of both the old and new OSD variant are calculated and equal to **0.8%** and **2.2%**, respectively.

- **Crack in crossbeam**

For the crack in the crossbeam, at some distance from the soft toe, the stresses cannot be captured well with the regular shell FE model. A weld modelling technique is needed for this investigated crack. After applying the combined weld modelling approach the mean value is equal to **0.80** (range:0.79-0.82) and **0.76** (range:0.75-0.79) for the old and new OSD variant, respectively. The coefficient of variation is equal to **1.9%** and **2.0%** for the old and new OSD variant, respectively. The standard deviation is equal to 0.02 for both the old and new OSD variant.

The location of the minimum and maximum stress perpendicular to the weld toe depends on the loading positions. The minimum stress occurs at a height of 28mm from the soft toe of the cut-out, while the maximum stress occurs at 12-14mm from the soft toe. At 12-14mm it is not possible to perform a hot spot stress surface extrapolation and thus an approximation technique is proposed to obtain a hot spot stress value. With this approximation technique it is possible to directly link the obtained hot spot stress value at 28mm with the hot spot stress value at 12-14mm. Three different levels are proposed to obtain this factor. With level one a predefined scaling factor, equal to 4.00, can be used, while with level 2 and 3 the scaling factor need to be defined again for the shell with combined weld and the solid FE model, respectively.

Several different options are investigated to see if the scatter in results between the solid and shell FE model can be further reduced. The local geometry of the cope hole of the shell FE model is adapted in which the length of the soft toe is changed to the same length as with the solid FE model: 10mm. The hot spot stress ranges remains the same even though it has some effects on the obtained minimum and maximum hot spot stress values.

The stiffness of the connection of the trough and crossbeam is also investigated by creating models with a local increased thickness of  $t+1.5a$  and  $t+2a$ . This results in a better match of the shell and solid FE model if the read out location of the stresses is fixed at 28mm from the soft toe. By applying the local increased thicknesses of  $t+1.5a$  and  $t+2a$  the location of the maximum stress in path 2 changed from 28mm to 30mm from the soft toe. No obvious improvement is found when comparing the hot spot stress of the shell model at this location with the solid model results.

### **Research on continuous open stiffener to crossbeam connection in OSD**

A similar research is also performed by (Pandit, 2020) who investigated the continuous open stiffener to crossbeam connection in OSDs. The same weld modelling techniques are investigated. In this research the following two crack locations are investigated: the crack in crossbeam near the lower cope hole from parallel to the weld toe, and the crack in the web of open stiffener parallel to the weld toe. For the crack in the stiffener the obtained mean value of the hot spot stress ratios is equal to **1.02** with a CV of **4%**. The obtained mean value of the hot spot stress ratios is equal to **1.07** with a CV of **5.4%** for the crack in the crossbeam.

## 8. CONCLUSIONS AND RECOMMENDATIONS

In this chapter the main conclusions are presented. Furthermore, an answer will be given to the main research question, and recommendations will be given. The main research question is given below:

*“What is the most consistent method to relate the stress range, obtained with shell FE modelling, with the hot spot stress range, obtained from solid FE modelling, at the rib-to-crossbeam connection with cope hole?”*

### 8.1. Conclusions

In the research regarding the single sided fillet welded longitudinal attachment joint a large scatter in hot spot stress results between the solid and shell FE model is observed which is equal to **0.85-1.12**. This scatter is depending on the thickness of the different plates and on the type of loading: tension or bending. With the uniform tension loading of the main plate the shell FE results in an overestimation of the hot spot stress, while the opposite is true for the bending load case. Applying the weld modelling technique from the IIW recommendations (Niemi, Fricke, & Maddox, 2018) has some limited effects on the hot spot stress.

A similar study is also performed for a single sided fillet welded transverse attachment joint, which is similar to the connection of the trough and crossbeam in the OSD. Additional weld modelling techniques are investigated, and it is concluded that the weld modelling technique proposed by Eriksson (Eriksson, Lignell, Olsson, & Spennare, 2003) shows good results when compared with the solid FE model. Those results are matching based on the hot spot stress, nominal stress, and the deformations of the transverse attachment plate.

After the weld modelling technique of Eriksson (Eriksson, Lignell, Olsson, & Spennare, 2003) proves to give good results for a simple specimen, the same comparison is made for the full OSD specimen. In a small parametric analysis several different load cases are investigated which results in in-plane and out-of-plane deformation of the crossbeam. For the in-plane load cases the difference between obtained hot spot stress of the shell and solid FE model, after applying the weld modelling technique, is small. The ratio is in the range of **1.00-1.10** for the crack in the trough, and **0.95-1.04** for the crack in the crossbeam. Both the stress gradient and the stress at 40mm from the weld toe of the shell and solid FE model are matching. With the out-of-plane load case a larger differences in the crossbeam are observed in which the ratio of the shell and solid hot spot stress is equal to 0.70. For this small parametric study also the comparison between the stress perpendicular and the maximum principal stress is made. Depending on the type of loading differences between those stress components are observed.

From the extensive parametric analysis the influence of the geometry and loading positions on the hot spot stress range are studied. The critical loading positions are calculated based on influence lines. The mean value of the obtained hot spot stress ratios is equal to **1.04** (range: 1.00-1.05). The coefficient of variation (CV) for the crack in the trough for both the old and new OSD variant are calculated and equal to **0.8%** and **2.2%** respectively. For the crack in the crossbeam the mean value is equal to **0.80** (range:0.79-0.82) and **0.76** (range:0.75-0.79) for the old and new OSD variant, respectively. The coefficient of variation is equal to **1.9%** and **2.0%** for the old and new OSD variant, respectively. The standard deviation is equal to 0.02 for both the old and new OSD variant. The coefficient of variation for both investigated cracks is low, i.e. below 5%, so the ratio between the obtained hot spot stress of the shell with combined weld and solid FE models is consistent.

Furthermore from the extensive parametric analysis it is observed that the location of the minimum and maximum stress perpendicular to the weld toe is depending on the loading positions. The minimum stress occurs at a height of 28mm from the soft toe of the cut-out, while the maximum stress occurs at a height of 12-14mm from the soft toe. Since with this latter location a regular surface stress extrapolation is not possible, the hot spot stress is approximated based on direct read out of the stress and linear curve fitting. Furthermore a scaling factor is proposed to directly link the hot spot stress from the shell with combined weld at a height of 14mm with the hot spot stress at a height of 28mm of the solid FE model. This scaling factor, equal to 4.00, is only valid for the investigated geometries.

When the obtained hot spot stress of the old and new OSD variants are compared with the hot spot stress values of the new OSD variant, the new variant is showing lower values. For the crack in the trough this reduction ( $\frac{\sigma_{HSS\_old}}{\sigma_{HSS\_new}}$ ) is equal to a factor **1.50-2.00**, while for the crack in the crossbeam it is equal to **1.40-1.70**, depending on the transverse loading position. Further investigation of the critical loading positions shows a stress gradient closest to the solid FE model for the shell FE model with combined weld modelling approach.

## 8.2. Recommendations

Based on the results of this master thesis, the recommendations for further research are listed below:

- Investigation of other geometries and shapes of the cope hole. Only the "Haibach" cope hole shape is investigated. It is recommended to also perform a similar study for the "normal" cope hole out shape to see if similar improvements are also valid for this geometry.
- This thesis is mainly focused on obtaining the hot spot stress based on surface stress extrapolation. As stated in the IIW recommendations (Niemi, Fricke, & Maddox, 2018), also through-thickness surface linearization can be further researched to make a further comparison which hot spot stress extrapolation technique is most suitable.
- To get a better understanding of the local stress behavior of the investigated crack in the crossbeam, the fatigue assessment based on the effective notch method need to be performed. This can result in a more accurate stress at the location of interest.
- More research on the different weld modelling techniques for the shell FE models to further reduce the differences in hot spot stress between the solid and shell FE model. Especially for the investigated crack in the crossbeam. Other weld element techniques like oblique elements or rigid links may be investigated.
- Further research is needed for the determination of the hot spot stress in case of multiaxial or biaxial stress state. To obtain the correct hot spot stress a distinction needs to be made between the maximum principal stress and the stress perpendicular to the weld toe or the minimum principal stress. As is observed in this research, differences occur between those different stress components cannot be ignored. A recommendation for the suitability of different stress, principal stress and stress perpendicular to weld toe, is needed based on further study.

# ANNEX A1

## Results tension

Table A1 0-1 Overview mesh sensitivity study tension loading

Element type and size	Ratio $\frac{\sigma_{HSS}}{\sigma_{nom}}$ solid	Ratio $\frac{\sigma_{HSS}}{\sigma_{nom}}$ shell	Ratio $\frac{\sigma_{HSS,shell}}{\sigma_{HSS,solid}}$
8mm linear reduced integration	1.118 (C3D8R)	1.182 (S4R)	1.06
8mm linear	1.173(C3D8)	1.336 (S4)	1.10
8mm quadratic reduced integration	1.212(C3D20R)	1.333 (S8R)	1.10
8mm quadratic	1.222(C3D20)	-	-
4mm linear reduced integration	1.161	1.184	1.02
4mm linear	1.195	1.255	1.06
4mm quadratic reduced integration	1.186	1.256	1.06
4mm quadratic	1.194	-	-
2mm linear reduced integration	1.182	1.204	1.02
2mm linear	1.197	1.225	1.03
2mm quadratic reduced integration	1.190	1.237	1.04
2mm quadratic	1.186	-	-
1mm linear reduced integration	1.189	1.204	1.01
1mm linear	1.191	1.212	1.03
1mm quadratic reduced integration	1.188	1.219	1.03
1mm quadratic	1.187	-	-
0.5mm linear reduced integration	-	1.205	-
0.5mm linear	-	1.208	-
0.5mm quadratic reduced integration	-	1.210	-

### Mesh sensitivity study solid element results tension

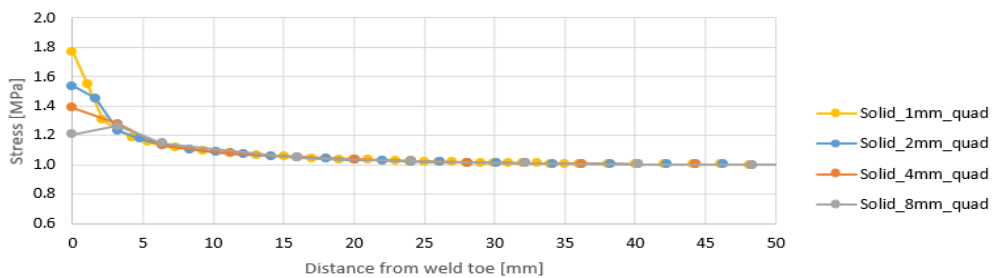


Figure A1 0.1 Overview results solid quadratic elements reduced integration

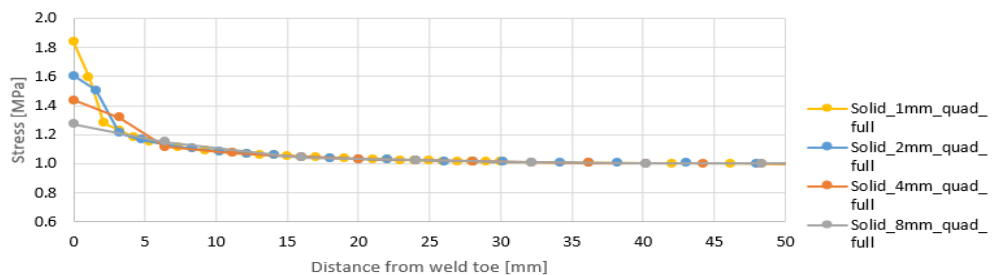


Figure A1 0.2 Overview results solid quadratic elements full integration

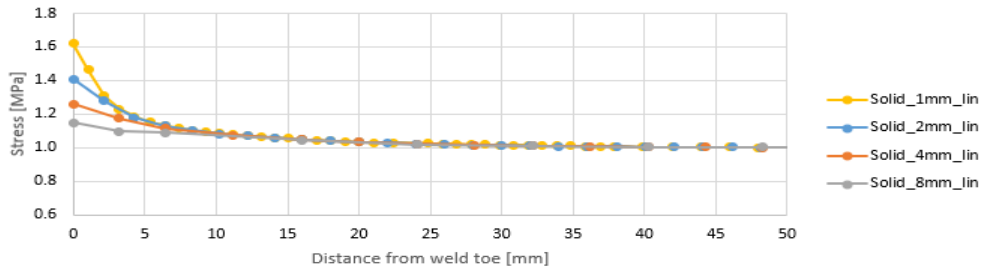


Figure A1 0.3 Overview results solid linear elements reduced integration

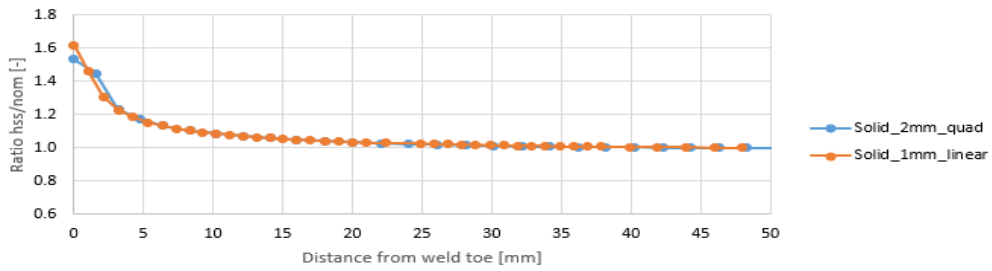


Figure A1 0.4 Overview results element type

**Parametric study solid element results tension**

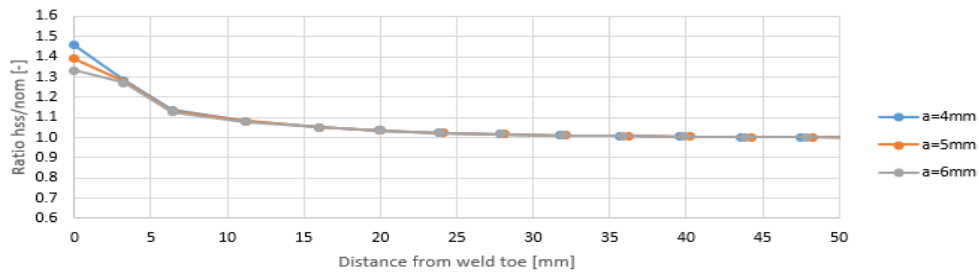


Figure A1 0.5 Overview results throat thickness

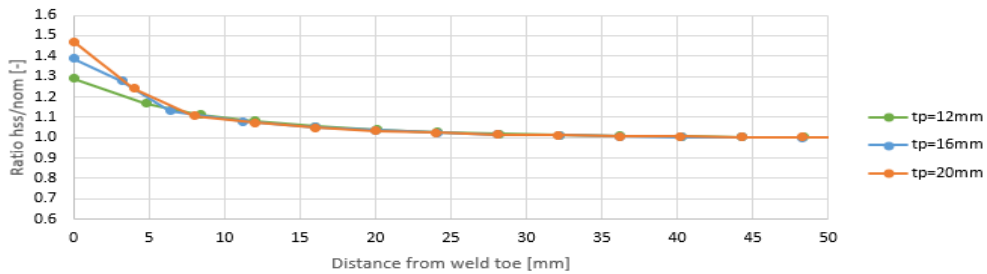


Figure A1 0.6 Overview results thickness main plate

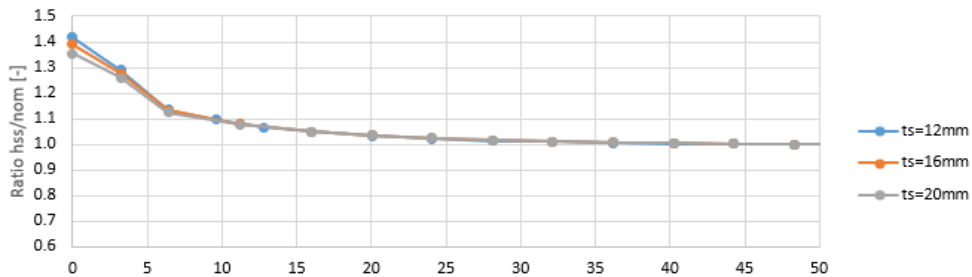


Figure A1 0.7 Overview results thickness stiffener plate

## Mesh sensitivity study shell element results tension

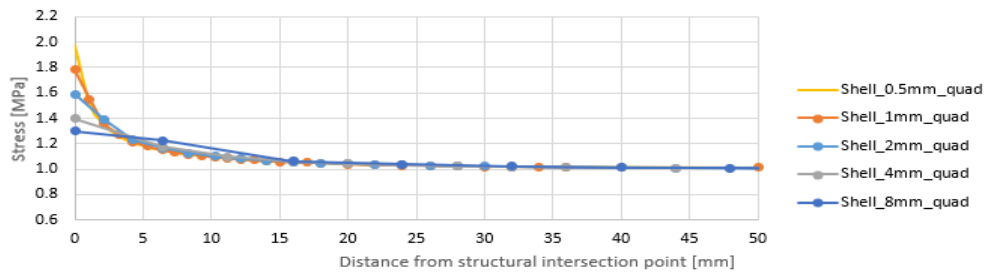


Figure A1 0.8 Overview results shell quadratic elements reduced integration

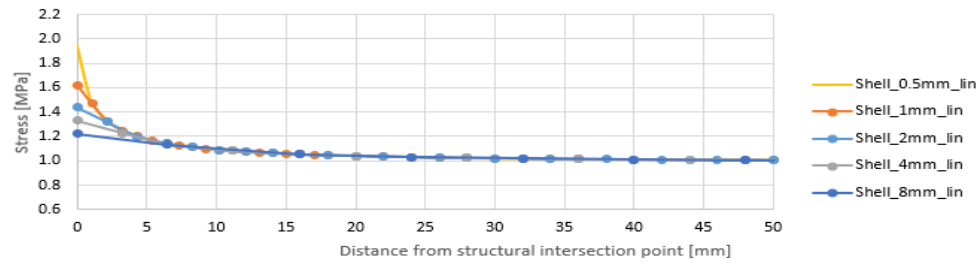


Figure A1 0.9 Overview results shell linear elements

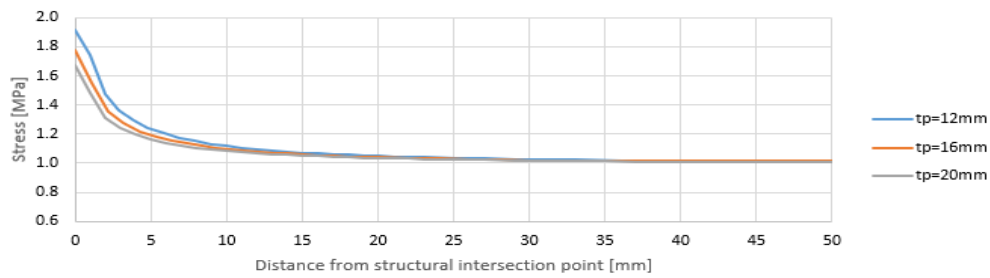


Figure A1 0.10 Overview results thickness main plate

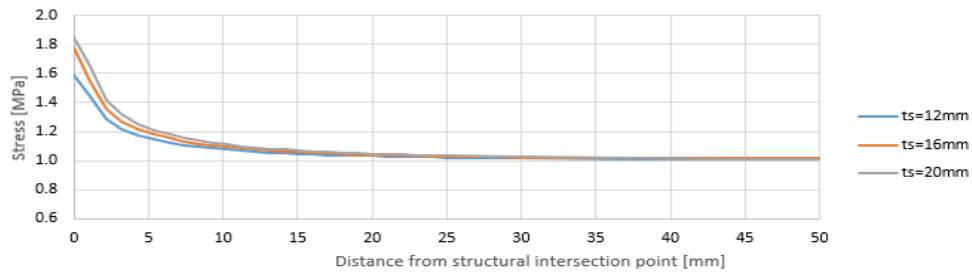


Figure A1 0.11 Overview results thickness stiffener plate

Results bending

Table A1 0-2 Overview mesh sensitivity study bending loading

Element type and size	Ratio $\frac{\sigma_{HSS}}{\sigma_{nom}}$ solid	Ratio $\frac{\sigma_{HSS}}{\sigma_{nom}}$ shell	Ratio $\frac{\sigma_{HSS,shell}}{\sigma_{HSS,solid}}$
8mm linear reduced integration	0.886 (C3D8R)	1.125 (S4R)	1.27
8mm linear	1.113 (C3D8)	1.229 (S4)	1.10
8mm quadratic reduced integration	1.300(C3D20R)	1.169 (S8R)	0.90
8mm quadratic	1.299(C3D20)	-	-
4mm linear reduced integration	1.051	1.094	1.04
4mm linear	1.197	1.120	0.94
4mm quadratic reduced integration	1.255	1.128	0.90
4mm quadratic	1.216	-	-
2mm linear reduced integration	1.153	1.094	0.95
2mm linear	1.225	1.103	0.90
2mm quadratic reduced integration	1.262	1.114	0.89
2mm quadratic	1.252	-	-
1mm linear reduced integration	1.207	1.094	0.91
1mm linear	1.239	1.097	0.89
1mm quadratic reduced integration	1.256	1.102	0.89
1mm quadratic	1.254	-	-
0.5mm linear reduced integration	1.219	1.091	0.90
0.5mm quadratic reduced integration	1.243	1.093	0.88

**Mesh sensitivity study solid element results bending**

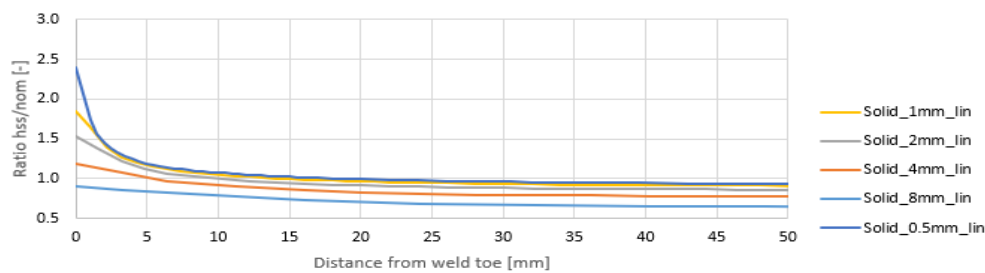


Figure A1 0.12 Overview results solid linear elements reduced integration

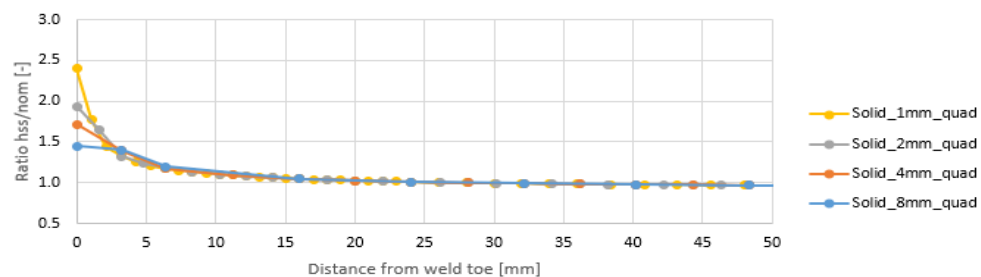


Figure A1 0.13 Overview results solid quadratic elements reduced integration

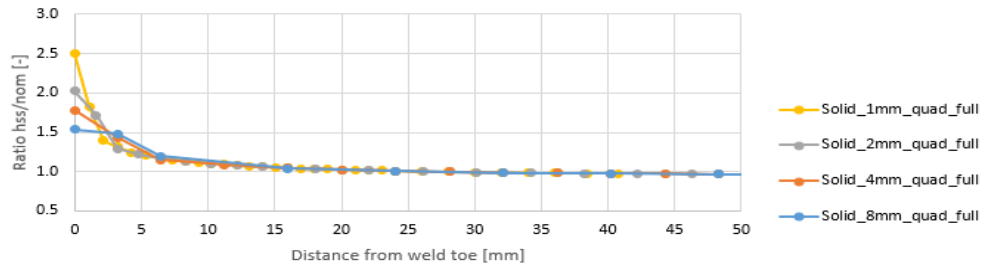


Figure A1 0.14 Overview results solid quadratic elements full integration

**Parametric study solid element results bending**

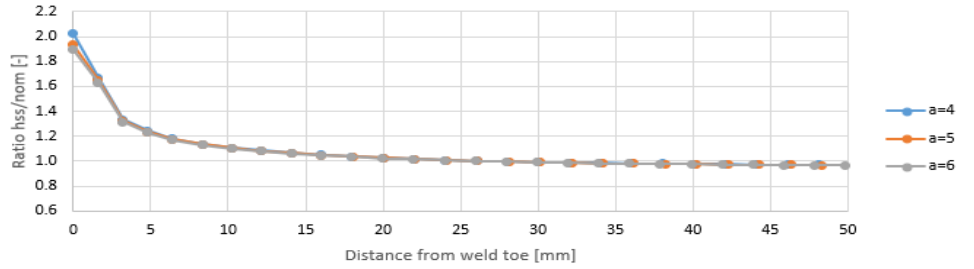


Figure A1 0.15 Overview results throat thickness

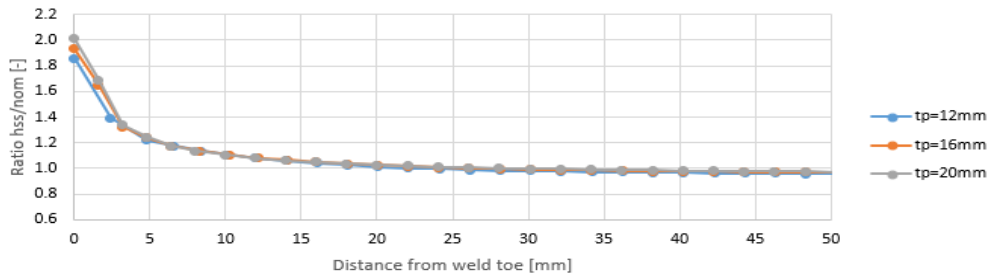


Figure A1 0.16 Overview results thickness main plate

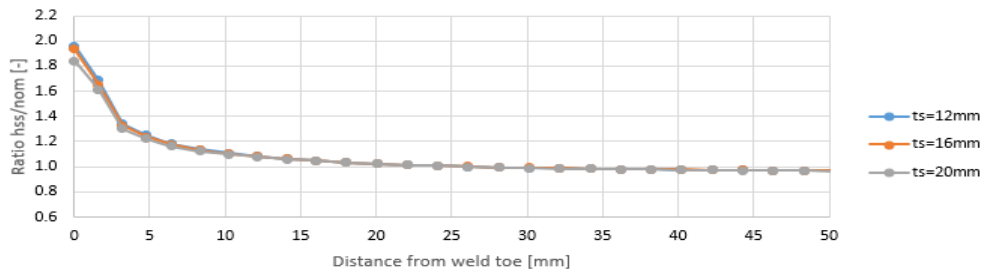


Figure A1 0.17 Overview results thickness stiffener plate

**Mesh sensitivity study shell element results bending**

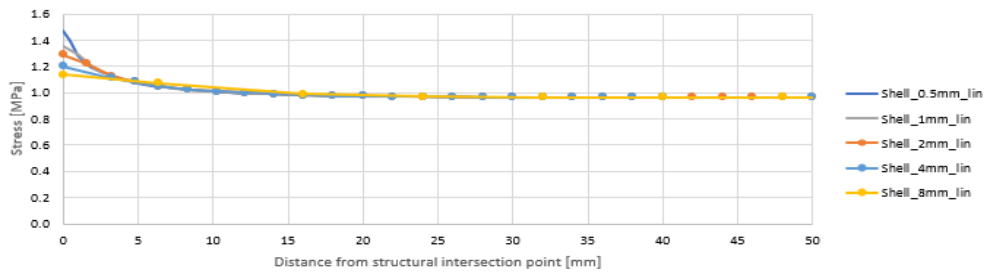


Figure A1 0.18 Overview results shell linear elements reduced integration



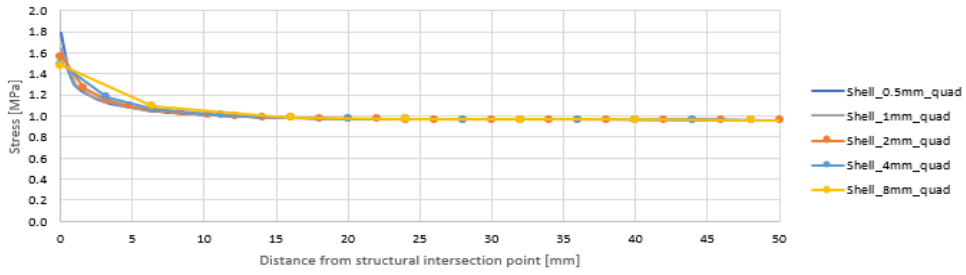


Figure A1 0.19 Overview results shell quadratic elements reduced integration

**Parametric study shell element results bending**

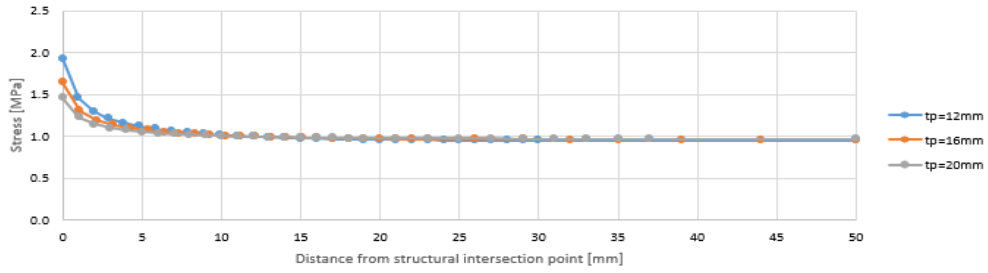


Figure A1 0.20 Overview results thickness main plate

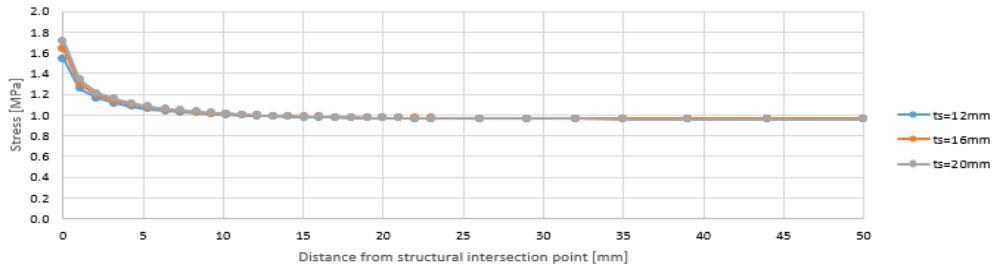
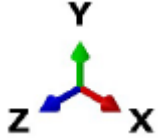


Figure A1 0.21 Overview results thickness stiffener plate

## ANNEX A2

### Results different modelling approaches shell element models tension

#### Used coordinate system:



#### Shell mid-surface uniform tension loading

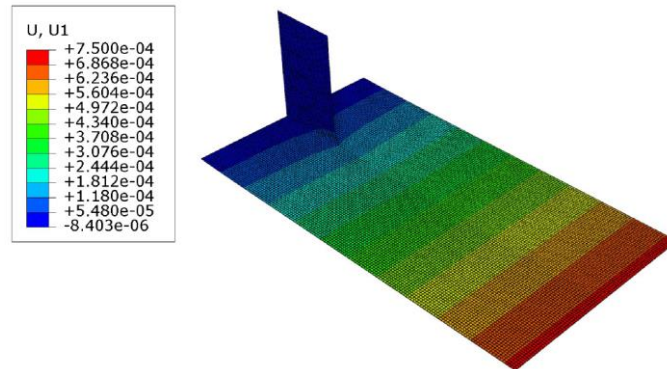


Figure A2 0.1 : Deformation U1, uniform tension load, shell mid-surface modelling FE model

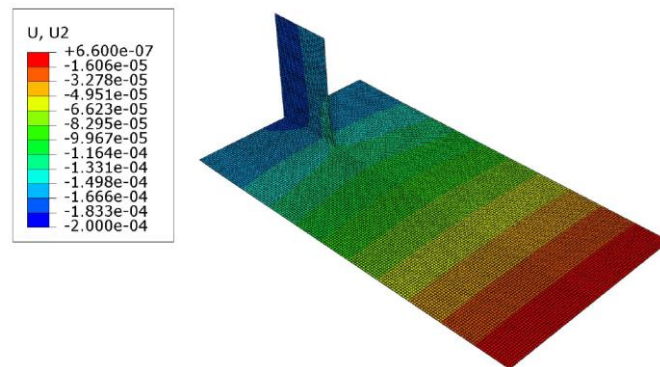


Figure A2 0.2 Deformation U2, uniform tension load, shell mid-surface modelling FE model

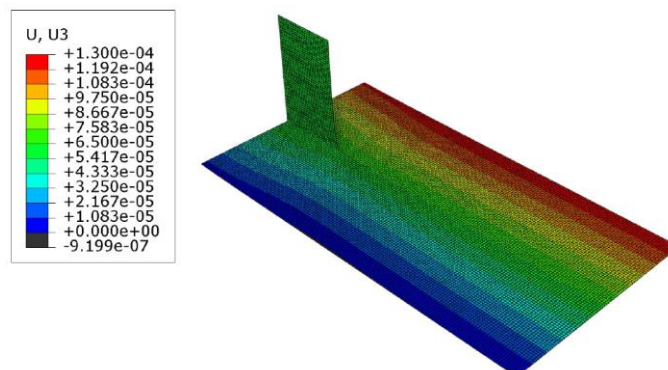


Figure A2 0.3 Deformation U3, uniform tension load, shell mid-surface modelling FE model

Solid uniform tension loading

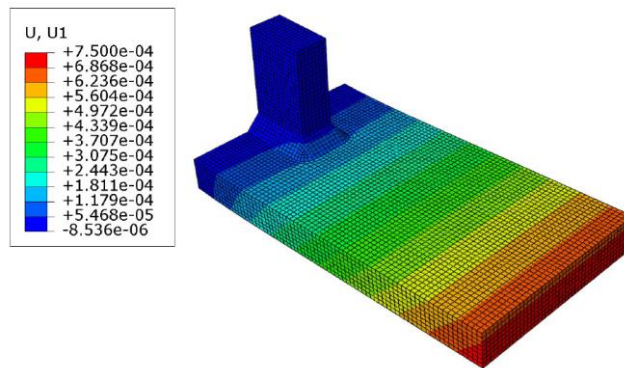


Figure A2 0.4 Deformation U1, uniform tension load, solid FE model

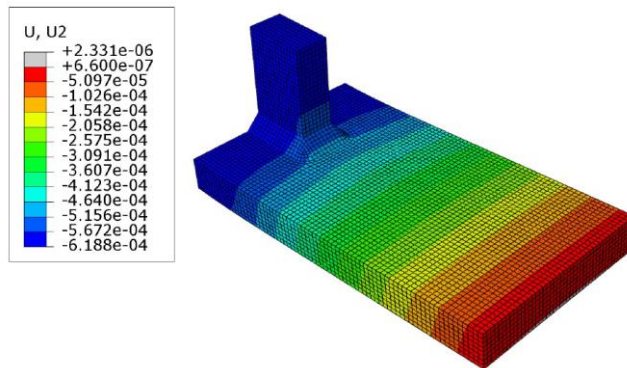


Figure A2 0.5 Deformation U2, uniform tension load, solid FE model

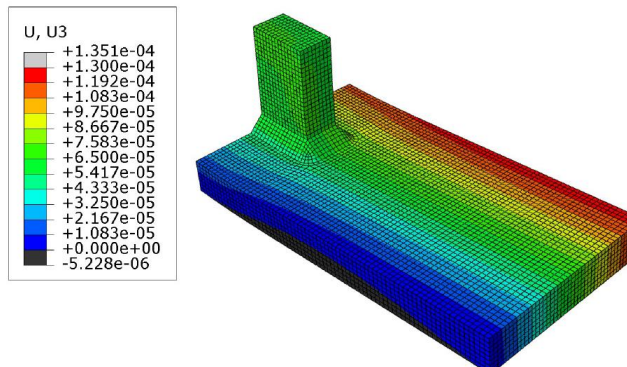


Figure A2 0.6 Deformation U3, uniform tension load, solid FE model

Shell bottom-surface offset modelling uniform tension loading

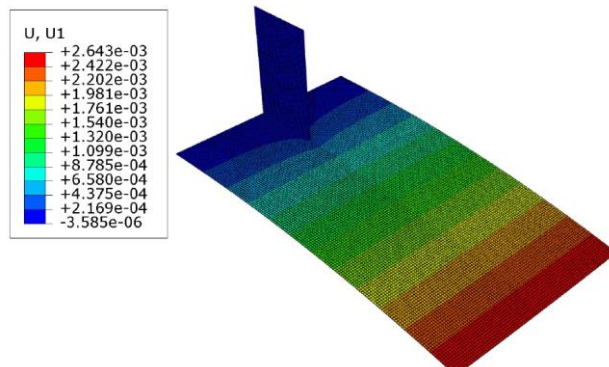


Figure A2 0.7 Deformation U1, uniform tension load, shell bottom-surface offset modelling FE model

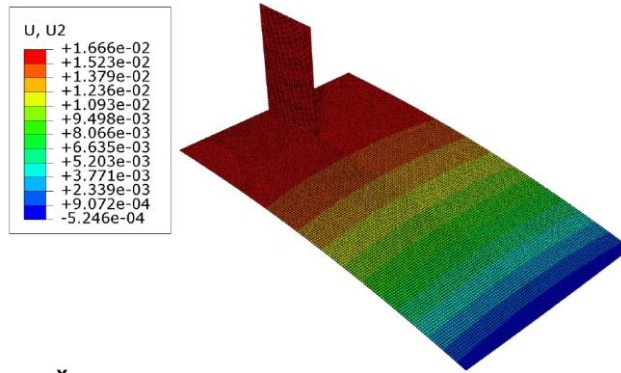


Figure A2 0.8 Deformation U2, uniform tension load, shell bottom-surface offset modelling FE model

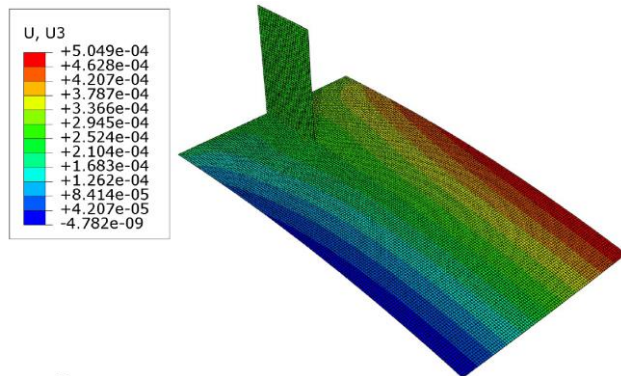


Figure A2 0.9 Deformation U3, uniform tension load, shell bottom-surface offset modelling FE model

## ANNEX B

In this annex the comparison between the different shell modelling approaches is investigated. In section 3.1.6 both the mid-surface modelling and bottom-surface modelling are investigated for the fillet welded transverse stiffener connection. It is concluded that the mid surface modelling approach is the best procedure, since with the top/bottom approach eccentricities are introduced due to shifting of the reference surface. The shell model can be divided in the following parts: deck plate, crossbeam I, II and III, troughs 1-8 and the bottom flange of the crossbeam. In Figure B 0.1 a graphical representation of the modelling approach is shown. In the left figure an overview of the connection is shown and in the right figure the render shell thickness option is on to show the thickness of the shell elements. The crossbeams form the central part of the structure and are modelled as middle surface. The bottom flange of the crossbeam is modelled as bottom-surface and thus it is not connected at the midplanes, but at the bottom of the crossbeam. Both the troughs and the deck plate are modelled as top-surface. By applying this modelling approach the overlap of the different shell element parts is limited as possible which can be clearly seen in Figure B 0.1.

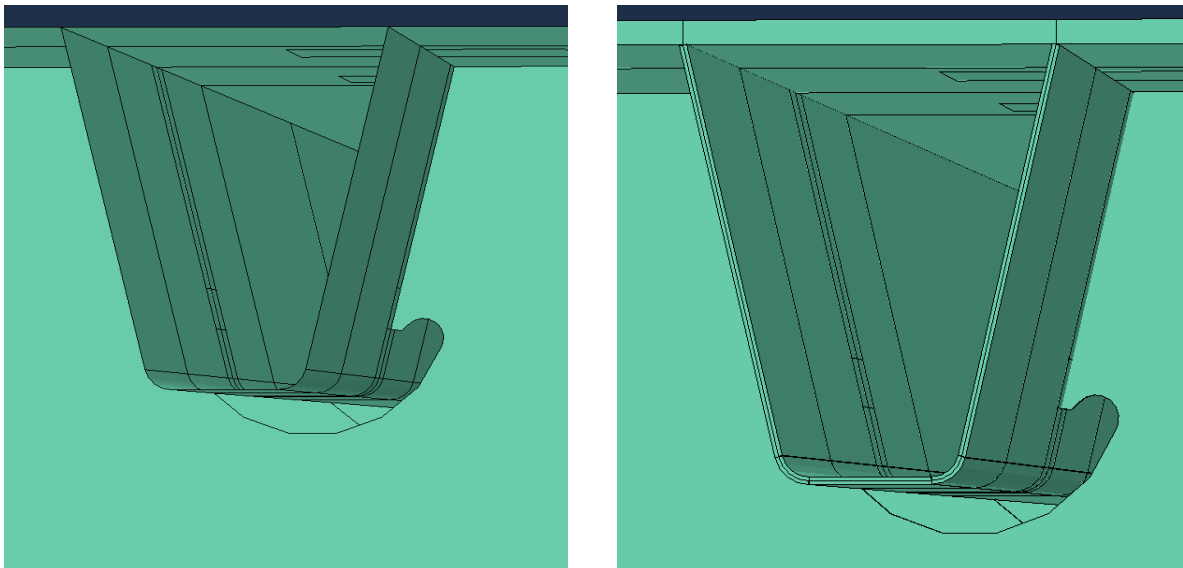


Figure B 0.1 Overview modelling approach top/bottom shell model

In the following figures the results for shell mid surface modelling, shell top/bottom modelling, and the solid model are shown.

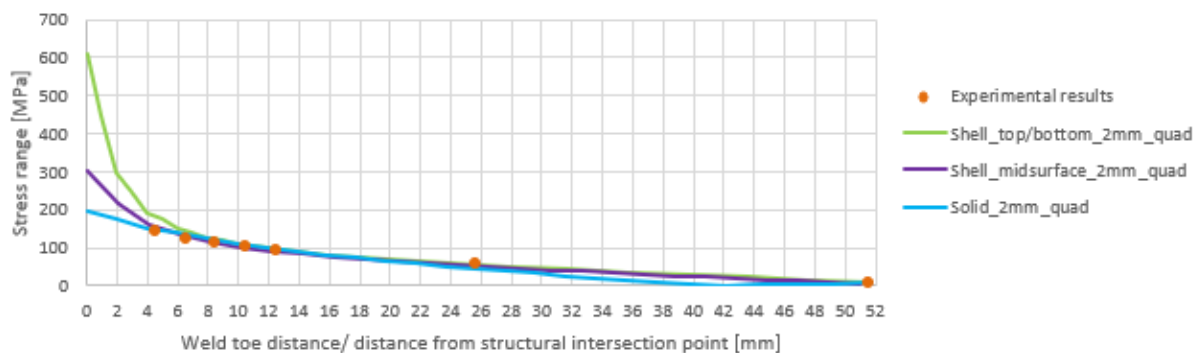


Figure B 0.2 Vertical direction: comparison shell element modelling techniques with solid element

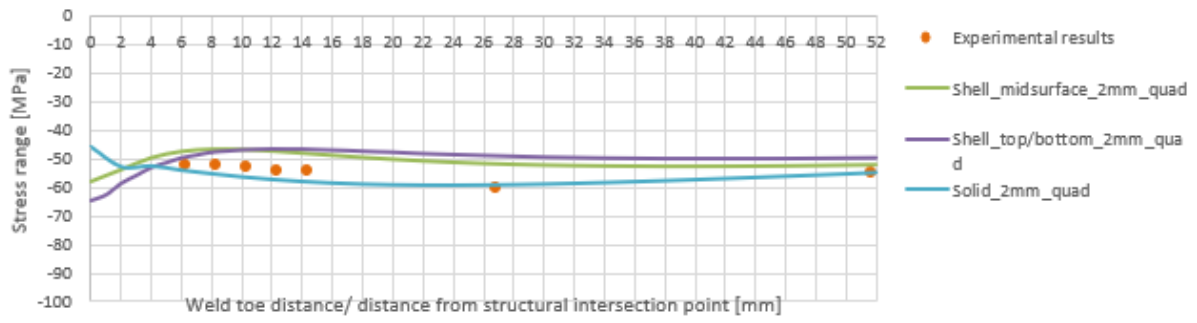


Figure B 0.3 Horizontal direction free edge: comparison shell element modelling techniques with solid element

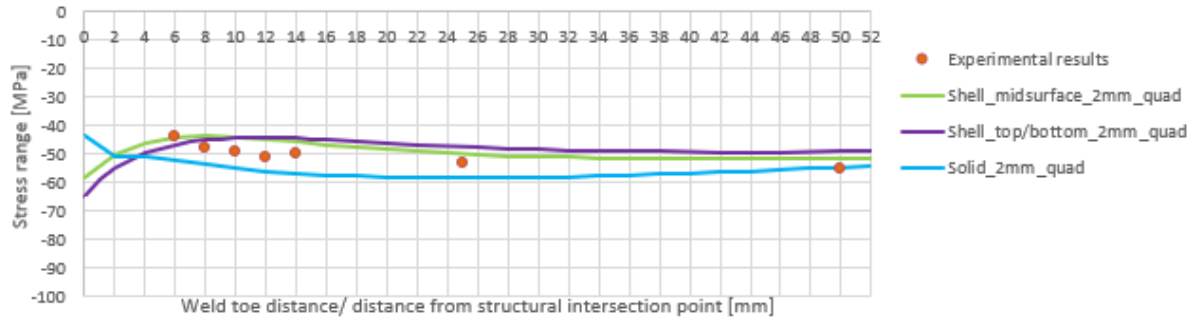


Figure B 0.4 Horizontal direction in span: comparison shell element modelling techniques with solid element

## ANNEX C

### Analysis of element size solid FE model horizontal direction

In Figure C 0.1 to Figure C 0.4 the results for the strain range in horizontal direction for the quadratic and linear solid models with different element sizes is shown. A distinction is made between the horizontal strain range at the free edge and the horizontal strain range in-span.

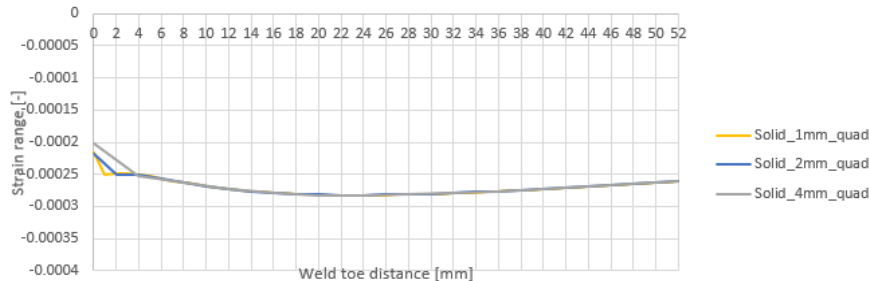


Figure C 0.1 Strain range in horizontal direction, free edge, for different linear solid element sizes

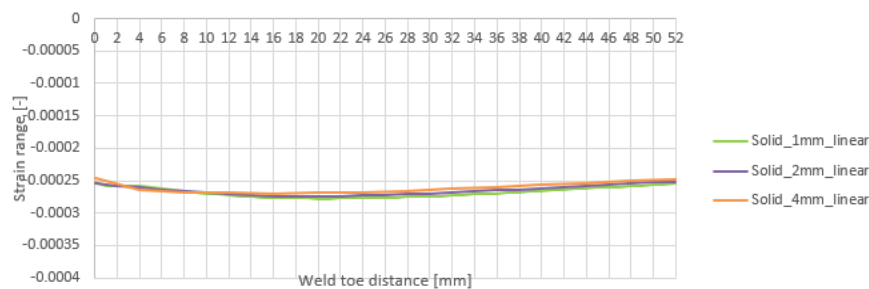


Figure C 0.2 Strain range in horizontal direction, free edge, for different linear solid element sizes

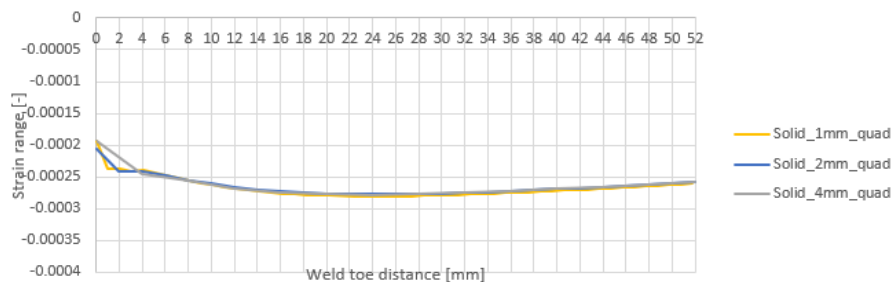


Figure C 0.3 Strain range in horizontal direction, in-span, for different quadratic solid element sizes

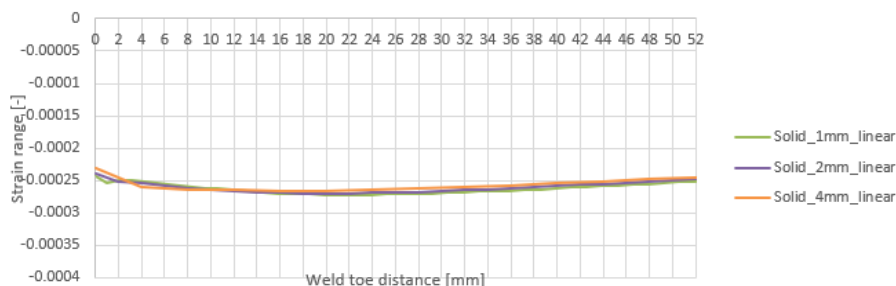


Figure C 0.4 Strain range in horizontal direction, in-span, for different linear solid element sizes

As can be seen from Figure C 0.1 and Figure C 0.3, the same conclusion as for the vertical quadratic elements is also valid for the results in horizontal direction. The element sizes of 1mm and 2mm show the same results after 2mm and the element size of 4mm shows the same results after 4mm. In Figure C 0.2 and Figure C 0.4 it can be seen that the, the large which is observed in the vertical direction, is not occurring in horizontal direction. The same conclusions as for the quadratic elements are also valid for the linear elements. To obtain the strain range at  $0,4t$  from the weld toe, it is advised to use linear or quadratic solid element with an element size of 2mm.

### Analysis and validation of global shell element model horizontal direction

A similar study as with the sub solid element model is performed to investigate the influence of the element size on the strain range. Five different local element sizes are investigated: 0.5, 1mm, 2mm, 4mm and 8mm for which the results are given in the following figures.

In Figure C 0.5 and Figure C 0.6 the results for the strain range in horizontal direction for the shell models with different element sizes is shown. A distinction is made between the horizontal stresses at the free edge, Figure C 0.5 and the horizontal stresses in-span, Figure C 0.6.

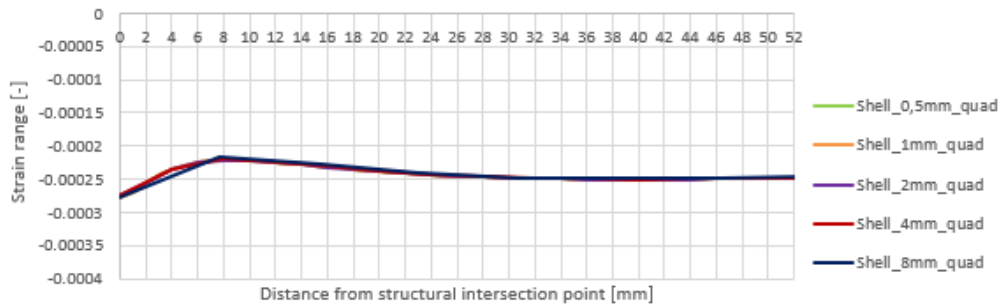


Figure C 0.5 Strain range in horizontal direction, free edge, for different element sizes

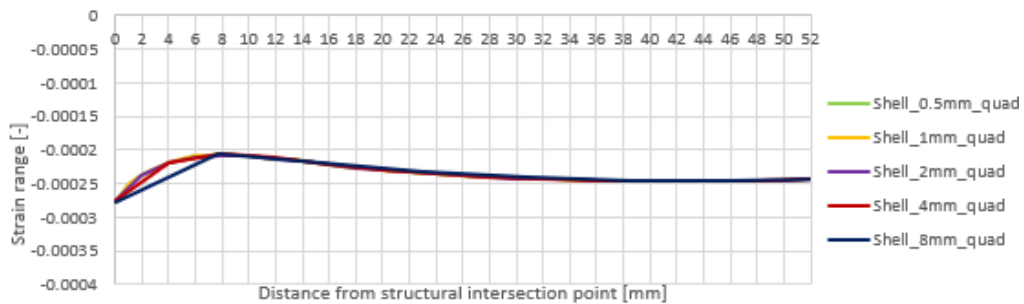


Figure C 0.6 Strain range in horizontal direction, in-span, for different element sizes

As can be seen from both figures, the strain range for the 0.5, 1 and 2mm elements size is almost the same over the measured length. The element sizes of 4 and 8mm show similar results at 8mm from the structural intersection point. Furthermore the strain range is more or less constant throughout the distance 8mm from the structural intersection point. After 8mm the results are not depending on the element size anymore. The difference in hot spot stress range for the 0.5, 1 and 2mm element size is very small, the difference is only 0.3%.



## ANNEX D

In this annex the results of mesh sensitivity study for loading positions 1, 2 and 4, are shown.

An overview of the local sub solid mesh can be found in Figure D 0.1 in which the detailed mesh for both crack locations is shown and an element size of 2mm is used. The welds in the solid FE model are fillet welds with a throat thickness of 5mm. In Figure D 0.2 the local mesh for the shell FE model is shown and an element size of 1mm is used.

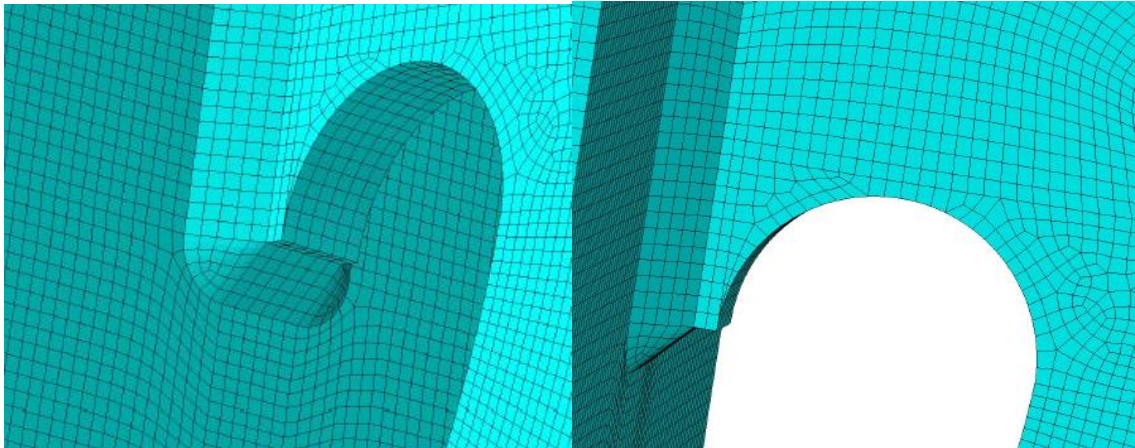


Figure D 0.1 Overview mesh sub solid model trough (left) and crossbeam (right)

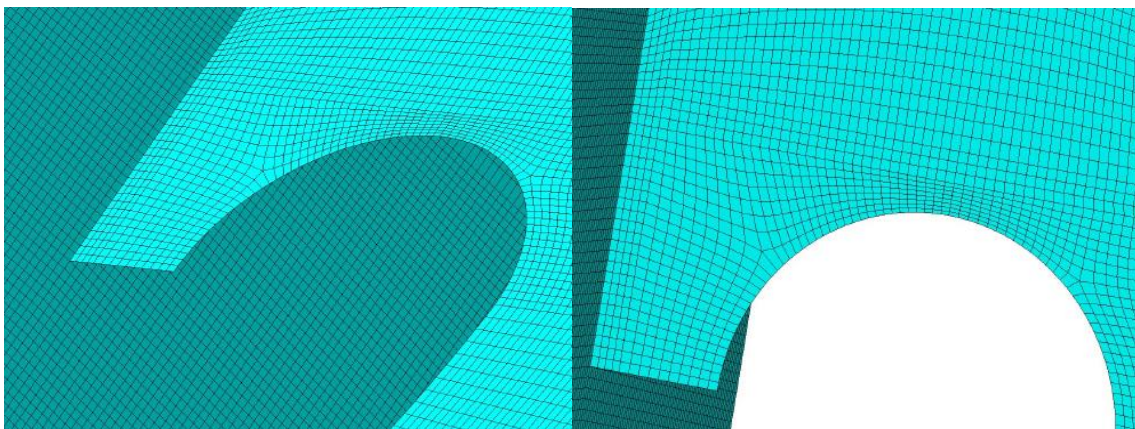


Figure D 0.2 Overview mesh shell model trough (left) and crossbeam (right)

**The stress perpendicular to the weld toe is used for obtaining the following graphs**

**Loading position 1: global in-plane loading: 500mm offset from crossbeam, loaded between webs**

**Solid**

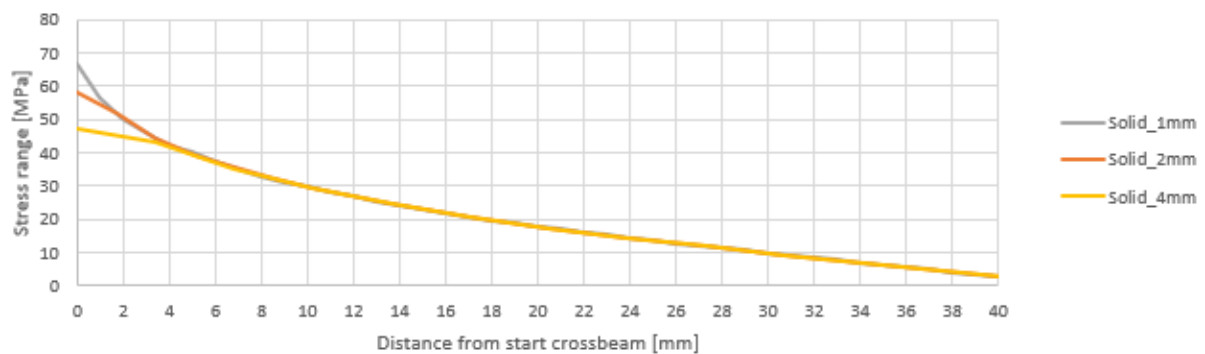


Figure D 0.3 Stress range in web trough for different quadratic element sizes

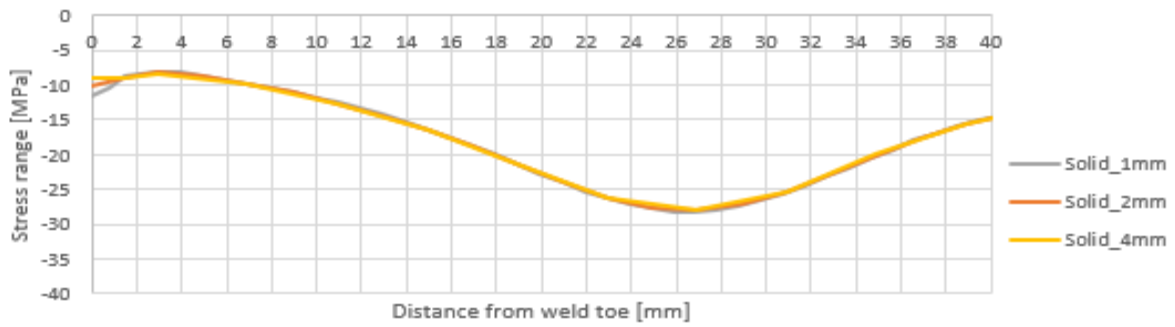


Figure D 0.4 Stress range in crossbeam for different quadratic element sizes

Shell

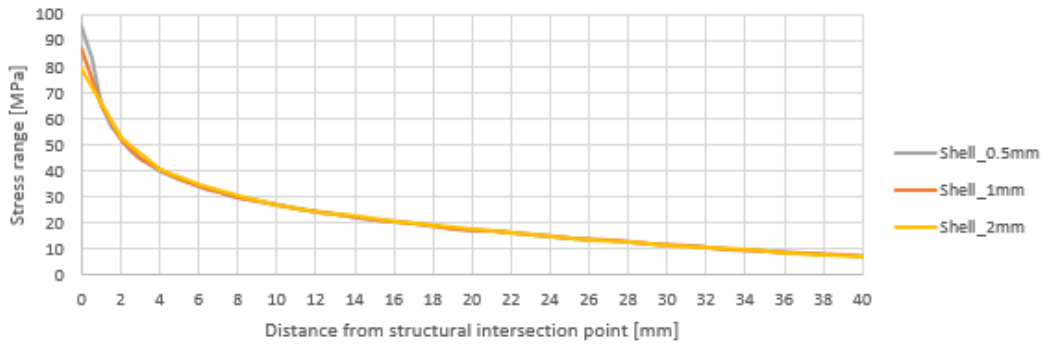


Figure D 0.5 Stress range in web trough for different quadratic element sizes

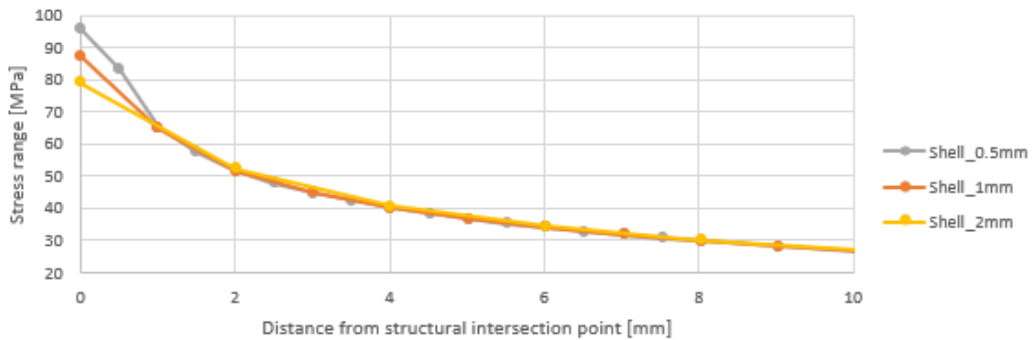


Figure D 0.6 zoomed in results stress range in web trough for different element

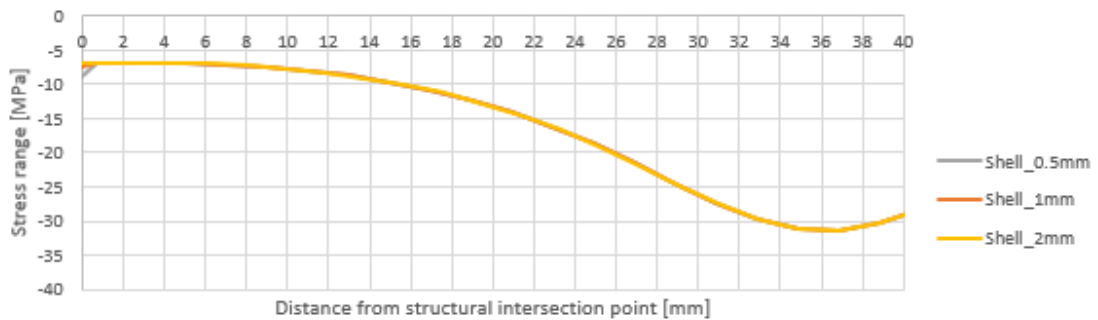
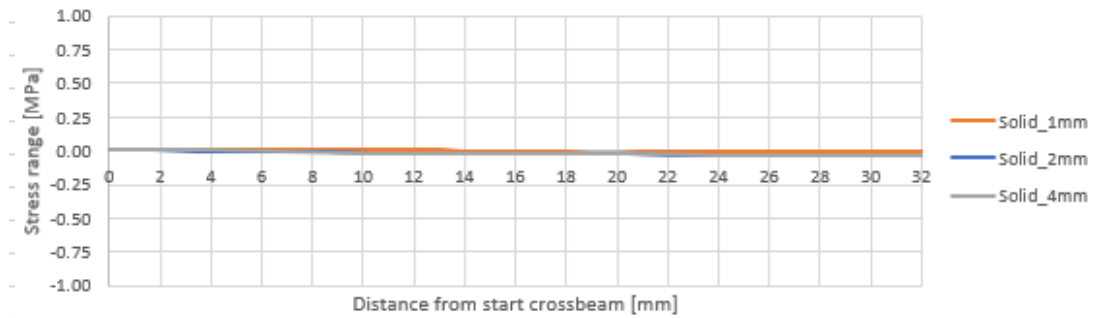


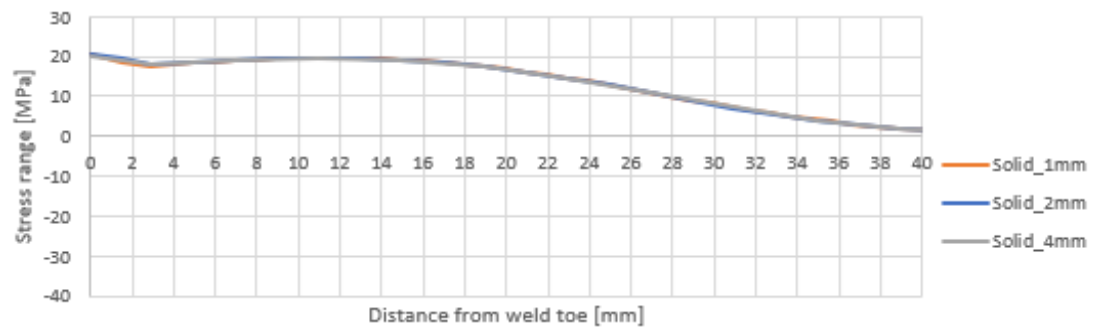
Figure D 0.7 Stress range in crossbeam for different quadratic element sizes

**Loading position 2: out-of-plane loading: 500mm offset from crossbeam, loaded between webs  
torsional load**

Solid:

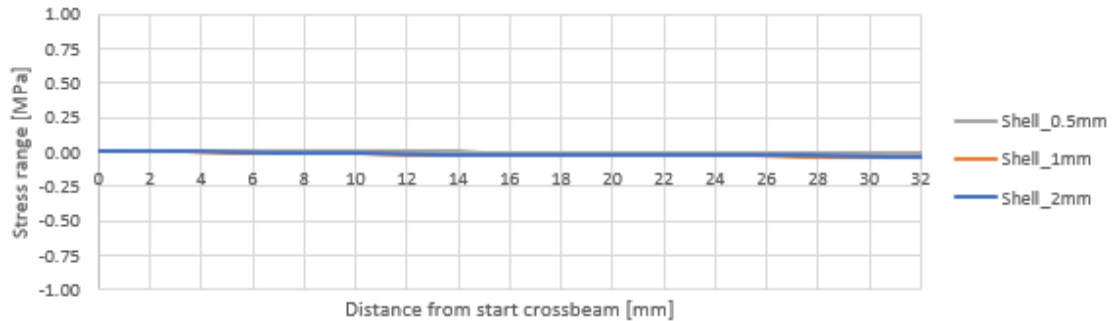


**Figure D 0.8 Stress range in web trough for different quadratic element sizes**

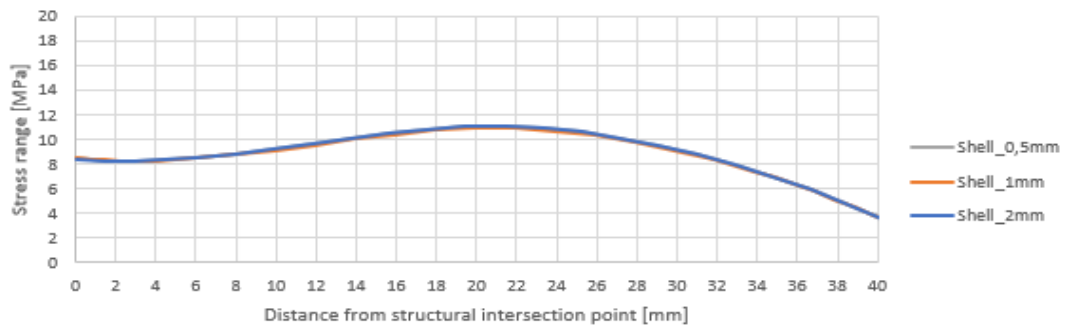


**Figure D 0.9 Stress range in crossbeam for different quadratic element sizes**

Shell:



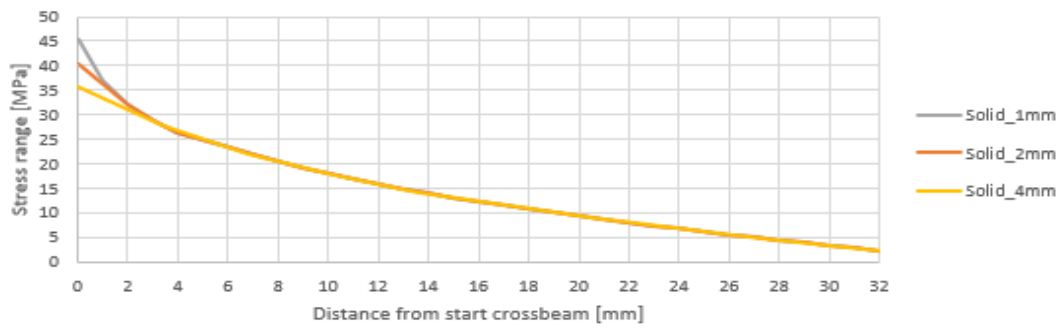
**Figure D 0.10 Stress range in web trough for different quadratic element sizes**



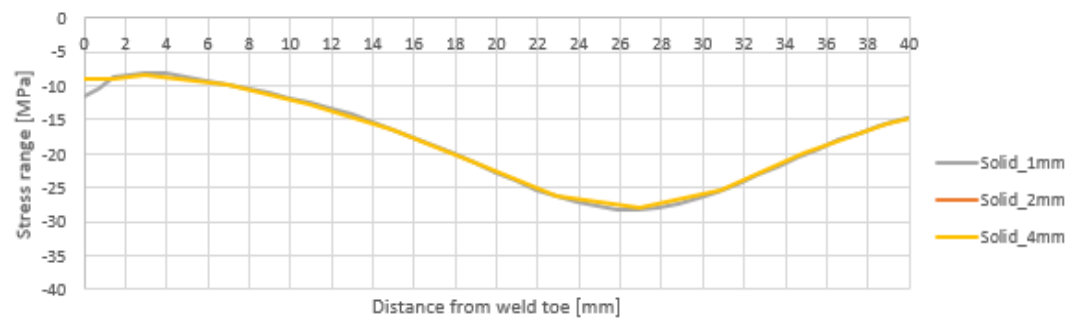
**Figure D 0.11 Stress range in crossbeam for different quadratic element sizes**

**Loading position 4: local in-plane loading, loaded between webs**

Solid:

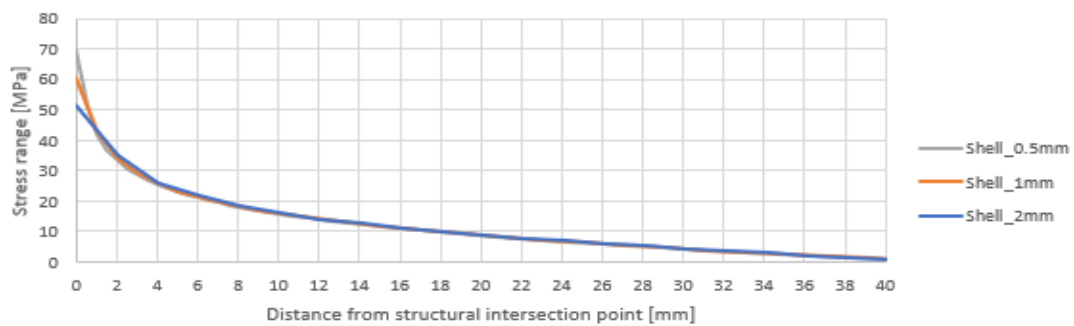


**Figure D 0.12 Stress range in web trough for different quadratic element sizes**

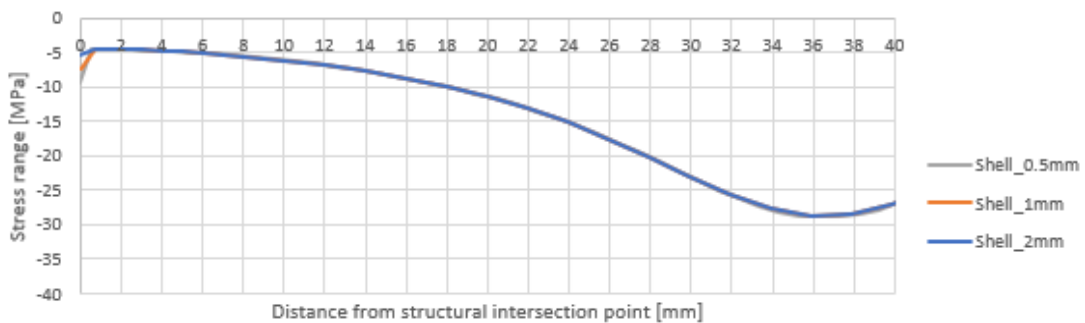


**Figure D 0.13 Stress range in crossbeam for different quadratic element sizes**

Shell:



**Figure D 0.14 Stress range in web trough for different quadratic element sizes**



**Figure D 0.15 Stress range in crossbeam for different quadratic element sizes**

## ANNEX E

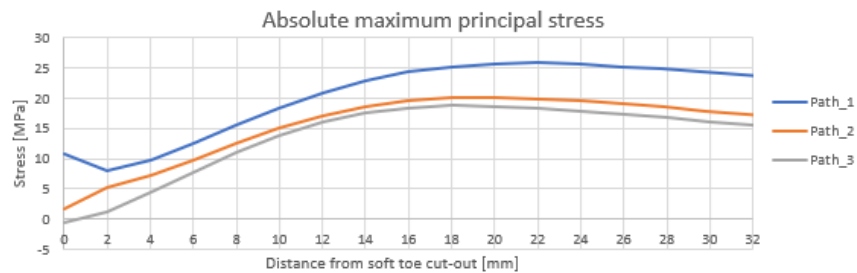
In this Annex the results for the crack location in the crossbeam is shown. This annex is divided in the following 4 parts:

- Part I: results absolute maximum principal stress and stress perpendicular to the weld toe for load positions 2 and 4;
- Part II: results weld modelling technique load positions 2 and 4;
- Part III: hot spot stress extrapolation shell, shell + weld, and solid for load positions 2 and 4;
- Part IV: deformation plots load position 2

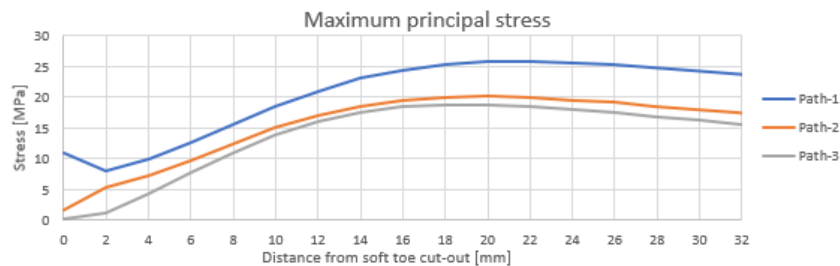
*Part I: results principal stresses and direct stresses*

### Load position 2

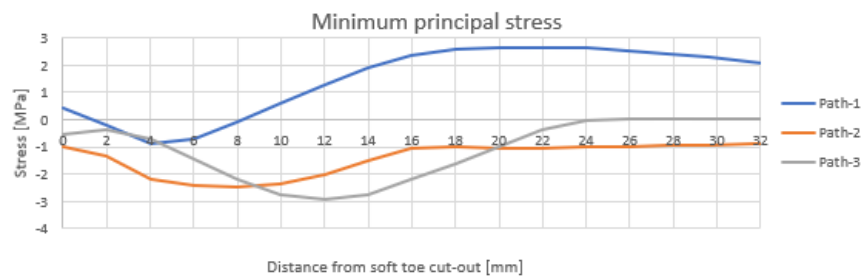
Solid:



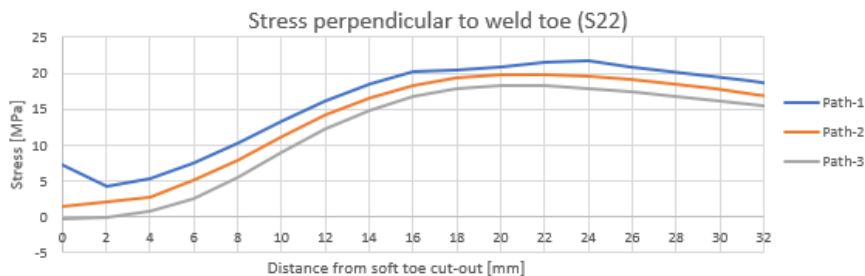
**Figure E 0.1 LP2: Absolute maximum principal stress for path 1,2 and 3 solid FE model**



**Figure E 0.2 LP2: Maximum principal stress for path 1,2 and 3 solid FE model**



**Figure E 0.3 LP2: Minimum principal stress for path 1,2 and 3 solid FE model**



**Figure E 0.4 LP2: Stress perpendicular to weld toe for path 1,2 and 3 solid FE model**



Figure E 0.5 LP2: Stress parallel to weld toe for path 1,2 and 3 solid FE model

Shell:

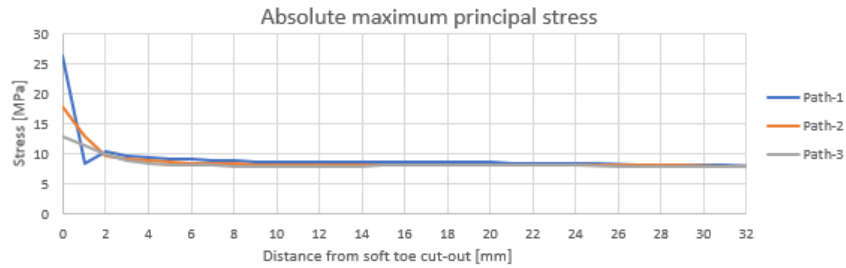


Figure E 0.6 LP2: Absolute maximum principal stress for path 1,2 and 3 shell FE model

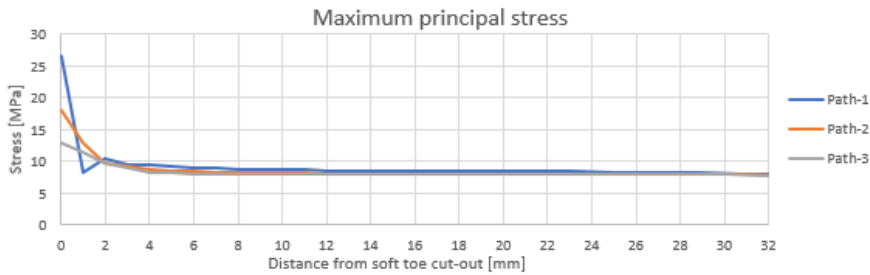


Figure E 0.7 LP2: Maximum principal stress for path 1,2 and 3 shell FE model

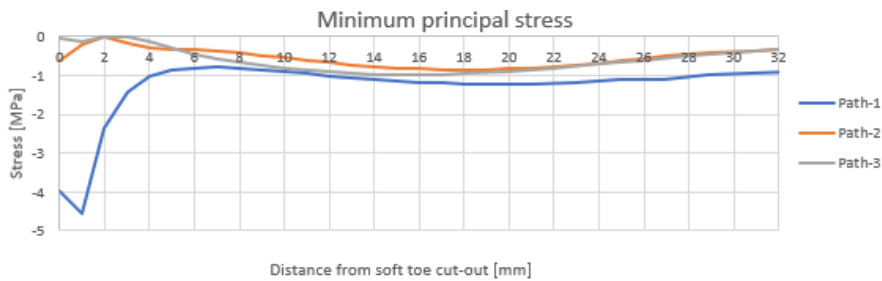


Figure E 0.8 LP2: Minimum principal stress for path 1,2 and 3 shell FE model



Figure E 0.9 LP2: Stress perpendicular to weld toe for path 1,2 and 3 shell FE model

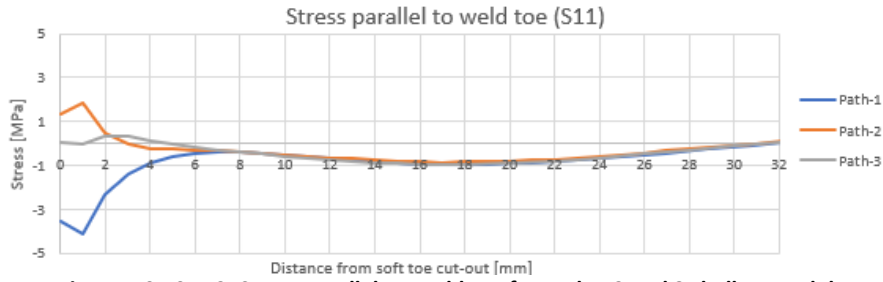


Figure E 0.10 LP2: Stress parallel to weld toe for path 1,2 and 3 shell FE model

Load position 3

Solid:

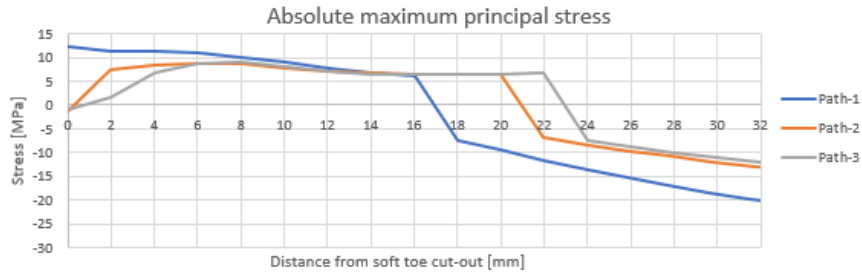


Figure E 0.11 LP3: Absolute maximum principal stress for path 1,2 and 3 solid FE model

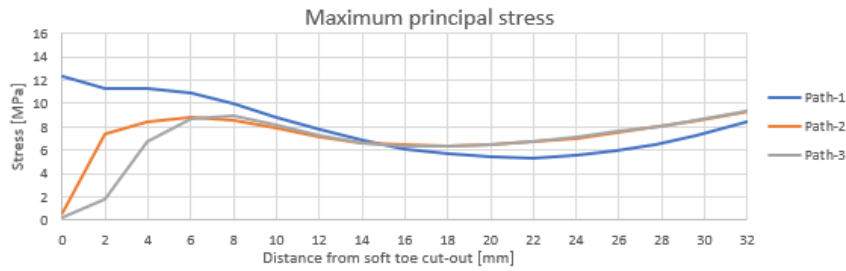


Figure E 0.12 LP3: Maximum principal stress for path 1,2 and 3 solid FE model

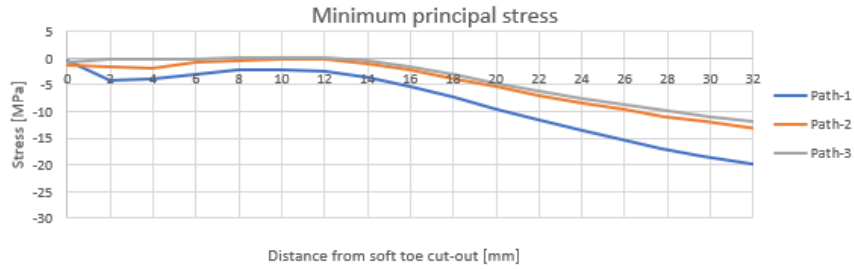


Figure E 0.13 LP3: Minimum principal stress for path 1,2 and 3 solid FE model

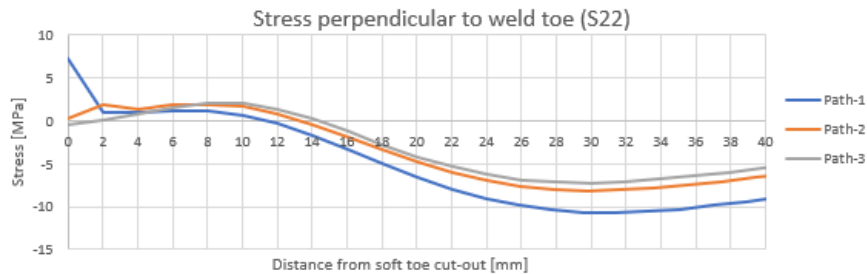


Figure E 0.14 LP3: Stress perpendicular to weld toe for path 1,2 and 3 solid FE model

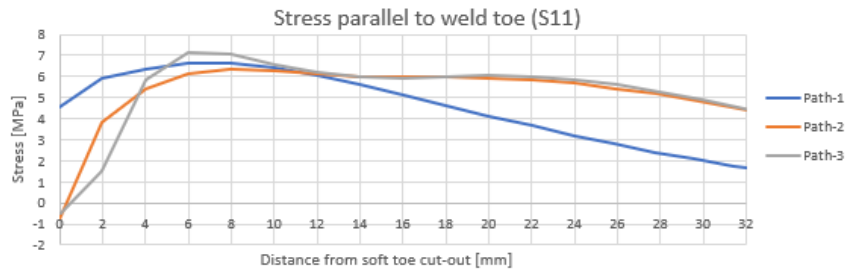


Figure E 0.15 LP3: stress parallel to weld toe for path 1,2 and 3 solid FE model

Shell:

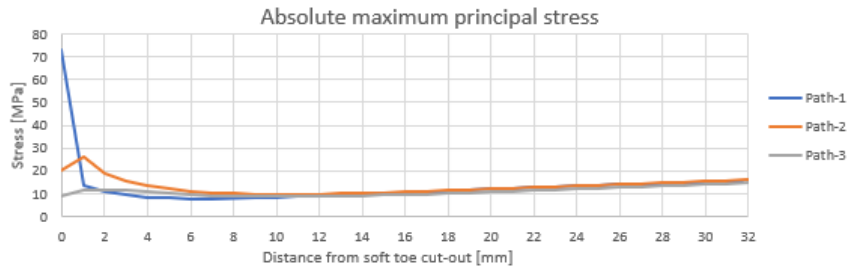


Figure E 0.16 LP3: Absolute maximum principal stress for path 1,2 and 3 shell FE model

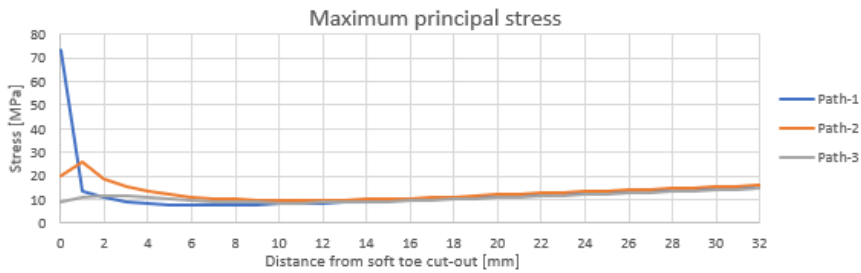


Figure E 0.17 LP3: Maximum principal stress for path 1,2 and 3 shell FE model

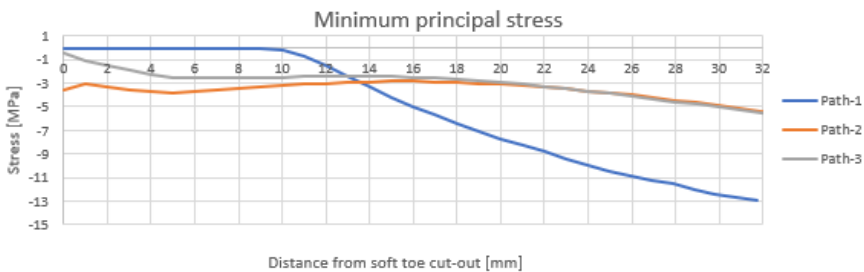


Figure E 0.18 LP3: Minimum principal stress for path 1,2 and 3 shell FE model

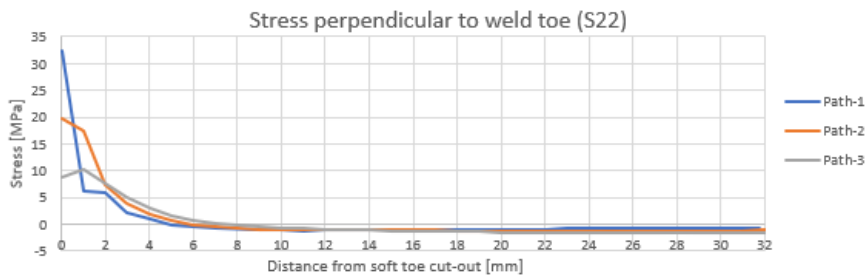


Figure E 0.19 LP3: Stress perpendicular to weld toe for path 1,2 and 3 shell FE model



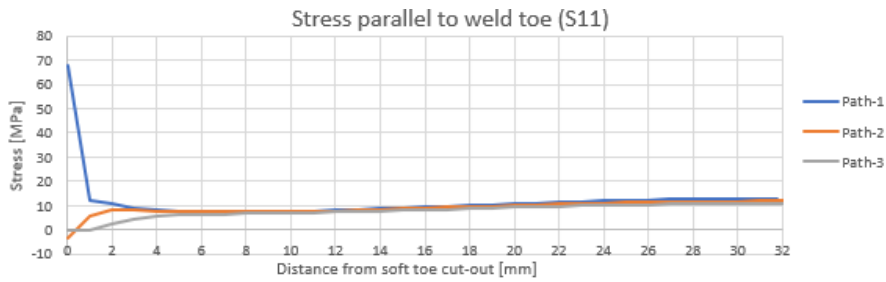


Figure E.0.20 LP3: Stress parallel to weld toe for path 1,2 and 3 shell FE model

Part II: results weld modelling techniques shell model Eriksson

Load position 1

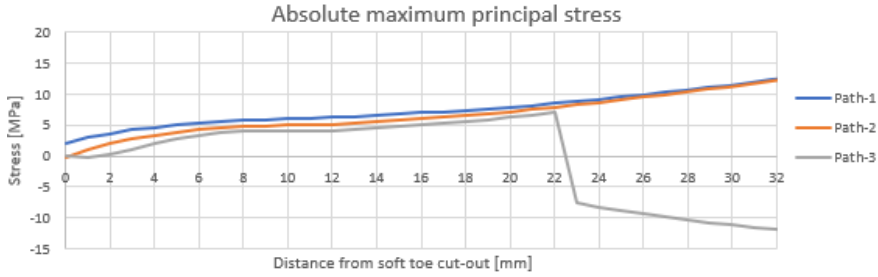


Figure E.0.21 LP1: Absolute maximum principal stress for path 1,2 and 3 shell FE model with weld Eriksson

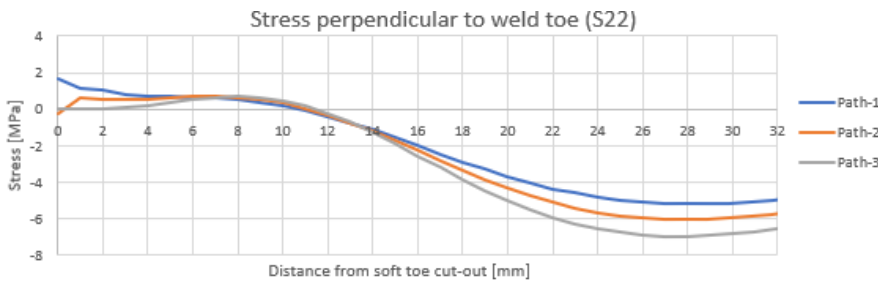


Figure E.0.22 LP2: Stress perpendicular to weld toe for path 1,2 and 3 shell FE model with weld Eriksson

Load position 2

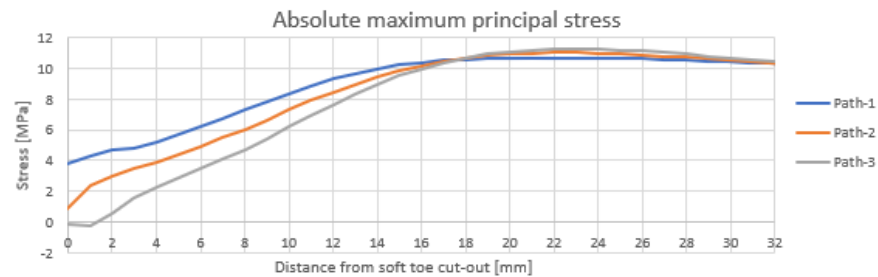


Figure E.0.23 LP2: Absolute maximum principal stress for path 1,2 and 3 shell FE model with weld Eriksson

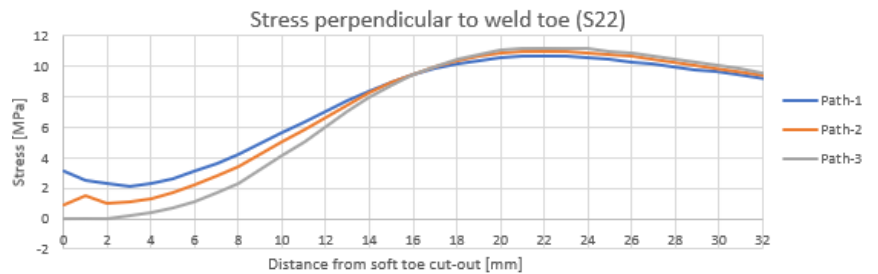
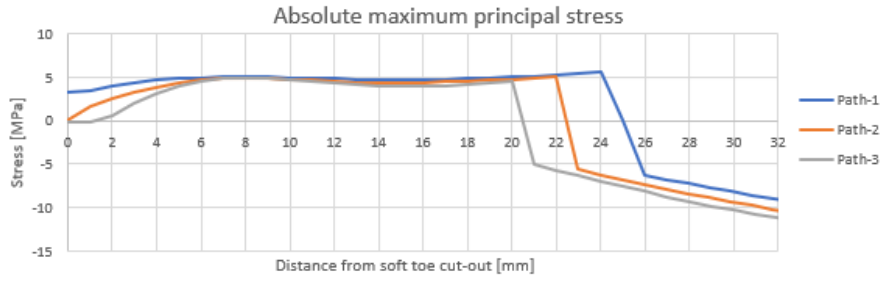
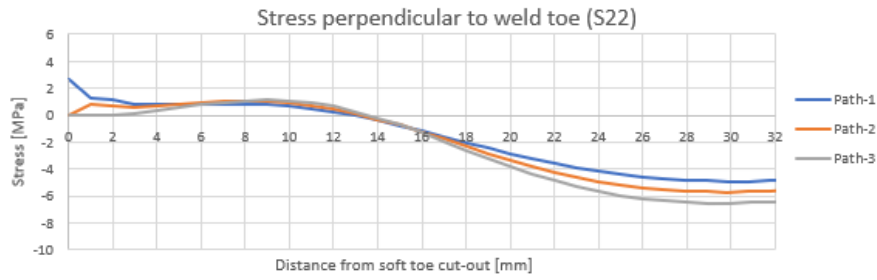


Figure E.0.24 LP2: Stress perpendicular to the weld toe for path 1,2 and 3 shell FE model with weld Eriksson

**Load position 3**



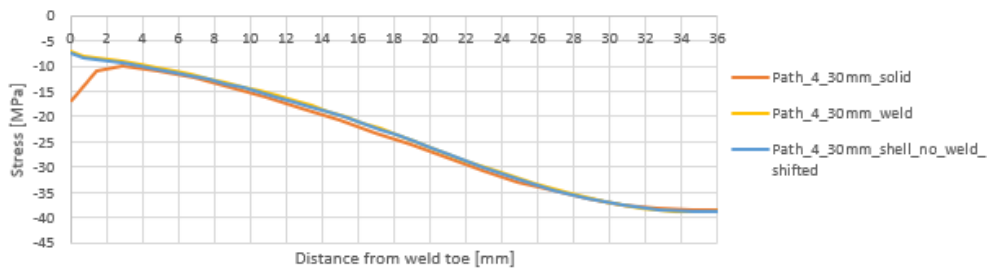
**Figure E 0.25 LP3: Absolute maximum principal stress for path 1,2 and 3 shell FE model with weld Eriksson**



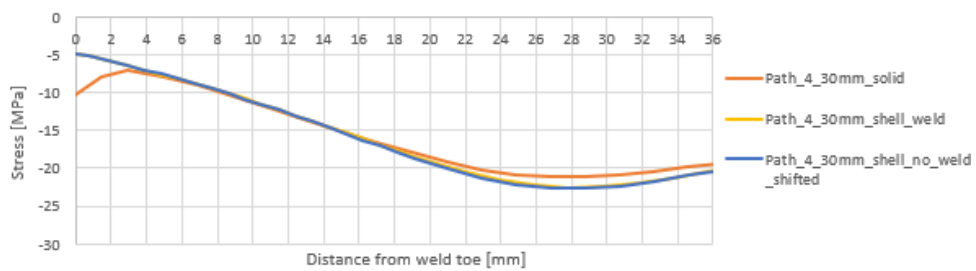
**Figure E 0.26 LP3: Stress perpendicular to the weld toe for path 1,2 and 3 shell FE model with weld Eriksson**

*Part III: results hot spot stress extrapolation shell, shell + weld and solid*

**Load position 3**



**Figure E 0.27 LP3 comparison results absolute maximum principal stress three different models path 4**



**Figure E 0.28 LP3: comparison results stress perpendicular to the weld toe three different models path 4**

## ANNEX F

The principal stress and the stress perpendicular to the weld toe (S22) will be compared for the following 2 cases: the red path with the green path and the yellow path with the purple path, which is shown in Figure F 0.1. The black dot, which is shown in Figure F 0.1 is a singular point and gives very high stresses. Due to this reason this point is not taken into account in the comparison of the different stresses. The yellow path has an offset from the red path which is equal to 1.46mm, which is half of the length from the weld toe to the curved part of the cut-out. For the through thickness stresses the X=0mm is at the location of the black dot in the figure below

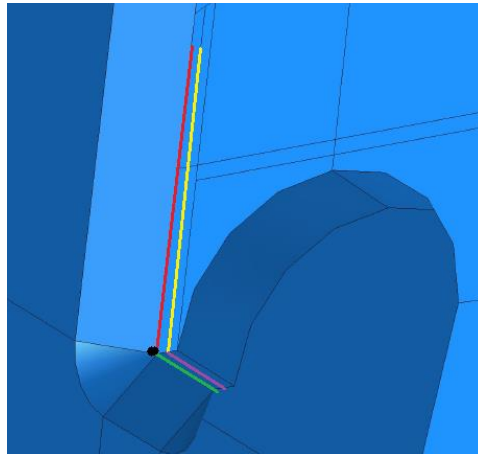


Figure F 0.1 Overview investigated paths

### Results loading positions

The results of the 5 different loading positions will be shown for every load position individually. First the stresses in path 1 and 2, will be shown and in the second figure the stresses through the thickness of the crossbeam will be shown. In those figures the absolute maximum principal stress and the stress perpendicular to the weld toe are shown.

#### Loading position 1:

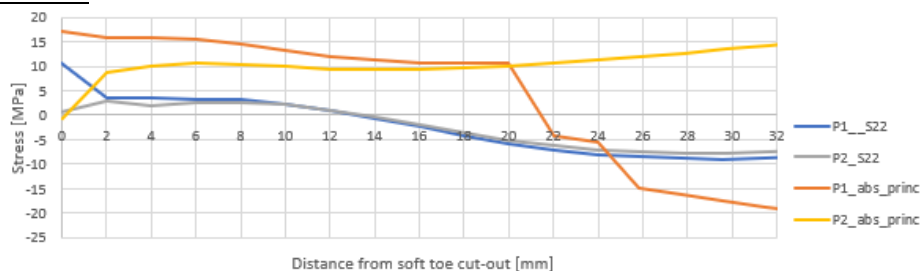


Figure F 0.2 LP1: absolute max principal stress and stress perpendicular to weld toe (S22) for path 1 and 2 (red and yellow path in Figure 0.1)

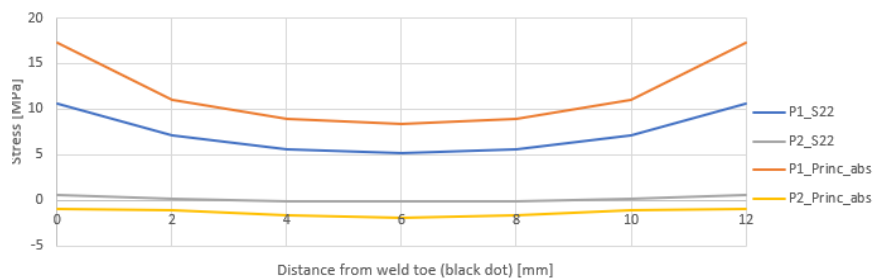


Figure F 0.3 LP1: absolute max principal stress and stress perpendicular to weld toe (S22) for path 1 and 2 through thickness crossbeam (green and purple path in Figure 0.1)

Loading position 2:

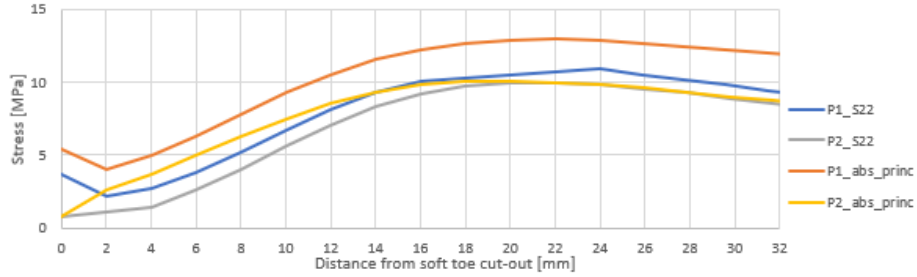


Figure F 0.4 LP2: absolute max principal stress and stress perpendicular to weld toe (S22) for path 1 and 2 (red and yellow path in Figure 0.1)

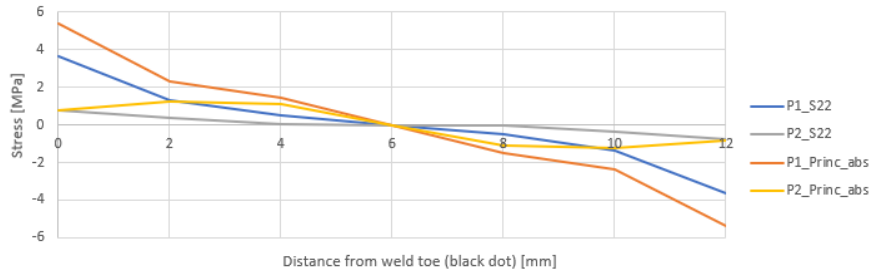


Figure F 0.5 LP2: absolute max principal stress and stress perpendicular to weld toe (S22) for path 1 and 2 through thickness crossbeam (green and purple path in Figure 0.1)

Loading position 3:

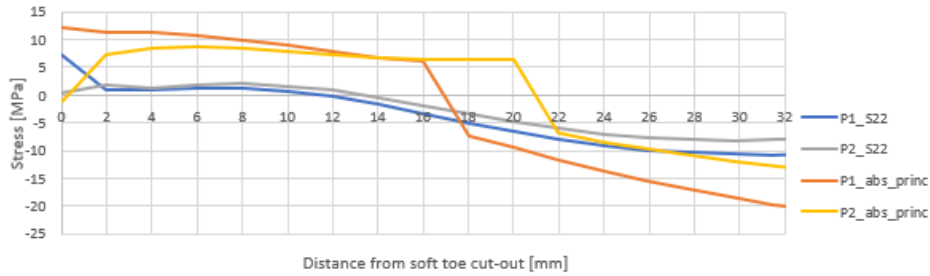


Figure F 0.6 LP3: absolute max principal stress and stress perpendicular to weld toe (S22) for path 1 and 2 (red and yellow path in Figure 0.1)

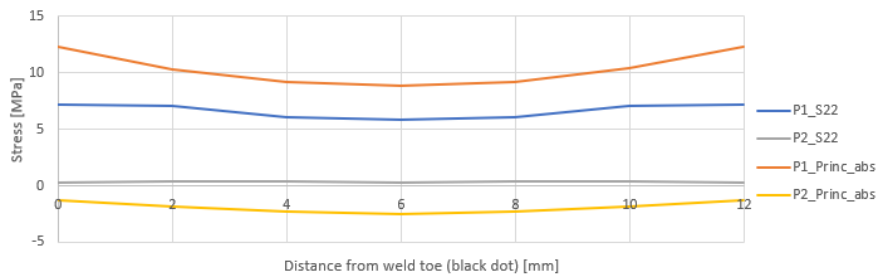


Figure F 0.7 LP3: absolute max principal stress and stress perpendicular to weld toe (S22) for path 1 and 2 through thickness crossbeam (green and purple path in Figure 0.1)

Loading position 4:

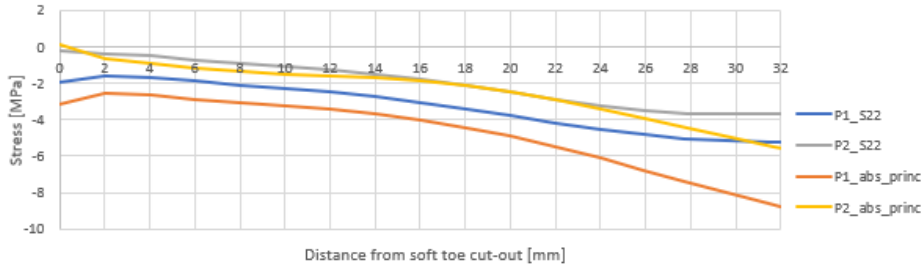


Figure F 0.8 LP4: absolute max principal stress and stress perpendicular to weld toe (S22) for path 1 and (red and yellow path in Figure 0.1)

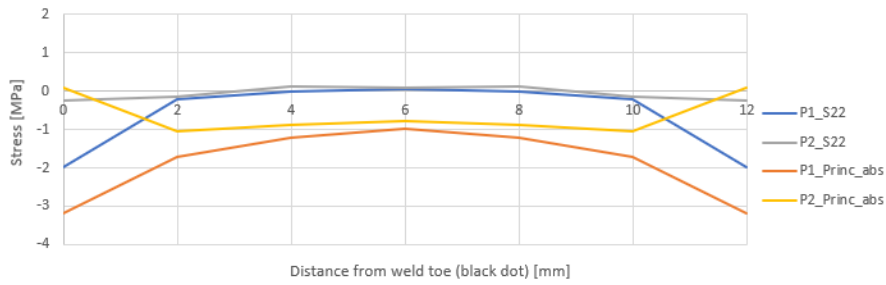


Figure F 0.9 LP4: absolute max principal stress and stress perpendicular to weld toe (S22) for path 1 and 2 through thickness crossbeam (green and purple path in Figure 0.1)

Loading position 5:

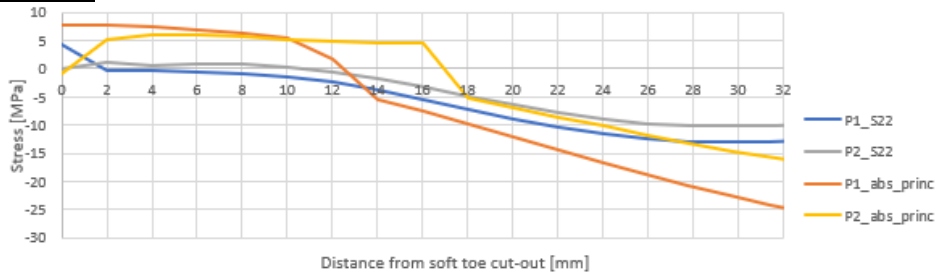


Figure F 0.10 LP5: absolute max principal stress and stress perpendicular to weld toe (S22) for path 1 and 2 (red and yellow path in Figure 0.1)

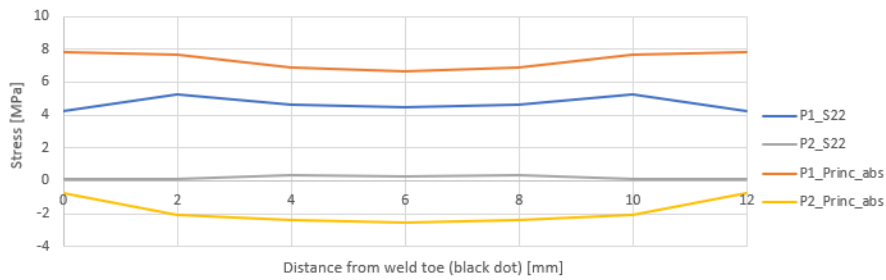


Figure F 0.11 LP5: absolute max principal stress and stress perpendicular to weld toe (S22) for path 1 and 2 through thickness crossbeam (green and purple path in Figure 0.1)

## ANNEX G

In this report the results for the deformation study of loading positions 2 are shown. With loading position 2, two wheel patches are placed with a offset of +500mm and -500mm from the middle crossbeam. One load of 50kN is facing upwards, while the other load of 50kN is facing downwards which is shown in Figure G 0.1.

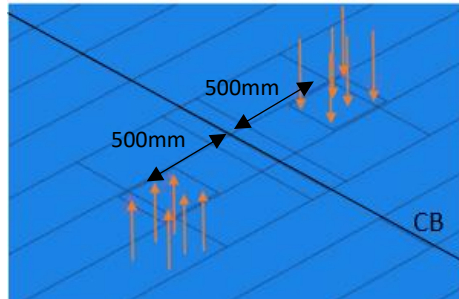


Figure G 0.1 Loading position 2

### Deformed mesh plots crossbeam loading position 2

In the following figures the results of the solid FE model are shown on the left figure and the results of the shell FE model with Eriksson weld on right figure. In this solid FE model the seam between the crossbeam and trough is modelled. To get a better visualization of the deformations, the thickness of the shell element is shown.

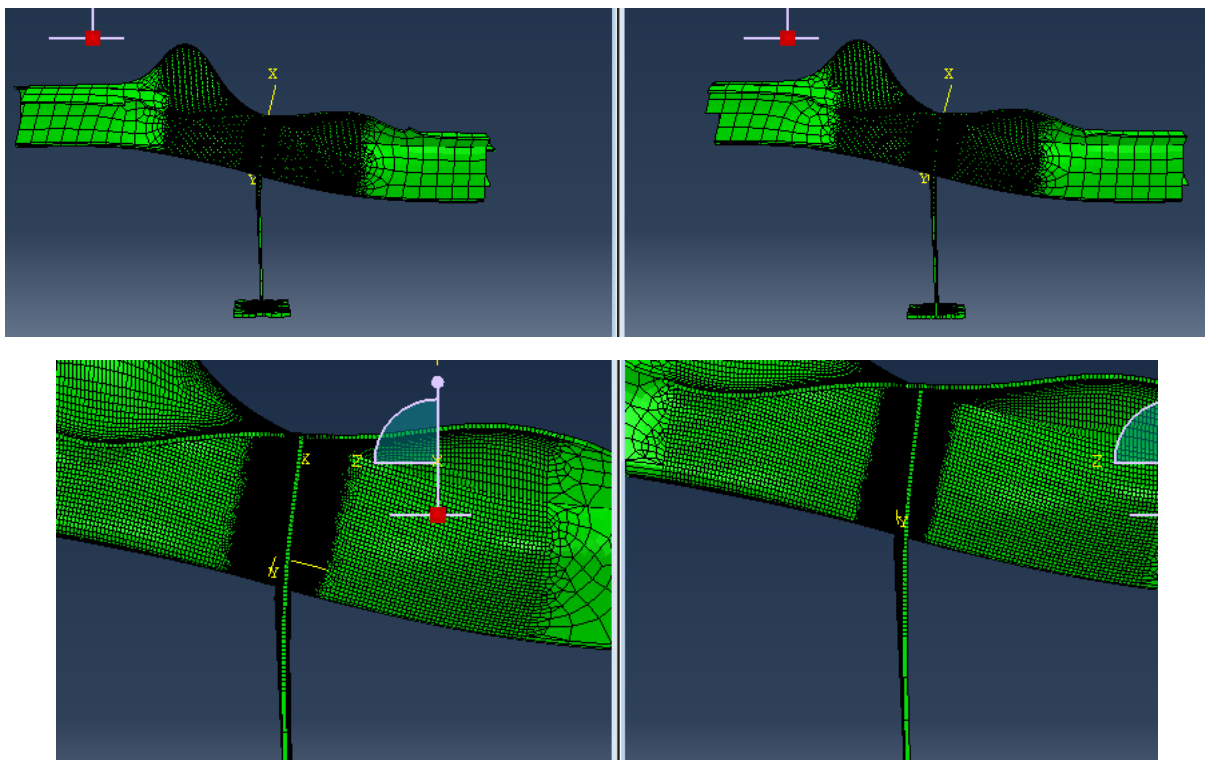


Figure G 0.2 Deformed mesh plot crossbeam, solid (left) and shell (right)

As can be seen from the above figures, the overall behavior of the solid and shell FE model is the same, which is as expected since they share the same overall shell model. In the following two figures the local deformation of the solid (right) and shell (left) FE model is shown, in which the shell render thickness option is put on to get a better representation of the local deformation.



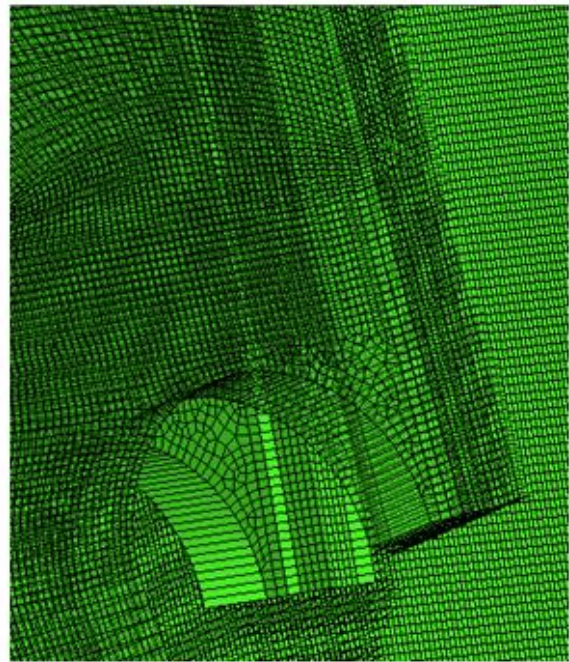
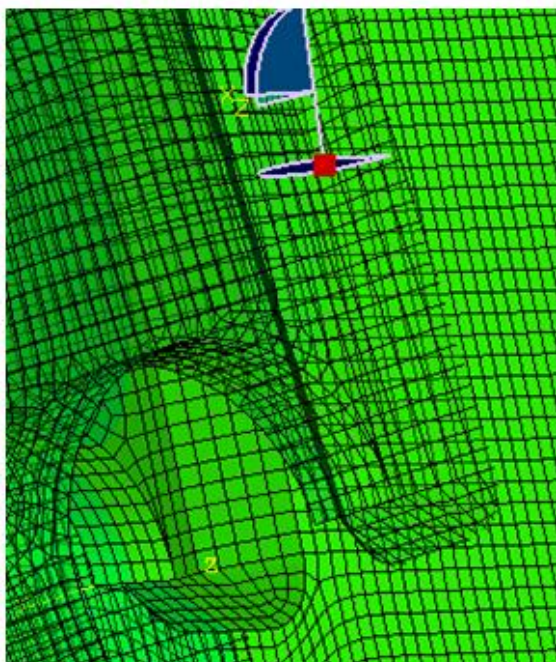
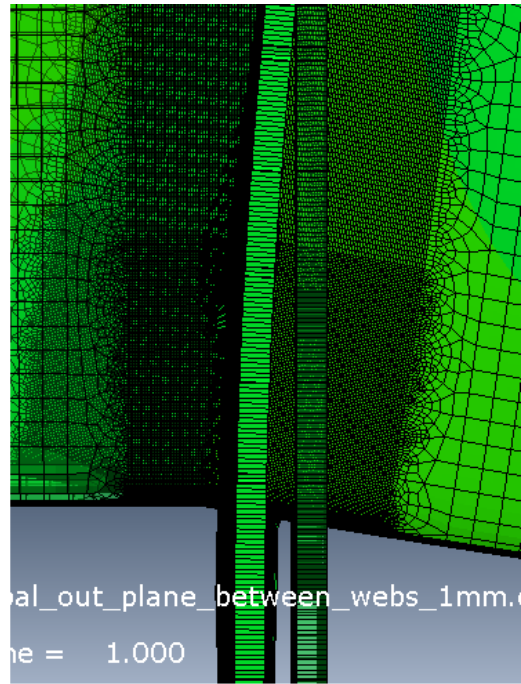
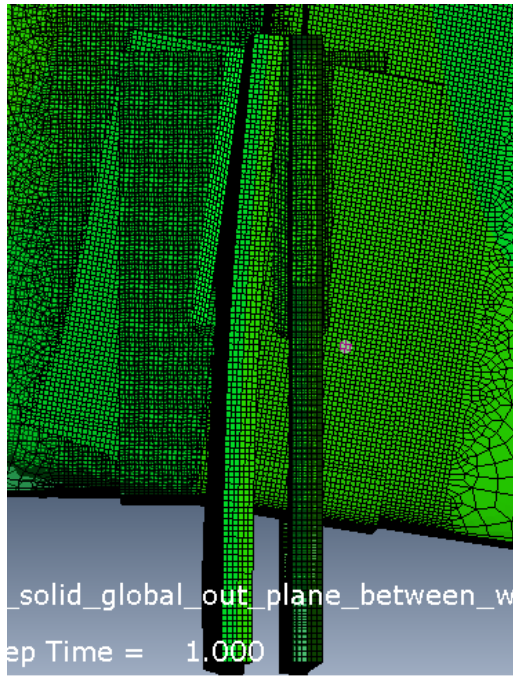
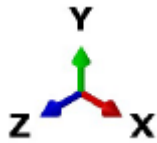


Figure G 0.3 Deformed and undeformed mesh local deformation at detail of interest, solid (left) and shell Eriksson (right), scaling factor 150

## Deformation contour plots

Used coordinate system:



In the next figures the overall deformation U, and the deformations in the three directions: U1,U2, and U3 will be shown. First a more zoomed out overview is shown and in the second figure the local deformations are shown. For both models the same minimum and maximum limits are used to make a proper comparison.

### Z-axis solid

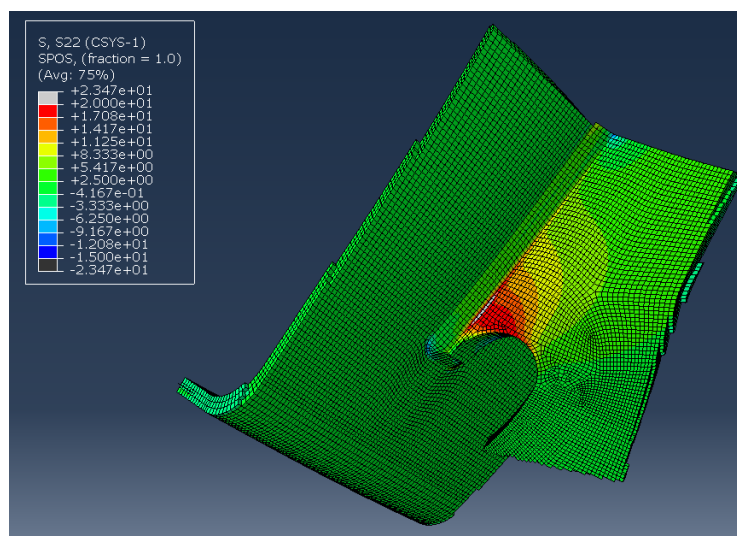


Figure G 0.4 Deformed mesh contour plot Z-axis solid FE model

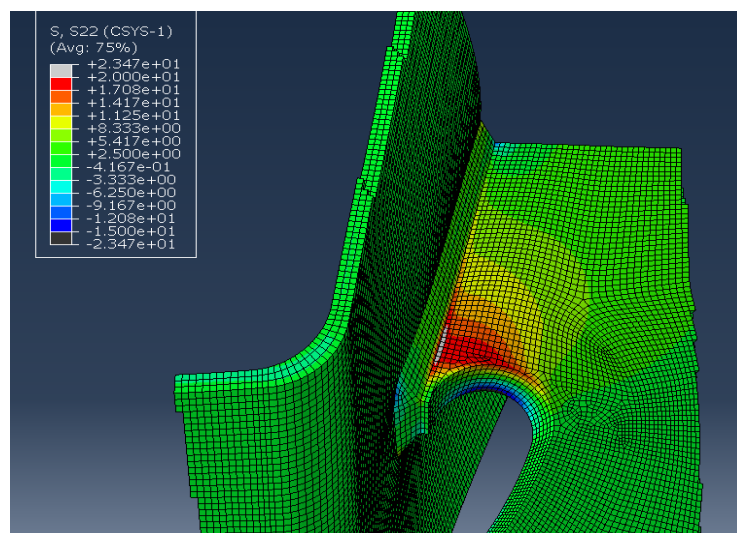


Figure G 0.5 Deformed mesh contour plot Z-axis solid FE model



### Z-axis shell weld Eriksson

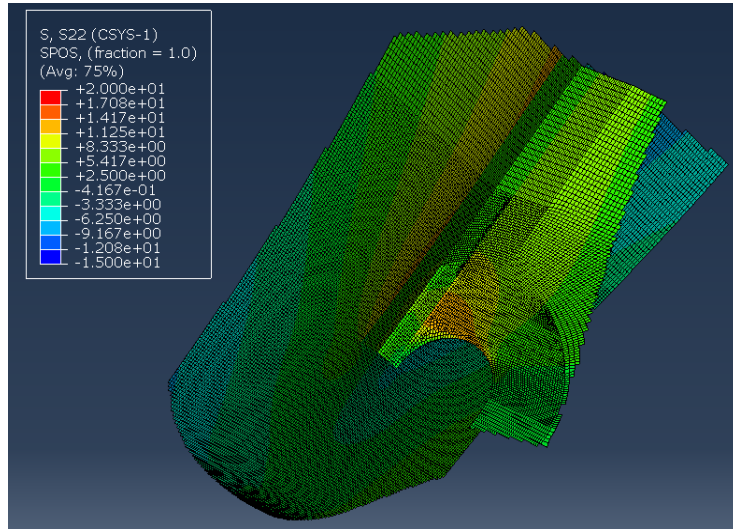


Figure G.0.6 Deformed mesh contour plot Z-axis shell Eriksson weld FE model

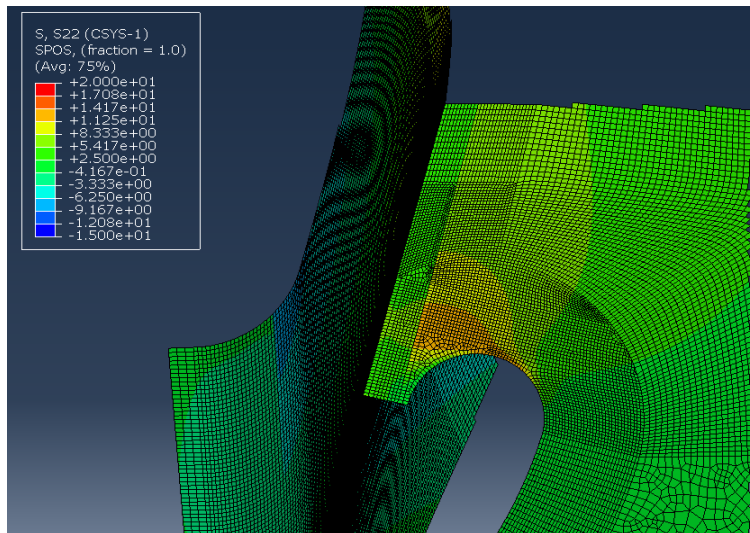


Figure G.0.7 Deformed mesh contour plot Z-axis shell Eriksson weld FE model

### Y-axis solid

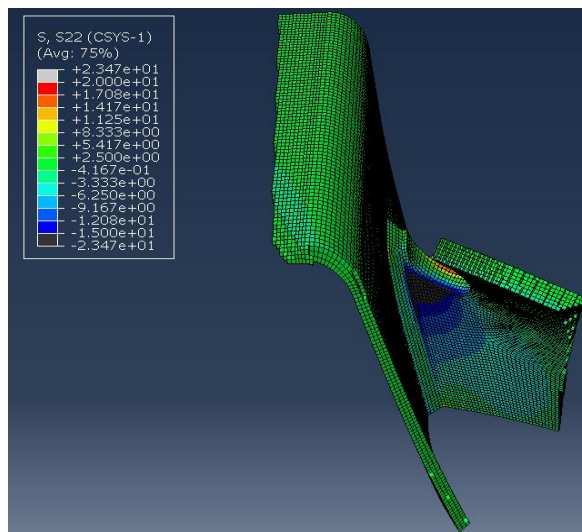


Figure G.0.8 Deformed mesh contour plot Y-axis solid FE model

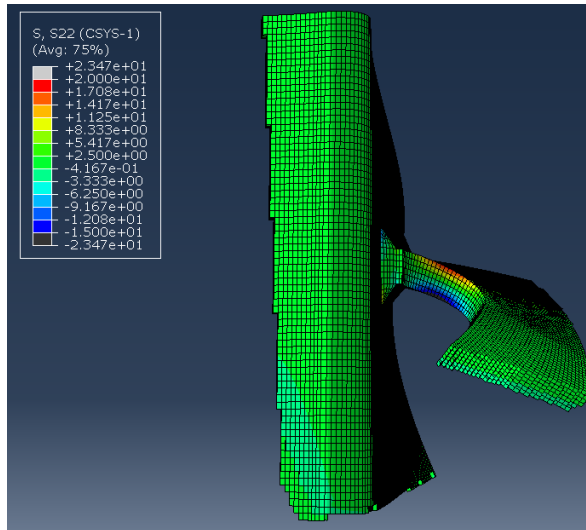


Figure G 0.9 Deformed mesh contour plot Y-axis parallel to weld toe solid FE model

**Y-axis shell weld Eriksson (thickness option on)**

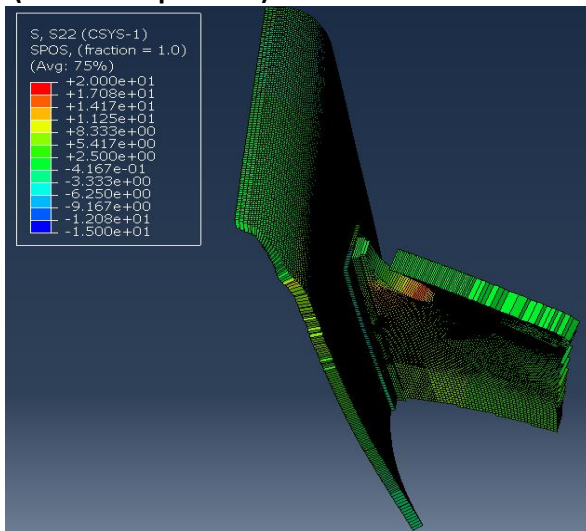


Figure G 0.10 Deformed mesh contour plot Y-axis shell Eriksson weld FE model (thickness option on)

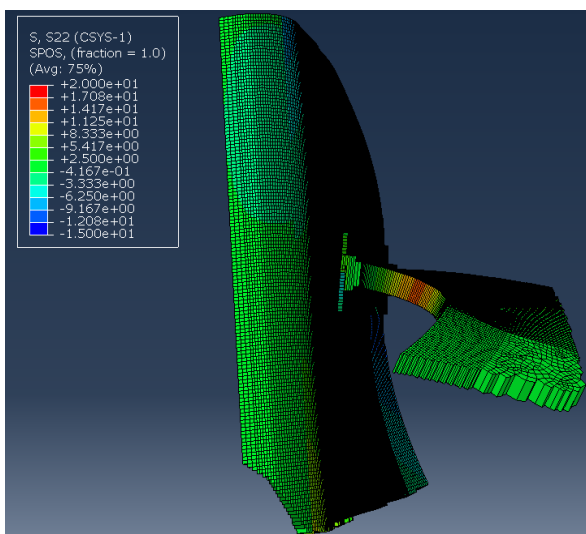


Figure G 0.11 Deformed mesh contour plot Y-axis parallel to lower weld toe shell Eriksson weld FE model (thickness option on)

### X-axis solid

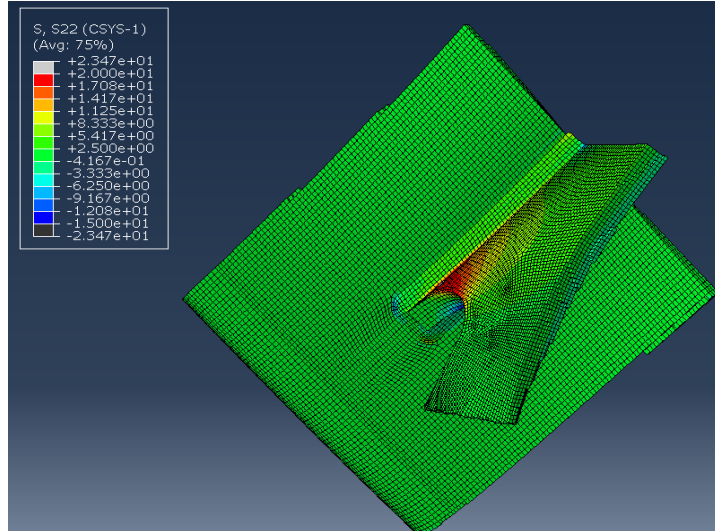


Figure G 0.12 Deformed mesh contour plot X-axis solid FE model

### X-axis shell weld Eriksson

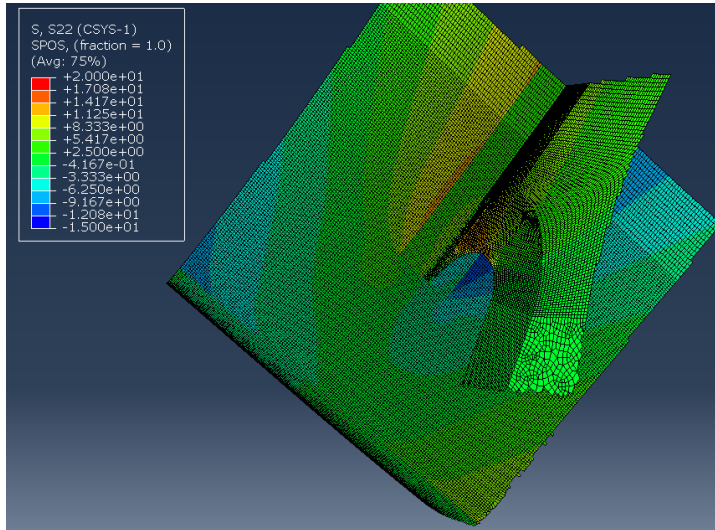


Figure G 0.13 Deformed mesh contour plot X-axis shell Eriksson weld FE model

### Local deformation at soft toe

In Figure G 0.14 and Figure G 0.15 the deformations of the “soft toe” with a scaling factor of 1000 is shown.

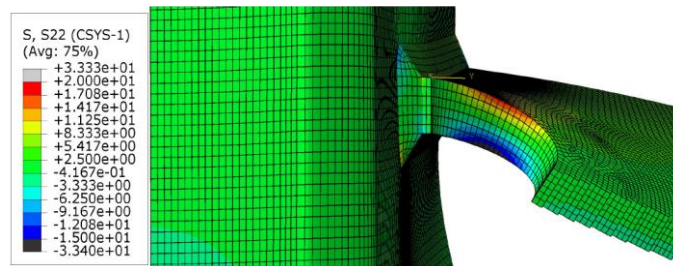


Figure G 0.14 Local deformation at soft toe solid FE model, scaling factor: 1000

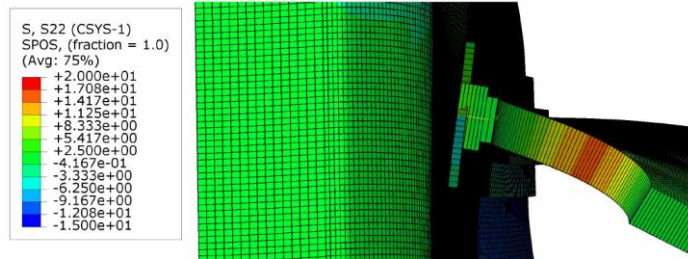


Figure G 0.15 Local deformation at soft toe shell with Eriksson weld FE model, scaling factor: 1000

## ANNEX H

### Comparison loading position 5 old and new OSD variant web of trough

In this Annex the comparison between the new and old OSD variant will be made for loading position 5, since the hot spot stress is higher for the new OSD variant when compared with the old variant. The stress perpendicular to the weld toe for the trough is shown in Figure H 0.1 for the old variant and in Figure H 0.2 for the new variant for the shell FE model without weld. As can be seen from the figures, in the case of the old OSD variant no stress concentration occurs at the structural intersection point of the trough and the crossbeam, while this stress concentration clearly occurs at the new variant.

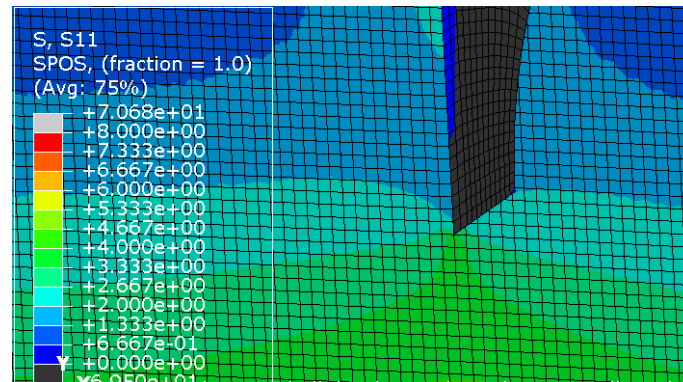


Figure H 0.1 Stress perpendicular to the weld toe old OSD variant

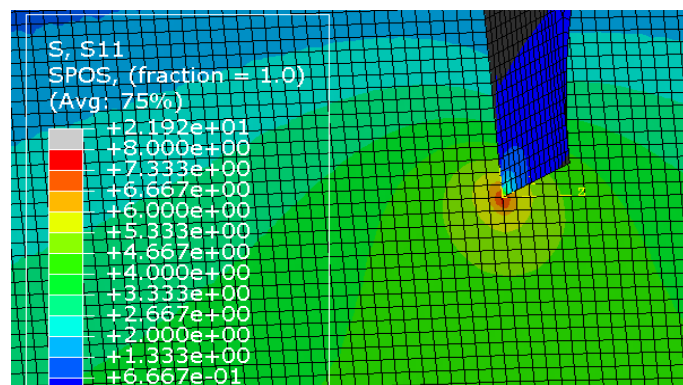


Figure H 0.2 Stress perpendicular to the weld toe new OSD variant

To investigate the stress in the trough two paths of 100mm length, 50mm to the left and right of the structural intersection point, are investigated. The first path is directly at the structural intersection point, see red line in Figure H 0.3, while the second path is 0.5t of the trough away from the structural intersection point, see green line in Figure H 0.3.

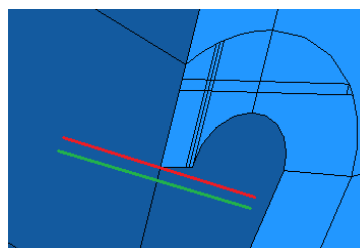
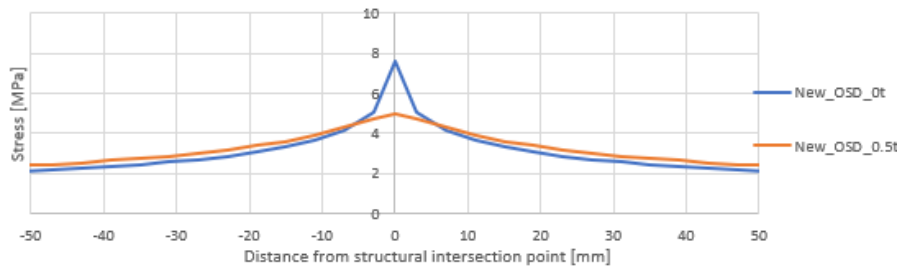


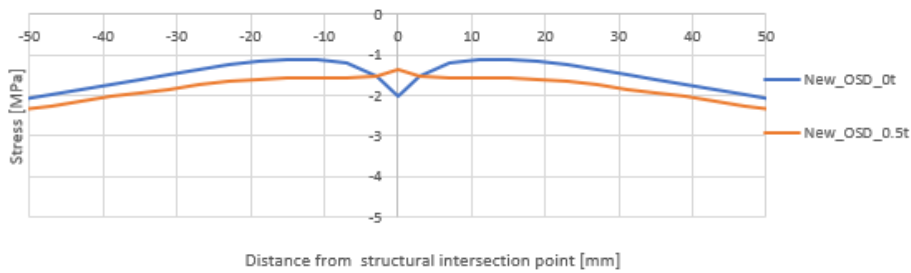
Figure H 0.3 Paths in trough 0t and 0.5t from structural intersection point.

To compare the behavior in those 2 paths, both the stresses perpendicular to weld toe for the inner and outer side of the shell elements are extracted. For both the new and old OSD both the stresses of the inner and outer side of the trough are extracted to see how the behavior in the trough is. The outer side is the at the outer face of the trough, while the inner side is at the inside face of the trough.

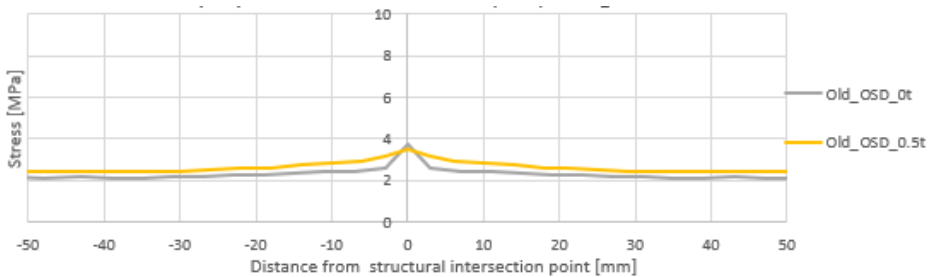
In Figure H 0.4 and Figure H 0.5 the results for the new OSD variant of the outer and inner side are shown, while in Figure H 0.6 and Figure H 0.7 the results of the old OSD variant are shown.



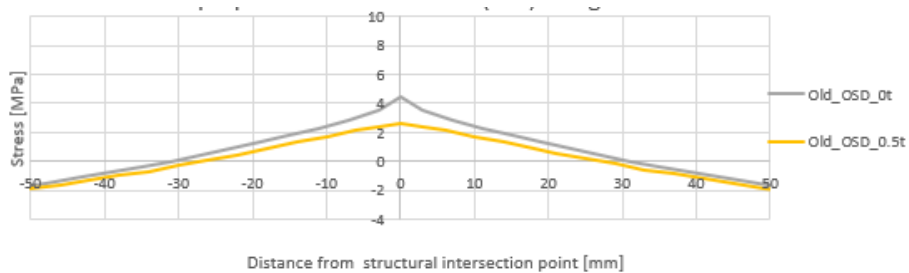
**Figure H 0.4 New OSD variant stress perpendicular to the weld toe trough outer side shell**



**Figure H 0.5 New OSD variant stress perpendicular to the weld toe trough inner side shell**



**Figure H 0.6 Old OSD variant stress perpendicular to the weld toe trough outer side shell**



**Figure H 0.7 Old OSD variant stress perpendicular to the weld toe trough inner side shell**

As can be seen from the graphs, the behavior of the old and new OSD is different locally at the structural intersection point. The new OSD variant shows a stress concentration at the outer side of the trough. On the outer side of the trough the stresses of the new OSD variant are all positive on the investigated paths, while on the inner side of the trough the stresses are all negative. This can only be caused by bending in the trough. For the old OSD not really a stress concentration occurs at the outer side of the trough, but as with the new OSD variant all values are also positive. The stress perpendicular to the weld toe on the outer side of the trough is more or less constant from -50 to -10 and +10 to +50mm.

The stress 50mm away for the structural intersection point, at the inner side of the trough for the old OSD variant, is also negative and thus at that location it is also predominantly loaded in bending. In



the local area something different occurs at -30mm from the structural intersection point: the stress is changing sign, it becomes positive. Directly at the structural intersection point the stress on the inner and outer side of the trough are more or less equal which means that at that location it is predominantly loaded by a membrane stress, and no bending.

Since the difference between the new and old OSD variant is only the thickness of the trough, crossbeam, and deck plate, one parameter is adapted at the time to see which parameter will result in this stress concentration for the new OSD. Since this can be easily done with a shell FE model, this model is used for the comparison. To compare the results first the contour plot of the stress perpendicular to the weld toe is shown and furthermore the hot spot stress is calculated. In the next three figures the contour plots of the stress perpendicular to weld toe are shown, when only one parameter is adapted.

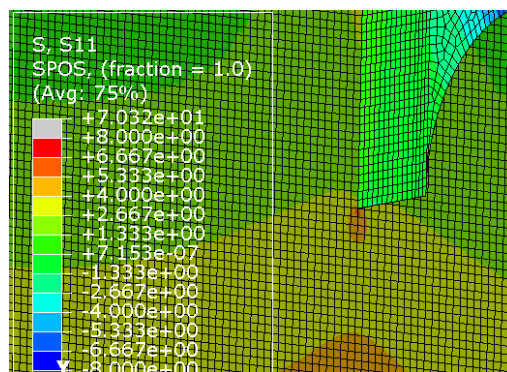


Figure H 0.8 Stress perpendicular to the weld toe thickness crossbeam increased

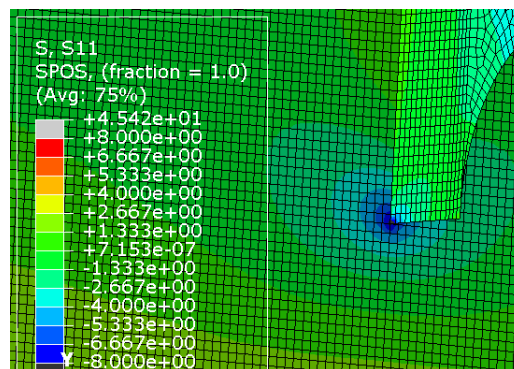


Figure H 0.9 Stress perpendicular to the weld toe thickness deck plate increased

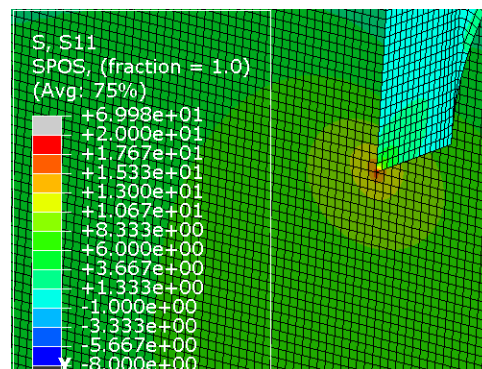


Figure H 0.10 Stress perpendicular to the weld toe thickness trough increased

As can be seen from Figure H 0.8, a small stress concentration will occur at the structural intersection point when the thickness of the crossbeam is increased from 12mm to 16mm. In Figure H 0.9 it can

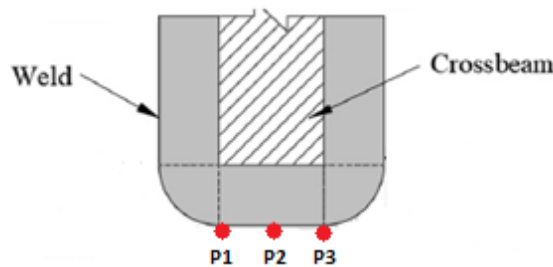
be seen that by increasing the thickness of the deck plate from 12mm to 22mm the stress concentration will change sign and becomes negative. Changing the thickness of the trough from 6mm to 8mm, will create a large stress concentration which can be seen in Figure H 0.10. The regular linear hot spot extrapolation, 0.4t and 1.0t, is performed to calculate the differences in obtained hot spot stresses and the results are shown in Table H 0-1.

**Table H 0-1 Results hot spot stress extrapolation web trough for different adapted parameters**

	Obtained hot spot stress in web trough [MPa]
Original HSS	+3.43
Increasing thickness crossbeam	+4.59
Increasing thickness deck plate	-5.19
Increasing thickness trough	+11.94

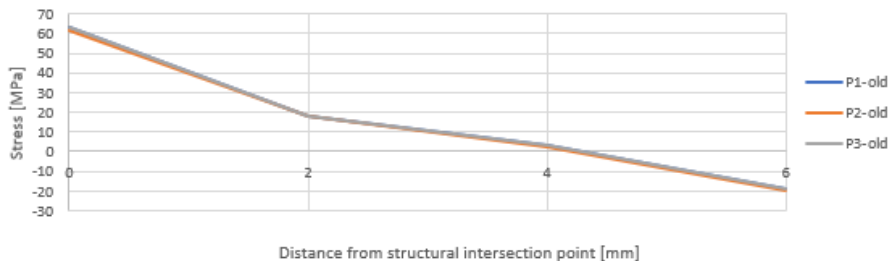
**Though thickness stress values solid FE model LC1 and LC5**

To investigate the local stress at the area close to the weld, the through thickness stress is extracted at three different locations which are marked in Figure H 0.11 from the solid FE model. This investigation is performed for both loading position 1 and loading position 5 for the new and old OSD variant to see which differences occur. First the results of load position 1 for both the new and old variant are shown and thereafter the results of loading position 5.

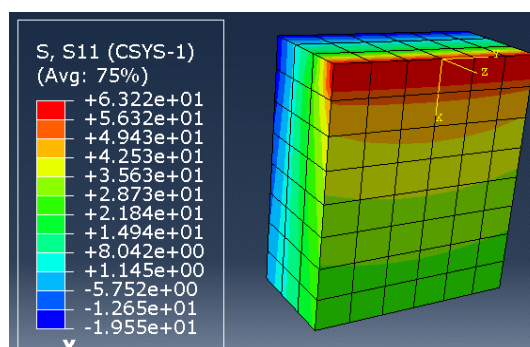


**Figure H 0.11 Overview through thickness locations solid FE model**

**LC1 old OSD variant**



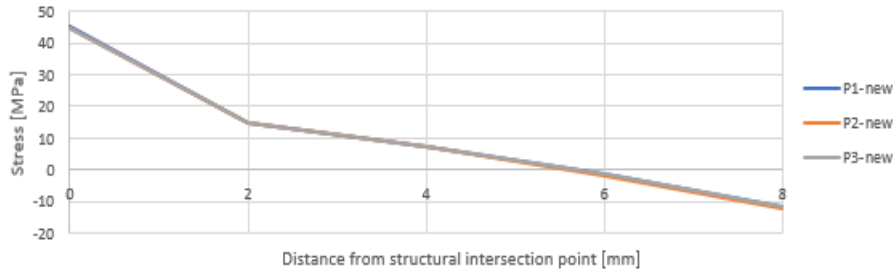
**Figure H 0.12 Old OSD variant LC1: stress perpendicular to weld toe through thickness trough**



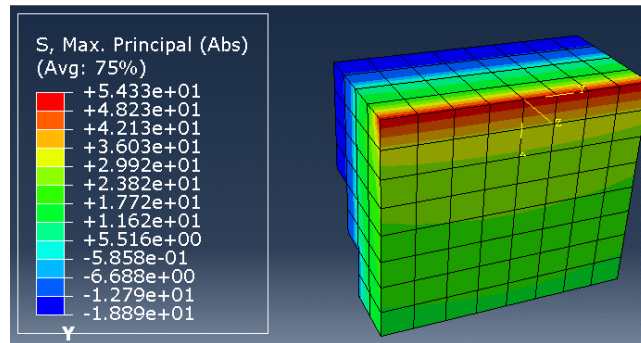
**Figure H 0.13 Old OSD variant LC1: stress perpendicular to weld toe through thickness trough contour plot**



**LC1 new OSD variant**

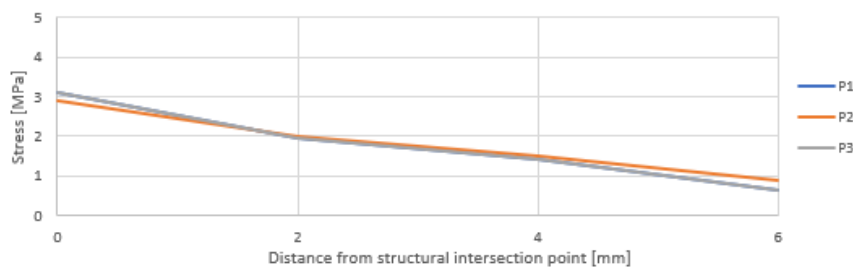


**Figure H 0.14 New OSD variant LC1: stress perpendicular to weld toe through thickness trough**

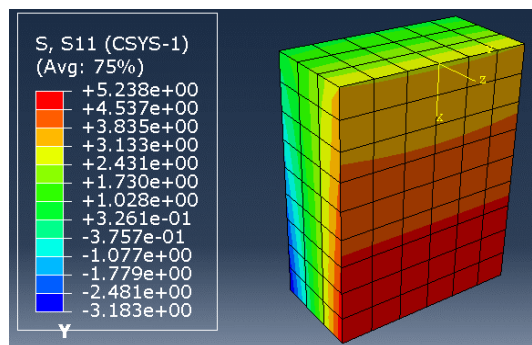


**Figure H 0.15 New OSD variant LC1: stress perpendicular to weld toe through thickness trough contour plot**

**LC5 old OSD variant**

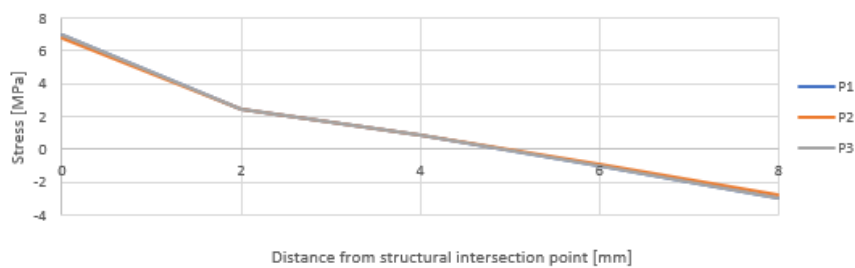


**Figure H 0.16 Old OSD variant LC5: stress perpendicular to weld toe through thickness trough**



**Figure H 0.17 Old OSD variant LC1: stress perpendicular to weld toe through thickness trough contour plot**

**LC5 new OSD variant**



**Figure H 0.18 New OSD variant LC5: stress perpendicular to weld toe through thickness trough**

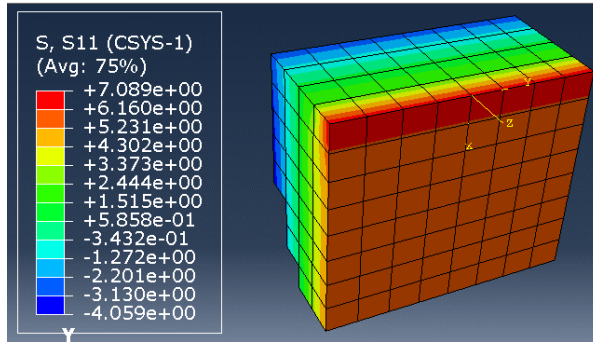
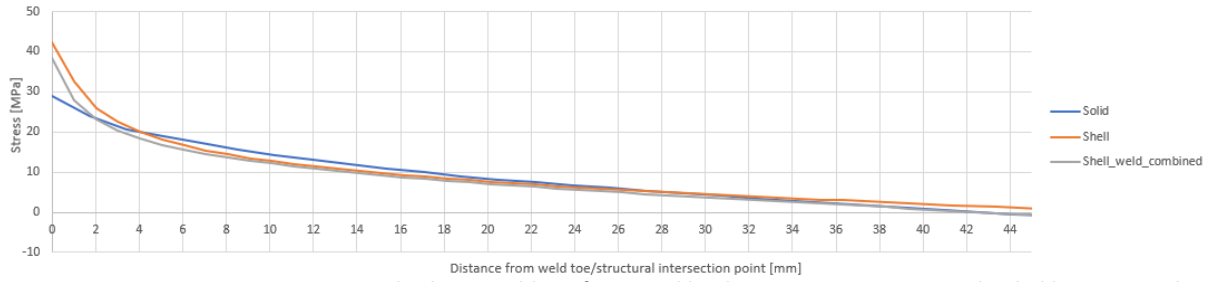


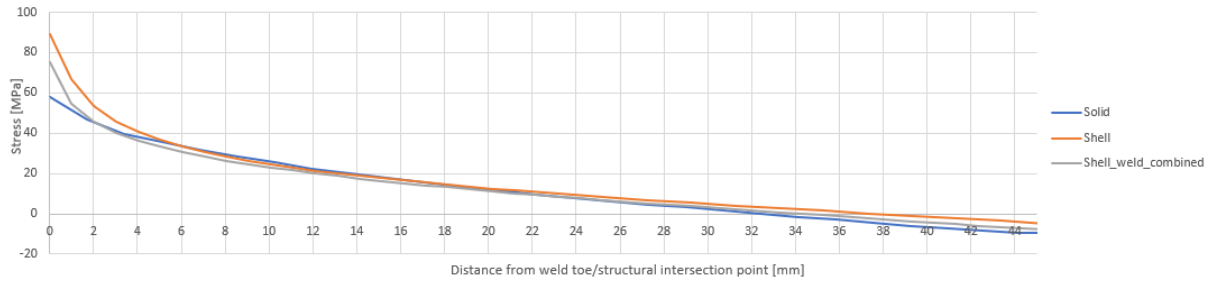
Figure H 0.19 New OSD variant LC5: stress perpendicular to weld toe through thickness trough contour plot

# ANNEX I

Stress path critical locations for crack in web of trough old OSD variant:

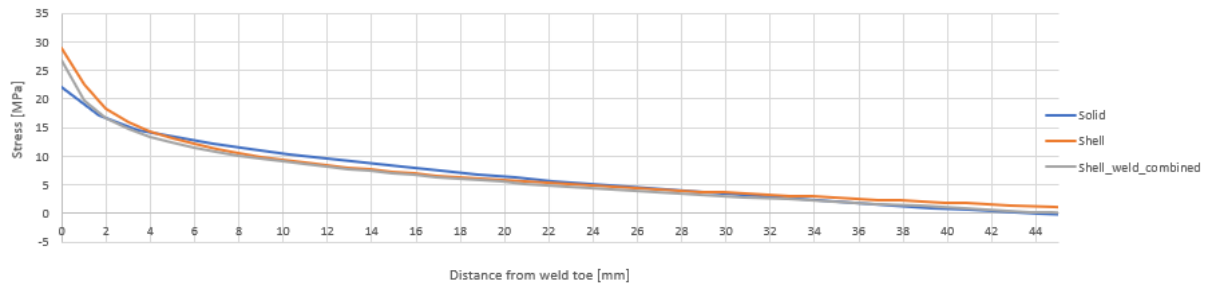


**Figure I 0.1 Comparison stress perpendicular to weld toe for critical loading position X=+375mm, loaded between webs trough, crack in web trough, old OSD variant**

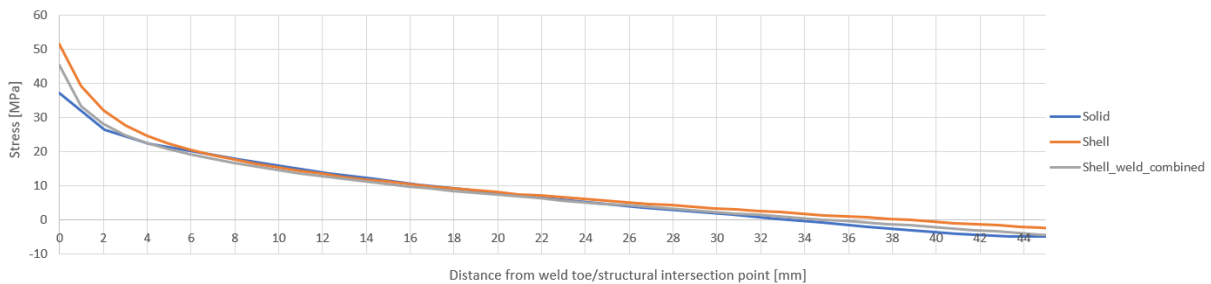


**Figure I 0.2 Comparison stress perpendicular to weld toe for critical loading position X=+1375mm, loaded between troughs, crack in web trough, old OSD variant**

Stress path critical locations for crack in web of trough new OSD variant:

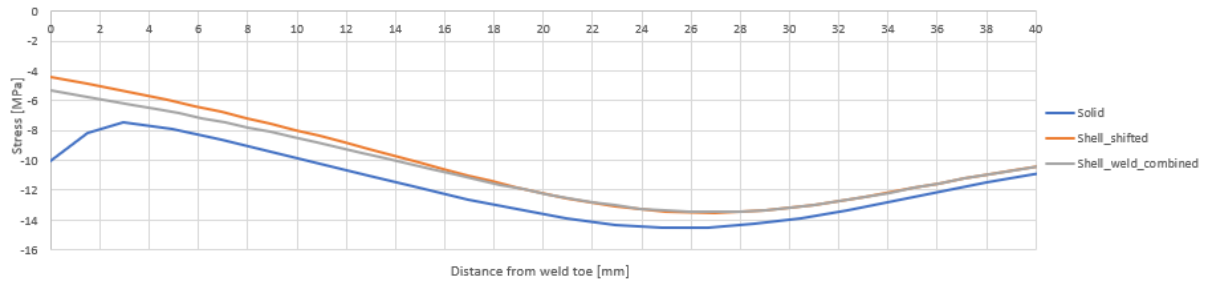


**Figure I 0.3 Comparison stress perpendicular to weld toe for critical loading position X=+375mm, loaded between webs trough, crack in web trough, new OSD variant**

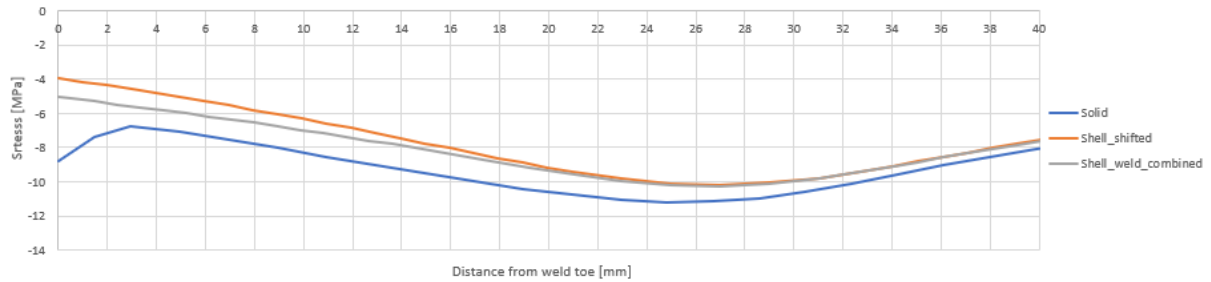


**Figure I 0.4 Comparison stress perpendicular to weld toe for critical loading position X=+1250mm, loaded between troughs, crack in web trough, new OSD variant**

**Stress path critical locations for crack in crossbeam P4 28mm old OSD variant (minimum HSS):**

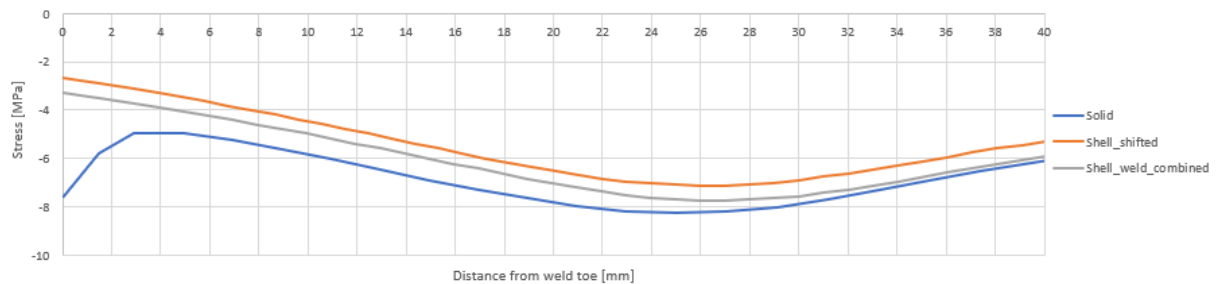


**Figure I 0.5 Comparison stress perpendicular to weld toe, P4\_28mm, for critical loading position X=+375mm, loaded between webs, crack in CB, old OSD variant**

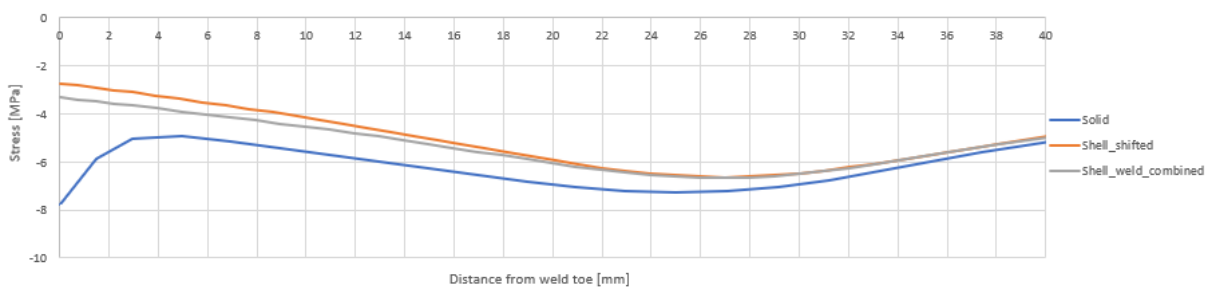


**Figure I 0.6 Comparison stress perpendicular to weld toe, P4\_28mm, for critical loading position X=+625mm, loaded between troughs, crack in CB, old OSD variant**

**Stress path critical locations for crack in crossbeam P4 28mm new OSD variant (minimum HSS):**

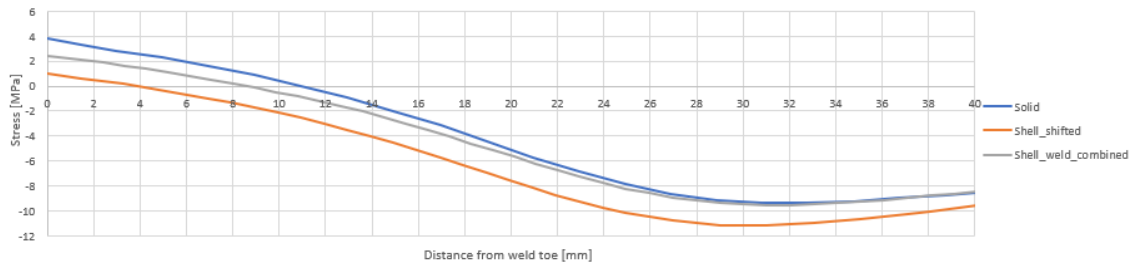


**Figure I 0.7 Comparison stress perpendicular to weld toe, P4\_28mm, for critical loading position X=+500mm, loaded between webs, crack in CB, new OSD variant**

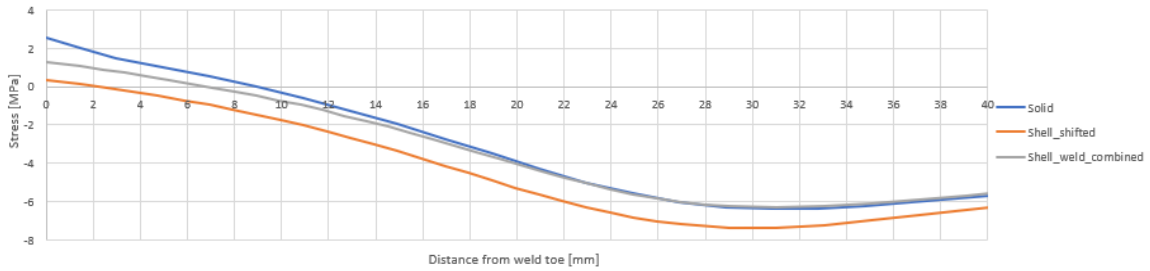


**Figure I 0.8 Comparison stress perpendicular to weld toe, P4\_28mm, for critical loading position X=+625mm, loaded between troughs, crack in CB, new OSD variant**

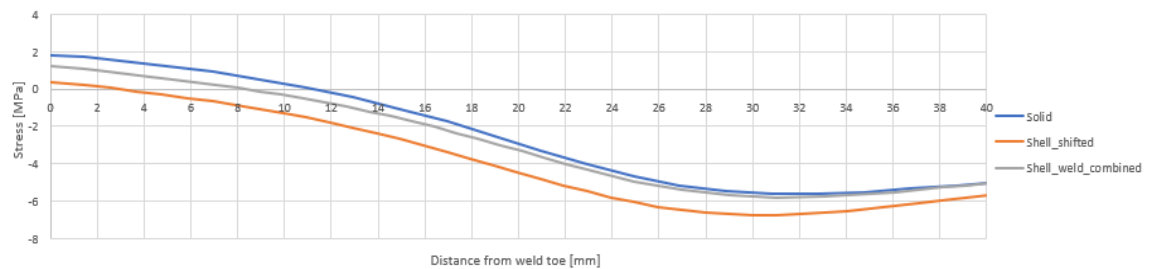
**Stress path critical locations for crack in crossbeam P4\_28mm old OSD variant (maximum HSS):**



**Figure I 0.9 Comparison stress perpendicular to weld toe, P4\_28mm, for critical loading position X=-750mm, loaded on top of web, crack in CB, old OSD variant**

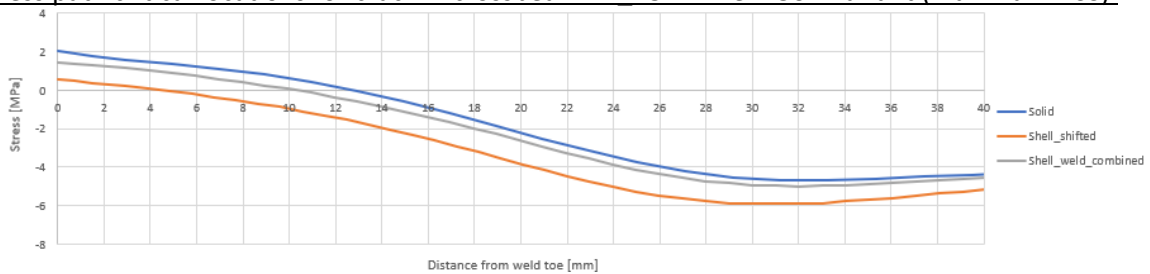


**Figure I 0.10 Comparison stress perpendicular to weld toe, P4\_28mm, for critical loading position X=-1375mm, loaded between webs, crack in CB, old OSD variant**

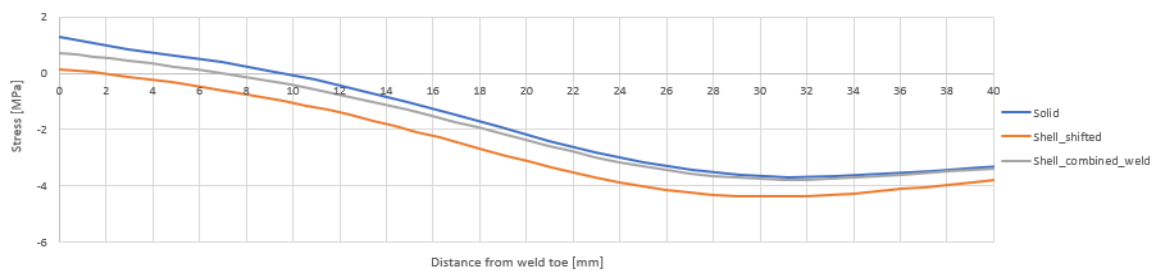


**Figure I 0.11 Comparison stress perpendicular to weld toe, P4\_28mm, for critical loading position X=-750mm, loaded between troughs, crack in CB, old OSD variant**

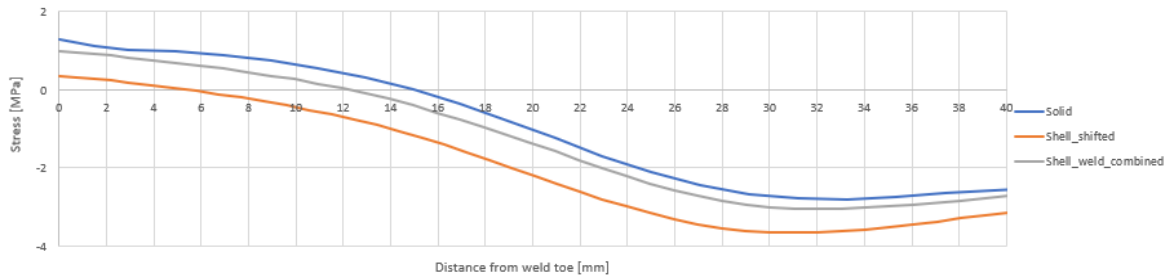
**Stress path critical locations for crack in crossbeam P4\_28mm new OSD variant (maximum HSS):**



**Figure I 0.12 Comparison stress perpendicular to weld toe, P4\_28mm, for critical loading position X=-750mm, loaded on top of web, crack in CB, new OSD variant**

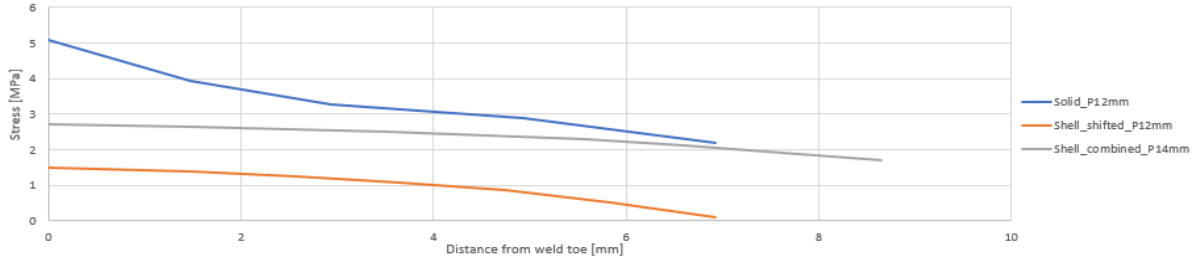


**Figure I 0.13 Comparison stress perpendicular to weld toe, P4\_28mm, for critical loading position X=-1250mm, loaded between webs, crack in CB, new OSD variant**

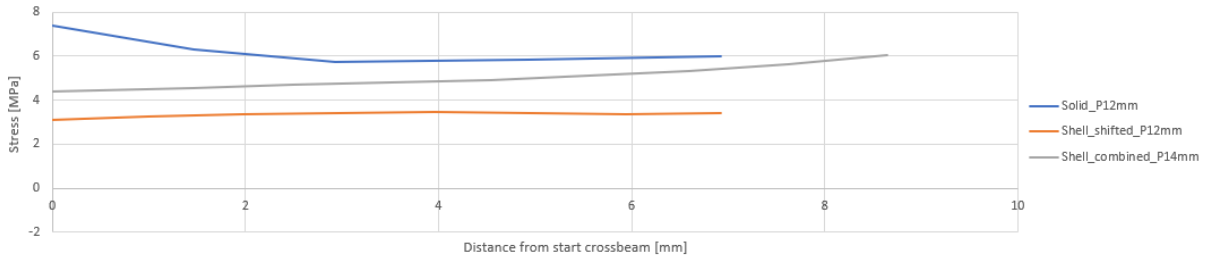


**Figure I 0.14 Comparison stress perpendicular to weld toe, P4\_28mm, for critical loading position X=-750mm, loaded between troughs, crack in CB, new OSD variant**

Stress path critical locations for crack in crossbeam P4\_12/14mm old OSD variant (maximum HSS):

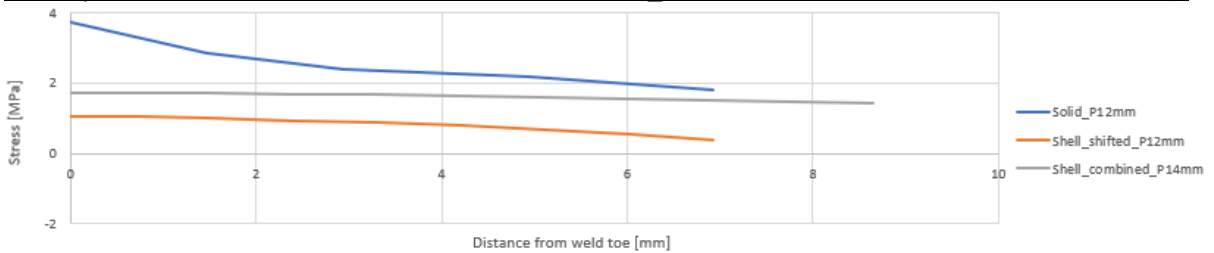


**Figure I 0.15 Comparison stress perpendicular to weld toe, P4\_12/14mm, for critical loading position X=-1375mm, loaded between webs, crack in CB, old OSD variant**

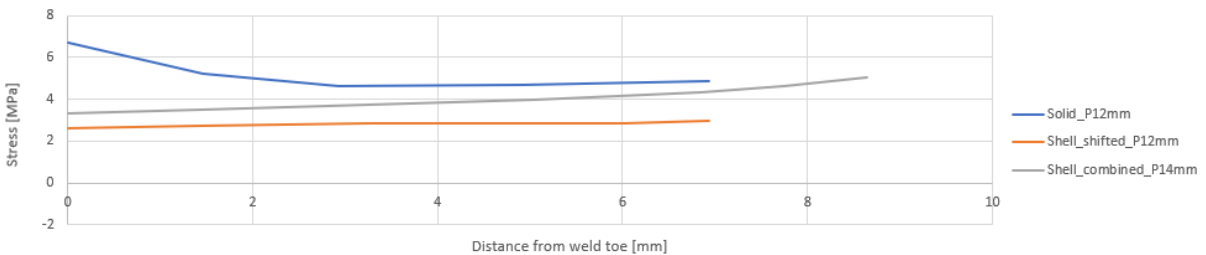


**Figure I 0.16 Comparison stress perpendicular to weld toe, P4\_12/14mm, for critical loading position X=-750mm, loaded between troughs, crack in CB, old OSD variant**

Stress path critical locations for crack in crossbeam P4\_12/14mm new OSD variant (maximum HSS):



**Figure I 0.17 Comparison stress perpendicular to weld toe, P4\_12/14mm, for critical loading position X=-1250mm, loaded between webs, crack in CB, new OSD variant**



**Figure I 0.18 Comparison stress perpendicular to weld toe, P4\_12/14mm, for critical loading position X=-750mm, loaded between troughs, crack in CB, old OSD variant**

## ANNEX J

### Comparison stresses

In Figure J 0.1 to Figure J 0.4 the comparison of the stress is made for the old OSD dimensions, thickness main plate 6mm, thickness stiffener 12mm, for four different load cases : LC1, LC2, LC3 and LC4.

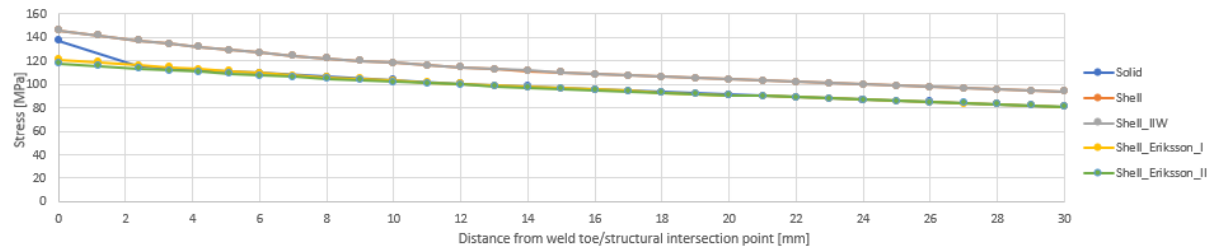


Figure J 0.1 Stress range LC I: in-plane, old variant

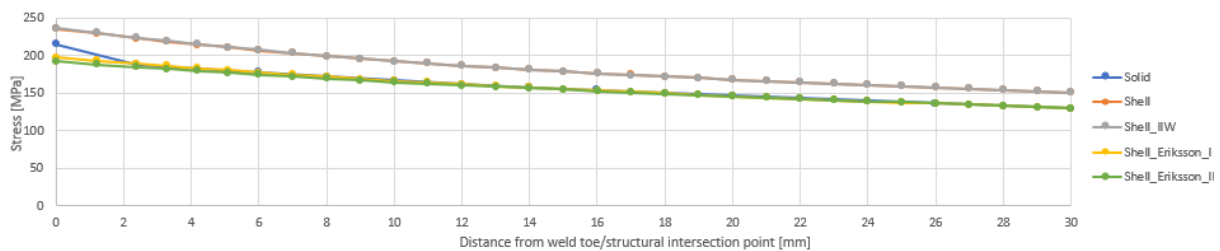


Figure J 0.2 Stress range LC II: out-of-plane I, old variant

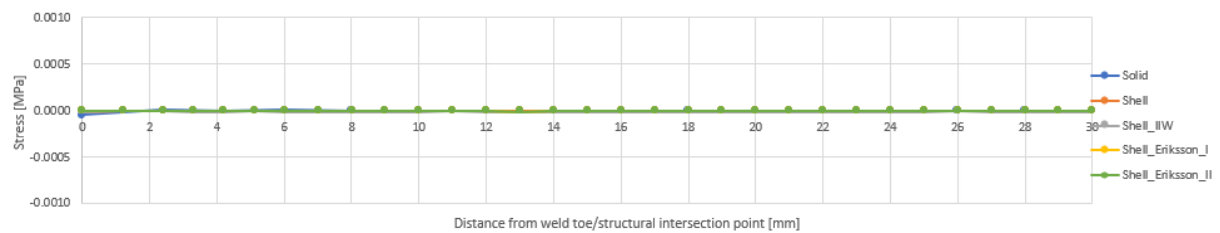


Figure J 0.3 Stress range LC III: out-of-plane II, old variant

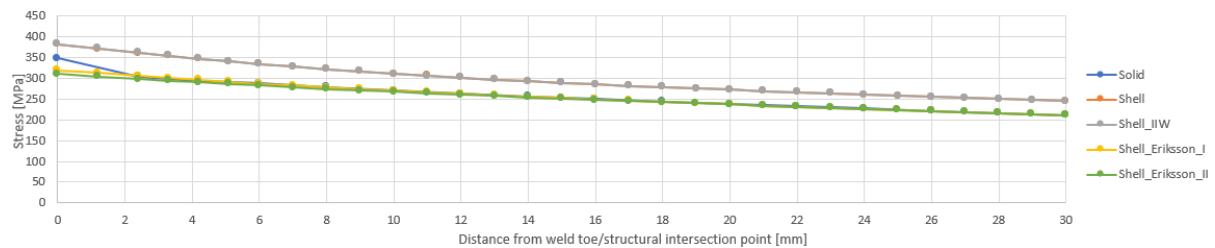


Figure J 0.4 Stress range LC IV: combination in-plane and out-of-plane I, old variant

In Figure J 0.5 to Figure J 0.8 the comparison of the stress is made for the new dimensions, thickness main plate 8mm, thickness stiffener 16mm, for four different load cases : LC1, LC2, LC3 and LC4.

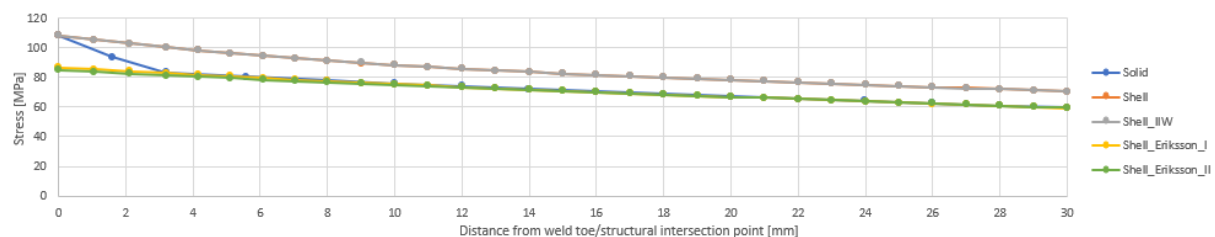


Figure J 0.5 Stress range LC I: in-plane, new variant

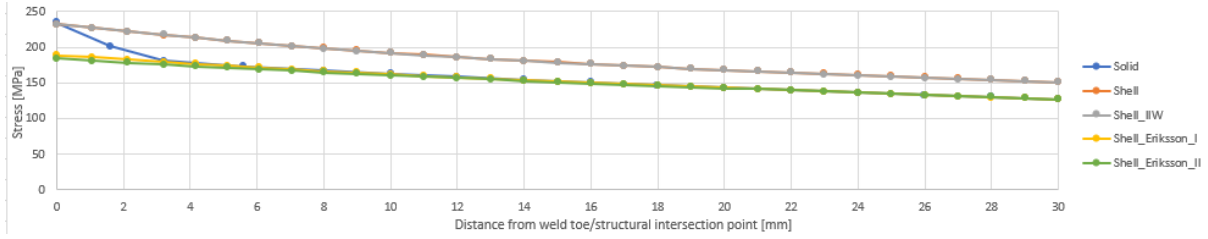


Figure J 0.6 Stress range LC II: out-of-plane I, new variant

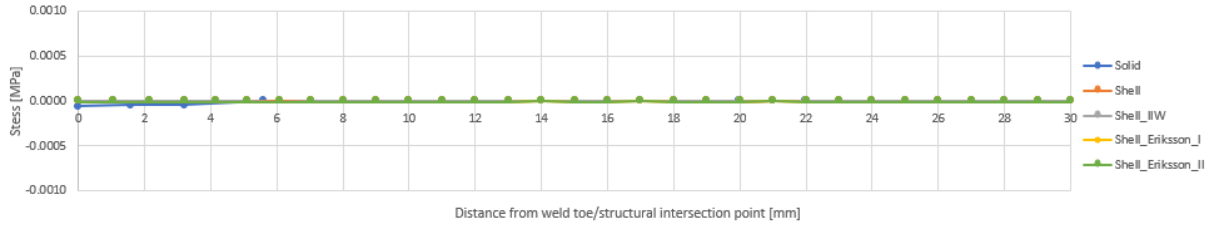


Figure J 0.7 Stress range LC III: out-of-plane II, new variant

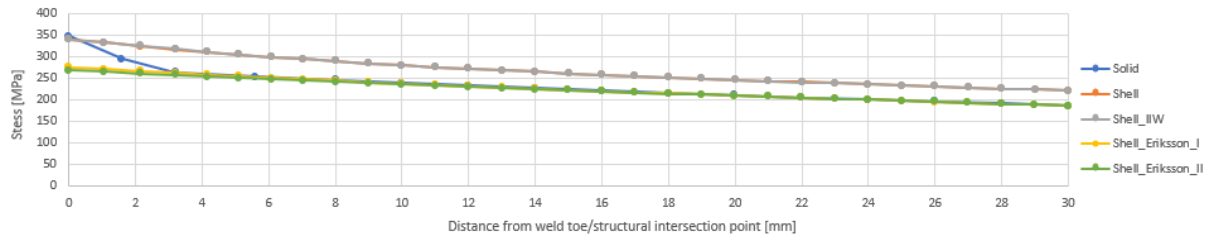


Figure J 0.8 Stress range LC IV: combination in-plane and out-of-plane I, new variant

### Comparison deformation

#### Load case I in-plane:

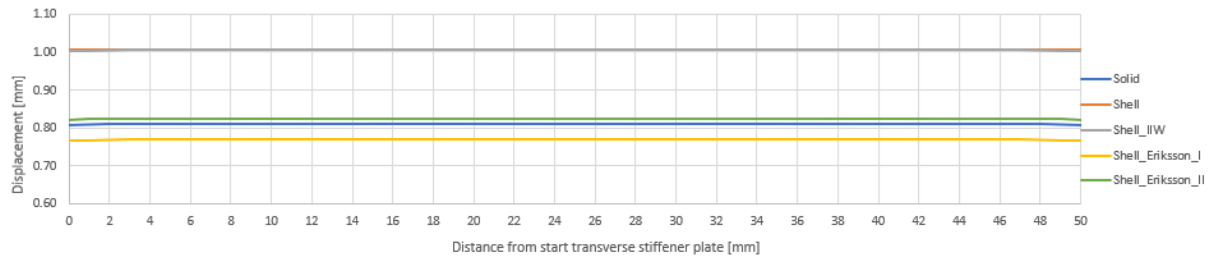


Figure J 0.9 Deformation U2 (Y-direction), loading type I: in-plane, old variant

#### Load case II out-of-plane I:

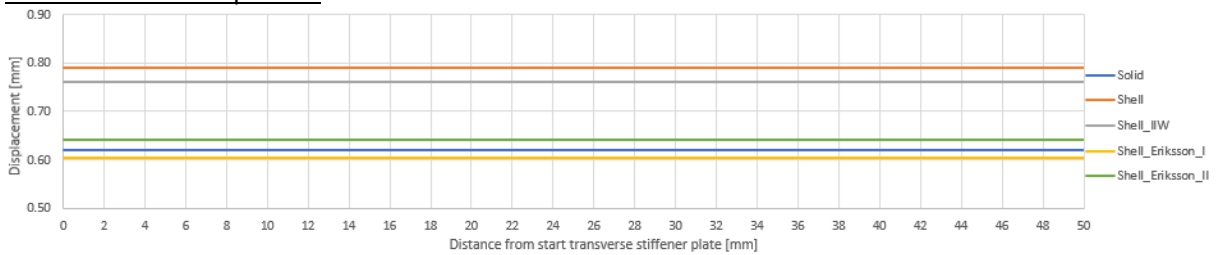
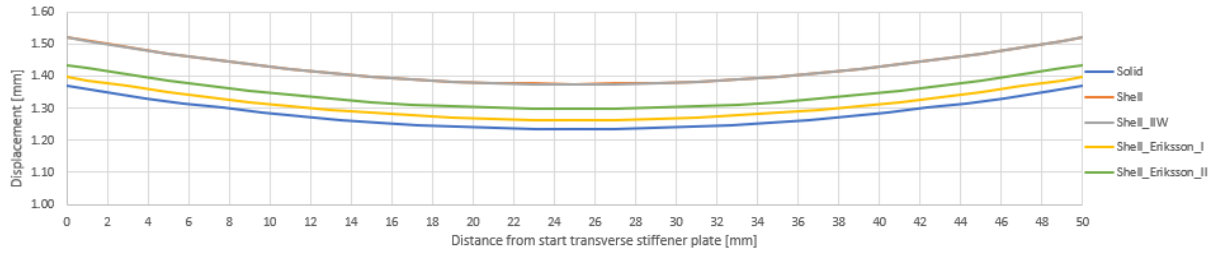


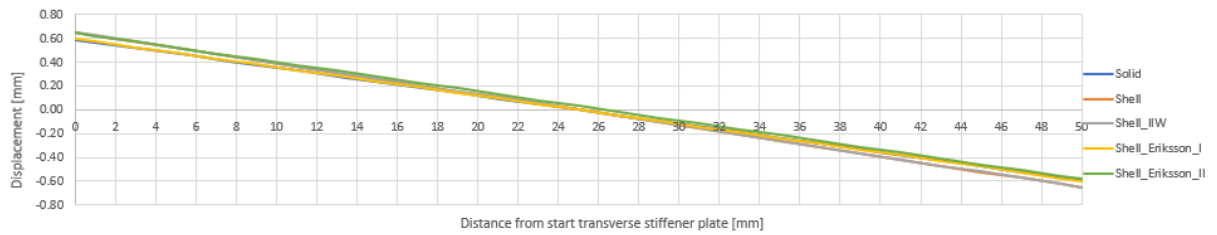
Figure J 0.10 Deformation U1 (X-direction), loading type II: out-of-plane I, old variant



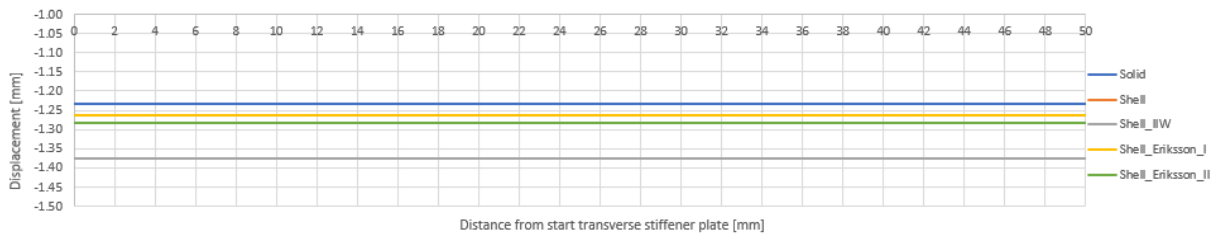
**Load case III out-of-plane II:**



**Figure J 0.11 Total deformation U, loading type III: out-of-plane II, old variant**

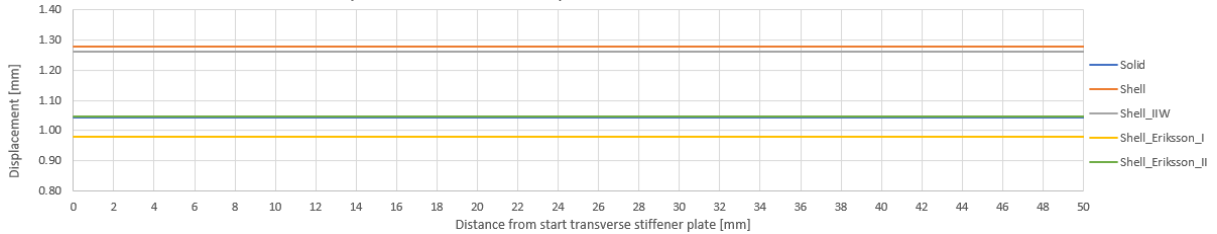


**Figure J 0.12 Deformation U2 (Y-direction), loading type III: out-of-plane II, old variant**



**Figure J 0.13 Deformation U3 (Z-direction), loading type III: out-of-plane II, old variant**

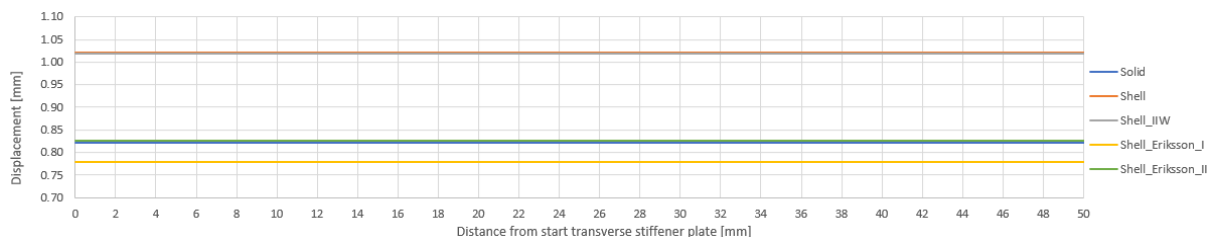
**Load case IV combination in-plane and out-of-plane I:**



**Figure J 0.14 Total deformation U, loading type IV: combination in-plane and out-of-plane I, old variant**



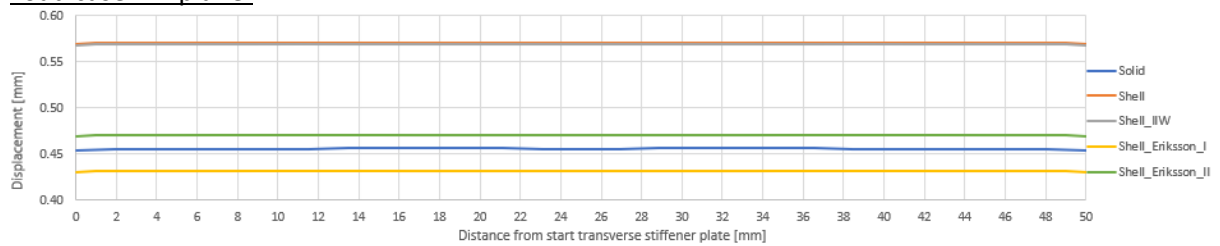
**Figure J 0.15 Deformation U1 (X-direction), loading type IV: combination in-plane and out-of-plane I, old variant**



**Figure J 0.16 Deformation U2 (Y-direction), loading type IV: combination in-plane and out-of-plane I, old variant**

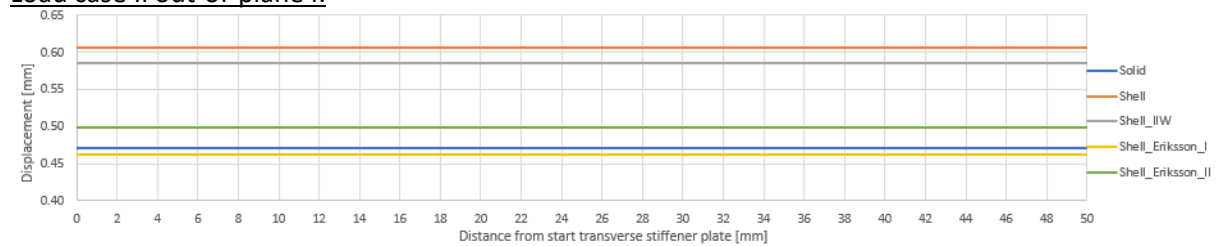
In the Figure J 0.17 to Figure J 0.24 the comparison of the predominant displacement is made for the new dimensions, thickness main plate 8mm, thickness stiffener 16mm.

**Load case I in-plane:**



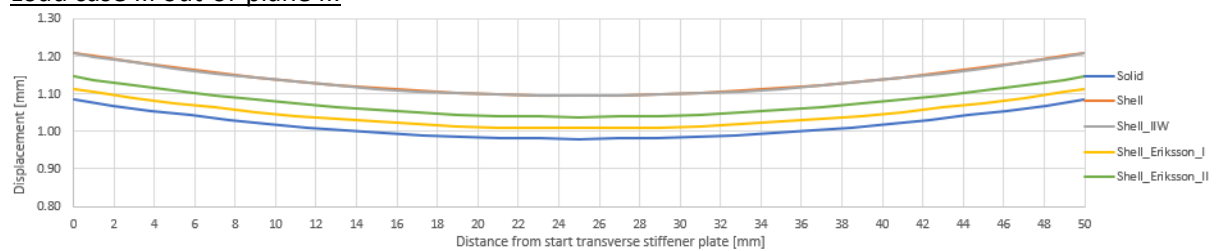
**Figure J 0.17 Deformation U2 (Y-direction), loading type I: in-plane, new variant**

**Load case II out-of-plane I:**

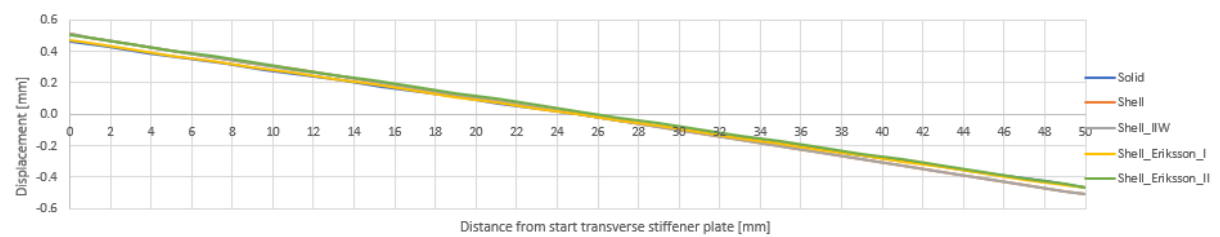


**Figure J 0.18 Deformation U1 (X-direction), loading type II: out-of-plane I, new variant**

**Load case III out-of-plane II:**



**Figure J 0.19 Total deformation U, loading type III: out-of-plane II, new variant**

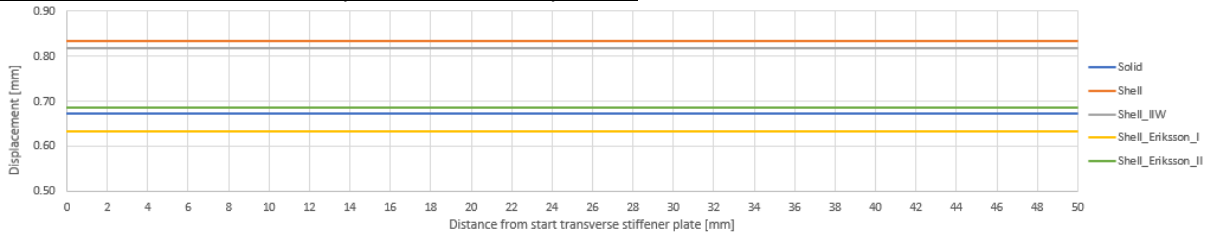


**Figure J 0.20 Deformation U2 (Y-direction), loading type III: out-of-plane II, new variant**



**Figure J 0.21 Deformation U3 (Z-direction), loading type III: out-of-plane II, new variant**

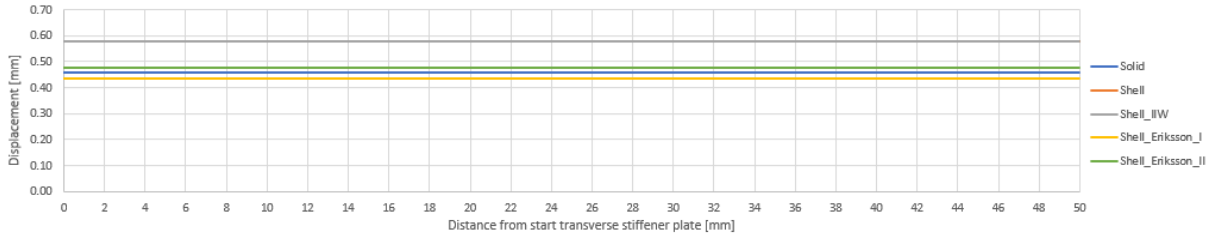
**Load case IV combination in-plane and out-of-plane I:**



**Figure J 0.22 Total deformation U, loading type IV: combination in-plane and out-of-plane I, new variant**



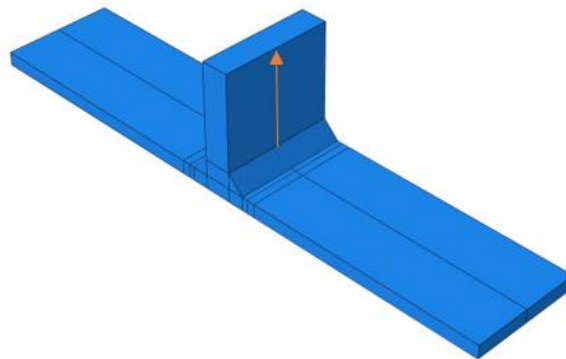
**Figure J 0.23 Deformation U1 (X-direction), loading type IV: combination in-plane and out-of-plane I, new variant**



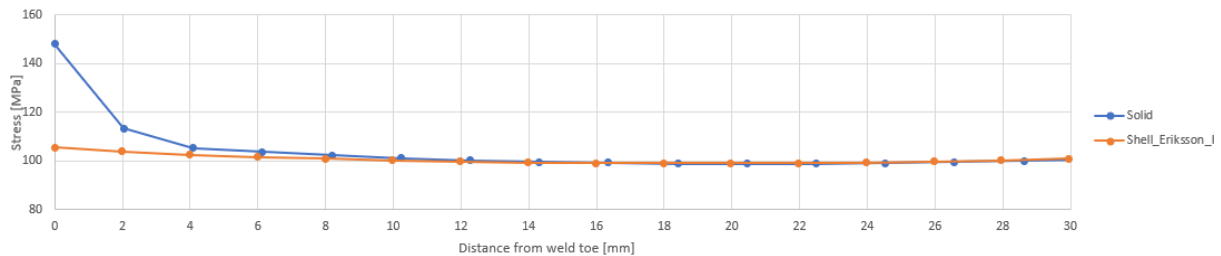
**Figure J 0.24 Deformation U2 (Y-direction), loading type IV: combination in-plane and out-of-plane I, new variant**

**Comparison hot spot stress in transverse attachment plate**

Also the hot spot stress in the stiffener is investigated for which the path is shown in Figure J 0.25. This analysis is performed for LC2 and LC4.



**Figure J 0.25 Path for hot spot stress extrapolation stiffener**



**Figure J 0.26 Stress range stiffener LC2, old variant**

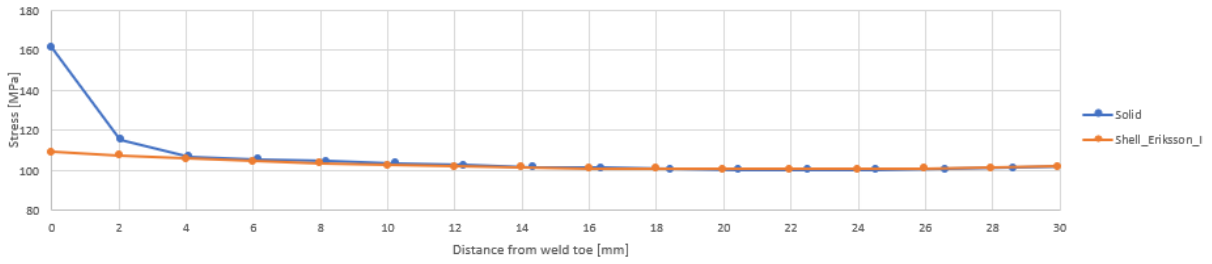


Figure J 0.27 Stress range stiffener LC4, old variant

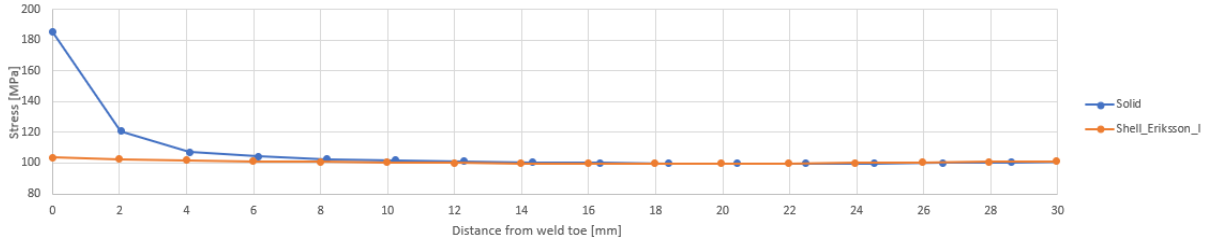


Figure J 0.28 Stress range stiffener LC2, new variant

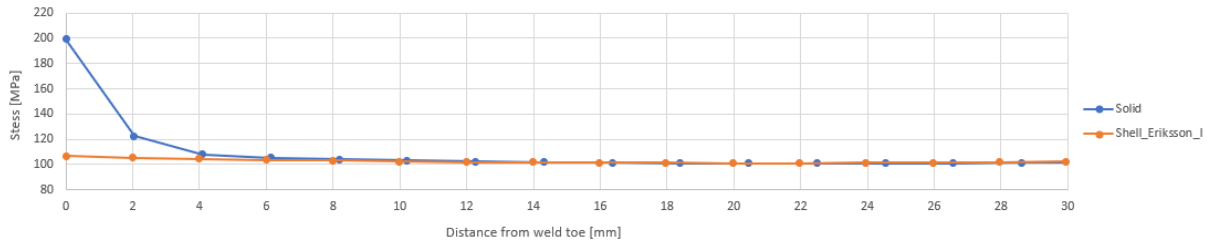
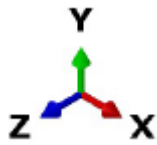


Figure J 0.29 Stress range stiffener LC4, new variant

Used coordinate system:



Deformed mesh and contour plots Abaqus old OSD variant thicknesses LC4:

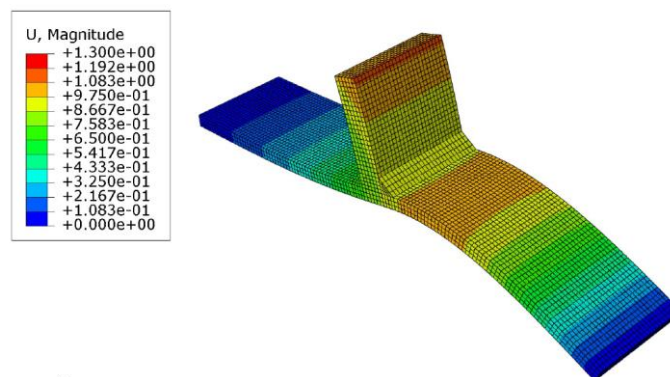


Figure J 0.30 Deformations plot LC4 old OSD thicknesses: solid FE model

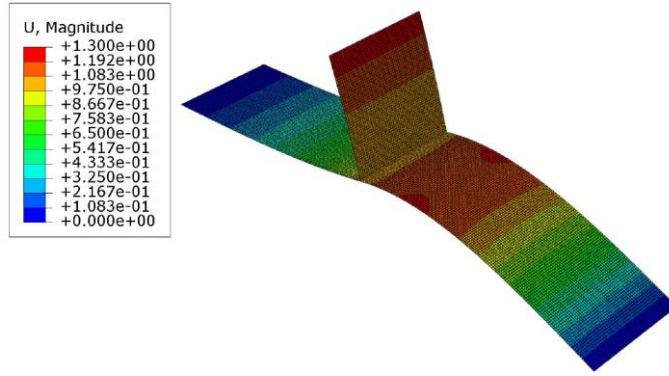


Figure J 0.31 Deformations plot LC4 old OSD thicknesses: shell FE model

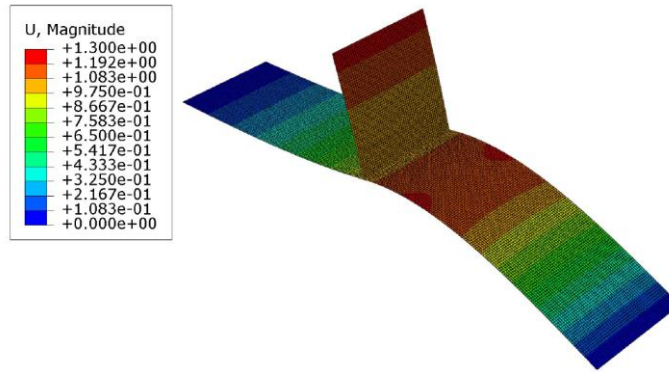


Figure J 0.32 Deformations plot LC4 old OSD thicknesses: shell with IIW weld FE model

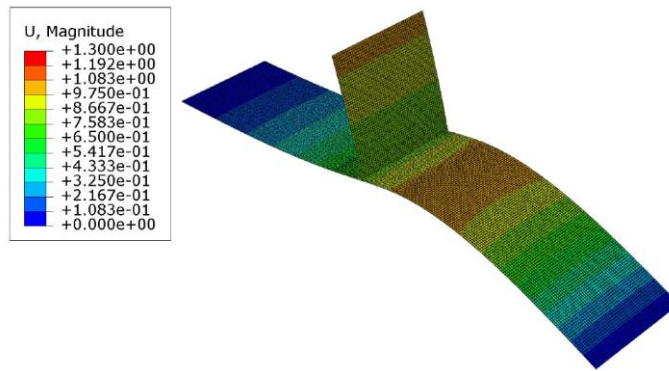


Figure J 0.33 Deformations plot LC4 old OSD thicknesses: shell with Eriksson (t+0.5a) weld FE model

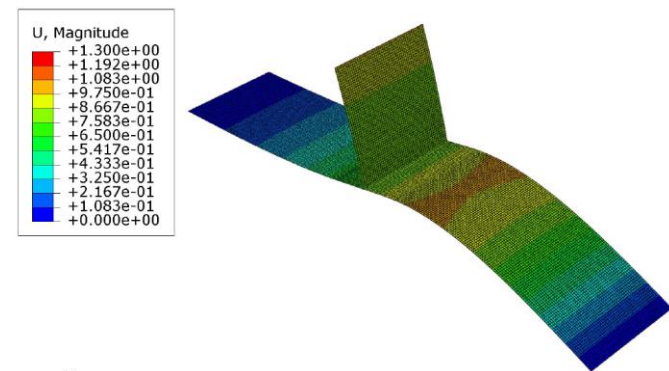
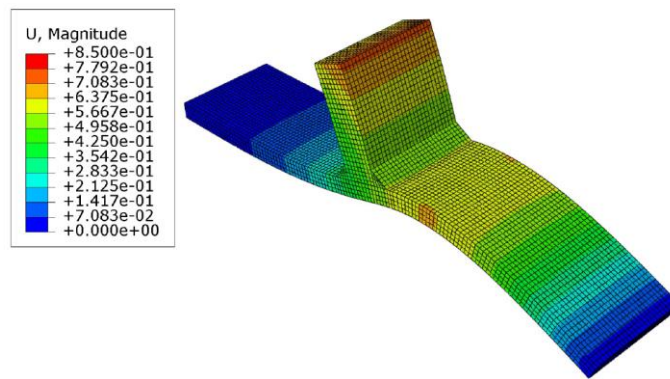
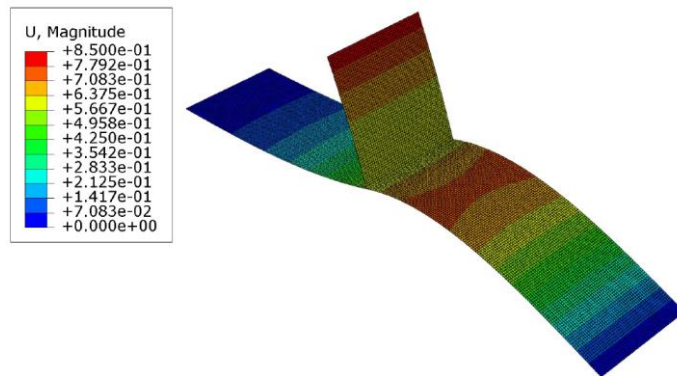


Figure J 0.34 Deformations plot LC4 old OSD thicknesses: shell with Eriksson (t+a) weld FE model

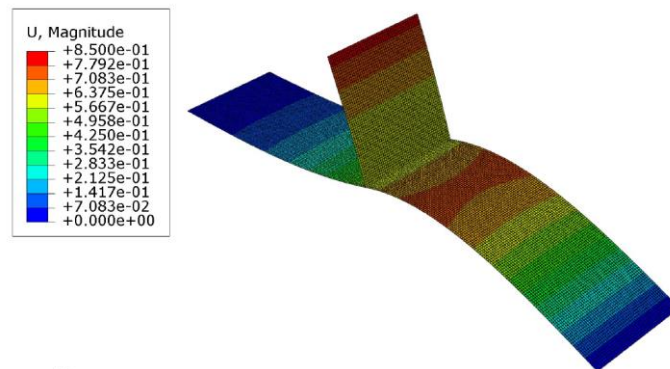
**Deformed mesh and contour plots Abaqus new OSD variant thicknesses LC4:**



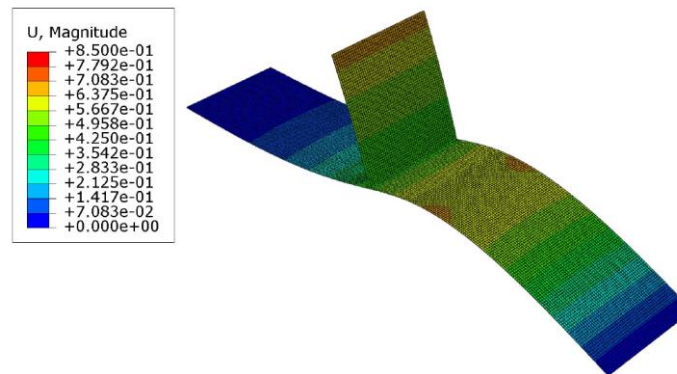
**Figure J 0.35 Deformations plot LC4 new OSD thicknesses: solid FE model**



**Figure J 0.36 Deformations plot LC4 new OSD thicknesses: shell FE model**



**Figure J 0.37 Deformations plot LC4 new OSD thicknesses: shell with IIW weld FE model**



**Figure J 0.38 Deformations plot LC4 new OSD thicknesses: shell with Eriksson (t+0.5a) weld FE model**

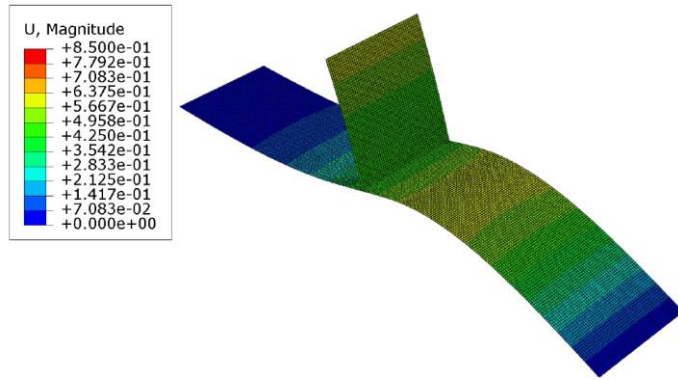


Figure J 0.39 Deformations plot LC4 new OSD thicknesses: shell with Eriksson (t+a) weld FE model

# ANNEX K

## Overview results stress in path 2:

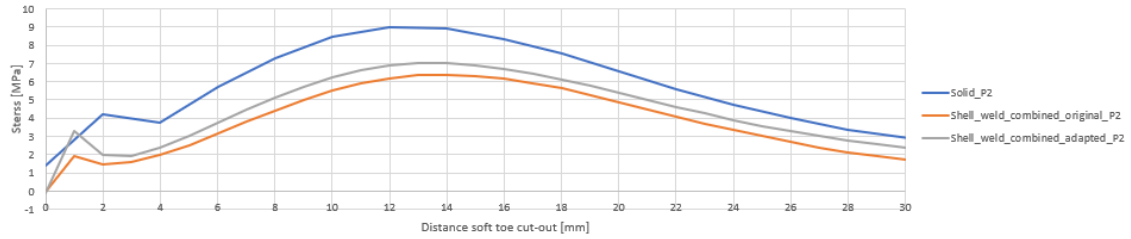


Figure K 0.1 Stress perpendicular to weld toe in path 2, loaded on web: X=-750mm, old OSD variant

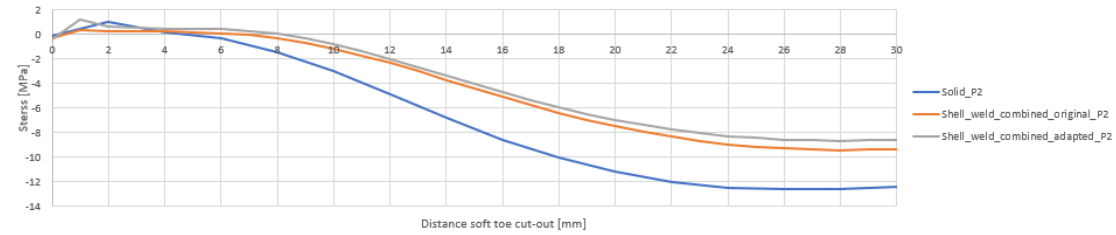


Figure K 0.2 Stress perpendicular to weld toe in path 2, loaded on web: X=+500mm, old OSD variant

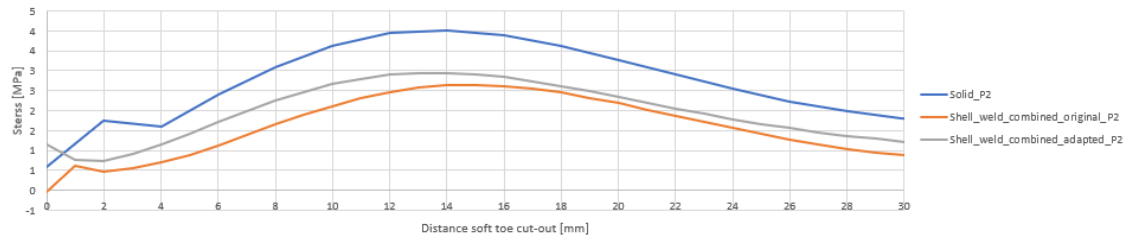


Figure K 0.3 Stress perpendicular to weld toe in path 2, loaded between webs: X=-1375mm, old OSD variant

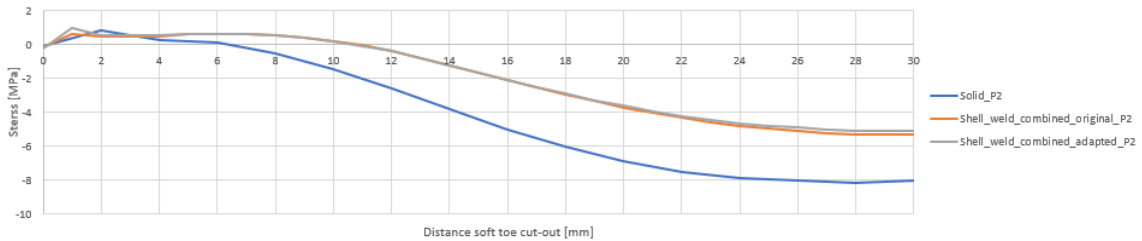


Figure K 0.4 Stress perpendicular to weld toe in path 2, loaded between webs: X=+375mm, old OSD variant

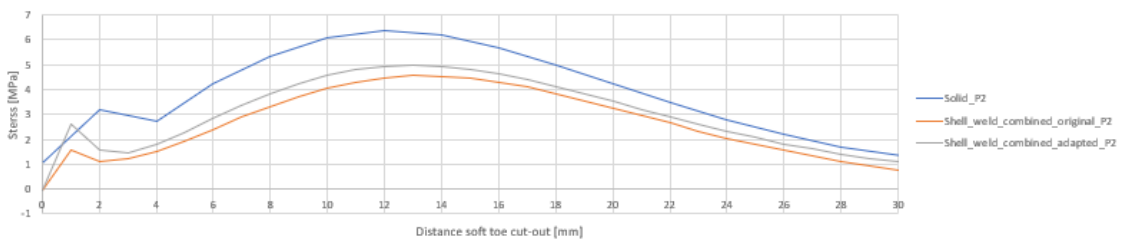


Figure K 0.5 Stress perpendicular to weld toe in path 2, loaded between troughs: X=-750mm, old OSD variant

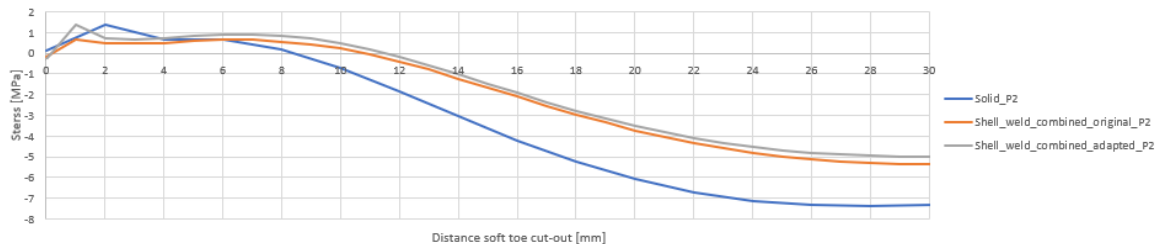
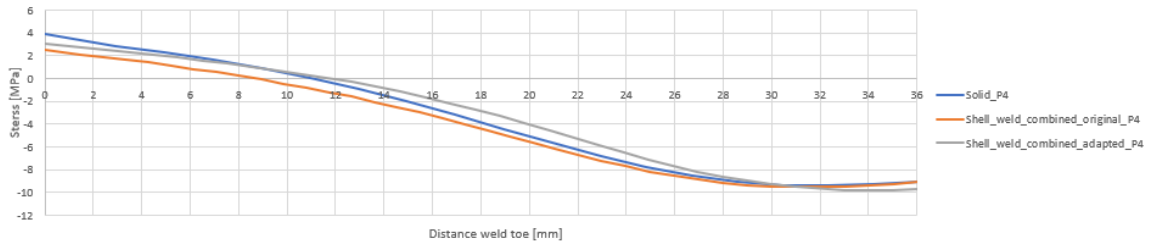


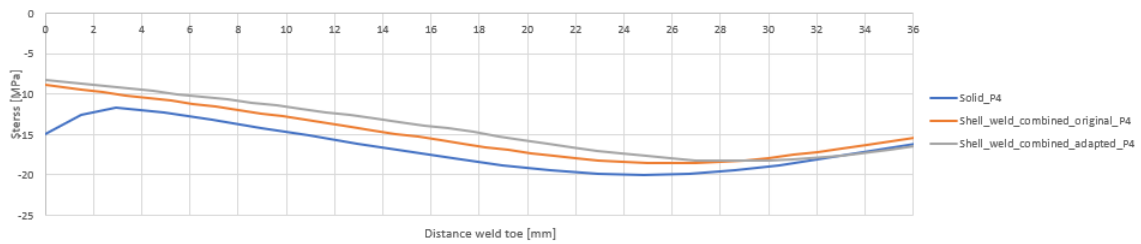
Figure K 0.6 Stress perpendicular to weld toe in path 2, loaded between troughs: X=+625mm, old OSD variant



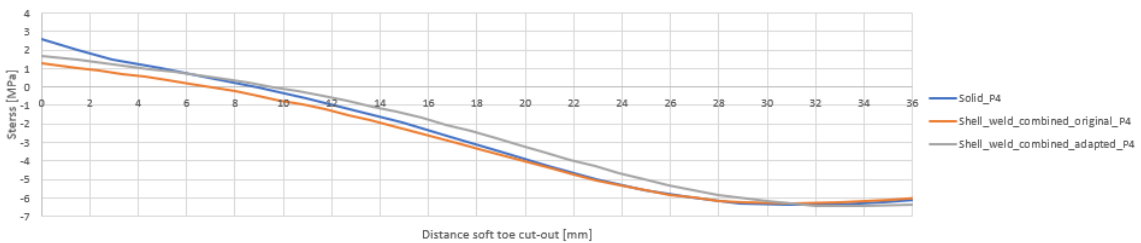
**Overview results stress in path 4:**



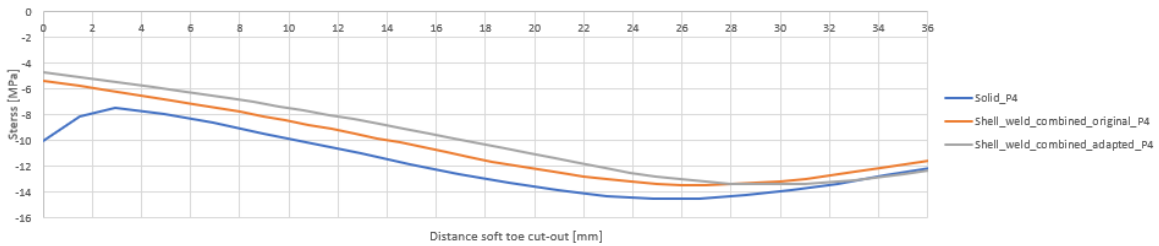
**Figure K 0.7 Stress perpendicular to weld toe in path 4, loaded on web: X=-750mm, old OSD variant**



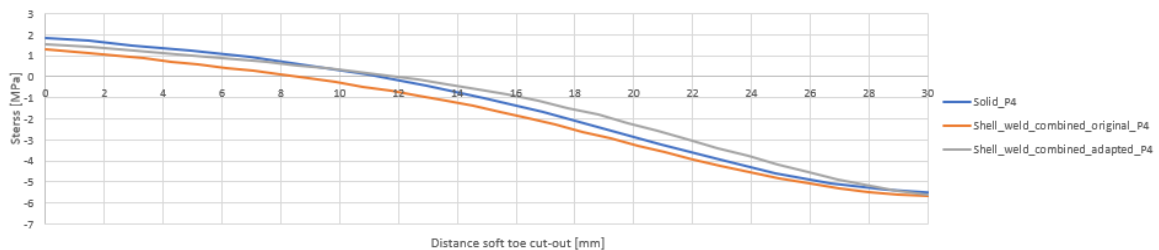
**Figure K 0.8 Stress perpendicular to weld toe in path 4, loaded on web: X=+500mm, old OSD variant**



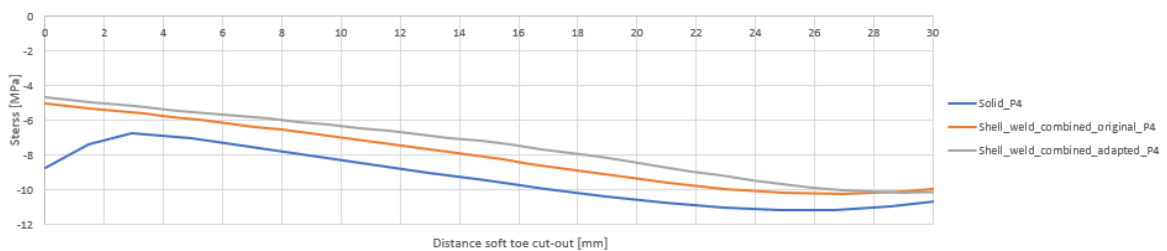
**Figure K 0.9 Stress perpendicular to weld toe in path 4, loaded between webs: X=-1375mm, old OSD variant**



**Figure K 0.10 Stress perpendicular to weld toe in path 4, loaded between webs: X=+375mm, old OSD variant**



**Figure K 0.11 Stress perpendicular to weld toe in path 4, loaded between troughs: X=-750mm, old OSD variant**



**Figure K 0.12 Stress perpendicular to weld toe in path 4, loaded between troughs: X=+625mm, old OSD variant**

## References

- Akhlaghi, F. (2009). *Fatigue life assessment of welded bridge details using structural hot spot stress method. A numerical and experimental case study*. Göteborg: Chalmers University of Technology.
- Al-Emrani, M., & Aygül, M. (2014). *Fatigue design of steel and composite bridges*. Göteborg: Chalmers University of Technology.
- ASM Handbook, Volume 19: Fatigue and Fracture*. (1996). Georgia: ASM International.
- Aygül. (2012). *Fatigue analysis of welded structures using the finite element method*. Gothenberg: Chalmers University of Technology.
- Aygül, M., Al-Emrani, M., & Urushadze, S. (2012). Modelling and fatigue life assessment of orthotropic bridge deck details using FEM. *International journal of fatigue*, 129-142.
- Bak, M. (2015, 05 15). *CAE associates*. Retrieved from How to account for fatigue data scatter: <https://caeai.com/blog/how-account-fatigue-data-scatter>
- Beales. (1990). *Assessment of trough to crossbeam connections in orthotropic steel bridge decks*. Berkshire: Transport and Road Research Laboratory.
- Beld, P. (2019). *Improvements for the prediction of the fatigue life of the deck plate in orthotropic steel decks*. Delft: Delft University of Technology.
- DNV GL. (2016). *Fatigue design of offshore steel structures*. Høvik, Norway: Det Norske Veritas Germanischer Lloyd.
- Dong, P. (2001). A structural stress definition and numerical implementation for fatigue analysis of welded joints. *International Journal of Fatigue* 23, 865-876.
- Echer, L., & Marczak, R. (2017). Parametric representation of weld fillets using shell finite elements—a proposal based on minimum stiffness and inertia errors. *Engineering optimization Volume 50*, 183-204.
- EN1991-2. (2011). *EN 1991-2 Eurocode 1: actions on structures - part 2: traffic loads on bridges*. Brussels: European committee for standardisation.
- EN1993-1-9. (2011). *EN 1993-1-9 Eurocode 3: design of steel structures - part 1-9 fatigue*. Brussels: European committee for standardisation.
- EN1993-2. (2011). *EN 1993-2 design of steel structures - part 2: steel bridges*. Brussels: European committee for standardisation.
- EN1993-2-NB. (2011). *En 1993-2/NB Dutch national annex to eurocode 3: design of steel structures - part 2: steel bridges*. Brussels: European committee for standardisation.
- Eriksson, A., Lignell, M., Olsson, C., & Spennare, H. (2003). *Weld evaluation using FEM - A guide to fatigue-loaded structures*. Gothenborg: Industrilitteratur AB.
- Fayard, J., Bignonnet, A., & Dang, K. v. (1996). Fatigue design criterion for welded structures. *Fatigue & Fracture of Engineering Materials & Structures* 19, 723-729.
- Federal highway administration. (2012). *Manual for designm construction, and maintenaice of orthotropic steel deck bridges*. Pittsburgh: US department of transportation.

- Freitas, S. d., Kolstein, H., & Bijlaard, F. (2011). Sandwich system for renovation of orthotropic steel bridge decks. *urnal of Sandwich Structures and Materials* 13, 279-301.
- Fricke, W. (2002). Recommended Hot-Spot Analysis Procedure For Structural Details of Ships And FPSOs Based On Round-Robin FE Analyses. *International journal of offshore and polar engineering*, 1-8.
- Gustafsson, J., & Saarinen, J. (2007). *Multiaxial fatigue in welded detail an investigation of existing design approaches*. Goteborg: Chalmers University of Technology.
- Haibach, E., & Plasil, A. (1983). Untersuchungen zur Betriebsfestigkeit von Stahlleichtfahrbahne mit Trapezhohlsteifen im Eisenbahnbrückenbau. *Der Stahlbau* 9, 269-274.
- Hänsch, H., & Müller, G. (1961). Dauerfestigkeitsversuche an geschweissten Hohlrippenanschlüssen. *Schweisstechnik* 11, 193-198.
- Hobbacher. (2014). *Recommendations for fatigue design of welded joints and components*. Wilhemshaven: International Institute of Welding (IIW).
- Hobbacher, A. (1996). *Fatigue design of welded joints and components*. Cambridge: Abington publishing.
- Hobbacher, A. (2009). The new IIW recommendations for fatigue assessment of welded joints and components - A comprehensive code recently updated. *International Journal of Fatigue*, 50-58.
- Hobbacher, A. (2016). *Fatigue design of welded joints and components*. Cambridge: Abington publishing.
- Huang, Y., Zhang, Q., & Bu, Y. (2019). Fatigue assessment of longitudinal rib-to-crossbeam welded joints in orthotropic steel bridge decks. *Journal of Constructional Steel Research*, 53-66.
- Kitner, K. (2016). *A study of manufacturable rib-to-floor beam connections in steel orthotropic bridge decks*. Bethlehem, Pennsylvania: Lehigh University.
- Klarholm, D. (2016). *Offset modeling of shell elements a study in shell element modeling using Nastran*. Linköping: Linköping institute of technology.
- Kolstein. (1997). *Out of plane bending tests on trough to crossbeam joints*. Delft: Delft University of Technology.
- Kolstein, H. (2007). *Fatigue classification of welded joints in orthotropic steel bridge decks*. Delft: Delft University of Technology.
- Kolstein, M., & Leendertz, J. (1989). *Fatigue design of European orthotropic steel bridge decks – Part 2: Trough to crossbeam connection*. Delft: Delft University of Technology.
- Krishnamoorthy, C. (1994). *Finite element analysis theory and programming second edition*. New Delhi: Tat McGraw-Hill publishing company limited.
- Lee, J.-M., Seo, J.-K., Kim, M.-H., Shin, S.-B., Han, M.-S., Park, J.-S., & Mahendran, M. (2010). Comparison of hot spot stress evaluation methods for welded structures. *Inter J Nav Archit Oc Engng* 2, 200-210.
- Leendertz, J. (2008). *Fatigue behaviour of closed stiffener to crossbeam connections in orthotropic steel bridge decks*. Delft: Delft University of Technology.

- Lehrke. (1990). Fatigue tests of stiffener to crossbeam connections. *IABSE Workshop Remaining Fatigue Life of Steel Structures*, 249-257.
- Leonetti, D., Allaix, D., Maljaars, J., & Hashemi, B. (2017). Fatigue Damage evaluation using S-N curves obtained by different data fitting methods. *IABSE Symposium*.
- Li, M., Suzuki, Y., Hashimoto, K., & Sugiura, K. (2017). Experimental study on fatigue resistance of rib-to-deck joint in orthotropic steel bridge deck. *Journal of bridge engineering volume 23*, 157-167.
- Liu, G., Huang, Y., Gao, M., & Li, Y. (2011). Comparison of Shell and Solid Elements for Hot Spot Stress Analysis of Complex Welded Joints. *International Society of Offshore and Polar Engineers (ISOPE)*, 19-24.
- Malikoutsakis, M., & Savaidis, G. (2009). An approach to the effective notch stress concept to complex geometry weld focusing on the FE modeling of weld ends. *3rd ANSA &  $\mu$ ETA International Conference*. Halkidiki: Aristotle University of Thessaloniki.
- Mashiri, F., & Zhao, X. (2007). Fatigue tests and design of thin chs plate t joints under cyclic in plane bending. *Thin-walled structures*, 463-472.
- Ministerie van Infrastructuur en Milieu, R. G. (2017). *Richtlijnen Ontwerp Kunstwerken ROK 1.4*. Utrecht: Rijkswaterstaat Technisch Document.
- Murakoshi, J., Hirano, S.-i., & Harada Hideaki. (n.d.). *Effect of the deck plate thickness of orthotropic steel deck on fatigue durability*. Japan: Center for advanced engineering structural assessment and research (CAESAR), PWRI.
- Nassif, H., & Linzell, D. (2013). Optimization of design details in orthotropic steel decks subjected to static and fatigue loads. *Transportation research record journal of the transportation research board*, 14-23.
- Niemi, E. (1995). *Stress determination for Fatigue Analysis of Welded Components*. -: International Institute of Welding.
- Niemi, E. (1995). *Stress Determination for Fatigue Analysis Of Welded Components*. Cambridge: Abington publishing.
- Niemi, E., Fricke, W., & Maddox, S. J. (2018). *Structural hot-spot stress approach to fatigue analysis of welded components designer's guide second edition*. Paris: International Institute of welding (IIW).
- Nunn, D. (1974). *An investigation into the fatigue of welds in an experimental orthotropic bridge deck panel*. Crowthorne: Transport and Road Research Laboratory, Structures Department, Bridges Division.
- Osawa, N., Yamamoto, N., Fukuoka, T., Sawamura, J., Nagai, H., & Maeda, S. (2011). Study on the preciseness of hot spot stress of welded joints derived from shell finite element analyses. *Marine structures volume 24*, 207-238.
- Pandit, S. (2020). *Finite element modelling of open longitudinal stiffener to crossbeam connection in OSD bridges for hot-spot stress determination*. Delft: Delft University of Technology.
- Radaj, D. (1990). *Design and analysis of fatigue-resistant welded structures*. Cambridge: Abington Publisher.

- Rikeros, D. (2019). *Fatigue assessment of rail track detail on movable bridge in Estonia based on 2D / 3D Finite Element Modelling using hot-spot stresses*. Delft: Delft University of Technology.
- SIMULIA. (2011). *Abaqus 6.11 Theory manual*. Providence: Dassault Systèmes Simulia Corp.
- Śledziewski, K. (2018). Fatigue assessment for selected connections of structural steel bridge components using the finite elements method. *AIP Conference Proceedings 1922*, 150001-1–150001-10.
- Smith, E. (1994). *Mechanical Engineer's Reference Book chapter 7: materials, properties and selection*. Oxford: Elsevier Ltd.
- Susmel, L., & Tovo, R. (2006). Local and structural multiaxial stress states in welded joints under fatigue loading. *International journal of fatigue (28)*, 564-575.
- Swierstra, E. (2017). *Fatigue assessment in finite element analysis a post-processor to FEA output for hot spot stress calculation*. Delft: Delft University of Technology.
- Wang, B. (2017). *A multiscale study on fatigue mechanism and life estimation on welded joints*. Gent: University of Gent.
- Wu, W., & Kolstein, M. (2020). *Out-of-plane fatigue tests of trough-crossbeam connection with 20mm deck plate*. Delft: Delft University of Technology.
- Wu, W., Kolstein, H., Veljkovic, M., Pijpers, R., & Vorstenbosch-Krabbe, J. (2017). Fatigue behaviour of the closed rib to deck and crossbeam joint in a newly designed orthotropic bridge deck. *CE Papers*, 2378-2387.
- Xiao, Z.-G., & Yamada, K. (2004). A method of determining geometric stress for fatigue strength evaluation of steel welded joints. *International Journal of Fatigue 26*, 1277-1293.
- Yokozeki, K., & Miki, C. (2016). Fatigue evaluation for longitudinal-to-transverse rib connection of orthotropic steel deck by using structural hot spot stress. *Weld World 60*, 83-92.
- Zhang, Q.-H., Cui, C., Bu, Y.-Z., Liu, Y.-M., & Ye, H.-W. (2015). Fatigue tests and fatigue assessment approaches for rib-to-diaphragm in steel orthotropic decks. *Journal of Constructional Steel Research*, 110-118.
- Zhao, X.-L., Wilkinson, T., & Hancock, G. (2005). *Cold-formed Tubular Members and Connections: Structural Behaviour and Design*. Oxford: Elsevier Ltd.